JOURNAL OF
EMERGING INVESTIGATORS

VOLUME 4, ISSUE 1 | JANUARY 2021
emerginginvestigators.org

Fractal chaos
Modeling and understanding chaotic behavior in the Mandelbrot Set

Bamboo bioplastic
Comparing a new formulation to conventional petroleum plastic

A look into lipases
How solvents affect industrial enzyme activity

Capturing humidity
A compact device for collecting water

Cannabinoid concerns
How CBD oil may correlate with depressive symptoms

JOURNAL OF EMERGING INVESTIGATORS

The Journal of Emerging Investigators is an open-access journal that publishes original research in the biological and physical sciences that is written by middle and high school students. JEI provides students, under the guidance of a teacher or advisor, the opportunity to submit and gain feedback on original research and to publish their findings in a peer-reviewed scientific journal. Because grade-school students often lack access to formal research institutions, we expect that the work submitted by students may come from classroom-based projects, science fair projects, or other forms of mentor-supervised research.

JEI is a non-profit group run and operated by graduate students, postdoctoral fellows, and professors across the United States.

Contents

VOLUME 4, ISSUE 1 | JANUARY 2021

JOURNAL OF
EMERGING INVESTIGATORS

Article

A statistical comparison of the Simultaneous Attack/ Persistent Pursuit Theory against current methods in counterterrorism using a stochastic model

Paarth Tara, Preeti Tara
Eastern Alamance High School, Mebane, North Carolina

SUMMARY

Though current strategies in counterterrorism are somewhat effective, various counterinsurgency theorists have raised doubts about the true efficacy of current methods. Established current strategies are fundamentally flawed, with an overemphasis on eliminating leaders and highly connected agents. Colonel Derek Jones, a counterinsurgency theorist, proposed the Simultaneous Attack/Persistent Pursuit (SAPP) Theory as a superior alternative to current methods. In this strategy, attacks are conducted equally across all fronts of a clandestine intelligence network, from which connections are pursued with further attacks. To determine whether current methods are more or less effective in counterterrorism than the method proposed by the SAPP Theory, a stochastic computational model was developed to represent a traditional eastern clandestine network for an isolated sub-cell of a terrorist organization. Attacks were modeled through the loss of agents within specific components of the network. After an analysis of relevant literature discussing the efficacy of current methods in counterterrorism, we hypothesized that the SAPP model would lead to a greater reduction in the number of terrorist attacks than other methods. We simulated five attack strategies, with each strategy being simulated for thirty trials, and the resulting final number of attacks of the terrorist network was recorded. Through four two-sample t-tests comparing each of the four non-SAPP strategies to the SAPP model, we concluded that the SAPP model was significantly more effective in reducing the final number of terrorist attacks. This demonstrates the comparative advantage of utilizing the SAPP model, which may prove to be critical in future efforts in counterterrorism.

INTRODUCTION

With a growing influence of terrorist organizations worldwide, human life and global peace are increasingly threatened throughout the world. These terrorist organizations often structure themselves in clandestine cell systems, which are a type of decentralized intelligence network in which individual members are not fully aware of either their role in the network, nor the existence of members outside of their localized group of agents (1). This research aims to understand both the nature of clandestine networks and strategies for combating these networks through computational methods.

Many terrorist organizations throughout the world have decentralized intelligence structures (2). Though many other intelligence systems are heavily dependent on leaders and plentiful connections between members (or agents), clandestine cell systems tend to place less of an importance on both of these components.

Most clandestine practitioners adopt clandestine networks in an effort to be resistant to the compromise—in the context of this research, the elimination of members through counterinsurgency—of agents within a network. Components of a clandestine network are isolated from one another to ensure that individual cells do not compromise information. This decentralized method of operation—referring to the nature of an intelligence structure to be arranged in such a manner that there are multiple leader agents distributed throughout the network, each with significant independence and control over localized portions of the whole network, yet bound together through their affiliation with the terrorist organization—also ensures that individual agents are sometimes unaware of their purpose in the network, uninformed of other members, and are unconnected to vital components of the network. Clandestine cells also place less of an importance on the loss of individual agents within a network, making the process of rebounding from an attack far more efficient.

Before analyzing strategies to combat these clandestine cell systems, it is important to differentiate between the various types. Western clandestine cell systems are more hierarchical in structure (**Figure 1**), with a more defined structure than eastern counterparts. Eastern clandestine cell systems are more loosely distributed (**Figure 2**), with many components of the network being structured in a ring-like form. In this research, we only considered eastern clandestine cell systems, for they are more closely linked to the form of major eastern terrorist organizations, which are the primary sources of modern global terrorism (1).

Due to the specific characteristics of clandestine networks, many counterinsurgency theorists question current strategies in counterterrorism (1, 3). Jordan *et al.* stated that these

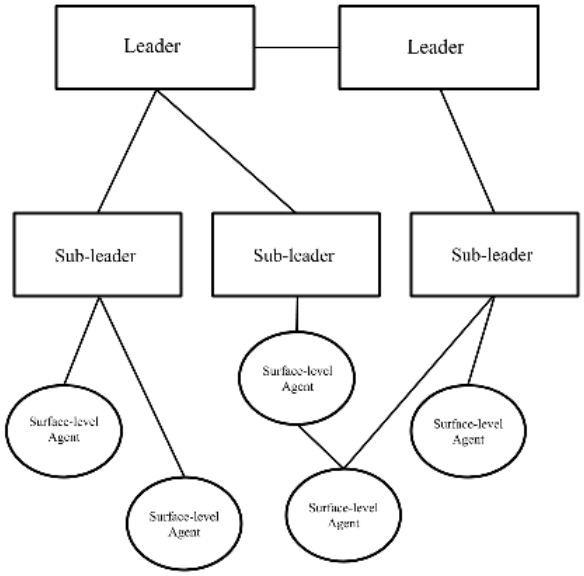

Figure 1. An abstract model of a western clandestine network. Boxes and circles both denote individual agents, and the text inside the enclosures indicates the position of the agent within the network. Lines from one enclosure to another indicate a connection. Connections occur from leaders to agents and from agents to agents in the real world. However, only the former is shown.

current strategies are too focused on the elimination of network leaders (3). These strategies are flawed because clandestine cell systems used by terrorist organizations often utilize their leaders to establish ideological unity (1). The group ideology of a terrorist organization motivates its actions and establishes a common purpose across all of its members (1). Without this group ideology, the organization could not function as effectively, for the decentralized nature of the organization would make it difficult to unite various components of the network under one common purpose. It is the job of the leaders of these organizations to enforce this ideological unity across the organization. Therefore, most leaders in these types of terrorist organizations rarely serve an operational role¬—one in which they conduct logistical and managerial tasks—instead opting to solely focus on establishing ideological unity across the organization. Through this, while it becomes clear how the rationale develops that eliminating the leaders of these types of terrorist organizations may lead to a reduction in the ideological unity of the organization, this strategy would not significantly affect the operational aspects of that organization.

Similarly, some counterinsurgency theorists claim that current strategies place an overemphasis on eliminating agents with large numbers of connections, as it is perceived that these agents have greater importance (1). Jones stated that these efforts only act to "cull the herd of poor clandestine practitioners" (1). Though in other intelligence networks, highly connected agents might be of greater importance than less-connected agents, this is not the case in clandestine networks. Instead, these networks aim to isolate components of the organization, especially those with vital roles. It is because of this that important agents are often less connected, as to minimize the probability of their compromise—that is, to minimize the probability of their elimination from the network due to a counterinsurgency effort (1). Those with larger amounts of connections are often highly prone to being compromised, and thus given less important roles, for they are less experienced clandestine practitioners. It is through this analysis that Jones asserted that current strategies in counterterrorism have failed to truly eliminate vital components of clandestine organizations, instead eliminating relatively useless agents of the organization (1). Through these criticisms, clandestine theorists have proposed novel strategies in combating terrorism.

The Simultaneous Attack/Persistent Pursuit (SAPP) Theory is a superior alternative to current methods in counterterrorism (1, 2). The SAPP Theory asserts that the simultaneous attack on all fronts of a clandestine terrorist network, followed by the pursuit of connected agents, will lead to the greatest damage to a clandestine system (**Figure 3**).

To compare the Simultaneous Attack/Persistent Pursuit (SAPP) Theory with other methods of counterterrorism, we developed a stochastic computational model of a clandestine network. Our model represented a traditional eastern clandestine network of an isolated sub-cell of a terrorist organization. We hypothesized that the SAPP Theory would lead to a statistically significant decrease in the number of terrorist attacks an organization was able to commit over a standard period of time, when compared to other strategies of counterterrorism. Our results supported our hypothesis, leading to the conclusion that it is probable that the SAPP

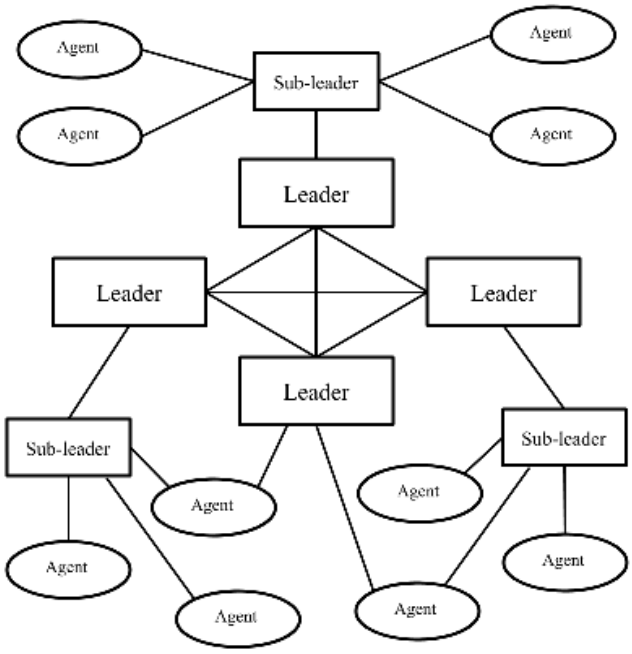

Figure 2. An abstract model of an eastern clandestine network. Boxes and circles denote individual agents, and the text inside the enclosures indicates the position of the agent within the network. Lines from one enclosure to another indicate a connection. Both leader-to-agent and agent-to-agent connections are shown.

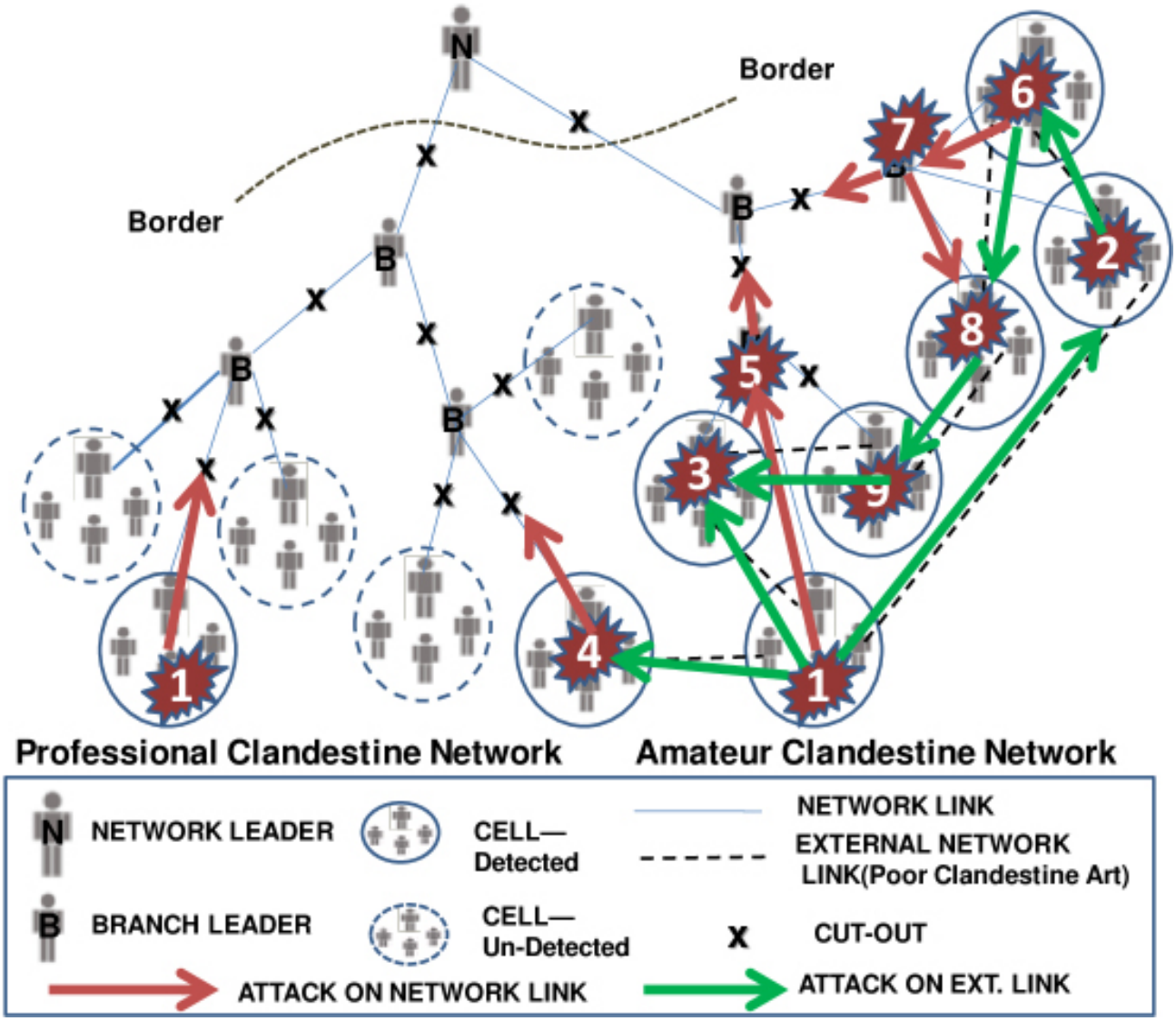

Figure 3. Visualization of pursuit through a clandestine network. Figure adapted from Jones (1). Agents are denoted with illustrations of people. Circles indicate that the agents within the enclosures are in individual units (referred to as cells). In appearance, undetected cells are solid, while detected cells are dotted. Lines between agents and cells denote connections. Solid connection lines indicate a strong link, while dotted lines indicate a weak link. Connections with dotted lines are easier to compromise. The label of the character "N" on an agent indicates that they are the leader of this portion of the clandestine network. The label of the character "B" on an agent indicates that they are a sub-leader of this portion of the clandestine network. The label of the character "X" on a connection indicates that it has been compromised. Solid red arrows indicate a counterinsurgent attack on a connection, while solid green arrows indicate a counterinsurgent attack on an agent or cell. SAPP Theory is demonstrated in this figure; the existence of multiple arrows indicates a simultaneous attack on all fronts of the exposed network, while the existence of multiple layers of arrows indicates a pursuit of agents through the network.

Theory is more effective in counterterrorism than current methods.

RESULTS

We developed a computational model to simulate a clandestine sub-cell network, and then applied various treatments onto the model to simulate different attack strategies. The simulated sub-cell network contained 4 simulated components: a propaganda cell, a recruitment logistics cell, a central logistics cell, and an operations cell. Using this model, it was possible to observe differences in the efficiency of the terrorist sub-cell network, operationally defined by the final number of terrorist attacks performed by the simulated terrorist network.

We ran the attack strategy associated with each of five treatments—Treatment O (attacks are only performed on the operations cell), Treatment P (attacks are only performed on the propaganda cell), Treatment C (attacks are only performed on the central logistics cell), Treatment R (attacks are only performed on the recruitment logistics cell), and Treatment S (attacks are performed using the SAPP strategy)—for 30 iterations and recording the final number of terrorist attacks

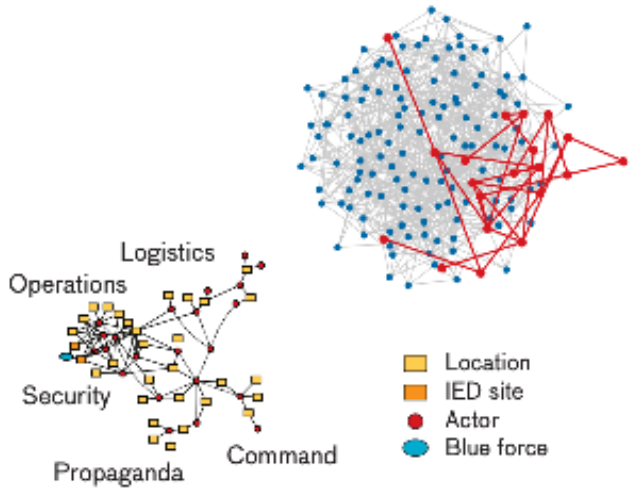

Figure 4. Inspiration for the structure of the simulated terrorist sub-cell. Figured adapted from Smith *et al.* (6). On the top right, the overall arrangement of the complete covert network is visualized. On the bottom left, a portion of that network is compartmentalized into five sections: Operations, Logistics, Security, Propaganda, and Command. Yellow boxes indicate physical locations within the network. Orange boxes indicate the existence of improvised explosive devices (IEDs). Red circles denote agents, or members of the terrorist organization. Blue circles represent sites where access of surface agents is available for counterinsurgency. The structure of this section of the covert network serves as an inspiration for the clandestine network in this research.

(A_{final}) at the end of 50 time steps for each iteration. These treatments were partially inspired by a model representing terrorist organizations as covert networks (**Figure 4**). We selected the amount of iterations to ensure the condition for sample-size was met to perform a two-sample t-test on any two of the treatments. Generally, the number of terrorist attacks (A_{final}) progressed linearly as the simulation proceeded for every iteration of every treatment. The specific rate of the linear progression differed between trials.

In this study, the probability of the elimination of an agent (member) from each cell differed. There was a 100% probability of removing an agent from the operations cell, a 90% chance of removing an agent from the propaganda cell, a 70% chance of removing an agent from the recruitment logistics cell, and a 20% chance of removing an agent from the central logistics cell. These probabilities were determined with the consideration of the inherent security some cells provide to their agents, which is related to how close agents within a cell have to interact with entities outside of the terrorist network. Members of the operations cell have to interact directly with entities outside the network, while agents from the propaganda cell have to interact less directly with those entities. Members from the recruitment logistics cell have to only collect and train incoming agents, which causes them to have an even less chance of being compromised. Members of the central logistics cell have mainly managerial roles, giving them little necessity to interact with the outside world. These probabilities were some of the most critical parameters in this experiment.

For the set of 30 values of A_{final} for each of the 5 treatments, we recorded the values of the sample size, mean, standard deviation, and standard error (**Table 1**). We performed t-tests on each individual treatment compared to Treatment S (**Table 2**).

Through the utilization of an α=0.01 significance level (as to minimize the probability of a Type I error), we established significance for each of the four two-sample t-tests. However, because multiple t-tests were made, erroneous results were more probable, and thus it was necessary to use multiple-testing adjustment of the significance level. To accomplish this, we used the Benjamini-Hochman Procedure. We used a standard false discovery rate of 5% throughout this procedure. We then recorded the critical values, ranking, adjusted p-value, and significance after the Benjamini-Hochman procedure for each of the four two-sample t-tests (**Table 2**). Through this, we determined significance for all two-sample t-tests, hinting that Treatment S was more effective in decreasing the value of A_{final} when compared to the other treatments.

DISCUSSION

The results from this experiment showed that the differences between the value of A_{final} for Treatment S and the values of A_{final} for the other treatments were statistically significant, supporting the hypothesis that the SAPP Theory was more effective in decreasing the number of terrorist attacks an organization was able to conduct when compared to other methods. We found that Treatment S was more effective in decreasing the number of terrorist attacks than any of the other treatments. Because Treatment S represented the SAPP model, we were able to support the hypothesis that the SAPP strategy would lead to a greater reduction in the number of terrorist attacks. It is important to understand that this data was only derived based on simulated attacks on a specific simulated configuration of a terrorist sub-cell. Because of this, further experimentation is necessary to decisively implement new strategies in counterterrorism.

The probabilities of the successful elimination of agents (members) from each cell in the model were critical parameters in the experiment. In order to simulate the security some cells inherently had from counterinsurgency attacks when

Treatment	N	Mean	SD	SE
Propaganda	30	70.4	4.95	0.9
Recruitment Logistics	30	70.6	4.11	0.75
Central Logistics	30	69.4	4.55	0.83
Operations	30	69.07	3.65	0.67
SAPP Theory	30	60.6	18.6	3.4

Table 1. Arrangement of all five treatments in this experiment with their associated sample size (N), mean of A_{final}, standard deviation (SD), and standard error (SE).

Rank	Treatment	Original P-value	Critical Value	Adjusted P-value	Significant at FDR = 0.05
1	Propaganda	0.004	0.0125	0.016	Yes
2	Recruitment Logistics	0.004	0.025	0.008	Yes
3	Central Logistics	0.008	0.0375	0.01067	Yes
4	Operations	0.01	0.05	0.01	Yes

Table 2. Arrangement of each treatment which was compared with Treatment S (SAPP Theory) with its rank, Original *p*-value, critical value, Benjamini-Hochberg Adjusted *p*-value, and significance. The Benjamini-Hochberg procedure was followed to ensure statistical significance when comparing the SAPP treatment group with all other treatment groups, and the critical value statistic is an intermediary value necessary to determine significance using the Benjamini-Hochberg procedure.

compared to others, we differed these probabilities across different cells (1). We determined the specific values used in this experiment with a combination of arbitrary intuition and academic evidence (1, 4).

A possible source of error in this research was the randomness which was introduced because of the nature of our stochastic model. It was possible that the recorded data occurred due to random chance. However, the randomness of this model would probably not have played such an important role, for 30 trials were taken to minimize the effects of this.

One of the largest possible sources of error was the model design itself. Though we designed the model with consideration of available scholarly information, it was possible that it did not truly reflect the realistic structure and conditions of an eastern clandestine terrorist network. This model was only one of many different types of models which could have been made to simulate a clandestine terrorist network. Because of this, further development of new models, as well as an increase in the amount of available information about real-world clandestine networks, is necessary. Only estimations of terrorist networks could be made computationally with the limited amount of information available. In order to minimize this source of error, it would be necessary to conduct further experiments on other models of clandestine terrorist networks, especially if future research and military disclosures reveal further insight into the nature of these networks.

These results indicate that it is important to continue studying clandestine terrorist networks computationally. Though these results on their own will not fully prove that the SAPP model is more effective than current strategies, the repetition of this experiment, as well as similar experiments, is necessary for the development of more complete results. This research can serve as a foundation for future research into the utilization of computational methods in studying clandestine networks.

Many questions about the nature of clandestine networks remain. Information on the true structure of many terrorist networks, as found in the real world, would be significantly important in the development of this field. The role of ideological uniformity in such an organization, the growth and development mechanics of full clandestine terrorist networks, as well as the comparative advantages of different types of strategies in counterterrorism are all important topics in this field of research which need to be studied in order to offer truly important and influential results. Without further research and experimentation of this model, as well as similar models, it is not possible to definitively assert that certain strategies for counterterrorism are superior to others. Nevertheless, this research provides very important results on the efficacy of the SAPP strategy when compared to current strategies in counterterrorism and presents a basis for discussions in the future on the use of computational tools in the efforts to optimize counterterrorist efforts.

METHODS

The code of the model used in this research was programmed in Python 3.6 and is available on GitHub (5).

Past research has shown five major components in a covert network, as shown in **Figure 4**—a network which attempts to conceal information about its structure and function from outside of the network: operations, logistics, security, propaganda, and command (6). Similarly, Li Bo, *et al.* gave an outline of five components of a sub-cell structure in a terrorist network: the action cell, the conduct cell, the resource cell, the recruit cell, and the training cell (4). Through these inspirations, the general model of the clandestine sub-cell in this research contained four components: the operations cell, the propaganda cell, the recruitment logistics cell, and the central logistics cell. The operations cell contained agents and resources which would be used to conduct simulated terrorist attacks. The propaganda cell dispersed propaganda to aid in the recruitment of new agents. The recruitment logistics cell aided in the collection and training of new recruits in the organization. The number of agents in the propaganda and recruitment logistics cell influenced the number of agents added into the organization after each time step of the simulation. The central logistics cell collected resources, directed attacks, provided ideological unification, and directed humans and weaponry throughout the network. Both the number of agents and resources in the operations cell and central logistics cell influenced the probability and frequency of successful terrorist attacks. In this simulation, each time step represented a single unit of time passing in the simulation. Equivalence to the length of this time step in the real world could not be determined without specific information about the form, function, and history of a particular terrorist organization.

$$G(\phi,\lambda) = \left\lceil \left\lfloor 1.2^{\phi} \right\rfloor \cdot \left(\frac{\left\lfloor \frac{51}{1+e^{-0.27(\lambda-15)}} \right\rfloor}{100} \right) \right\rceil$$

Figure 5. Mathematical equation of the *G*(ϕ,λ) equation.

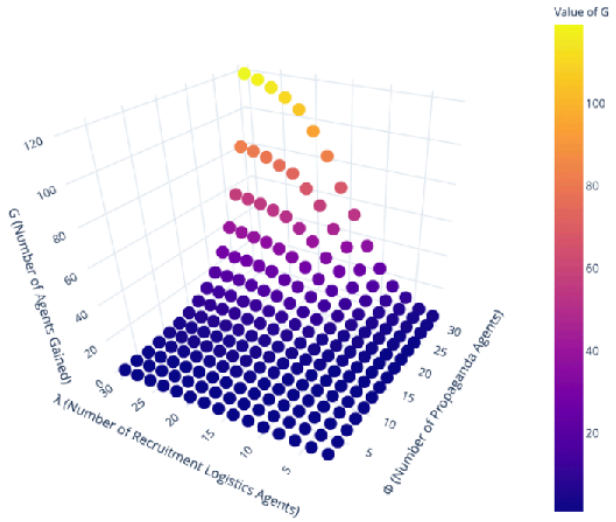

Figure 6. A three-dimensional scatter plot representing values of the G function for a total of 225 value-pairs of ϕ and λ. ϕ ranges from 2 to 30, increasing by steps of 2. λ ranges from 2 to 30, increasing by steps of 2. *G* ranges from 1 to 119.

We applied five treatments to this simulated network. Treatment O only attacked the agents in the operations cell. Treatment P only attacked the agents in the propaganda cell. Treatment R only attacked the agents in the recruitment logistics cell. Treatment C only attacked the agents in the central logistics cell. Treatment S attacked all cells of the network pseudo-randomly, with each cell being given an equal probability to be attacked, leading to a relative equivalence in the attack distribution across all cells of the network. In this case, the best representation of current strategies was with Treatments O and C, while the best representation of the SAPP strategy was with Treatment S (1, 2).

The number of terrorist attacks which occurred in a certain time step depended on the number of agents within the central logistics cell and the operations cell. For each terrorist attack to occur, four agents were required from the operations cell, while only two agents were required from the central logistics cell. This means that a total of six members from the central logistics and operations cell were required to conduct a terrorist attack. Depending on the number of agents within each of the two cells, the maximum possible number of terrorist attacks would be conducted. Each terrorist attack had a 70% chance of being successful. If a terrorist attack was successful, the number of terrorist attacks in the simulation was increased by 1 (A := A + 1). If not, the number of terrorist attacks remained constant.

We represented the number of agents entering a terrorist network through the $G(\phi,\lambda)$ function (**Figure 5**). ϕ represented the number of agents within the propaganda cell, while λ represented the number of agents within the recruitment logistics cell. With consideration of the nature of eastern clandestine terrorist networks, we determined that an increase in the number of agents in the propaganda cell would lead to an exponential increase in the number of individuals available for recruitment (4). It was also determined that the recruitment logistics cell would always perform only to a threshold in its recruitment efforts, as going beyond that threshold would risk an increased probability in the members of the cell being compromised (4). Thus, we determined that the percent of the available pool of recruits which would be recruited would be determined by the capacity of the recruitment logistics cell to operate, which was operationally defined as the number of agents within the Recruitment Logistics cell, or \lambda. Thus, we developed a logistic expression based on the value of \ lambda was to return a value between 0 and 50%, depending on the number of agents within the recruitment logistics cell. We multiplied this expression with the exponential expression of the propaganda cell and put the result through a ceiling operator. The logistic expression contained a flooring operator in order to ensure that the value of the expression remained between 0 and 50%. We floored the exponential expression arbitrarily. The flooring or ceiling of the exponential expression, as well as the overall expression, would not have mattered for the general results, as they would have only produced relatively small deviations. We added $G(\phi,\lambda)$ agents into the network, with each agent being assigned to a component pseudo-randomly, and with equal probability of entering each component. When computing the value of $G(\phi,\lambda)$ across a range of values of ϕ and λ, it was possible to see that the value of G was a product of a logistic and exponential expression (**Figure 6**).

For every time step, we removed a random number of agents—operationally equivalent to members of a terrorist organization— (from 0 to 3) from the components of the sub-cell network by the treatment applied. This variation was used to simulate the security some cells inherently have when compared to other cells (1).

The model started with eight members in the operations cell, six members in the propaganda cell, six members in the recruitment logistics cell, and four members in the central logistics cell. Optimal initial conditions for this simulation, in this context, referred to the conditions which best allow for the minimization of the time it takes to perform the simulation fully. We determined the initial values for each cell through testing the optimal initial conditions of the simulation on our system.

ACKNOWLEDGEMENTS

I would like to thank my science and math teachers, especially Mrs. Shelley Casey and Mr. Brian Ewbank, for consistently supporting my work.

Published: December 1, 2020

REFERENCES

1. Jones, Derek. *Understanding the Form, Function, and Logic of Clandestine Cellular Networks: The First Step in Effective Counternetwork Operations*. Defense Technical

Information Center, 2009, *Defense Technical Information Center*, apps.dtic.mil/sti/pdfs/ADA505161.pdf.
2. Jones, Derek. *A Military Theory for Destroying Clandestine Insurgent and Terrorist Organizations.* United States Army War College, 2017, https://publications.armywarcollege.edu/pubs/3434.pdf.
3. Jordan, Jenna. "Attacking the Leader, Missing the Mark: Why Terrorist Groups Survive Decapitation Strikes." *The MIT Press Journals*, 28 May 2014, www.mitpressjournals.org/doi/pdf/10.1162/ISEC_a_00157.
4. Li, Bo, *et al*. "Agent Based Modeling on Organizational Dynamics of Terrorist Network." *Hindawi,* 11 Nov. 2015, www.hindawi.com/journals/ddns/2015/237809/.
5. hello.py. isef2020, commit b6eb7bcac0a66b70e80964f320a6cfb33a80c751, Paarth Tara, 2020. GitHub, https://github.com/VioletIzHere/isef2020/blob/master/hello.py.
6. Smith, Steven T., *et al*. "Covert Network Detection." *MIT Lincoln Laboratory,* Jan. 2013, www.ll.mit.edu/sites/default/files/page/doc/2018-05/20_1_4_Smith.pdf.

JOURNAL OF
EMERGING INVESTIGATORS

Article

Leveraging E-Waste to enhance water condensation by effective use of solid-state thermoelectric cooling

Soham Joshi, Santosh Joshi
Columbus Academy, Columbus, Ohio

SUMMARY

Water scarcity affects upwards of a billion people worldwide today. Multiple cities, such as Cape Town, Mexico City, Melbourne, and Jakarta have been threatened by water crises in the past. However, these cities are perfect for harnessing the power of water condensation. Fog nets and condensation towers have been used as water condensation devices, but these mechanisms are expensive, require preexisting infrastructure, and need certain geographic features to function. This project leverages the potential of capturing humidity to build a high-efficiency water condensation device that can generate water and be used for personal and commercial purposes. In addition, the device is portable, environment-friendly, inexpensive, scalable, and can be incorporated into existing water storage infrastructure. The device uses the principle of solid-state thermoelectric cooling and the Peltier effect to function. The Peltier effect is based on the phenomenon that when changing electric currents are applied between the junctions in a thermocouple, it causes a change in temperature. Change in temperature causes one of the junctions in the thermocouple to heat and another junction to cool. Thermoelectric modules can be packaged as part of a device that at room temperature causes cooling, thereby causing effective water condensation. This compact environment-friendly device would have low power requirements, which would potentially allow it to utilize renewable energy sources and collect water at the most needed location.

INTRODUCTION

Because 785 million people lack even a basic drinking-water service, a mechanism is needed to increase access to water throughout the day and night in an affordable and environmentally friendly way (1). One way this can be achieved is through condensation of water from humid air.

Traditionally, fog nets and condensation towers have been used as water condensation devices. Although these mechanisms require low investment in technology, installation, and operation, they can be expensive when compared to their output, making them less optimal in the long term. Additionally, fog water collection methods such as fog nets and condensation towers require specific environmental and topographical conditions for optimal results, making their placement and reliability challenging (2). Fog nets and condensation towers are most productive in mountainous regions and areas close to the ocean. Fog nets are effective in areas with long-lasting fog on a frequent basis throughout the year and locations at least 1,000 meters above sea level. Most fog nets have been measured to perform at an average efficiency of 20% meaning large scale devices are necessary generate enough water for a family (1).

Additionally, these structures are massive and must be built outside city limits, limiting their use to suburban and rural areas. This can be a big constraint for large cities with water accessibility issues, like Jakarta and Melbourne, that are looking for new ways to acquire water to serve large populations. The infrastructure needed to collect the condensed water and transport it to residential localities could become cost prohibitive. Because of these shortcomings, fog nets and condensation towers have had limited use in small local communities. Further, they are not meant for commercial use or for portable, personal use.

There are four refrigeration techniques to produce condensation: mechanical compression refrigeration, absorption refrigeration, evaporative cooling refrigeration, and thermoelectric refrigeration. Other than thermoelectric refrigeration, all other ways involve the use of a refrigerant or water (9). Oftentimes, the refrigerants are non-environmental, flammable chemicals (9). Also, traditional refrigeration mechanisms are noisy, prone to vibrations, and need specific positioning or risk failure if tilted (9). Systems that use water as a coolant are at a disadvantage in areas facing drought. Peltier systems are designed to be quiet, free of vibrations and without moving parts (10). They are small and lightweight devices that are less complex, easier to replace, and require comparatively less maintenance. Additionally, thermal cooling from Peltier systems outperform all the others as an effective way to cause reduction of temperature (10). Thermoelectric refrigeration, though effective, is premature for large-scale commercialization, but this concept and technology is apt in the scenario being considered here.

Therefore, we hypothesized that solid-state thermal cooling Peltier modules would lower the ambient temperature to the dew point temperature in a glass tank with sizable surface area to enhance condensation.

This project will use thermodynamic cycles for refrigeration. Cooling is caused by a change in the entropy

of thermoelectric materials. The Peltier effect is a change in temperature caused by applying differing electric currents at the junctions in a thermocouple. "When the current flows through the junctions of the two conductors [of the Peltier tile], heat is removed at one junction and cooling occurs" (3). Peltier cooling modules and CPU cooling fans from computers that are disposed as e-waste can be leveraged as effective cooling materials. Therefore, this study will use thermoelectric Peltier elements as thermal diodes to bring the normal temperature (T) down to the dew point temperature (TD) in the condensation device and start a consistent cycle of prolonged periods of water condensation based on the ambient humidity. Peltier, or thermoelectric cooling (TEC) elements, are widely used in portable cooling appliances. This disposed e-waste could become a potential cost-saving source of material for the water condensation device.

This project aims to develop a way to affordably and efficiently condense water to provide water for local communities by capturing humidity in the air and converting it into water, benefiting all. This mechanism can be highly customized depending on the purpose of use. More than half of the cost of the device can be eliminated, since the essential materials needed to build the mechanism comes from electronic waste or e-waste.

RESULTS

A sample dataset of meteorological data from Reliable Prognosis, a weather news source, for Cape Town, South Africa from 2015 to 2020 was extracted for analysis (7). Statistical analysis was conducted to demonstrate that climatic conditions, temperature, and relative humidity, supported the utility of a condensation device. The results show potential to leverage the free humidity in the environment as an alternative source of water.

A set of 38,502 records (hours) was used as a sample. The data set included the following information for all hours of all days since 2015: temperature, relative humidity, and dew point temperature.

Three sets of information were derived based on the above data. The first set comprised the number of times when the normal temperature was equal to or less than the dew point temperature causing ideal natural conditions for water condensation. The second set comprised the number of times the difference between the normal temperature and the dew point temperature was 10°F or less. The third set comprised the number of times the relative humidity was 60% or more. The rationale for choosing the above two thresholds (10-degree difference between normal temperature and the dew point temperature and percent of relative humidity) was to allow for process inefficiencies. Relative humidity of more than 60% would provide ample opportunity for condensation to start faster. An average of the relative humidity of the 38,502 records was taken and calculated as 72%. An average of the ambient temperature of the 38,502 records was taken and calculated as 63°F. An average of the ambient dew point temperature of the 38,502 records was taken and calculated as 54°F. Rounding the difference of two averages, which was 9°F, the 10°F was used for the experiment. The basis was that, in most cases, a cooling to an extent of 10°F was required to reach the dew point temperature.

The analysis revealed that out of 38,502 hours, the normal temperature was equal to or less than the dew point temperature only 954 times. In all these cases, the humidity was 60 percent or more. Hence, out of 38,502 hours, there were 954 hours when the city benefitted from natural conditions that caused water condensation. As expected, these hours were mostly between midnight and 8:00 AM. These conditions existed for only 217 days out of 1600 days, and 75 percent of the hours existed in the months of May to September (**Figures 1 and 2**). There were 29,022 hours during the analysis period when the humidity was 60 percent or more. Of these 29,022 hours, there were 21,481 hours when the difference between the normal temperature and the dew point temperature was 10-degree Fahrenheit or less. These include the 954 hours when the normal temperature was equal to or less than the dew point temperature. Excluding natural conditions, there were 20,527 hours which could have been used to condense water if a device existed that could have created conditions to cause water condensation. In short, there were 20,527 opportunities lost to use a natural resource like humidity and extract water. The hours when these opportunities existed were spread across several days in all the months and during various parts of the day, making it a reliable and consistent source (**Figures 3 and 4**).

Next, we created an environment that resembled a real-life scenario and performed testing at home under controlled conditions to benchmark and compare testing results for four scenarios.

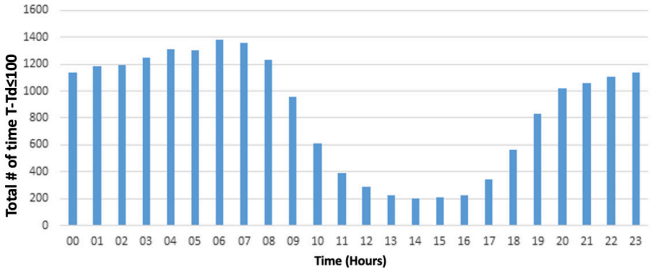

Figure 1. Total number of times T ≤ TD during every hour of the day from 2015 to 2019.

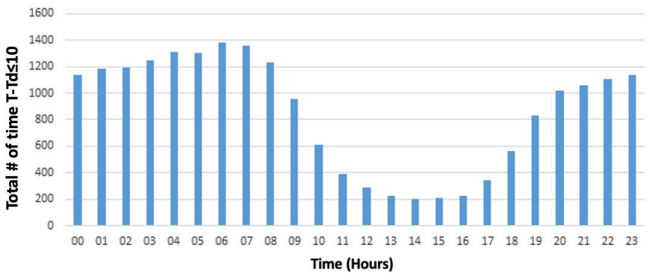

Figure 2. Total number of times T ≤ TD during a given month since 2015.

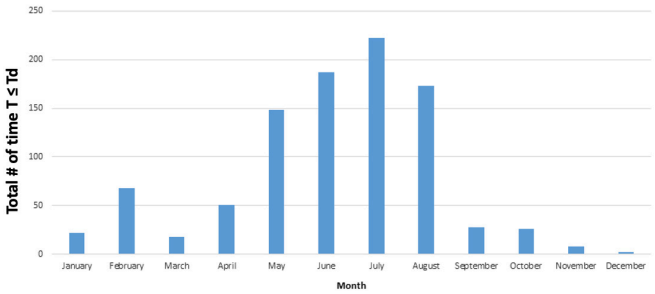

Figure 3. Total number of times T-TD ≤ 10 during a given hour of the day since 2015.

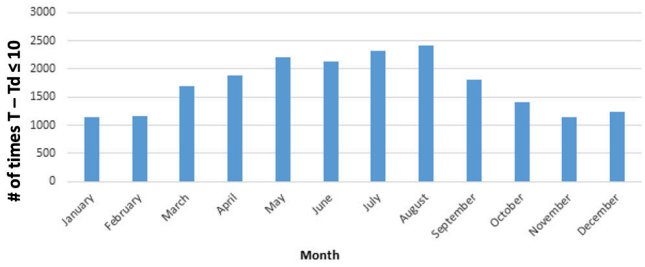

Figure 4. Total number of times T-TD ≤ 10 during a given month since 2015.

The below scenarios served as the benchmark for the later tests. Condensation was measured every 15 minutes over a 1-hour period. In the first test scenario, all independent variables were kept constant. We monitored water condensation under natural conditions with no thermo-cooling to simulate a natural as-is scenario. No condensation was observed since the ambient temperature was higher than the dew point temperature. In the second scenario, all independent variables except the total surface area were kept constant; no thermo-cooling was applied. No condensation was observed since the ambient temperature was higher than the dew point temperature. The increased surface did not have any impact on the condensation of water. In the third scenario, all independent variables except relative humidity were kept constant; no thermo-cooling was applied. Negligible condensation was observed since the ambient temperature was higher than the dew point temperature. The increased humidity did not have any impact on the condensation of water. In the fourth scenario, all independent variables except relative humidity and total surface area were kept constant; no thermo-cooling was applied. Negligible condensation was observed since the ambient temperature was higher than the dew point temperature. The increased surface area and humidity did not have any impact on the condensation of water. All four scenarios were repeated with thermo-cooling i.e. with constant reduction on temperature by the Peltier cooling module. The goal of this series of tests was to simulate the conditions of a working device.

When the Peltier cooling module was turned on, there was a consistent drop in the temperature inside the glass tank. The initial temperature at the start of the test was 82°F. The thermo-cooling was effective in dropping the temperature to the dew point temperature, which was 75°F. It took about 20 minutes to reach the dew point temperature. After 20 minutes, early signs of water condensation were visible. At the end of the one hour, about six ounces of water were collected with the base surface area exposed for condensation. As the surface area exposed for condensation was increased by about 35%, the quantity of water collected was eight ounces. A similar correlation was also observed when the relative humidity percent was increased (i.e. increase in the relative humidity caused an increase in the quantity of water collected). The testing results summary also confirmed that the Peltier module caused enough cooling and helped reach the dew point temperature. Condensation was observed when the dew point temperature was reached (**Figures 5 and 6**).

DISCUSSION

Based on the observed water collection, a standard device would conservatively be able to collect 78 ounces in a day if the device were run for 9 hours. The Constitutional Court of South Africa has quantified that 42 liters or 11 gallons of water is needed to meet the basic needs of 1 person. However, the device is meant to collect water for drinking purposes, which

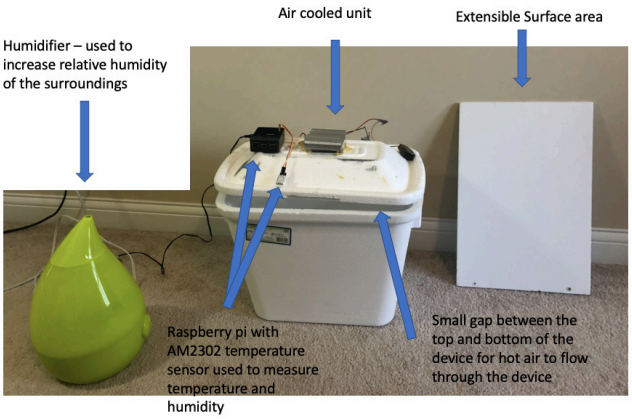

Figure 5. Photograph of testing setup.

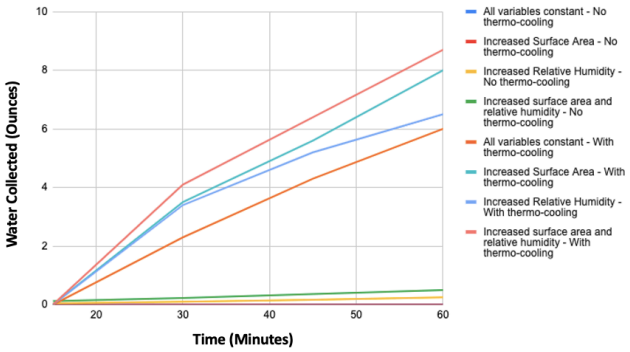

Figure 6. Condensation over time in different testing conditions.

is only about half a gallon. Based on this need, one device would be needed to collect the required drinking water for one person. As the surface area of the device increases, it will become more economical and can serve multiple people.

We hypothesized that if solid-state thermal cooling Peltier modules are used to lower the ambient temperature to the dew point temperature in a glass tank with sizable surface area, enhanced condensation would be observed. Through testing, the hypothesis was supported as water was generated using solid-state refrigeration.

Through the analysis of the data, a potential source of reduction in efficiency of the device was found. The most effective times to cool water, in the area where testing occurred, is from April to September (**Figure 3**). However, in regions such as Cape Town, these are the wet winter months and often have less sun exposure. Additionally, the hours where the dew point temperature and temperature were the same or within 10°F was primarily from 12:00 A.M. to 9:00 A.M. The average sun curve during midwinter in Cape Town shows that the sun rises at around 8:00 A.M. and sets at 4:19 P.M. (8). This means about eight hours of sunlight is available. The device will not have immediate power as the unit will run most of the night, so a battery is required to supply energy. During testing, the power requirements of the device were measured. It was deciphered that with a singular 9-volt battery the Peltier tile could run for 11.3 hours, and the CPU fan with a 9-volt battery could run for 21.25 hours. This means that the device would only require two rechargeable 9-volt batteries that are charged by solar panels. Assuming that a single cell in a solar panel generates 0.5 volts, a 40-cell solar panel that generates approximately 20 volts per day would be sufficient for the power needs of the device.

Additionally, a comparative analysis of available E-Waste and number of devices needed for Cape Town was performed. For the example of Cape Town, the city has a population of 433,688 people. One person would require one unit of the current prototype, which equals 433,688 units. This would mean approximately 433,688 solar panels and double the number of 9-volt batteries are required. The device does hinge on the fact that E-Waste Peltier tiles are accessible. Though there are not specific numbers for how many computers with Peltier tiles are disposed of each year, 7 million tons of heating and freezing equipment were recycled and daily 142,000 computers were recycled, which means that at least some portion of the Peltier tiles could be sourced through E-Waste (2). Additionally, the product utilizes solar energy, but depending on different regions the power of the device is customizable. In large cities where electricity is cheaper, the device could be plugged in, or in cities where wind energy or hydropower are more readily accessible, those could be used to power the device.

Although the device can generate 78 ounces of water per day, there are some limitations to the device. Firstly, weather conditions will affect the function of the device. For example, after heavy rains, this device would be able to generate significantly more water. However, in regions plagued by drought, the device would not be able to generate as much water. Without testing in those specific regions, it is hard to estimate the amount of water that can be generated, but combining this testing and the historical Cape Town weather data used, it can be estimated that during off-months, September through January, the efficiency of the device will drop 50%. Although the device will be affected by off-months, during the night from approximately 8 P.M. to 8 A.M., the device will still run at peak efficiency as the relative humidity is high enough for condensation occur. If the weather conditions are not ideal and the device runs at 82% efficiency, it would still produce 64 ounces of water, meeting the recommended amount of daily drinking water.

An advancement in future iterations of the prototype would be the use of metal organic frameworks (MOFs) which are organic-inorganic hybrid compounds that are crystalline and highly porous in nature. MOFs have pores with diameters less than 2 nanometers, and hence are referred to as microporous materials. The porous nature of the MOFs helps them build extremely high surface areas. So much so that 1 gram of a MOF could have surface area of 15 million square inches or upwards, which is more than the area of 2 football fields (6). MOFs possess water adsorption (not absorption) properties that provide hydrolytic stability and make them less reactive with water. MOFs have been tested to capture as much as 200% water of their own weight (6). An improved metal organic framework, hydrophobic MOFs, can not only capture and store water due to their large surface area but are effective in releasing water when heated. This is a viable option for the product, as during the night, condensing water is most effective. This means the MOF's could collect the water the unit generates through the night and release it in the morning when the temperature rises.

MATERIALS AND METHODS

A glass tank was used to collect water. One Peltier Thermoelectric Cooling Module with the following specifications was used for thermo-cooling: 15 volt, 6-ampere and Melcor type: CP1.4-127-06L unit with two 70mm, 2,900 RPM CPU cooling fans, which move about 18.58 cubic feet of air per minute. An aluminum heat sink was used for better heat dissipation. A Raspberry Pi 3 was used to run the python script that provided real-time data on the temperature and humidity. A temperature and humidity sensor (AM2302/DHT22) that uses a capacitive humidity sensor and a thermistor to measure the surrounding air was used to measure the temperature and humidity. The sensor can be used for 0–100% humidity readings with 2–5% accuracy and can be used for -40 to 80°C temperature readings positive or negative 0.5°C accuracy.

Actual testing of the device was performed to support the hypothesis. All the test cases were performed with an initial starting temperature of 82°F. This will be referred to as the base temperature. The base humidity was maintained

at 70%. An increased humidity of 80% was used for those test cases that measured the impact on condensation when ambient humidity changes. A glass tank (22 in x 12 in x 13.5 in) with base surface area of 1182 square inches was used. Ten rectangular prisms (1 in x 1 in x 10 in) and an additional total surface area of 400 square inches were used to test scenarios of increased surface area. Quantity of Water Collected was measured for all the test scenarios. Dew point temperature in degrees Celsius was calculated using $T - ((100 - RH)/5)$, where T is observed temperature, and RH is relative humidity in percent.

Relative humidity, temperature, dew point and total surface area were the independent variables in the experiment. Rate of water condensation was the dependent variable. Time for ingestion of steam was the control variable.

An important concept in consideration for the solution is the dew point temperature, which "is the temperature the air needs to be cooled to (at constant pressure) in order to achieve a relative humidity (RH) of 100%" (4). The dew point is the temperature to which air must be cooled to become saturated with water vapor (5). The third important concept is the exposed surface area. Surface area is a one of the most important factors since humidity needs a surface to condense. Lack of a large area can become a huge constraint for compact portable water condensation devices. The laws of thermodynamics can help solve the problem of reducing the normal temperature to the dew point temperature to create optimal conditions for condensation, but the lack of sufficient exposed surface area would underutilize the created conditions and render the device ineffective.

The testing of the device was completed in four different scenarios to test the maximum efficiency and ideal working conditions of the device. Each measurement was completed five times, and the given data is the average of the five tests. Additionally, the varied conditions exposed the device to different climatic conditions to evaluate its use in different climates.

To complete the first scenario where all independent variables were kept constant and no thermo-cooling was applied, the temperature was set to the constant 82°F and the humidity was maintained at 70%. In the second scenario, all independent variables except the total surface area was kept constant and no thermo-cooling was applied. In this test, the temperature was set to 82°F and the humidity was set to 70%. In addition, rectangular prisms where attached to the top of the lid. In the third scenario, all independent variables except relative humidity were kept constant and no thermo-cooling was applied. In this case, the temperature was constant at 82°F and the humidity was increased from 70% to 80%. In the fourth scenario, all independent variables except relative humidity and total surface area were kept constant and no thermo-cooling was applied. Finally, the temperature was constant at 82°F, but the humidity was increased to 80% in conjunction with the rectangular prisms, which were attached to the top of the lid. These 4 scenarios were repeated, but the thermo-cooling was applied. During the tests where the thermo-cooling was applied, air channels were created for the cold air to flow through the rectangular prism, so that they total surface area would be increased.

Received: January 2, 2020
Accepted: November 21, 2020
Published: December 2, 2020

REFERENCES

1. Fessehaye, M., Abdul-Wahab, S.A., Savage, M.J., Kohler, T., Gherezghiher, T., Hurni, H. "Fog-water collection for community use." *Renewable and Sustainable Energy Reviews*, vol 29, 2014, pp. 52–62.
2. Button, Kimberly ButtonKimberly, and Healthy Home. "20 Staggering E-Waste Facts." *Earth911.com*, 24 May 2018, earth911.com/eco-tech/20-e-waste-facts/
3. Buel, Zander. "The Four Types of Refrigeration Systems You Need to Know." *Refrigeration School, Inc. (RSI)*, 27 Dec. 2018, www.rsi.edu/blog/hvacr/four-types-refrigeration-systems-need-know/.
4. "How Do Thermoelectric Coolers (TEC) Work: II-VI Incorporated." *II*, www.ii-vi.com/how_do_thermoelectric_coolers_tec_work/.
5. "How Do Thermoelectric Coolers (TEC) Work: II-VI Incorporated." *IIVI Incorporated*, www.marlow.com/how-do-thermoelectric-coolers-tecs-work.
6. https://rp5.ru/Weather_in_the_world. Weather for 243 Countries of the World, 18 Jan. 2020, rp5.ru/Weather_in_the_world.
7. "Sunrise and Sunset Times for Cape Town, South Africa by Suncurves." *Suncurves*, suncurves.com/en/v/1310/.
8. Notman, Nina. "MOFs Find a Use." *Chemistry World*, 28 Mar. 2017, www.chemistryworld.com/feature/mofs-find-a-use/2500508.article#commentsJump.
9. US Department of Commerce, and NOAA. "Dew Point vs Humidity." National Weather Service, NOAA's National Weather Service, 18 June 2019, www.weather.gov/arx/why_dewpoint_vs_humidity.
10. Lallanilla, Marc. "What Is Dew Point?" *LiveScience*, Purch, 11 Feb. 2014, www.livescience.com/43269-what-is-dew-point.html.

JOURNAL OF
EMERGING INVESTIGATORS

Article

Fingerprint patterns through genetics

Gabriel O'Brien, Kristen Murphy
Hopkinton High School, Hopkinton, Massachusetts

SUMMARY

Fingerprints are unique identifiers, but it is unclear how much similarity/variation closely-related family members exhibit. This study explores the link between fingerprints and genetics by analyzing familial fingerprints to show how the fingerprints between family members, and in particular siblings, could be very similar. The left and right thumb and ring fingerprints were taken from seven related individuals (immediate family and grandparents) and were classified to see which fingerprint feature was dominant and how it was inherited through the different generations of the individuals tested. Ridge features between the three siblings out of the seven individuals were measured and analyzed. The hypothesis was that the fingerprints between siblings would be very similar and the dominant fingerprint features within the family would be the same throughout the generations. The experimental data suggested that these same common patterns were passed down, helping to support this link. Also, the fingerprints between the siblings showed a trend of similarity, with only very small differences which makes these fingerprints unique. This work helps to support this fascinating link between fingerprints and genetics while providing a modern technological application.

INTRODUCTION

This study investigates if basic fingerprint patterns are inherited through genetics. Fingerprint patterns have multiple levels of classifications; in this work, we focus on level one and level two features, which identify basic fingerprint patterns without going into their individual complexity. Level one features include three main types of fingerprints: a loop, a whorl, and an arch. Of course, there are many variations of these patterns such as a double loop or a tented arch, which could be considered level two features (1). A loop is a pattern where the ridges enter from either side, re-curve, and pass out or tend to pass out the same side they entered (1). A whorl is where the ridges are usually circular, and the circles get smaller and smaller until they form a dot (1). The third type of pattern, the arch, is a pattern where the ridges enter from one side, make a rise in the center and exit generally on the opposite side (1). Since the DNA that a person inherits from their parents determines many characteristics and traits, such as whether someone is right- or left-handed or which color their eyes are, all biological siblings inherit a mixture of their parents' DNA and possess similar traits (2). The goal of this work was to examine if fingerprint patterns are also a genetically inherited trait, as well as how similar familial fingerprint patterns are. Fingerprints develop during gestation in the womb, and the environment of the womb can greatly influence specific ridge distances, making fingerprints unique (3).

MIT Technology Review gave a simple experiment that had aspects that were similar to this project in the way that they were able to take the fingerprints, using ink and tape. Some current research in this area is focused on new methods of being able to take fingerprints by forensic scientists to establish a link between biological evidence and a suspect in a criminal investigation. That method uses DNA samples to create different fingerprint fragments whose size and shape are compared between different individuals (4). Heng et al. conducted an experiment that studied the distribution of fingerprint patterns among Malaysian populations (5). The hypothesis of the experiment stated that it is impossible for two individuals to have identical prints, but highly similar fingerprints between closely related individuals are likely to exist (5). One of the groups that this study focused on was the distribution of fingerprint patterns between siblings within these populations. About 96 siblings were recruited from families around Kuala Lumpur and 96 public citizens were selected from around the same area, and the study revealed that siblings demonstrated greater similarity of all fingerprint patterns than non-siblings (5).

The purpose of the Heng et al. study was to examine the genetic link between fingerprint patterns utilizing examples from a family of individuals to understand how these prints are inherited and which fingerprint pattern is dominant. This work also compares the ridge features between siblings who developed in the same womb to investigate their similarity. Specific measurements of the ridge features of the center and outermost ridges from the siblings' fingerprints were taken, and those values were averaged to see if they fit within a boundary of being considered similar. Then, a statistical analysis was performed to show that the fingerprints of two people who developed in the same womb will be very similar. The testable question developed from the desire to find the link between fingerprints and apply the link to a modern purpose: can fingerprint patterns be inherited through genetics and how does that relate to how the fingerprint technology on

smartphones works? Here, we explore if fingerprint patterns could be inherited and, in doing so, compare, contrast, and classify the fingerprints within the family tested to see which pattern is dominant. Further, my fingerprints and my brothers' fingerprints were closely examined to see how the ridge features are different. Statistical analysis on the thumb and ring finger prints of seven family members was performed to evaluate whether the ridge features were significantly different. Only a few ridges were suggested to be significantly different, supporting that these small, subtle differences within the fingerprints of siblings are what allow the fingerprint technology on smartphones to work.

This question helped to influence the hypothesis that fingerprint patterns can be inherited through genetics; since a person inherits half of their DNA from each parent, those patterns should prevail among relatives' fingerprints (6). After comparing the ridge feature measurements for the left and right thumbs and ring fingers between siblings, I found the ridge features varied between my brothers and I, and in terms of magnified millimeters (mm) under a hover camera and a microscope, there were not significant differences between the ridge features on the same fingers since we developed in the same womb. This topic is meaningful to study because fingerprint identification is used in forensics to help find criminals and it is used to protect your phone. I wanted to learn about how these specific patterns are similar and different among family members which allows this technology to work. Scientists are still exploring how much of an individual's fingerprint is inherited through genetics. This study provides a new analysis technique (using the press-and-roll method) to find the small subtle differences in the fingerprints between family members and even between siblings who developed in the same womb by virtue of having a shared mother.

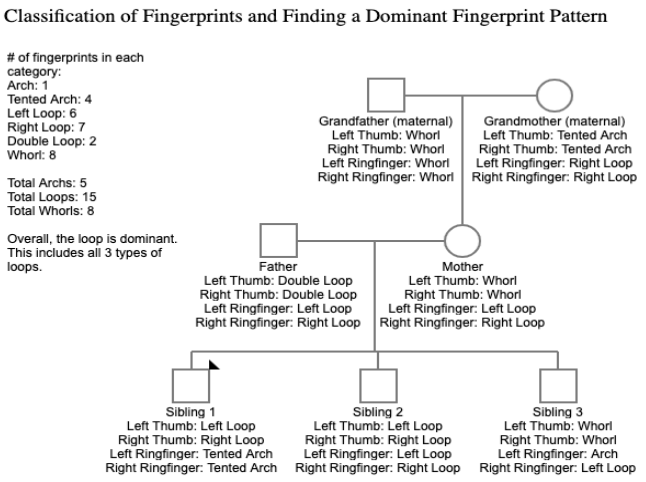

Figure 1: Classification of fingerprints and finding a dominant fingerprint pattern as a pedigree. Fingerprints were obtained from seven related individuals across three generations. Fingerprints were then classified using a microscope and a classifications guide. Using progenygenetics.com, classifications along with the individuals were put into the website to create a pedigree to better visualize how the individuals are related to each other as well as how the different fingerprint characteristics could have possibly been inherited.

RESULTS

Two experiments were performed where the fingerprints (obtained using the press and roll method) (4) of seven related individuals were documented and classified using the guidelines displayed in the introduction (4), to find the dominant fingerprint pattern and figure out if a trend suggests that it wasinherited through family lines. (**Figure 1**). The second experiment focused on the fingerprints of the three siblings, where the center and outermost ridges were measured for the left and right thumb and ring finger prints taken for each sibling, and then the measurements were averaged and analyzed for differences with student t-tests (**Table 1, Figures 1, 2**). **Figure 2** displays the actual ridge feature measurements as well as the average measurement for each finger tested for all three of the siblings. Nearly all of the error bars displayed in **Figure 2** overlap, showing that the fingerprint patterns between siblings are suggested to be statistically similar. Table 1 shows the student t-tests that were performed to show that the ridge feature measurements between siblings were statistically similar. Notably, the dominant fingerprint pattern in my family was a loop, and the student t-tests assessing the statistical similarities between ridge feature measurements between siblings showed that the fingerprints between my brothers and I were not statistically different. Most of the student t-tests produced a p-value that did not display a significant difference. These results support our hypothesis, suggesting that the loop is the pattern that is most likely to be inherited throughout my family lines. More specifically, the results suggest that the dominant fingerprint pattern in my family is the right loop. It is a trait commonly shared on the maternal and paternal sides of my family, as seen in **Figure 1**.

One surprising result from the student t-tests was that

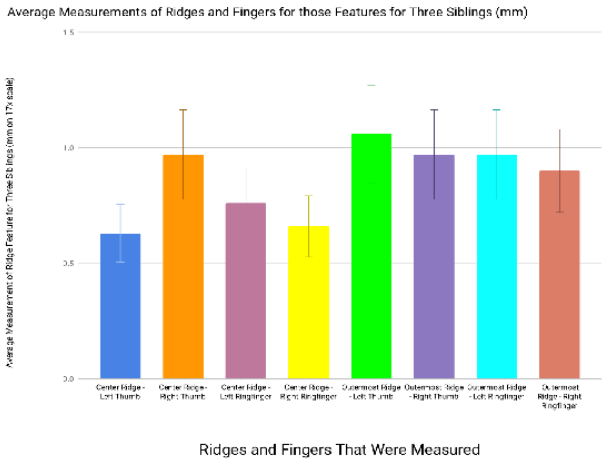

Figure 2: Graph comparing group averages for measurements per finger. Ridge features were measured in millimeters for three siblings. Average measurements for the ridge features are presented; error bars depict the standard deviation of the recorded measurements. Student t-tests were performed on the data, but very few significant differences were noted.

	Center Ridge Left Thumb vs. Central Ridge Right Thumb	Center Ridge Left Thumb vs. Central Ridge Left Ringfin-ger	Center Ridge Left Thumb vs. Central Ridge Right Ringfin-ger	**Center Ridge Left Thumb vs. Outer Ridge Left Thumb**	Center Ridge Left Thumb vs. Outer Ridge Right Thumb	Center Ridge Left Thumb vs. Outer Ridge Left Ringfin-ger	Center Ridge Left Thumb vs. Outer Ridge Right Ringfin-ger	Center Ridge Right Thumb vs. Center Ridge Left Ringfin-ger	**Center Ridge Right Tumb vs. Central Ridge Right Ringfin-ger**	Center Ridge Right Tumb vs. Outer Ridge Left Thumb
p-value	**0.04**	0.45	0.68	**0.01**	0.07	0.11	0.12	0.30	**0.03**	0.35
Statistically Significant	**Yes**	No	No	**Yes**	No	No	No	No	**Yes**	No
	Center Ridge Right Thumb vs. Central Ridge Right Thumb	Center Ridge Right Thumb vs. Central Ridge Left Ringfin-ger	Center Ridge Right Thumb vs. Central Ridge Right Ringfin-ger	Center Ridge Right Thumb vs. Outer Ridge Left Thumb	Center Ridge Right Thumb vs. Outer Ridge Right Thumb	Center Ridge Right Thumb vs. Outer Ridge Left Ringfin-ger	Center Ridge Right Thumb vs. Outer Ridge Right Ringfin-ger	Center Ridge Left Thumb vs. Center Ridge Left Ringfin-ger	**Center Ridge Left Tumb vs. Central Ridge Right Ringfin-ger**	Center Ridge Left Tumb vs. Outer Ridge Left Thumb
p-value	1.00	1.00	0.67	0.54	0.11	0.35	0.39	0.51	**0.01**	0.07
Statistically Significant	No	No	No	No	No	No	No	No	**Yes**	No
	Center Ridge Right Ringfin-ger vs. Outer-Ridge Left Ringfin-ger	Center Ridge Right Ringfin-ger vs. Outer-Ridge Ridge Ringfin-ger	Outer Ridge Left Thumb vs. Outer Ridge Right Thumb	Outer Ridge Left Thumb vs. Outer Ridge Left Ringfin-ger	Outer Ridge Left Thumb vs. Outer Ridge Right Ringfin-ger	Outer Ridge Right Thumb vs. Outer Ridge Left Ringfin-ger	Outer Ridge Right Thumb vs. Outer Ridge Right Ringfin-ger	Center Ridge Left Ringfin-ger vs. Outer Ridge Right Ringfin-ger		
p-value	0.11	0.12	0.47	0.54	0.24	1.00	0.71	0.74		
Statistically Significant	No	No	No	No	No	No	No	No		

Table 1: Statistical analysis of ridge feature measurements between siblings. Ridge features were measured for three siblings. Student t-tests were performed on the data and the p-values and significance (p-value < 0.05) are reported here. The four statistically significant relationships are emphasized in bold.

there were only four statistically significant comparisons: Center Ridge Left Thumb vs. Central Ridge Right Thumb, Center Ridge Left Thumb vs. Outer Ridge Left Thumb, Center Ridge Right Thumb vs. Central Ridge Right Ring Finger, and Center Ridge Right Ring Finger vs. Outer Ridge Left Thumb. These are very small differences which is why only four student t-tests showed a significant difference in ridge feature measurements.

DISCUSSION

Overall, the data collected did support the hypothesis that fingerprint patterns can be inherited through genetics. It also supported that the dominant fingerprint patterns in the data would be a loop and an arch. Those patterns are the dominant patterns from my left and right thumb and ring finger, and since a person inherits half of their DNA from each parent, those patterns would prevail among my relatives' fingerprints. Also, the ridge features did show some variation between my siblings and me, and in terms of magnified millimeters under a hover camera and a microscope, there were only small, subtle differences between ridges since which are suggested to be due to the fact that we developed in the same womb.

The dominant pattern within my family lines could have been passed down directly to my mother by her parents, and then again to my brothers and me. Consequently, basic

fingerprint patterns could be passed down through genetics. There are other factors that shape fingerprints, such as the environmental exposure during gestation, making every fingerprint unique, but these basic patterns are linked to a person's DNA and are passed along through family lines.

The main takeaway from our study is that this research suggests that basic fingerprint patterns can be inherited through genetics, which was shown by having the same common pattern passed down through members of the different generations in my family, and the analysis suggests that there are only very small differences in the fingerprints between siblings. Statistically, these differences are small and the fact that fingerprint recognition is able to pick-up on that is what allows that technology to work. Everyone has their own unique fingerprint, but that is a factor of every fingerprint linked through genetics (differential inheritance of parent's DNA) and environmental exposure during gestation. This is why the fingerprints between siblings were not exactly the same. The data suggests that if two people developed in the same womb, their fingerprints, could be very similar. Fingerprint recognition is impressive technology because it is able to recognize every individual user, even if they have a sibling with a very similar fingerprint. Since the ridge feature measurements between siblings showed only four statistically different tests, this shows how intricate fingerprint recognition technology is because the data suggests that these differences are rather subtle. These results are important because they help to begin to reveal this fascinating link between fingerprints and genetics, which not many people are aware of, and these ideas are fundamental to how big companies like Apple use fingerprint recognition for their iPhones.

At the conclusion of this study, some questions remain unanswered. I still want to know more about the specific algorithms used in fingerprint technology that allow this technology to recognize subtle differences, and I also want to see if there is an inheritance factor of fingerprint patterns within other families that would make that part of the data more significant. As for the fingerprint technology, very similar fingerprints can still be differentiated. I think that fingerprint technology is safe because fingerprints partially depend on the environment, causing a few significant differences in the fingerprints between siblings. Some limitations of this study include the fact that only one family of related individuals was tested. A family of unrelated individuals could be tested as well and the data could be compared. I could also possibly test the ridge features of other siblings and see if those fingerprints are statistically similar. There are multiple possibilities but, from the data that I have provided, fingerprints between siblings are statistically similar and there is an inheritance factor throughout the fingerprint patterns of family members.

MATERIALS AND METHODS

Generational Fingerprint Pedigree

Left and right thumb and ring finger fingerprint patterns from seven family members in three generations were collected and classified. The fingerprints were collected by gently rolling each subject's left and right thumb and ring fingers in ink, making sure to cover the whole fingerprint with ink and pressing and rolling onto a piece of labeled printer paper. The clearest prints from each of the four fingers for each subject were selected for analysis; each fingerprint pattern was placed under a microscope to observe the ridge features and classify the fingerprint. If multiple prints from the same finger were taken for clarity, the classification that was most present was deemed the dominant fingerprint pattern. This process was repeated for each of the four fingerprints for each of the seven subjects.

Magnifed Fingerprint Measurement and Analysis

A hover camera was used to zoom in on each fingerprint that was collected for each of the three brothers in the family. The ridges were extremely small, so a 1 mm sheet of paper was zoomed in until it was 17 mm, and the ridges were measured on this consistent 17 mm scale with a constant 1 mm error boundary for the fingerprints to be considered similar. Then, a millimeter ruler was used to measure the center and outermost ridge features of that fingerprint. This process was repeated for the fingerprint patterns of each of the four fingers for each brother. The results were averaged and student t-tests were used to compare ridge feature measurements between siblings to identify statistically significant differences (p-value < 0.05).

Received: January 26, 2020
Accepted: July 31, 2020
Published: December 2, 2020

REFERENCES

1. International Association for Identification. "Fingerprint Sourcebook." *National Institute of Justice*, nij.ojp.gov/library/publications/fingerprint-sourcebook?ncjnumber=225320.
2. "Are One's Fingerprints Similar to Those of His or Her Parents in Any Discernible Way?" *Scientific American*, www.scientificamerican.com/article/are-ones-fingerprints-sim/.
3. "Are Fingerprints Determined by Genetics? - Genetics Home Reference - NIH." U.S. National Library of Medicine, National Institutes of Health, ghr.nlm.nih.gov/primer/traits/fingerprints.
4. Bourzac, Katherine. "Finding Evidence in Fingerprints." *MIT Technology Review*, 22 Oct. 2012, www.technologyreview.com/s/410573/finding-evidence-infingerprints/.
5. Heng, Gan S. *et al.* "Distribution of Fingerprint Patterns Among Young Adults and Siblings in Malaysia." *The*

in-fingerprints/.
5. Heng, Gan S. *et al*. "Distribution of Fingerprint Patterns Among Young Adults and Siblings in Malaysia." *The International Journal of Medicine and Sciences*, vol. 3, no. 1, 2018, pp 11-17.
6. "DNA Fingerprinting - GeneEd - Genetics, Education, Discovery." U.S. National Library of Medicine, National Institutes of Health, geneed.nlm.nih.gov/topic_subtopic.php tid=37&sid=38.
7. Medland *et al*. "Linkage analysis of a model quantitative trait in humans: finger ridge count shows significant multivariate linkage to 5q14.1" PLoS Genet, 3 (2007), pp. 1736-1744.
8. Progeny Free Online Pedigree Tool - 9.101.9047.00, pedigree.progenygenetics.com

JOURNAL OF
EMERGING INVESTIGATORS

Article

Comparing the biodegradability of petroleum-based plastic with a novel, sustainable bio-plastic alternative

Lana Van Note, John Wnek
Marine Academy of Technology and Environmental Science, Manahawkin, New Jersey

SUMMARY

The convenience and affordability of single-use plastic products makes them an attractive option for consumers. The toxic constituents of these traditional plastics, however, are known to cause a variety of health issues in thousands of species. These environmental hazards, along with the issue of white plastic and microplastic pollution, causes increased interest in biodegradable alternatives to petroleum-based hydrocarbons. In this research, a novel bioplastic inclusive of bamboo tannins and chitosan is selected from more than 60 trial formula variations based on resulting strength, fatigue, and transparency attributes. The biodegradability of the finalized bioplastic is compared to that of conventional polyethylene, in addition to investigating its solubility and water absorbance. Biodegradation rates of the bio-based plastic exceeded that of the petroleum-based formula, as determined with Fourier Transform Infrared Spectroscopy (FTIR-ATR) analysis. The behavior of the experimental product in water deviated from the initial hypothesis, with substantial weight increase of approximately 193% after 60 minutes. A cost analysis displayed a difference of $0.0016 between the two products, with the natural additives of the experimental being more expensive. This research displays the potential of a legitimate, fully biodegradable plastic alternative to current marketplace bioplastics.

INTRODUCTION

The reliance on single-use, synthetic plastic polymers dominates hundreds of industries despite the variety of environmental and health risks they pose (1). Accumulating at a rate of eight million metric tons per year, the practice of recycling plastics, such as polystyrene and polyethylene, is being abandoned, and facilities are resorting solely to incineration or landfill usage to dispose of plastics (2). Such methods endanger thousands of species via air pollution, water contamination, and the production of toxic residue (3). Plastic substitutes with at least 20% of their constituents considered renewable are currently seen as the key to combating white pollution (4). Additionally, bioplastics are evolving in the commercial market which appeal to environmentally conscious consumers; however, most of these new products are not capable of complete degradation (5-6).

A majority of bioplastics include corn or cassava starches, which are converted to polylactic acid prior to use (7). The incorporation of carbohydrates is responsible for the tendency of such substances to break down with prolonged contact with water or soil (8). However, utilizing a food source as the backbone of such a ubiquitous material may not be ideal due to the potential increase in land and fertilizer usage. In this research, a bioplastic film incorporating tannins, a derivative of *Bambusa sp.* (bamboo), chitin, derived from *Gryllus sp.* (field cricket), and agar agar, originating from seaweed, was developed over the course of nine months with over 60 formulas tested.

Hydrolyzable tannins, a group of amorphous substances commonly found within bamboo, form complexes with a variety of proteins and carbohydrates, mainly those rich in proline (PRPs), such as gelatin and agar (9-10). While there is some debate as to whether tannins cause the precipitation of proteins or the formation of a complex of weak and strong chemical bonds, it is crucial that the solution is the proper acidity to reach its isoelectric point in order for any notable interactions to occur (11). Bamboo was selected as the source material from which to extract tannins because of its sustainability and wide availability (12). Certain species of the *Bambusa* genus are beginning to be considered nuisances because of their rapid growth and ability to repopulate in a multitude of conditions (13). These features make bamboo particularly attractive for costing models.

Chitosan, derived from the carbohydrate chitin, is an example of a substance that interacts with tannins (14). An abundant polysaccharide, chitin's occurrence in nature is only second to cellulose. It can be found in the cell walls of fungi, marine invertebrates, insect exoskeletons, as well as numerous plants and animals (15). Chitin is a natural polymer with a varied cellulose structure, containing an N-acetyl group instead of a hydroxyl group at the second carbon (16). Its low solubility usually requires a deacetylation process for conversion to chitosan **(Figure 1),** which is necessary for proper complex formation (17-18).

In this investigation, the degradation rate of the innovative bioplastic in both water and soil, in addition to its absorbance, was compared against a traditional, petroleum-based film after initial formula selection. Serving as a potential substitute for single-use plastic wraps/films, poor transparency and mediocre strength, biodegradation, and fatigue resistance

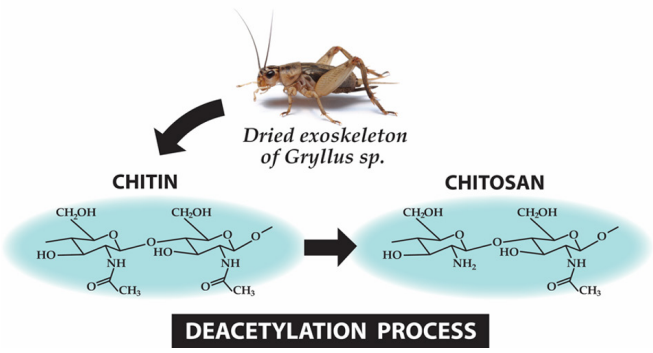

Figure 1. Converting chitin to chitosan. The reaction requires the degree of deacetylation to be between 60% and 90%. Once deacetylated, the product is then soluble in organic acids, such as acetic acid.

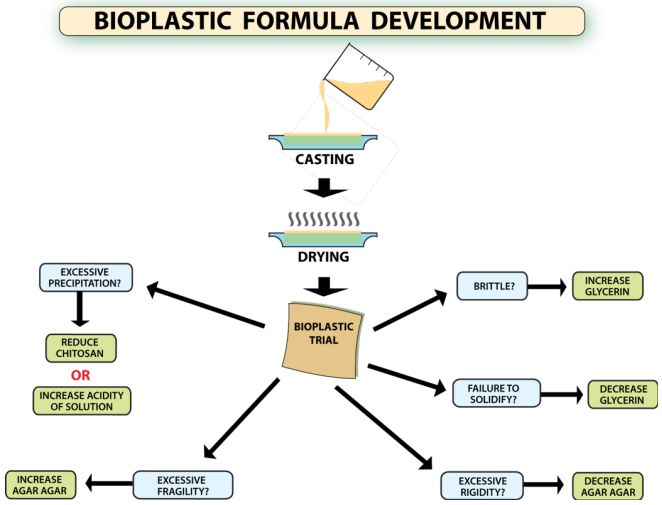

Figure 2. Flow chart demonstrating the experimentation process. Trial and error led to the creation of the novel formula. Frequent adjustments were made to ensure the product was pliable and able to withstand handling during strength, flexibility, transparency, biodegradation, water absorption, and solubility tests.

are acceptable, but low solubility and water absorption are imperative. We hypothesized that the bioplastic formula would biodegrade much more rapidly than the polyethylene film but have little solubility and absorption. The ideal biodegradable film for application in the packaging industry should undergo a lag phase, sustained from synthesis to disposal, before the biodegradation process accelerates.

RESULTS

Part I: Preliminary Testing and Selection

The nature of this research required a two-part procedure for an adequate product comparison. The first component involved the formation of a novel bioplastic, primarily incorporating chitosan, tannins, and agar agar. Additional elements, such as acetic acid and glycerin, were included to ensure successful interactions that generated a stable material. The final product was developed through a process of trial and error with more than 60 created bioplastics **(Figure 2, Table 1).**

The experimental bioplastic formula used in the comparison was selected based off the results of three preliminary tests—strength, transparency, and fatigue—for nine final film compositions. A grading scale was constructed to simplify the selection process **(Table 2)**. Data collected from a simulated tensile strength test and UV-spectrophotometry were favorable for obtaining a basic profile of each film tested and determining which is most suitable for further examination. Fatigue resistance was used to simulate repetitive use as well as gauge flexibility; a value greater than 100 represented a material with adequate flexibility for sustained usage and comfortable handling **(Figure 3A)**. The minimum strength requirement was arbitrarily decided to be

Table 1. Characteristics/scores of nine bioplastic formulations.

Trial	Agar agar	Tannin	Chitosan	Acetic Acid	AA Treatment	Glycerin	Solidification	Transmittance (%)	Strength (N)	Fatigue (Cycles)	Final Score
1	4.000%	2.000%	0.100%	8.000%	No	0.150%	Yes	6.20%	8.92	>100	7
2	4.000%	2.000%	<0.001%	8.000%	N/A	0.100%	No	N/A	N/A	N/A	0
3	4.000%	2.000%	<0.001%	<0.001%	N/A	1.000%	No	N/A	N/A	N/A	0
4	4.000%	2.000%	<0.001%	8.000%	N/A	2.000%	No	N/A	N/A	N/A	0
5	4.000%	2.000%	2.000%	8.000%	No	0.200%	Yes	<0.01%	20.14	29	5
6	7.500%	2.000%	<0.001%	8.000%	N/A	0.150%	Yes	18.65%	7.19	>100	8
7	7.500%	2.000%	2.000%	8.000%	No	0.150%	Yes	<0.01%	20.34	1	4
8	7.500%	2.000%	2.000%	8.000%	No	0.100%	Yes	<0.01%	6.43	<1	1
9	7.500%	2.000%	0.100%	8.000%	Yes	0.150%	Yes	12.52%	11.72	>100	8

Note: The final experimental plastics were ranked based on ability to solidify, transparency, and flexibility using a grading scale for each attribute. The final score was the summation of points from the three areas of evaluation. No points were awarded for solidification; however, a failure to solidify resulted in a final score of zero. The formula with the highest point total was selected for further experimentation. Formula #9 was selected due to the preference of a strong film for biodegradation comparison.

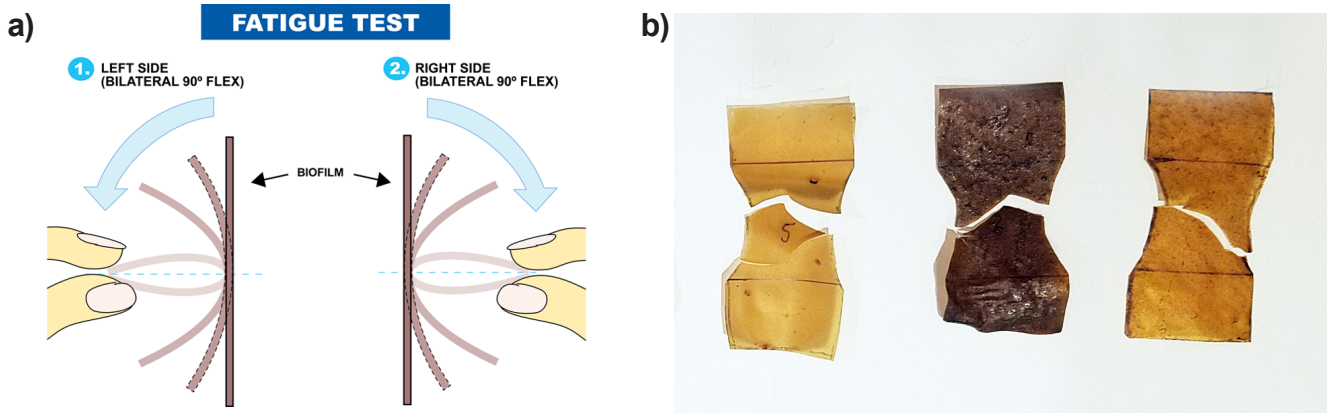

Figure 3. Preliminary flexibility and strength testing procedures. a) Each 70 mm x 20 mm x 0.1mm bioplastic trial was subjected to a flex test to examine its ability to withstand fatigue. One 90-degree bilateral flex to each side was termed one cycle. The trial was given the full 5 points if it was able to complete 100 cycles with no signs of breakage. **b)** Samples were cut into a dog bone shape to maintain a strong grip and limit error. Breakage occurred within a range of approximately 500-1850 mL of water. The maximum weight (in kilograms) each sample could sustain was multiplied by the gravitational constant to obtain the force in newtons.

9.81 N, meaning that the optimal film would be able to support the weight of one kilogram, sufficient for its intended use **(Figure 3B)**. Transparency is trivial when compared to the other mechanical properties but was considered when tasked with designing an aesthetically pleasing commercial product. Trial 9, with a 75:1 ratio of agar agar to chitosan, received the highest rating with the ability to withstand approximately 11.72 newtons of force and the maximum number of flexes, in addition to its fair transmittance of 12.52% **(Table 1)**.

Part II: Water Absorption and Solubility Comparison

After initial testing, ten 10 mg samples of both the selected bioplastic and polyethylene film were used for an *in vitro* biodegradation test, using soil as the source of microorganisms. Subsequent to the 168-hour period, Fourier Transform Infrared Spectroscopy (FTIR) with the Attenuated Total Reflection attachment (ATR) was utilized to determine the percent degradation, using unexposed samples as controls. The FTIR-ATR analysis of three peaks for the biodegraded bioplastic film produced an average peak ratio (control:experimental) of 1.000:0.778 **(Figure 4A, areas #1-3)**, while a peak ratio of 1.000:0.978 was calculated for the petroleum-based plastic **(Figure 4B, areas #1-2)**. Negligible change was seen in the polyethylene film, unlike the tannin and chitosan-based formula, which achieved approximately 22% biodegradation in the 168-hour period. A *t*-test suggested that the difference in biodegradation rates was not significant ($p = 0.0635$; $\alpha = 0.05$).

Fifteen 10 mg samples of each plastic type were submerged in distilled water for one of five possible timespans, then reweighed using an analytical balance to conclude the water absorption testing. The turbidity of the remaining solution, in addition to FTIR analysis as a secondary method, was used to calculate percent solubility. Solubility was examined to determine if the material would break down when deposited into a marine system, while water absorption was assessed to estimate the film's practicality as a consumable wrapping or similar product. Absorbance significantly increased across all bioplastic trials, which was confirmed by a *t*-test assuming unequal variances ($p = 0.0191$; $\alpha = 0.05$). The average percent absorption for the bioplastic samples for 1, 5, 15, 30, and 60 minutes were 110%, 168%, 176%, 206%, and 193% respectively **(Figure 5A)**. Around the 60-minute mark, the bioplastic samples reached peak solubility, with the average turbidity of the remaining solutions increasing from 20 FAU at the 1-minute mark to 66 FAU after the full 60

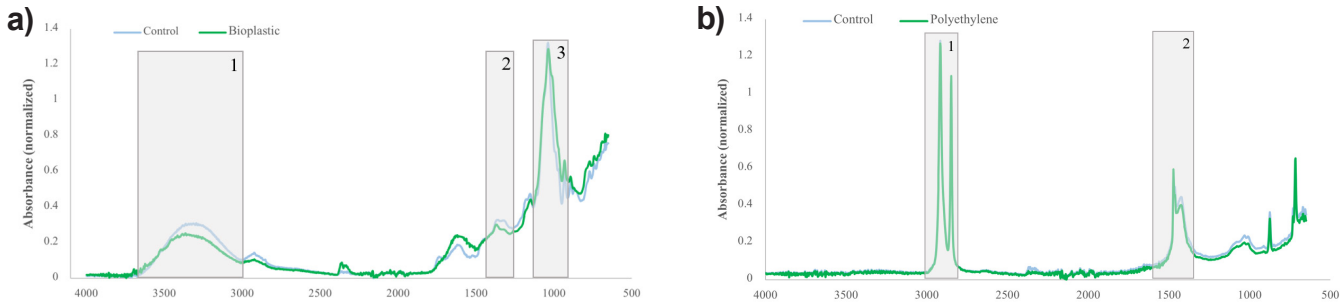

Figure 4. Results of biodegradation analysis. FTIR-ATR spectra of the biodegraded a) bioplastic (1.000:0.778) and **b)** polyethylene (1.000:0.978) samples after an exposure period of 168 hours at 25±2°C. Unexposed bioplastic and polyethylene samples were used as controls to calculate the peak ratios. 64 iterations of each sample were taken to reduce error from outside factors (sound, carbon dioxide, etc). Shaded regions indicate analyzed peaks used to produce the final ratio of the control to the experimental.

minutes, translating to 5.5% and 18.2% solubility. The FTIR supported these results by producing an average peak ratio of 1.000:0.9373:0.9349:0.7133 (control:5min:15min:60min) **(Figure 5B, areas #1-2)**. Unlike the experimental bioplastic film, the polyethylene samples were consistently insoluble (p = 0.006; α = 0.05) and had low absorption values **(Figure 5A)**.

DISCUSSION

The chitosan and tannin bioplastic formula designed in this investigation demonstrates potential after analyzing its effectiveness compared to petroleum-based plastic film. The mean biodegradation rates of each material suggested that the 10.0 mg sample of the experimental bioplastic biodegraded 11 times faster than its petroleum-based counterpart. The average biodegradation rate of approximately 22% per week is particularly impressive when considering other biodegradable plastics currently on the retail market which, in fact, do not fully biodegrade as implied (19). The product's ability to biodegrade is mainly due to the utilization of organic constituents in the formula (20). The unnatural bonding in polyethylene is responsible for its indestructible nature, as few microorganisms are equipped with the metabolic pathways needed to weaken the long chains of such interactions (21). Evidence of this is seen in the FTIR spectra between 1400 and 1600 cm^{-1} (region III), where a peak indicating carbon-carbon double bonding is visible for polyethylene (22). The presence of C-H bonds (1050 cm^{-1}) in the bioplastic, commonly observed in organic compounds, allows for increased biodegradation (23).

Though the usage of environmentally friendly constituents was responsible for rapid biodegradation, it was also responsible for the film's water absorbance and dissolution in distilled water (24). Shortly after submersion, the absorption of the bioplastic plateaued and eventually decreased. The slight decrease in weight may have been due to dissolution. We inferred that this trend would continue to increase inversely with time. The FTIR-ATR analysis confirmed these findings, suggesting that a minimum exposure time of 60 minutes is necessary to achieve considerable dissolution. Distortion of the carbon-carbon bond within the film as a result of its introduction to water is evident near 1600 cm^{-1}, indicated by the varying peaks (25). The FTIR-ATR analysis differed from the colorimetry solubilities by an average of 12.4%. The discrepancy is likely due to excess water remaining on the samples at the conclusion of testing, resulting in continuous dissolution; however, the FTIR result still mirrors the incremental differences over the 60-minute period that the colorimetry provided. A sharp peak is seen in the fingerprint region near 1,020 cm^{-1} within the FTIR spectra of the experimental plastic, a possible indicator of the presence of aliphatic amines, molecules that interact with water to form hydrogen bonds (26-27). Another peak is visible in region I (4,000 to 2,500 cm^{-1}), unlike the polyethylene samples, revealing that the suggested hydrogen bonding is present (28). The existence of O-H or N-H single bonds indicate polarity, justifying the film's solubility in a polar solute (29).

The pricing of polyethylene was approximately $0.0031 per square centimeter, while the bioplastic was approximately $0.0047 per square centimeter. When considering the additional cost for maintaining a landfill for the polyethylene products (including after closure costs), the price rises to $0.0035, meaning the bio-based film costs 34% more than its competitor (30).

The data supports the hypothesis that the bioplastic has an enhanced biodegradation capability, displaying an average degradation rate of 22% per week. However, the results do not support the hypothesis in that the water absorption and solubility percentages were significantly higher in the bio-based formula. Excessive water absorption may inhibit its application as a single-use product because of the weakened structure and durability. A product with solute capabilities is of value, under certain conditions. Rapid dissolution is a hindrance that must be addressed in order to consider its usage as a legitimate alternative. Despite this, the bioplastic

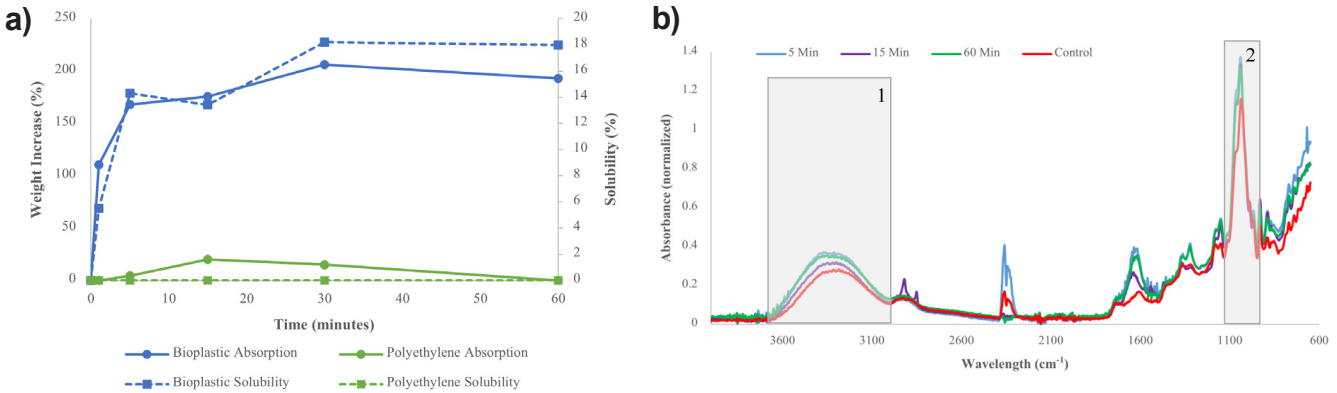

Figure 5. Results of water absorption/solubility testing. a) Both plastic films were subjected to distilled water at 22°C for five exposure times — 1, 5, 15, 30, and 60 minutes (n = 3). Mean absorbance values of the bio-based plastic were significantly higher than those of the polyethylene film (p = 0.0191; α = 0.05). **b)** Subsequent to solubility testing, further evaluation of the experimental samples determined moisture effects on the structural integrity of the bioplastic film. Shaded regions indicate peaks that were investigated to produce the final ratio of the control to the experimental samples (by increasing exposure time: 0.9373:0.9349:0.7133).

film was successful in that it displayed the basic mechanical properties fundamental to plastic packaging and achieved considerable biodegradation within the experiment's timeframe.

Adjustments to the formula of the bioplastic could be considered as certain properties made testing cumbersome (i.e. stiffness due to lack of glycerin). With the improvements, tensile strength testing in addition to film elongation testing at breaking point will be warranted choices. Supplementary testing may also be conducted to test the film's effectiveness as a wrapping for consumables, which may be applied as a spray or an immersive solution. Besides its application in the food and packaging markets, this biodegradable, moldable plastic may be useful in the medical industry as well. One of its uses may include bioabsorbable surgical implants which assist with tendon-to-bone repair, or for improved methods of implanted drug delivery due to its biodegradability and possible limitation of bacterial growth. Coupled with copolymer blending, this novel bioplastic formula shows much future ability.

MATERIALS AND METHODS

Part I: Bioplastic Formulation and Selection

Formula Constituents

The solution-casting method was utilized to synthesize the bioplastic in this research. The primary constituent of the most successful formula was agar agar (7.50 wt%), which acted as the base substance of the film. Hydrolyzable tannins derived from members of the subfamily *Bambusoidae* (common bamboo) were incorporated into the mixture (4.00 wt%), obtained through boiling of sheared, young culms approximately 2.50 cm in diameter in distilled water for upwards of 200 hours. The ability of tannins to form a complex of chemical bonds with proline-rich proteins and carbohydrates, including chitin, was the reasoning for its inclusion (31). Dried exoskeleton of *Gryllus sp.* was ground into a fine powder using a spice mill and added to the formula; however, due to the incomplete solubility of granular particles, 0.300 g of commercial grade powdered chitosan (X002ATKNGV, MarkNature) was dissolved within 5.00 mL of 5% acetic acid and added as a supplementation. In an effort to reduce the pH of the solution and effectively reach the isoelectric point calculated prior to experimentation (approximately 5), acetic acid was selected as the solvent for the chitosan solution (32). Additionally, glycerin, a plasticizer responsible for the flexibility of the product, was included at a concentration of approximately 0.200 wt%. A solution was produced with all additives using distilled water as the solvent at a ratio of 11:2. The solution was heated to 95±5°C with constant stirring, then filtered through a sieve with a 2 mm aperture diameter. Once cast into silicone molds, gelatinization occurred, and the films dried at room temperature (23°C) for 48–72 hours. A similar procedure applied to all films, with only the concentrations being altered according to **Table 1**. Formulas that failed to produce a solidified product or displayed excessive brittleness were ineligible to proceed to preliminary testing. The final experimental formula described was selected from the favorable trials using a grading scale which considered transparency, strength, ability to solidify, and ability to withstand fatigue **(Table 2).**

Table 2. The grading scale of the three preliminary tests.

Score	Transmittance (%)	Force (N)	Number of Cycles
0	<0.01	<0.01	<1
1	0.01-12.50	0.01-10.0	1-25
2	12.51-25.00	10.1-20.0	26-50
3	25.01-37.50	20.1-30.0	51-75
4	37.51-50.00	30.1-40.0	76-100
5	>50.00	>40.1	>100

Note: Each bioplastic received a score of 0–5 based on the percent transmittance of light, the force of weight (in newtons) each dog-bone shaped samples could withstand, or the number of flexing cycles that were completed before tearing/breaking was imminent.

Transparency Testing

Transparency was determined using the transmittance (%T) obtained through UV-spectrophotometry using a Shimadzu UV-1201 spectrophotometer at 600 nm. Each of the nine formulas were cut to fit the spectrophotometer cell (approx. 70 mm x 20 mm x 0.1 mm), and the resulting transmittance was an average of three trials. Testing was conducted in low-light areas in order to reduce the amount of error from stray light.

Strength Testing

Strength was estimated by determining the maximum force of weight (N) each 60 mm x 30 mm x 0.1 mm dog bone-shaped bioplastic sample could withstand. Each solidified sample (6 in total) was suspended vertically at each wide dog bone end between two 5.1 cm spring clamps. A container was attached via nylon cording to the lower clip, freely suspended. Water was added in 100 mL increments into the container attached to the apparatus. After breakage, the force in newtons was calculated by multiplying the mass of water by gravitational acceleration **(Figure 3B)**.

Fatigue Testing

Each film's ability to withstand fatigue was tested by performing 90-degree bilateral flexes in series until tearing was visible **(Figure 3A)**. Testing concluded if a sample was able to withstand one hundred bilateral flexes in series without disturbing the film's structural integrity.

Part II: Polyethylene Comparison

Biodegradation Rate Analysis

Five months prior to collection, several polyethylene plastic products were buried near the location of the soil sample extraction to mimic the conditions of a typical landfill and attract native soil microorganisms known to gradually biodegrade plastics, such as *Pseudomonas putida* (33). Ten

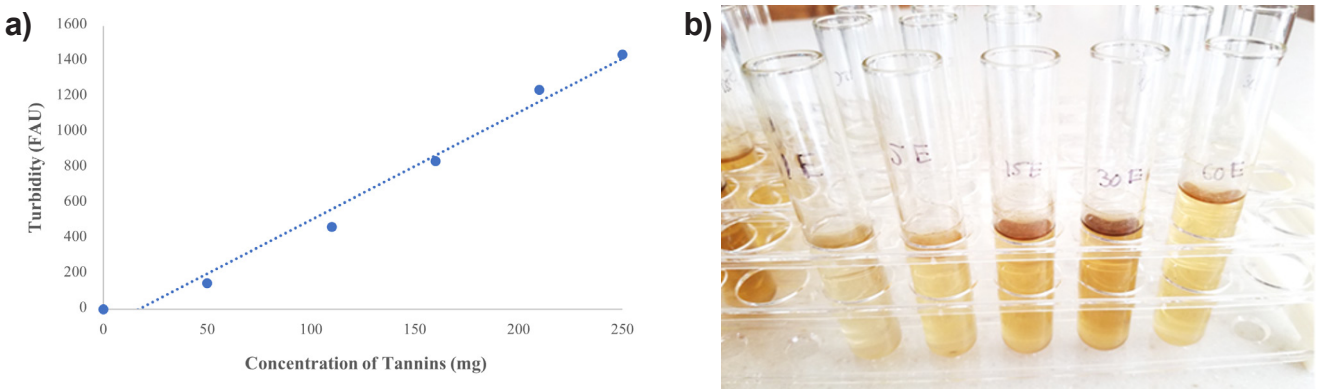

Figure 6. Tannins standard curve used in calculating solubility of bioplastic samples. a) The equation of the standard curve (y = 6.072x - 101.03) was utilized to calculate the concentration of tannins within the remaining solution of the absorption trials. The R^2 value was 0.9829, indicating strong correlation between the two variables. **b)** The turbidity of the remaining solution at the conclusion of the water absorption test was sufficient for estimating the solubility of the plastics (n = 3).

10 mg strips of the experimental bioplastic and traditional polyethylene film were placed in borosilicate test tubes containing 8.00 g of soil. 0.50 mL of distilled water was added for proper moisture content, and trials were incubated at 25±2°C for 168 hours, with an additional 0.50 mL of distilled water introduced to the system at the 85-hour mark to maintain moisture. Samples were removed and allowed to dry. The comparison of peak ratios from the FTIR-ATR analysis determined the average percent biodegraded. A *t*-test (assuming unequal variances) was utilized to detect a significant difference in the percentages between the two products (α = 0.05).

Water Absorbance Testing

Fifteen 10 mg samples of the novel bioplastic and an LDPE polyethylene plastic film shopping bag were obtained. An *in vitro* water absorption test was performed using borosilicate test tubes in accordance with the ASTM D570-98 procedure (with modification) (34). Samples were weighed using an Ohaus analytical balance (+/- 0.0001 g) then submerged in 8.00 mL of distilled water at 22°C for 1, 5, 15, 30, and 60 minutes. After exposure, samples were dried to remove excess water on the film's surface, then reweighed. A *t*-test assuming unequal variances was performed on the weight differences after the full 60-minute period to compare the absorbances of the two plastics examined (α = 0.05).

Solubility Testing

Solubility was determined via colorimetry using a LaMotte Smart3 Colorimeter (absorption method) and compared using a second *t*-test. Testing was conducted in a dark room to minimize the error in the turbidity values (FAU) by reducing light interference. Prior to processing experimental solutions, a standard curve was created using the turbidity of six standards, with each successive standard containing an increasing ratio of hydrolyzable tannins to distilled water **(Figure 6A)**. The curve determined the turbidity, and therefore, the concentration of tannins of the remaining solutions at the conclusion of the water absorption testing **(Figure 6B)**. Fourier Transform Infrared Spectroscopy (FTIR) with the Attenuated Total Refraction (ATR) attachment was utilized to further assess the bioplastic samples after being submerged for 5, 15, and 60 minutes. Sixty-four iterations were captured for each test to limit any error from interferences such as sound and carbon dioxide.

Cost Analysis

A cost analysis was performed to compare the pricing (per square centimeter) of the novel bioplastic formula with current single-use plastic products. Only the major components of each film were included in the calculation (i.e. agar agar, tannins, and chitosan for bioplastic, and petroleum for polyethylene).

Received: June 8, 2020
Accepted: November 25, 2020
Published: December 1, 2020

REFERENCES

1. Vierira, Melissa, *et al*. "Natural-Based Plasticizers and Biopolymer Films: A Review." *European Polymer Journal*, vol. 47, no. 3, Mar. 2011, pp. 254–263., doi: 10.1016/j.eurpolymj.2010.12.011.
2. Lea, W. Reid. "Plastic Incineration versus Recycling: a Comparison of Energy and Landfill Cost Savings." *Journal of Hazardous Materials*, vol. 47, no. 1-3, 1996, pp. 295–302., doi:10.1016/0304-3894(95)00117-4.
3. Song, Jim H., *et al*. "Biodegradable and Compostable Alternatives to Conventional Plastics." *Philosophical Transactions of the Royal Society B: Biological Sciences*, vol. 364, no. 1526, 2009, pp. 2127–2139., doi:10.1098/rstb.2008.0289.
4. Gironi, Fausto, and Vincenzo Piemonte. "Bioplastics and Petroleum-Based Plastics: Strengths and Weaknesses."

Energy Sources, Part A: Recovery, Utilization, and Environmental Effects, vol. 33, no. 21, 2011, pp. 1949–1959., doi:10.1080/15567030903436830.

5. Razza, Francesco, and Francesco Innocenti. "Bioplastics from Renewable Resources: the Benefits of Biodegradability." *Asia-Pacific Journal of Chemical Engineering*, vol. 7, 2012, pp. S301–S309., doi:10.1002/apj.1648.
6. Kitamoto, Hiroko, *et al*. "Phyllosphere Yeasts Rapidly Break down Biodegradable Plastics." *AMB Express*, vol. 1, no. 1, 2011, p. 44., doi:10.1186/2191-0855-1-44.
7. Baumberger, Stephanie, *et al*. "Use of Kraft Lignin as Filler for Starch Films." *Polymer Degradation and Stability*, vol. 59, no. 1-3, Jan. 1998, pp. 273–277., doi:10.1016/s0141-3910(97)00193-6.
8. Sanyang, Muhammed, *et al*. "Effect of Plasticizer Type and Concentration on Tensile, Thermal and Barrier Properties of Biodegradable Films Based on Sugar Palm (Arenga Pinnata) Starch." *Polymers*, vol. 7, 2015, pp. 1106–1124., doi:10.3390/polym7061106.
9. Adamcyzk, Bartosz, *et al*. "Tannins and Their Complex Interaction with Different Organic Nitrogen Compounds and Enzymes: Old Paradigms versus Recent Advances." *ChemistryOpen*, vol. 6, no. 5, Aug. 2017, pp. 610–614., doi:10.1002/open.201700113.
10. Van Buren, Jerome, and Willard Robinson. "Formation of Complexes between Protein and Tannic Acid." *Journal of Agricultural and Food Chemistry*, vol. 17, no. 4, 1969, pp. 772–777., doi:10.1021/jf60164a003.
11. Obreque-Slier, Elías, *et al*. "Tannin-Protein Interaction Is More Closely Associated with Astringency than Tannin-Protein Precipitation: Experience with Two Oenological Tannins and a Gelatin." *International Journal of Food Science & Technology*, vol. 45, no. 12, 2010, pp. 2629–2636., doi:10.1111/j.1365-2621.2010.02437.x.
12. Yeasmin, Lucina, *et al*. "Bamboo: an Overview on Its Genetic Diversity and Characterization." *3 Biotech*, vol. 5, no. 1, 2014, pp. 1–11., doi:10.1007/s13205-014-0201-5.
13. Canavan, Susan, *et al*. "The Global Distribution of Bamboos: Assessing Correlates of Introduction and Invasion." *AoB Plants*, vol. 9, no. 1, 2017., doi:10.1093/aobpla/plw078.
14. Younes, Islem, and Marguerite Rinaudo. "Chitin and Chitosan Preparation from Marine Sources. Structure, Properties and Applications." *Marine Drugs*, vol. 13, no. 3, 2015, pp. 1133–1174., doi:10.3390/md13031133.
15. Tharanathan, Rudrapatnam N., and Farooqahmed S. Kittur. "Chitin — The Undisputed Biomolecule of Great Potential." *Critical Reviews in Food Science and Nutrition*, vol. 43, no. 1, 2003, pp. 61–87., doi:10.1080/10408690390826455.
16. Kaczmarek, Michal Benedykt, *et al*. "Enzymatic Modifications of Chitin, Chitosan, and Chitooligosaccharides." *Frontiers in Bioengineering and Biotechnology*, vol. 7, 2019, p. 243., doi:10.3389/fbioe.2019.00243.
17. Schmitz, Christian, *et al*. "Conversion of Chitin to Defined Chitosan Oligomers: Current Status and Future Prospects." *Marine Drugs*, vol. 17, no. 8, 2019, p. 452., doi:10.3390/md17080452.
18. Furuike, Tetsuya, *et al*. "Preparation of Chitosan Hydrogel and Its Solubility in Organic Acids." *International Journal of Biological Macromolecules*, vol. 104, 2017, pp. 1620–1625., doi:10.1016/j.ijbiomac.2017.02.099.
19. Jain, Roopesh, and Archana Tiwari. "Biosynthesis of Planet Friendly Bioplastics Using Renewable Carbon Source." Journal of Environmental Health Science and Engineering, vol. 13, no. 11, 15 Feb. 2015., doi:10.1186/s40201-015-0165-3.
20. Amin, Ruhul, *et al*. "Characterization and Performance Analysis of Composite Bioplastics Synthesized Using Titanium Dioxide Nanoparticles with Corn Starch." Heliyon, vol. 5, no. 8, 28 Aug. 2019., doi:10.1016/j.heliyon.2019.e02009.
21. Atiq, Naima, *et al*. "Isolation and Identification of Polystyrene Biodegrading Bacteria from Soil." *African Journal of Microbiology Research*, vol. 4, no. 14, 2010, pp. 1537–1541.
22. Barbes, Lucica, *et al*. "ATR FTIR Spectrometry Characterisation of Polymeric Materials." *Romanian Reports in Physics*, vol. 66, no. 3, 2014, pp. 765–777.
23. Ismail, Nurul Aina, *et al*. "Synthesis and Characterization of Biodegradable Starch-Based Bioplastics." *Materials Science Forum*, vol. 846, 2016, pp. 673–678., doi:10.4028/www.scientific.net/msf.846.673.
24. Santana, Renata Ferreira, *et al*. "Characterization of Starch-Based Bioplastics from Jackfruit Seed Plasticized with Glycerol." *Journal of Food Science and Technology*, vol. 55, no. 1, 2017, pp. 278–286., doi:10.1007/s13197-017-2936-6.
25. Svatoš, Aleš, and Athula B. Attygalle. "Characterization of Vinyl-Substituted, Carbon−Carbon Double Bonds by GC/FT-IR Analysis." *Analytical Chemistry*, vol. 69, no. 10, 1997, pp. 1827–1836., doi:10.1021/ac960890u.
26. Chiu, Yie-Chan, *et al*. "Effect of Aromatic and Aliphatic Amines as Curing Agents in Sulfone Epoxy Monomer Curing Process." *Polymer Bulletin*, vol. 70, no. 4, 2013, pp. 1367–1382., doi:10.1007/s00289-013-0942-z.
27. Spencer, J. N., *et al*. "Hydrogen Bonding by Alcohols and Amines." *Journal of Solution Chemistry*, vol. 14, no. 11, 1985, pp. 805–814., doi:10.1007/bf00646002.
28. Khan, F, *et al*. "FTIR Studies of Hydrogen Bonding Interaction between Alkyl Esters and Hexanol, p-cresol in Carbon." *Indian Journal of Pure & Applied Physics*, vol. 46, 2008, pp. 12–19., doi:10.1039/c6ra17819g.
29. Armstrong, Steven R., *et al*. "Effects of Polar Solvents and Adhesive Resin on the Denaturation Temperatures of Demineralized Dentine Matrices." Journal of Dentistry, vol. 36, no. 1, 2008, pp. 8–14., doi:10.1016/j.jdent.2007.10.003.
30. Hirshfeld, Stephen, *et al*. "Assessing the True Cost of Landfills." *Waste Management & Research*, vol. 10, no. 6, 1992, pp. 471–484., doi:10.1016/0734-242x(92)90088-3.

31. Koopmann, Ann-Kathrin, *et al*. "Tannin-Based Hybrid Materials and Their Applications: A Review." *Molecules*, vol. 25, no. 21, 2020, pp. 4910., doi:10.3390/molecules25214910.
32. Xu, Peisheng, *et al*. "Zwitterionic chitosan derivatives for pH-sensitive stealth coating." *Biomacromolecules*, vol. 11, no. 9, 2010, pp. 2352–2358., doi:10.1021/bm100481r.
33. Nikel, Pablo, and Victor de Lorenzo. "Pseudomonas putida as a functional chassis for industrial biocatalysis: From native biochemistry to trans-metabolism." *Metabolic Engineering*, vol. 50, 2018, pp. 142-155., doi:10.1016/j.ymben.2018.05.005.
34. Judawisastra, Hermawanm, *et al*. "Water absorption and its effect on the tensile properties of tapioca starch/polyvinyl alcohol bioplastics." IOP Conference Series Materials Science and Engineering, vol. 223, no. 1, 2017., doi:10.1088/1757-899X/223/1/012066.

JOURNAL OF
EMERGING INVESTIGATORS

Article

A juxtaposition of airborne microplastics and fiber contamination in various environments

Trucy Truong-Phan, Joe Rasmus
Williamston High School, Williamston, Michigan

SUMMARY

Microplastics can have detrimental effects on various wildlife, as well as pollute aquatic and atmospheric environments. The term microplastics refers to miniscule pieces of plastic that are either deliberately produced at that small size or are broken down from larger pieces of plastic. This study focused on air samples collected from five locations to investigate microplastic concentrations in atmospheric fallout from indoor and outdoor settings, through a process utilizing a hand-held vacuum pump and a rotameter. The samples were collected over a five-month period, and the number, as well as the morphologies, of the microplastics were recorded for each of the five sample locations. The amount of microplastic debris found in the urban setting was larger compared to the amount found in the rural setting. Furthermore, we found that the difference between the average number of microplastic fragments and fibers collected from all locations was not large enough to be statistically significant. Since the amount of published research on airborne microplastics is very minimal, the results collected in this study will help us better understand the prevalence of airborne microplastics.

INTRODUCTION

Plastic has become an integral feature of everyday life, especially with the commercial industry of polymers rapidly expanding every year. Due to the high demand for this synthetic material, concerns regarding its long-term effects on humans and the environment have gained more attention. Over time, plastic disintegrates into microscopic particles called microplastics which are usually 5 mm or less (1). Microplastics can accumulate in the atmosphere, resulting from fragmentation of plastic products (2). The contamination of microplastics in varying environments has become a pressing issue in the scientific community. As plastic production increases, more microplastics are released into the atmosphere. Although there have been several studies completed that examine the impacts of microplastic in different water sources, there is a limited amount of published work on airborne microplastics. Previous studies investigated the impacts of airborne microplastics on human health and explored different methods to collect microplastic debris (2).

Mass production of plastics has significantly surged within the past decade, increasing the atmospheric exposure to synthetic particles, including microplastic fibers and fragments. Fibers are long strands of microplastics that are the same width throughout their entire length, while fragments resemble a small droplet or stain. Both morphologies of the microplastics are characterized during the fragmentation of the original piece of plastic and have the same impact on the environment. Roughly 8.3 billion metric tons of plastic have been produced in the past six decades (3). This quantity of plastic distributed by commerce has resulted in high amounts of plastic particles throughout the environment. These plastic particles have been identified in urban centers, freshwater sources, uninhabited islands, sea surfaces, as well as polar regions (3). Additionally, research has shown that microplastics and synthetic fibers are found in indoor settings and residential areas (4).

The objective of this study of airborne microplastics is to expand public knowledge of atmospheric contamination, which can be utilized to find potential solutions to combat the issue. The research focused on examining the difference in airborne microplastic concentrations in various environments and the potential factors that may impact concentration levels. Because of the considerable rise in plastic production, this concern is expected to expand into a more serious problem that can negatively impact ecosystems and human health (2). Microplastics are 5 mm or smaller, which means that they are often difficult to identify and analyze (1). Common sources of these microscopic contaminants include microbeads from cosmetics, microfibers from clothes, and synthetic polymers from motor vehicle tires (2). Airborne microplastics has been linked to environmental pollution, airborne contamination, as well as human health degradation, including serious health concerns such as chronic bronchitis, asthma, sinusitis, and interstitial fibrosis (4). Workers in certain industries, specifically synthetic textile and flock production, are exposed to high concentrations of airborne fibers and contaminants, which may lead to occupational diseases (4).

The goal of this study was to determine whether measurable quantities of airborne microplastics were present in the atmosphere of various locations tested in mid-Michigan. We hypothesized that airborne microplastic debris would be significantly different between an urban and rural environment. We also hypothesized that the number of microplastics from areas with a higher population density or more human movement would differ from the number of

microplastics from areas with less movement and people. Airborne microplastic accumulation may be primarily driven by human activity, industrial debris, motor vehicle pollution, and synthetic fibers from clothes dryer discharge (3). All four of these can be sourced and found outdoors. Our data provides evidence to support the claim that the number of microplastics from the atmosphere of the urban location was statistically different to those from the rural location. Furthermore, the results showed that the hallway compared to the lunchroom concentrations, as well as the lunchroom compared to the research classroom concentrations, were not statistically different. Comparing the collected microplastics from the locations to each other provided insight into the varying levels of airborne contamination in different regions.

RESULTS

We examined the concentrations of airborne microplastics by collecting numerous air samples from each location selected and calculating the microplastics per cubic meter in the air samples. At least four samples were collected from each location to investigate the varying quantities of airborne microplastics. We used a handheld vacuum that is attached to a Buchner funnel, which is equipped with Whatman filter paper, to collect air particles. Additionally, air flow rate, the amount of air being vacuumed into the funnel over time, was controlled using a rotameter. While analyzing each sample, the specific qualities of the microplastics were recorded, as well as the type of the microplastic (fiber or fragment).

We collected airborne microplastic samples from varying locations that associate with varying levels of human activity and movement. We selected a rural location to simulate an environment with reduced human and automobile traffic, while an urban location is selected to simulate an environment with high levels of human and automobile traffic. Furthermore, a high school classroom represented an area with low human activity, the lunchroom characterized an area with moderate human activity, and the performing arts hallway represents an area with high human activity (**Figure 1**). The raw number of microplastics on each filter was another key focus. A

Table 1. Summary data of measured microplastics by site.

Sample Location	Sample Size	Mean	Median	Std. Dev.
		MPs per m³	MPs per m³	MPs per m³
Research Classroom	4	5.1	3.9	3.5
Rural Location (Lounsbury Rd.)	4	3.7	3.4	2.2
Urban Location (W Oakland Ave.)	6	31.9	25	21.2
Lunchroom	4	16.2	16.2	3.7
Performing Arts Hallway	4	64.6	62.4	19.8

Note: "MP" is the abbreviation for microplastics.

condensed summary table comparing all five locations using the data collected for each sample is shown in **Table 1**.

For each location, four to six individual samples were collected, and every sample contained at least one cubic meter of filtered air. In total, 22 air samples were collected over the five-month period. After we examined and analyzed the samples, a 2-tailed Mann-Whitney U-test was used for the four hypotheses (5). This was done by dividing the original alpha value of 0.05 by three, which was the number of comparisons being made. Therefore, the adjusted alpha value for the three hypotheses comparing microplastics between each location was 0.017; a result was considered statistically significant if the *p*-value was found to be less than 0.017. Next, we wanted to examine the average number of microplastic fragments from all locations versus the average number of microplastic fibers from all locations. Since this hypothesis was evaluated independently, the alpha value remaining was 0.05.

Using the air filtering setup described previously, samples were collected from urban and rural locations (**Figures 2 and 3**). We found that the airborne microplastic concentration was significantly higher in urban samples (Mann Whitney U, 2-tailed; urban $n = 6$; rural area $n = 4$; $p = 0.0095$). The number of total microplastics collected in the urban samples greatly outnumbered the total number of microplastics from the rural

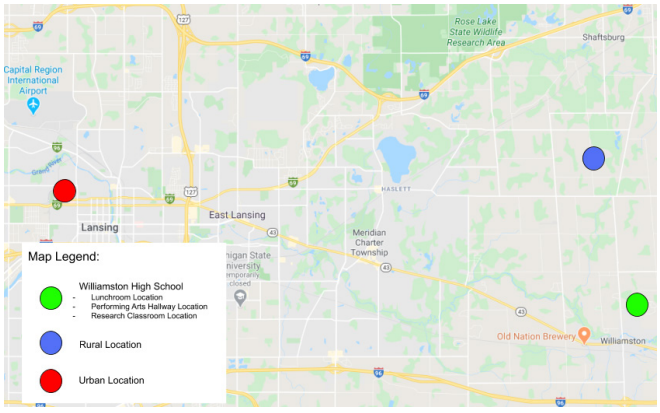

Figure 1. Map displaying the five different locations that were sampled. The research classroom, the lunchroom and the performing arts hallway were all located within the same building.

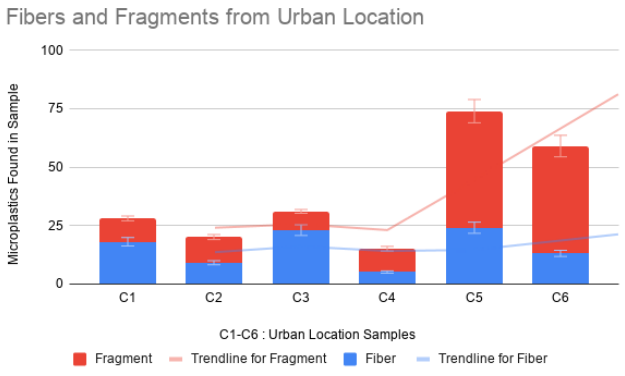

Figure 2. Microplastic fragments and fibers found across the urban location samples (C1-C6). The moving average and error bars (estimated error) are displayed.

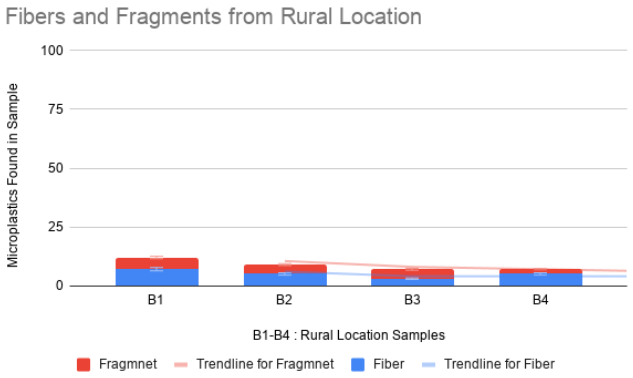

Figure 3. Microplastic fragments and fibers found across the rural location samples (B1-B4). The moving average and error bars are displayed.

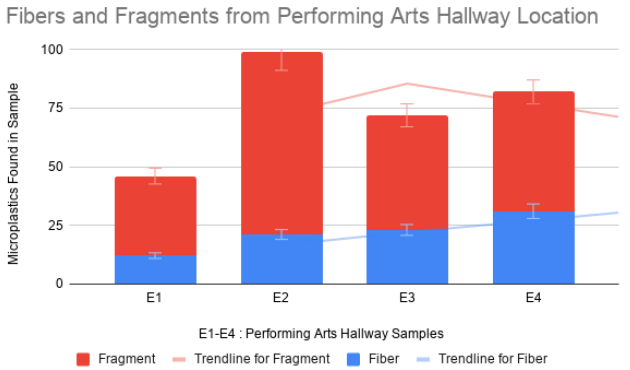

Figure 4. Microplastic fragments and fibers found across the performing arts hallway samples (E1-E4). The moving average and error bars are displayed.

samples. The raw data showed how these two locations varied immensely, in regard to airborne microplastics concentrations.

We wanted to examine an environment that could simulate a high and moderate traffic level. The Williamston High School performing arts hallway and the lunchroom, respectively, were the locations utilized to collect the data (**Figures 4 and 5**). The difference between the amount of microplastics per cubic meter in a hallway sample was not significantly different than that of the lunchroom (Mann Whitney U, 2- tailed; hallway $n = 4$; lunchroom $n = 4$; $p = 0.0286$).

The lunchroom simulated a location with moderate traffic, while the research classroom simulated a location with low traffic (**Figure 5 and 6**). We did not observe a significant difference between the amount of microplastic debris collected from the lunchroom air compared to the classroom air (Mann Whitney U, 2- tailed; lunchroom $n = 4$; classroom $n = 4$; $p = 0.0286$).

Lastly, we sought to compare the average number of microplastic fragments and microplastic fibers from all locations (**Table 1**). There was no significant difference between the average number of microplastic fragments versus fibers across all sample locations (Mann Whitney U, 2- tailed; fibers $n = 5$; fragments $n = 5$; $p = 1.000$).

DISCUSSION

The samples collected during this experiment yielded varying results regarding the comparison of airborne microplastics in multiple locations. The data showed that the concentration of microplastics per cubic meter of air from the urban location was not equal to the microplastics per cubic meter of air from the rural location. The number of airborne microplastics collected from the urban area had higher concentrations compared to those of rural areas. The data indicated that the difference between the microplastics per cubic meter of air from the performing arts hallway compared to the lunchroom, as well as the difference between the microplastics from the lunchroom and research classroom, were both too small to be considered statistically significant. Additionally, we found that there was insufficient evidence to support the hypothesis that the average concentration of fragments versus fibers across all locations were different from each other.

The samples were collected at each different location

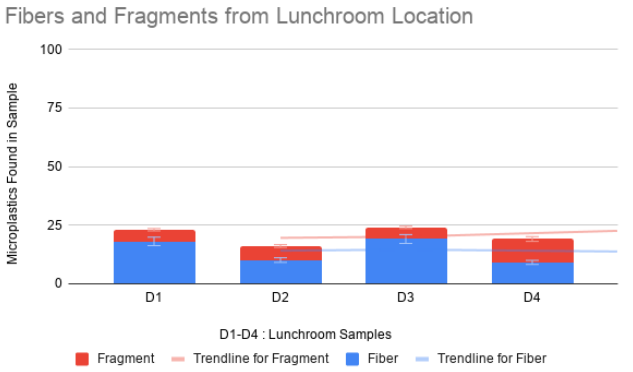

Figure 5. Microplastic fragments and fibers found across the lunchroom location samples (D1-D4). The moving average and error bars are displayed.

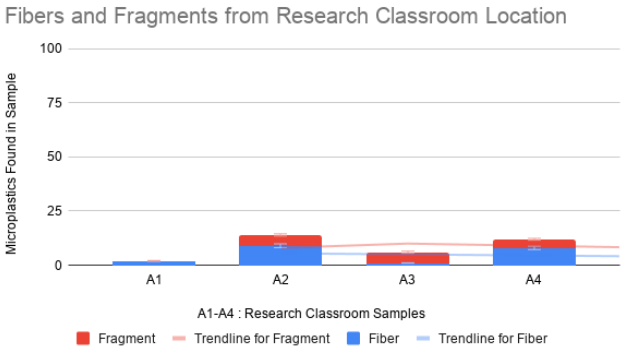

Figure 6. Microplastic fragments and fibers found across the research classroom samples (A1-A4). The moving average and error bars are displayed.

on different days due to time restrictions. This was a key limitation in the study because the varying conditions, such as weather, that each collection date could have an impact on the quantity of microplastics. Another limitation that was encountered during this experiment was how samples that were collected for the urban and rural location had more exposure time to factors that could confound the results. Since these were the two locations that were away from the high school and research room where the data was analyzed, the filter paper had to be transferred outside of the building with glass microscopes slides. During this process, the filters for the urban and rural samples had a higher risk of capturing microplastics from other sources of contamination.

The urban sample was collected with a setup facing W Oakland Avenue, a road that often experiences heavy traffic throughout the day. This location was selected to simulate a metropolitan area with high levels of human and automobile traffic. Cars and other motor vehicles often release microplastics pollutants through mechanical abrasions of the tires (2). Another factor to consider was that the location was next to a residential neighborhood. Since textiles and fabrics are known to release large quantities of microplastic fibers and fragments, clothes washers and dryers can impact the amount of fibers released into the air in certain areas. Previous research has shown that each garment may release approximately 1900 fibers per wash (3). Additionally, regarding the urban samples, the fluctuation in the number of microplastics, specifically fragments, could be due to the various dates and times in which the samples were collected. Samples C1, C2, C3 and C4 were collected on the same Sunday at various points of the day. Sample C5 was collected on a Friday at around 5 PM, and sample C6 was collected on a different Friday at around the same time. Samples C5 and C6 were collected during similar conditions and yielded similar results.

The rural sample was taken in Williamston, Michigan. The setup was facing Lounsbury Road, which did not receive much traffic. Additionally, the location was surrounded by farmland. This location was selected to mimic an agricultural area with low human and automobile traffic. These factors may have contributed to the difference in the number of microplastic debris in the urban and rural sample. The Mann-Whitney U-test gave evidence that the urban air sample contained significantly higher amounts of microplastics, compared to rural air samples (p-value = 0.0095). The urban location was in an area exposed to more factors that could potentially release more microplastics, as opposed to the rural sample, which did not get as much exposure to these elements.

The lunchroom samples were collected by a wall on the edge of the lunchroom in the school building, an area that a limited number of students walked through. On the contrary, the setup for the performing arts hallway was in an area that many students frequently walked through. Both locations had the setup placed on ground level. The number of microplastics in the performing arts hallway was not significantly different from the microplastics in the lunchroom (p-value = 0.0286). An interesting feature of the performing arts hallway samples was that they all contained many microplastics fragments compared to the other locations (**Figure 4**).

The performing arts hallway samples were the only ones to contain these concentrated fragments in small clusters throughout the filter paper. Heavy walking traffic, the height of the air collection setup from ground level, and different air ventilation patterns could possibly explain this difference. Additionally, since the sample was taken at ground level in an area with heavy human exposure, synthetic materials from shoes and fabric could also contribute to the explanation of the microplastic fragments. Even though the lunchroom sample was taken on ground level, there was little human movement.

With a p-value of 0.0286, we did not observe a difference in microplastics between the research classroom and the lunchroom. The classroom sample was collected along a wall of the room on a counter at approximately waist level. There were roughly ten students in the classroom during the times of the air collection. Students in the classroom were required to wear cotton lab coats, which prevented the transfer of microplastics from clothing into the air. Also, since the classroom air sample was taken on a counter, it was not directly exposed to foot movement, or the synthetic materials from shoes.

The goal of this research was to determine whether quantifiable values of airborne microplastics could be detected in varying outdoor and indoor locations. Previous studies have shown similar results regarding the presence of microplastics in the atmosphere. Specifically, one study discussed how the number of airborne microplastics found in an indoor environment will be dependent on the “lifestyle” of the residents and environment of the tested location (6). The conductors of that study concluded that humans are exposed to natural and synthetic fibers when indoors (6). Similarly, our data, collected from the three indoor locations, demonstrated how airborne microplastics can be found in areas with humans. The results of this study showed how human activity can have an impact on microplastic values too.

Although a few possibilities explaining variations in the numbers of microplastics for each location were explored, a limited amount of research has been done to support how these parameters could impact the airborne microplastics concentration. Since only four to six samples were collected per location, the results came from a limited sample size. Additionally, time to collect all the samples was limited, since the data collection period was cut short due to the COVID-19 pandemic.

Future research studies and experiments could focus on the sample intake location, specifically looking at how the floor level, the waist level and the head level could affect results. Another interesting aspect to explore is whether the temperature of the environment impacts the number of airborne microplastics collected. In addition, we recommend

measuring the specific lengths of microplastics detected, as well as whether they are fibers or fragments. Further research should use a larger sample size in terms of the number of air collections from each location. These suggestions will help determine the origin of the microplastics and can be applied to find possible solutions to combat this category of airborne pollution. Understanding the influx of airborne microplastics in various areas is a critical component in learning about the overall quality and conditions of the environment. The data compiled demonstrated how microplastics are currently present in various atmospheres and are more concentrated in certain areas. These findings can be utilized to find realistic measures to prevent the release of more plastic contaminants into the atmosphere. By looking at areas with higher concentrations and narrowing down the sources of this pollution, scientists and engineers can develop new technologies for essential items, such as automobile cars and clothes dryers that release lower amounts of plastic into the air. Although the findings of this experiment yield useful information in the understanding of airborne microplastic contamination, there is still a need for additional research to further the knowledge in this scientific area.

MATERIALS AND METHODS

For each sample that was collected, a blank No. 1 Whatman filter paper (diameter of 42.5 mm) was first examined under the 10x microscope. A ⅛ inch grid was printed on each individual filter to easily quantify the number of microplastics examined. Looking at the filter prior to the air collection ensured that the microplastics that may have been on the filters beforehand were taken into account. To collect reliable samples, a PVC rotameter with a brass flow control valve and an EPR O-Ring was utilized. The rotameter was first mounted onto a retort stand. Using a piece of rubber tubing, a handheld vacuum was connected to the top outlet of the rotameter. The bottom outlet of the rotameter was connected to the outlet in a glass Buchner flask, using a piece of plastic tubing. A rubber bung was inserted at the top of the flask, and the Buchner funnel was placed firmly within the bung. The filter paper was then placed in the Buchner funnel (**Figure 7**). This setup allowed the suction from the vacuum to create a partial vacuum within the flask. When the vacuum was turned on, the suction was able to hold the filter paper in place, while also collecting the circulating air.

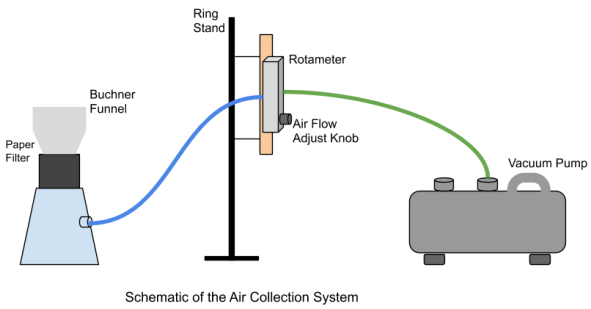

Figure 7. A schematic diagram of the air collection system involving the Buchner funnel, the rotameter and the vacuum pump.

Previous research suggested that there was an average of 5-50 plastic particles found in one cubic meter of air (2). The rotameter was monitored to ensure it ran long enough to collect at least one cubic meter of air to have a reliable sample size. This was done by controlling the volumetric flow of the air collected through the Buchner funnel using the rotameter's valve, which then dictated how long to collect each independent sample. The duration time for all the samples collected ranged from 40-75 minutes. For each location, four to six samples were collected over different days and times to examine the overall numbers of microplastic particles per cubic meter of air. The number of samples that were collected for each location varied because time limitations impeded the ability to collect the same number of samples from each site. The samples were then taken back to the research room at Williamston High School and examined for air contamination on the filter under a 10x microscope. The filter papers were placed under the microscope and visually inspected. Each microplastic fiber or fragment was manually identified, counted, and recorded. Since the filter was examined before the air collection was taken place, we could accurately identify which were the new particles from the sample location.

Five independent locations were tested, which included both urban and rural settings, as well as indoor settings with minimal to heavy human interaction to simulate a low and high population density. The first air samples were taken from inside the research classrooms at Williamston High School on four different days, and each sample was examined independently. These collections spanned from late November to early December. The rural samples were collected from a classmate's house on Lounsbury Road in Williamston, which was surrounded by several large farm fields, over the span of four days in December of 2019. The vacuum was plugged in using an electrical outlet by the side of the house and collected each sample independently. Next, the urban air samples were collected from metropolitan downtown Lansing at St. Andrew Dung Lac Catholic church, located on Oakland Avenue in January to February of 2020.

Indoor samples taken in the lunchroom simulated an area with a low population density. These were collected over the range of two weeks in February of 2020 and occurred during the lunch period, approximately 11:15 AM to noon. The samples for the performing arts hallway took place during the same time of the day. These were collected in February and March of 2020. However, this sample location was by the entrance of the performing arts hallway. Band class took place during this time, which meant that many students walked past this area in the hallway to get to their class. These samples took into account the heavy human interaction and movement and simulated an area with a high population density.

Once all locations were sampled, analyzed, and recorded,

the total count of plastic particles, the color, and the type (fragment or fiber) were recorded in a Google Spreadsheet. The mean and standard deviation of microplastics 5 mm or less per cubic meter of air for each sample location was calculated. Since the three hypotheses evaluate the same issue simultaneously, the alpha value used for these significance tests needed to be adjusted to avoid the probability of making a false statistical inference. The Bonferroni adjustment was used to control the increased chances of making a false inference.

The last hypothesis of this study was looking at a different issue: the average number of microplastic fragments from all locations versus the average number of microplastic fibers from all locations. Since this hypothesis was evaluated independently, the alpha value remained as 0.05. The data for each location was put on separate bar graphs, and the centered moving average was also included. This trendline calculates the average several times for the several subsets within the data. Moving average values were placed at the center of the range for the subset in which the mean value was computed, so the result's average may shift the trendline past the first sample.

These results were then compared using a 2-tailed Mann-Whitney U Test for each hypothesis. This nonparametric test was used because the sample sizes for each location did not meet the statistical guidelines for a parametric test, and normality could not be assumed with the data. A popular factor that is often considered when deciding whether to use a parametric or nonparametric statistical test is the sample size. Oftentimes, a sample size of 30 or more observations is considered sufficient to use a parametric test and assume normality. Since each location in this study had only four to six samples, the sample sizes were too small to meet this requirement. Additionally, with small sample sizes, we had difficulties determining the distribution of the data because the normality tests had inadequate power to provide useful results. Furthermore, a 2-tailed test was performed for each hypothesis to avoid bias of the results. It tested the possibility for both positive and negative differences in the sample distribution and made it possible to distinguish the various statistical relationships among the data, while also avoiding prior assumptions regarding which location would have more microplastics.

ACKNOWLEDGEMENTS

I would like to give a special thank you to Dr. Kurt Guter for all the guidance and advice he has given me throughout this research study.

Received: June 13, 2020
Accepted: November 30, 2020
Published: December 4, 2020

REFERENCES

1. US Department of Commerce, and National Oceanic and Atmospheric Administration. "What Are Microplastics?" *NOAA's National Ocean Service*, 13 Apr. 2016.
2. Gasperi, Johnny, *et al*. "Microplastics in Air: Are We Breathing It in?" *Current Opinion in Environmental Science & Health*, vol. 1, 2018, pp. 1–5., doi:10.1016/j.coesh.2017.10.002.
3. Geyer, Roland, *et al*. "Production, Use, and Fate of All Plastics Ever Made." *Science Advances*, vol. 3, no. 7, 2017, doi:10.1126/sciadv.1700782.
4. Prata, Joana Correia. "Airborne Microplastics: Consequences to Human Health?" *Environmental Pollution*, vol. 234, 2018, pp. 115–126., doi:10.1016/j.envpol.2017.11.043.
5. Chen, Shi-Yi, *et al*. "A General Introduction to Adjustment for Multiple Comparisons." *Journal of Thoracic Disease*, vol. 9, no. 6, 2017, pp. 1725–1729., doi:10.21037/jtd.2017.05.34.
6. Dris, Rachid, *et al*. "A First Overview of Textile Fibers, Including Microplastics, in Indoor and Outdoor Environments." *Environmental Pollution*, vol. 221, 2017, pp. 453–458., doi:10.1016/j.envpol.2016.12.013.

JOURNAL OF
EMERGING INVESTIGATORS

Article

Statistically Analyzing the Effect of Various Factors on the Absorbency of Paper Towels

Lynn Tao[1], Angie Zhang[1], Jane Chi[2]
[1] Thomas Jefferson High School for Science and Technology, Alexandria, VA
[2] Northrop Grumman Mission Systems, Fairfax, VA

SUMMARY

The spread of SARS-CoV2 virus and COVID-19 has caused a surge in demand for paper towels, with a 264% increase in sales growth as customers enhance their hygiene efforts. Though there have been many studies on the characteristics of various paper towels, relatively little research has been performed on how different types of liquid, different fat concentrations, and different properties of paper towels impact their absorbency. In this study, we examined the effect of these factors using samples of the Bounty Select-a-Size paper towels obtained by simple random sampling, and random assignment procedure. We constructed comparative graph displays, verified the data's normal distribution, and performed statistical analysis. A two-sample mean significance test gave us strong statistical evidence to reject the null hypotheses in favor of the alternative hypotheses at the alpha level of 0.05. We found that different liquid types did impact the absorption capability of a paper towel — milk tended to have a higher absorption amount into paper towels than water, and vegetable oil tended to have a higher absorption amount than milk. We also found to a certain degree that fat concentration tended to increase a liquid's absorption amount into paper towels. We reported a cause and effect relationship from the paper towels' properties (whether folded or not) and its absorbency. Our results could help restaurants and other businesses save expenses by minimizing paper towel usage according to spill types and by using paper towels in more efficient ways.

INTRODUCTION

The emergence of SARS-CoV2 and COVID-19 has caused a surge in demand for paper towels and other disposable paper products. Consumers are moving away from reusable cleaning cloths in favor of disposable paper towels out of concerns that reusable cloths may harbor germs if not properly disinfected. Some health experts have also advised using paper towels to disinfect bathroom faucets and door handles to avoid contamination (1). The Bangladesh government further suggested that people should use paper towels instead of jet dryers because paper towels are more effective in removing pathogens missed by ineffective washing (2). Due to suggestions such as this, the paper towel industry saw a 264% increase in sales growth as consumers enhance their hygiene efforts (3). Paper towel companies have advertisements on television, radio, newspapers, magazines, billboards, and even packaging, claiming they are the superior brand. There have also been many studies and projects on the characteristics and evaluation of various paper towels. Five different paper towels were rated on absorption, scrubbing strength, and strength when wet (4). Other studies went further to perform cost analysis based on the absorption of paper towels, questioning if the expensive option is always the most effective (5), or discussed the importance of absorption, strength, and ease of separation among various paper towels (6). A similar study concluded that the paper towel brand Bounty won the comparison in terms of absorption quality (7).

We chose to conduct this experiment for the following three purposes: (i) to learn the effect of liquid type on the absorption ability of paper towels by studying the average absorption of water, milk, and vegetable oil, (ii) to learn how the fat content of a liquid impacts paper towel absorption, and (iii) to assess how different the structure of a paper towel, such as whether they are folded or not, affects their absorption. We identified milk with different fat concentrations (whole milk versus skim milk) and compared their absorption into the same brand of paper towels. We found that paper towels had a significantly higher absorption capacity for vegetable oil, when compared to milk or water. We also found that paper towels when folded absorbed more liquid than when not folded at all. This information would help estimate the number of paper towels required to clean a particular type of spill. In particular, businesses such as restaurants that are seeking to save expenses would be able to minimize the number of paper towels according to the types of the spill and by using paper towels in ways more efficiently. Other than seeking to answer interesting questions, this project aims to add further knowledge on paper towels currently lacking in the literature.

RESULTS

Effect of liquid type

We chose tap water and 2% reduced fat milk as the two experiment groups for this study to determine the effect of liquid spill type because of their easy availability and different properties. For each test, we used one sheet of Bounty Select-a-size paper towel and submerged it into a liquid, either water or milk, in a large graduated cylinder. We then pulled the towel out of the liquid, keeping it above the

JOURNAL OF
EMERGING INVESTIGATORS

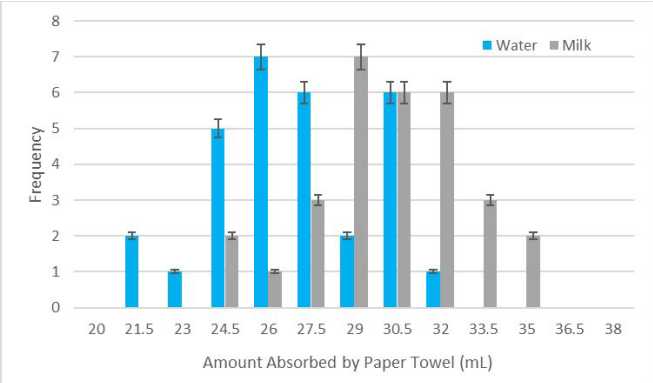

Figure 1. Paper towels absorb more milk than water. The number of times that a paper towel absorbed a specific volume (mL) of milk (grey) or water (blue) was recorded (n = 30 trials per liquid). Error bars denote standard error.

cylinder until it stopped dripping. Next, we measured the absorbency as the volume (mL) of liquid absorbed by one sheet of the paper towel, reflected as the changes between the initial and final marks on the cylinder. We observed the shape, outliers, center, and spread of the data distribution for each experiment group before conducting two-sample t-test analysis.

The shape of the distribution displayed a slight right skew for the water treatment and a slight left skew for the milk treatment on the comparative histogram (bar graph) (**Figure 1**). Right skewing indicated that the mean was greater than the median for water treatment, while left skewing indicated that the mean was less than the median for milk treatment. Data from the final summary statistics (**Table 1**), as 27.738 mL (mean) > 27.60 mL (median) in the case of water treatment and 30.993 mL (mean) < 31.60 mL (median) in the case of milk treatment, confirmed the shape distribution tendency on the histogram. However, the skews were miniscule enough that they did not affect the assumption about the normal distribution of the experiment data.

We calculated outliers using the summary statistics (**Table 1**). The interquartile range (IQR) was multiplied by 1.5, added to the third quartile (Q3) and subtracted from the first quartile (Q1) to produce a range of non-outlier values. The range of non-outlier values for the water treatment was 18.95 – 37.35 mL. There were no outliers for the water treatment dataset as no value was less than 18.95 mL or more than 37.35 mL. On the contrary, two low outliers appeared for the milk group dataset but with minimal significance due to their closeness to the range of non-outlier values.

The central tendency analysis showed that a paper towel tended to absorb approximately 27.60 mL of water and approximately 31.60 mL of milk on average (**Table 1**). Therefore, the central tendency for the absorption for the milk was greater than water. In fact, 14.50% more milk than water could be absorbed into a paper towel on average.

Because of the slight skew of the datasets, the interquartile range is the most appropriate measure of spread in this context compared to the sample standard deviations (8). The interquartile range (IQR) was 4.60 mL and 2.80 mL for the water and milk treatment datasets respectively (**Table 1**). The spread of the water treatment was approximately 1.64 times that of the milk, as there tended to be more variability in the water data values than in the milk data values. Since the sample sizes were equal for both treatments, there may have been other factors between the two liquids that influenced this variability. The normal quantile plots for the water vs. milk treatment groups (**Figure 2**) suggested the experiment data for water and milk treatment groups followed the normal distribution.

Based on the two-sample t-test, the *p*-value was 9.038 x 10^{-6} and the confident interval at a 95% confidence level

Experiment Test	Treatment Group	Sample Size	Mean	Standard Deviation (S)	Min	Quartile 1 (Q1)	Median (Q2)	Quartile 3 (Q3)	Max
effect of liquid type	water	30	27.738 mL	2.741 mL	22.30 mL	25.85 mL	27.60 mL	30.45 mL	33.20 mL
	milk	30	30.993 mL	2.653 mL	25.10 mL	29.50 mL	31.60 mL	32.30 mL	36.30 mL
effect of fat concentrations	whole milk	30	23.983 mL	1.095 mL	21.5 mL	23.5 mL	24.0 mL	24.5 mL	27.0 mL
	skim milk	30	26.833 mL	0.735 mL	25.0 mL	26.5 mL	27.0 mL	27.38 mL	28.5 mL
	vegetable oil	30	37.667 mL	0.968 mL	35.5 mL	37.0 mL	37.5 mL	38.0 mL	40.0 mL
effect of a paper towel's structure	no folding	30	22.759 g	1.826 g	19 g	21g	23 g	24 g	26 g
	folded	30	34.897 g	2.110 g	30 g	34 g	35 g	36 g	39 g

Table 1. Summary Statistics for Each Treatment Group. The experiments testing the effect of liquid type and the effect of fat concentrations measured the amount of liquid absorbed by paper towels in milliliters (mL). The experiments testing the effect of the structure of paper towels measured the mass of paper towel after fully absorbed in water, in grams (g).

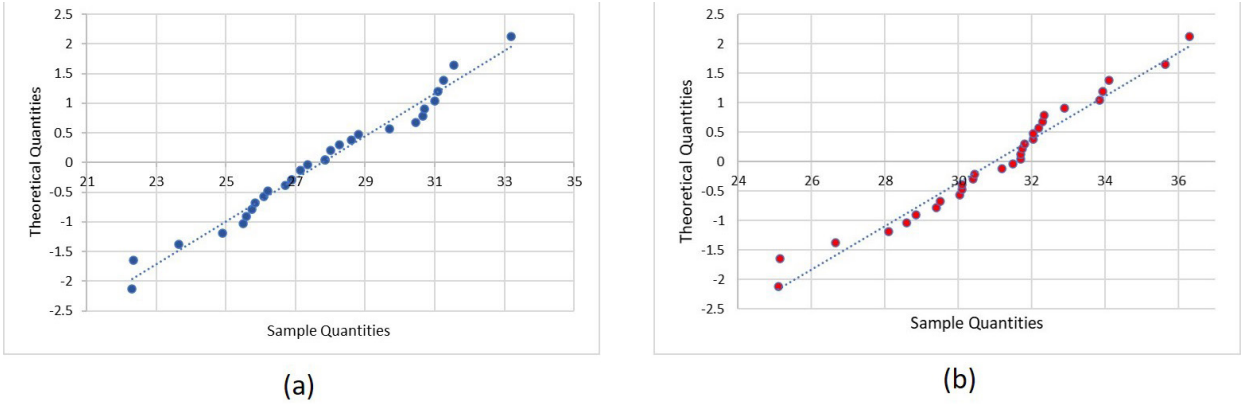

Figure 2. Sample data are in a normal distribution. We plotted the sorted data vs. values selected for the samples (n = 30). The data points are roughly close to a straight dotted line. (a) Water sample data passed the pencil test. (b) Milk sample data passed the pencil test.

was (1.827, 4.683) mL for the study of the effect of liquid type (**Table 2**). Since the *p*-value was less than 0.05, we rejected the null hypothesis in favor of the alternative hypothesis at the alpha (α) level of .05. The mean volume of water absorbed was less than the mean volume of the milk absorbed by the Bounty paper towels, and the difference between the mean volume of absorption was within the confident interval.

Our results were significant due to the fact that zero did not fall within this interval, confirming that the *p*-value obtained in our two-sample t-test was statistically significant. This suggested a cause and effect relationship between the type of liquid (water or milk) and its absorbency into paper towels.

Effect of fat concentrations

In order to determine the effect of fat concentrations, we used whole milk, skim milk and vegetable oil as the three experiment groups. These three types of liquids are widely available at grocery stores and have distinct fat concentrations. Whole milk has approximately 3.5 percent fat by weight while skim milk has 0 gram of fat, and both have 8 grams of protein per 8-ounce glass (9, 10). On the other hand, vegetable oil contains 100% fat. We followed a similar procedure as the above experiment for the effect of liquid type. For each test, one sheet of Bounty Select-a-size paper towel was fully saturated by dipping it into a liquid. The towel was then pulled out of the cylinder and hung in the air until it stopped dripping. The amount of liquid absorbed was measured as the changes between the initial and final marks on the cylinder. We observed the shape, outliers, center, and spread of the data distribution for each experiment group before conducting two-sample t-test analysis.

The distribution displayed a slight left skew for the whole milk and the skim milk treatment groups and a slight right skew for the vegetable oil treatment on the comparative histogram (bar graph) (**Figure 3**). Data from the final summary statistics (**Table 1**) confirmed the shape distribution tendency on the histogram. The skews were too insignificant to affect the assumption about the normal distribution of the experiment data.

Based on the data from the summary statistics (**Table 1**), the whole milk group had one lower and one upper outlier. There was one upper outlier for the vegetable oil group and no outlier for the skim milk group. All the outliers

Experiment Test	Treatment Group	Df	Test Statistic	p-value	T-critical Value	Confident Interval at 95% Confidence Level
effect of liquid type	water vs. milk	57.9	-4.67	9.038×10^{-6}	2.0018	(1.827, 4.683) mL
effect of fat concentrations	whole vs. skim Milk	51	-11.84	2.995×10^{-16}	2.0078	(2.376, 3.333) mL
	skim milk vs. vegetable oil	54	-48.82	2.314×10^{-46}	2.0048	(10.388,11.278) mL
effect of a paper towel's structure	flat vs. folded paper towel	56	-23.73	6.696×10^{-31}	2.0032	7.673, 15.763 g

Table 2. Two-Sample T-test Results (at significance level an alpha (α) = .05) and the Confidence Interval (at 95% Confidence Level). *p*-value (< 0.05) indicates that the experiments support the alternative hypothesis. The comparison of water vs. milk, and skim milk vs. vegetable oil shows that liquid type affects the absorption capacity of paper towels. The comparison of whole milk vs. skim milk vs. vegetable oil suggests that fat contents in liquid potentially impact how much paper towels absorb a liquid. The comparison of flat vs. folded paper towel indicates that certain property of paper towels makes a difference in their absorption ability.

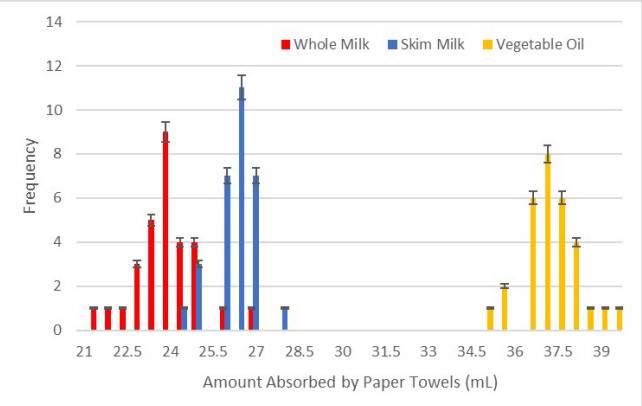

Figure 3. Paper towels absorb much more vegetable oil than milk. Among milk, paper towels absorb more skim milk than whole milk. The number of times that a paper towel absorbed a specific volume (mL) of whole milk (red), skim milk (blue), or vegetable oil (yellow) was recorded (n = 30 trials per liquid). Error bars denote standard error.

were not significant enough to affect the data analysis.

The central tendency analysis revealed that the absorption for the skim milk is 3 mL greater, or 12.5% greater than that for the whole milk. The absorption for vegetable oil was 10.5 mL, or 39.62%, greater than skim milk. The interquartile range (IQR) was 1.0 mL, 0.875 mL, and 1.0 mL for the whole milk, skim milk, and vegetable oil treatment group, indicating their having similar variability among the samples.

Based on the two-sample t-test, the *p*-value was 2.99461×10^{-16} for the whole milk vs. skim milk test (**Table 2**) and was much less than 0.05, so we rejected our null hypothesis in favor of the alternative hypothesis at the alpha (α) level of 0.05, which showed that the mean amount of whole milk absorbed (mL) was less than the mean amount of skim milk absorbed (mL) by the same type of Bounty paper towels. The t-critical value was 2.0078 and the confidence interval was (2.376, 3.333) mL (**Table 2**). As this interval did not include zero, we were 95% confident that the difference between the mean volume of absorption for whole milk vs. skim milk was within this interval, and thus our results were statistically significant at a 95% confidence level. This experiment suggested a cause and effect relationship from the fat concentrations of milk to its absorbency into paper towels.

Similarly, the two-sample t-test for skim milk vs. vegetable oil yielded a *p*-value of 2.314×10^{-46}, so we rejected our null hypothesis in favor of the alternative hypothesis at the alpha (α) level of 0.05 — the mean amount of vegetable oil absorbed (mL) was much more than the mean amount of skim milk absorbed (mL) by the paper towels. The t-critical value was 2.0048 and the confidence interval was 10.388 – 11.278 mL (**Table 2**), thus we were 95% confident that the difference between the mean volume of absorption for skim milk vs. vegetable oil was within this interval, and that our results was statistically significant at 95% confidence level in showing a cause and effect relationship from the fat concentrations of a liquid to its absorbency into paper towels.

Effect of the structure of a paper towel

In this experiment, we chose to compare a folded vs. not-folded paper towel to determine the effect of a paper towel's structure because folding a towel is an easy operation to implement. It also addresses an interesting question in daily life about whether we should fold a towel to efficiently clean up a spill. In this experiment, we folded half of the total paper towels on a flat surface and pressed them tightly to compact them into smaller, thicker squares. We soaked a paper towel, either folded or not-folded, thoroughly with water, hung it in the air until it stopped dripping, and put it on a scale. We measured the amount of liquid absorbed as the mass (gram) of the paper towel. We observed the shape, outliers, center, and spread of the data distribution for each experiment group before conducting two-sample t-test analysis.

The shape of the distribution displayed a slight left skew for both the flat paper towel and the folded paper towel groups on the comparative histogram (bar graph) (**Figure 4**). Data from the final summary statistics (**Table 1**) confirmed these slight and insignificant skews, which did not affect much the data distribution characteristics.

Based on the data from the summary statistics (**Table 1**), two low outliers (30 g) showed up for the folded paper towel group while no outlier appeared for the flat paper towels. The interquartile range IQR was same for both the folded and flat paper towel groups, which also indicated that these two groups tended to have similar variability among the samples.

The central tendency analysis for folded vs. flat paper towels showed that folded paper towels are much more absorbent than flat paper towels. The absorption for the folded paper towels was 12g, about 52.18% greater than flat paper towels that were not folded.

The t-test gave a *p*-value of 6.696×10^{-31}, and the confidence interval of (7.673, 5.763) g (**Table 2**), thus

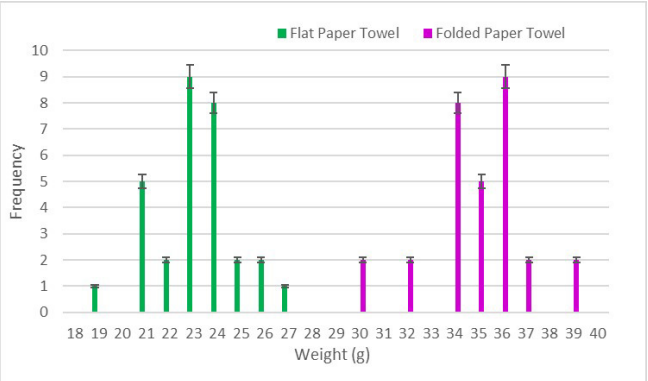

Figure 4. Paper towels absorb more liquid when folded up. The number of times that a paper towel absorbed a specific mass (gram) of flat paper towel (green) or folded paper towel (purple) was recorded (n = 30 trials per liquid). Error bars denote standard error.

we rejected our null hypothesis in favor of the alternative hypothesis at the alpha (α) level of 0.05 for this experiment. The average mass of water absorbed by a paper towel when folded was much more than the average mass absorbed by the same type of Bounty paper towel when not folded. Our results were statistically significant at the 95% confidence level and indicated a cause and effect relationship between different paper towel structures (folded vs. flat) and absorbency into paper towels.

DISCUSSION

We found that paper towels had a significantly higher absorption capacity for milk when compared to water. A possible explanation to support these findings may be because of the higher viscosity of milk due to its fat content (11). Fat molecules tend to cling to layers of paper material (12). Another reason could be because 2% milk fat has an average density ranging from 1.026–1.034 g/cm^3, while water has an average density of 1 g/cm^3 (13, 14). The slightly higher density of milk could influence the higher absorption amount of milk into Bounty paper towels.

To understand the effect of fat content on the absorption, we compared the absorption of whole milk, skim milk, and vegetable oil by the Bounty paper towels. It was surprising to see that skim milk had a higher absorbance than whole milk when whole milk should have a slightly higher viscosity than skim milk. However, a possible explanation could be that when the fat is stripped from whole milk to become skim milk, the skim milk is fortified with synthetic vitamins and milk solids to replace the lost proteins and calcium. These vitamins and solids may have greater attractive properties to the material of the paper towel. These substances could also have a substantially large mass that trapped them between the molecular spaces, increasing the overall absorbance for skim milk.

As expected, we found that paper towels had a significantly higher absorption capacity for vegetable oil, when compared to milk. Vegetable oil is mainly composed of fat and thus has a much higher viscosity than milk. Due to the large size of the fatty acid chains in vegetable oil, the triglycerides may be more easily trapped between the molecules of the paper towel. Hydrophobic interactions could also group fat molecules closely together in an otherwise hydrophilic surrounding due to the polar composition of paper towels (15). Furthermore, oil's high viscosity decreases leakage from the towel after the liquid has been absorbed. On the other hand, milk has a less viscous composition and smaller molecules (lactose, water, minerals, proteins, less fat) compared to vegetable oil that allow milk to escape from the paper towel more easily.

When testing the structure of paper towels, we found that paper towels when folded had a higher absorption capacity than when not folded at all. This may be explained by the properties of paper. In general, paper readily absorbs water because it is made of cellulose, which is hydrophilic. Paper towels are made to have empty spaces between their cellulose fibers to be especially absorbent. Water molecules tend to fill these empty spaces as they are absorbed by the cellulose in paper towels. Folding a paper towel creates more layers for water to fill, which is why the folded paper towels could hold more water and higher mass in the experiment. The study suggests that folded paper towels are more efficient at cleaning up spills and that we could use fewer paper towels for the same job if we use them properly.

One important note is that we were not able to purchase the exact same type of Bounty paper towels for the part two and part three of the experiment as the first part (the blank white vs. flowery print type). Our initial thought was to compare the results from all parts of the experiment together, but the difference in the paper towel type (though from the same brand) forced us to limit the comparison. We also question whether absorption potential is specific to brand, towel, or roll type.

For further study, we recommend data collection of the absorption of several different liquid types to obtain a wider range of knowledge about the properties of a variety of liquids. For example, we could test fruit juice, carbonated soda, and amongst others. Comparing these results would help us learn more about the effect of viscosity and/or surface tension on the amount absorbed. Another interesting experiment may be to test the impact of other properties of paper towels such as different types (i.e. flowery vs. bland Bounty) from the same brand.

METHODS

The experimental design description (**Figure 5**) outlines the experimental design, which can also be visualized in a simple graphic (**Figure 6**). To carry out our experiment, we ran independent trials, one paper towel sheet for each

Experimental Design Description

Explanatory Variable (IV):	The explanatory variable in this experiment is the "type of the liquid spill" (water vs milk, whole milk vs skim milk, milk vs vegetable oil), or the "property of paper towel" (folded vs flat). This variable is categorical and binary.	
Treatments:	Water (100 mL)	Milk (100 mL)
	Whole Milk (100 mL)	Skim Milk (100 mL)
	Milk (100 mL)	Vegetable Oil (100 mL)
	Folded Paper Towel	Flat Paper Towel
Number of Repeated Trials:	30 repeated trials (using one sheet of paper towels in each independent trial)	30 repeated trials (using one sheet of paper towels in each independent trial)
Response Variable (DV):	The response variable in this experiment is the "amount of liquid absorbed by one sheet of paper towel" (measured in mL) or the "mass of paper towel fully absorbed with water" (measured in gram). This variable is quantitative.	
Constants:	- Type (brand) of paper towel - Size of paper towel - Types (brands) of milk - Type of water - Measuring tool (graduated cylinder) - Measuring unit (mL,g) - Tool used to saturate the paper towel with the liquid (tweezer) - Location in which the experiment is performed.	

Figure 5. Experiment Design Description. Explanatory Variable is also called Independent Variable (IV). Response Variable is also known as Dependent Variable (DV). Four pairs of treatments are listed, each will test one hypothesis regarding to the experiment purpose.

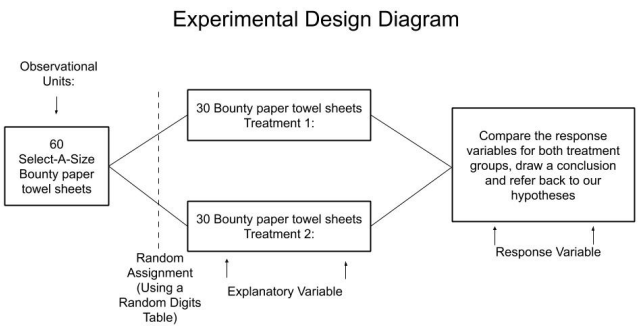

Figure 6. Experiment Design Diagram. During the experiment, a treatment (i.e. type of liquid) is imposed onto observational units (paper towels) in order to gather data on a response variable. The confounding variables balance out through random assignment of paper towels to treatments. Random Assignment creates treatment groups that are similar in all aspects, so the statistically significant difference in the data collected can be attributed to a cause and effect relationship.

trial. Each trial was independent because we measured the absorbance amount of each sheet of paper one at a time so that the trials did not affect one another.

We used two types of hypotheses in this study: a null hypothesis and an alternative hypothesis. The null hypothesis (H_0) was the one we attempted to disapprove. The alternative hypothesis (H_a) was the one we suspected to be true and attempted to prove.

For example, for the experiment of water vs. milk, we let μ_W and μ_M represent the mean amount of water (mL) and milk (mL) absorbed by all Select-a-Size paper towels by the paper towel brand Bounty. The Mathematical null hypothesis is H_0: $\mu_W = \mu_M$. The contextual null hypothesis H_0 was: the mean amount of water absorbed by all Bounty Select-a-Size paper towels is equal to the mean amount of milk absorbed by all Bounty Select-a-Size paper towels at the α-level of .05. The Mathematical alternative hypothesis is H_a: $\mu_W < \mu_M$. The contextual alternative hypothesis was: the mean amount of water absorbed by all Bounty Select-a-Size paper towels is significantly less than the mean amount of milk absorbed by all Bounty Select-a-Size paper towels at the α-level of .05

Experiment Setup

During the experiment, we randomly assigned the observational units to the treatment groups. Thirty sheets of paper towels were randomly assigned to each of the two treatment groups (water or milk, whole milk or skim milk, etc.) to be measured of each of their amounts of absorbance of liquid. The random assignment process of paper towels was done using a Random Digits Table as described below.

Randomization

Randomization was key in the experiment. We implemented both simple random sampling and random assignment in this study. Simple random sampling was implemented into the process to obtain our observational units. In our experiments, we took 60 sheets from one roll of paper towels (regarded as independent) as the paper towels were formed as a large sheet before they were cut and randomly sorted into packages during the manufacturing process. This gave all of them an equal chance to be part of this study. In addition, random assignment was implemented into the process to sort our observational units into our two treatment groups to limit the influence of confounding variables. We numbered each paper towel sheet with a number from 1–60 and using a Random Digits Table to determine which digits belonged to which group.

The randomization protocol in the experiment was as follows: We numbered each of the 60 sheets of paper from 1–60. Then, using a Random Digits Table and starting at any row, we began counting the first two numbers of the five-digit numbers, disregarding any values greater than 60 and any repeats. If necessary, we chose another row of random numbers. The occurrence of the digit zero allowed for the possibility of choosing a towel marked with one digit (01, 03, 09). After recording 30 distinct numbers between 1 and 60, the corresponding paper towel sheets (the ones with the same numbers given to them) would be part of one treatment group (i.e. water) and the remaining 30 would be part of the other group (i.e. milk). These two treatment groups each had their own separate towel stack.

Data Collection

For each trial in experiment part one (water vs. milk) and part two (whole milk vs. skim milk vs. vegetable oil), we measured 100 mL of liquid with a graduated cylinder and dipped the sheet of paper towel in the liquid until it was fully saturated and could absorb any more liquid. We then recorded the milliliters of liquid absorbed into each sheet. Then, we subtracted the remaining amount of water in the graduated cylinder from the original amount, thus obtaining the number of milliliters of liquid that was absorbed into a sheet of paper.

For the experiment regarding paper towel structure (folded vs. flat paper towel), we placed a paper towel flat on the table surface, wet it thoroughly using water, and then hung it until all of the excess water dripped out. We then weighed the paper towel on the kitchen scale, and recorded the mass. For each trial of the folding paper towel, we followed a similar procedure as for a flat paper towel, except that we first folded it twice by the middle line so it turned into a rectangular-shaped small paper towel in four layers before wetting it. We kept it still folded when we hung it.

Statistical Analysis

In Rossman and Chance (2011), three conditions are required for a two-sample t-test (8): 1) populations are greater than ten times the sample sizes, 2) random assignment of subjects to treatments (experiment) or independent random samples from two populations (observational study) is

satisfied by using random assignment, and 3) sample size (n) is greater than or equal to 30 or population is normally distributed. This condition is satisfied by a sample size of 30 paper towels.

The standard error of the sample mean can be calculated by the following formula (16):

$$SE_{\bar{x}} = \sqrt{\frac{s_W{}^2}{n_W} + \frac{s_M{}^2}{n_M}}$$

Test Statistic can be obtained by this expression (16):

$$\frac{\bar{x}_W - \bar{x}_M}{\sqrt{\frac{s_W{}^2}{n_W} + \frac{s_M{}^2}{n_M}}}$$

The degree of freedom is one less than the sample size. It can also be found on a TI-84 calculator (Stat=>Tests=>TwoSampleT-test). Similarly, *p*-value can be obtained on calculator as well where *p*-value = Pr (T_{df} < t).

To construct a Confidence Interval: we use a 95% confidence level (t-interval) which can be calculated using formula (16):

$$(\bar{x}_W - \bar{x}_M) \pm t^* \sqrt{\frac{s_W{}^2}{n_W} + \frac{s_M{}^2}{n_M}}$$

where the critical value can be obtained on calculator by t* of 95% CI = InvT (probability, df) = InvT (0.975, df). The probability is calculated as the sum of confidence level (95%) and the left tail (2.5%).

ACKNOWLEDGEMENTS

We would like to take this opportunity to sincerely thank our teacher and supervisor, Mr. Jurj. Because of your teaching, we've come to love statistics and really enjoy the project. Your advice on our research, from topic selection, to randomization of data collection, and to statistical analysis methods are really crucial. Your encouragement and timely response brightened our day and we learned a lot.

We also really appreciate our parents for their support and unconditional love during the project. You helped us get all the supplies and materials that we needed. You don't mind us making a mess in the kitchen. Because of your support, we really enjoyed the project.

Received: June 9, 2020
Accepted: November 23, 2020
Published: December 4, 2020

REFERENCES

1. Research and Markets. "Paper Towel Industry sees 264% Growth due to the Coronavirus as Consumers Move Away from Reusable Cleaning Cloths." *GlobeNewswire*, 28 Apr. 2020, www.globenewswire.com/news-release/2020/04/28/2023224/0/en/Paper-Towel-Industry-sees-264-Growth-due-to-the-Coronavirus-as-Consumers-Move-Away-from-Reusable-Cleaning-Cloths.html. Accessed 11 Nov. 2020.
2. McNamara, Kelly. "Paper towels may remove virus missed by poor hand washing: study." *Bangladesh Government News*, 17 Apr. 2020, www.thejakartapost.com/life/2020/04/17/paper-towels-may-remove-virus-missed-by-poor-hand-washing-study.html. Accessed 11 Nov. 2020.
3. "COVID-19's Impact on the Paper Towel Market; 264% Sales Growth as Consumers Enhance Their Hygienic Efforts." *PR Newswire*, 27 Apr. 2020, www.prnewswire.com/news-releases/covid-19s-impact-on-the-paper-towel-market-264-sales-growth-as-consumers-enhance-their-hygienic-efforts-301047562.html.
4. Napsha, Joe. "Students bring home science awards at Queen of Angels in North Huntingdon." *The Pittsburgh Tribune-Review*, 15 Mar. 2016, archive.triblive.com/news/students-bring-home-science-awards-at-queen-of-angels-in-north-huntingdon/. Accessed 11 Nov. 2020.
5. "Top scientist leads school." *Albert & Logan News*, 1 June 2011 Accessed 11 Nov. 2020.
6. Ciaramidaro, Rebecca. "The Wipe Stuff." *Choice*, Apr. 2019, pp. 47-49.
7. Ritchie, Paulette Lash. "New experiments, experiences." *The St. Petersburg Times*, 7 Dec. 2006 Accessed 11 Nov. 2020.
8. Rossman, Allen, and Beth Chance. Workshop Statistics: *Discovery with Data*. 2006, ISBN: 978-0-470-54209-5. Accessed 11 Nov. 2020.
9. Ferdman, Roberto. "The whole truth about 'whole milk.'" *Washington Post*, 3 Oct. 2014, www.washingtonpost.com/news/wonk/wp/2014/10/03/whole-milk-is-actually-3-5-milk-whats-up-with-that/. Accessed 11 Nov. 2020.
10. "Get the Facts: Types of Milk Explained." *Milk Life*, edited by MilkPep, America's Milk Companies, milklife.com/articles/nutrition/types-of-dairy-milk. Accessed 11 Nov. 2020.
11. Sarma, K. S. *Physical Chemistry of Milk*. 2012. *e-Krishi Shiksha*, ecoursesonline.iasri.res.in/mod/page/view.php?id=4164. Accessed 12 Nov. 2020.
12. Blamire, John. "The Giant Molecules of Life: Lipids and Polysaccharides." *Science at a Distance*, 1999, www.brooklyn.cuny.edu/bc/ahp/SDPS/SD.PS.LipPol.html. Accessed 12 Nov. 2020.
13. Paar, Anton. "Density measurement of milk and dairy products." *The Engineer*, 28 Feb. 2017, www.theengineer.co.uk/supplier-network/product/density-measurement-of-milk-and-dairy-products/. Accessed 12 Nov. 2020.
14. "Water Density." *United States Geological Survey*, www.usgs.gov/special-topic/water-science-school/science/water-density?qt-science_center_objects=0#qt-science_center_objects. Accessed 12 Nov. 2020.
15. Karapanagiotis, Ioannis, *et al*. "Facile Method to Prepare Superhydrophobic and Water Repellent Cellulosic

Paper." *Journal of Nanomaterials*, 11 Feb. 2015, www.hindawi.com/journals/jnm/2015/219013/. Accessed 12 Nov. 2020.
16. Tabor, Starnes, *et al*. *The Practice of Statistics*. Bedford, Freeman & Worth, 2018. Accessed 11 Nov. 2020.

JOURNAL OF
EMERGING INVESTIGATORS

Article

Effects of Prolonged Azithromycin Therapy on Bacterial Resistance to Functionally Analogous Antibiotics

Ethan Gibbs[1] and Jennifer Gibbs[1]
[1] Olentangy High School, Lewis Center, Ohio

SUMMARY

Bacteria may be innately resistant to antibiotics or acquire antimicrobial resistance through a variety of mediums. Under certain conditions, bacteria develop cross-resistance, a reduction in susceptibility to many antibiotics they have never been exposed to before. Most frequently, chemical similarities between antibiotics cause cross-resistance since bacterial defenses are counteractive to a specific molecule. However, cross-resistance to many chemically different antibiotics can occur when bacteria mutate to develop non-specific defenses. This study investigated a subject who had received prolonged azithromycin therapy for a neuropsychiatric condition related to chronic Group A Streptococcus infection. Given the possibility of cross-resistance, we hypothesized that, after prolonged azithromycin therapy, any bacteria collected from the subject would be resistant to structurally analogous antibiotics. We also hypothesized that, if bacteria from the subject had developed metabolic mutations, resistance to functionally analogous antibiotics would be present. From a series of antibiotic susceptibility tests, we concluded that the subject bacteria were resistant to erythromycin, a structural analog of azithromycin, but exhibited standard sensitivity to functional antibiotic analogs. The results of our study will help identify the risks associated with prolonged antibiotic therapy for a variety of conditions.

INTRODUCTION

The positive effects of antibiotics on human health have been unparalleled by any other pharmaceutical for the past five decades. Within recent years, however, bacterial resistance to antibiotics has grown exponentially as new resistant mutants continue to develop and spread (1). The World Health Organization (WHO) states that excessive prescription of antibiotics is a primary contributor to the development of resistance, which can occur for many reasons, such as over-the-counter availability (2). Our ability to control the spread of human pathogens has slowed as the rate that bacteria gain resistance far exceeds the rate at which we create new antibiotics. Additionally, studies have shown that the use of antibiotics limits the ability of human systems to perform vital functions and shield against future infections (3, 4). Because of these factors, many common infections associated with antibiotic therapy are becoming more difficult, if not impossible, to treat, making antibiotic resistance one of the biggest threats to universal health (2).

Bacteria may have innate resistance or gain resistance to one or more classes of antibiotics through genetic mutations and gene transmission from one bacterium to another. Bacteria survive by employing these resistance mechanisms to counteract the effect of the antimicrobial agents (5). In the context of this study, antibiotics that function by inhibiting protein synthesis are rendered less effective when bacteria change their ribosome structure (6). Modifications, such as this, are how bacteria develop cross-resistance, a reduction in susceptibility to many antibiotics they have never been exposed to before (7). Szybalski and Bryson (1952) reported that chemical similarities between antibiotics are most often the cause of cross-resistance because bacterial defenses are counteractive to a specific molecule (8). However, cross-resistance to many chemically different antibiotics can also occur when the metabolic pathway they attack is altered (8). For example, macrolide antibiotics rely on inhibiting the translation of mRNA into protein. If bacteria alter their ribosomes in response, the efficacy of all functionally similar antibiotics decreases. Following these findings, a study by Gutmann and colleagues (1988) found that mutations correlated with cellular metabolic activity, such as reduced membrane permeability, can cause resistance to multiple antibiotic classes as well (9).

In this case study, we studied the effect of prolonged antibiotics on bacterial resistance development on a subject who had received azithromycin therapy for over five years to treat a pediatric autoimmune neuropsychiatric disorder associated with streptococcus (PANDAS) (10). PANDAS is a disorder characterized by the development of obsessive-compulsive disorder (OCD), motor tics, and abnormalities in behavior. The disease traditionally manifests in younger patients and is associated with the presence of Group A streptococcus (GAS) infections. Prolonged use of antibiotics (most commonly beta-lactams and macrolides) to prevent future streptococcal infections is appropriate for severe cases of this disorder (10). Currently, we are limited in our understanding of the effects of extensive azithromycin therapy on bacterial resistance in patients. Affected bacteria may have directly evolved mutations to counteract the mechanisms of antibiotics or received resistance genes from other bacteria.

Considering the possibility of cross-resistance, the

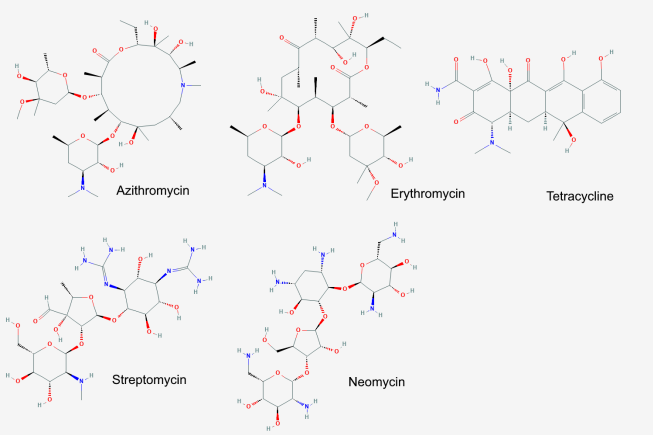

Figure 1. Molecular structures of azithromycin, erythromycin, tetracycline, streptomycin, and neomycin. Top row, from left to right: azithromycin, erythromycin, tetracycline. Bottom row, from left to right: streptomycin, neomycin. Note the similarities between macrolides erythromycin and azithromycin. Also, note the similarities between aminoglycosides neomycin and streptomycin. Depictions of molecular structures obtained from PubChem.

aim of this work was to elucidate the effects of prolonged azithromycin therapy on bacterial resistance in the subject. Erythromycin, tetracycline, streptomycin, and neomycin were selected because they are functionally analogous to azithromycin. These antibiotics have similar ways of inhibiting bacterial growth; however, they do not all have similar chemical structures (11-15). Of the four antibiotics, erythromycin is the only one structurally analogous to azithromycin, while tetracycline, streptomycin, and neomycin have dissimilar structures (**Figure 1**). We hypothesized that after prolonged azithromycin therapy, any bacteria collected from the subject would be resistant to structurally analogous antibiotics. Additionally, under the condition that bacteria from the subject had developed mutations, we predicted that resistance to antibiotics that are functionally analogous to azithromycin would be present.

Our results indicated that the bacteria collected from the subject were completely resistant to erythromycin while having above standard sensitivity to tetracycline, streptomycin, and neomycin. Overall, the results of this case study will aid in identifying the risks associated with antibiotic treatment significantly longer than the standard duration.

Trial #	Erythromycin (mm)	Tetracycline (mm)	Streptomycin (mm)	Neomycin (mm)	Control (mm)
1	0	40	20	32	0
2	0	40	22	36	0
3	0	38	18	34	0
4	0	42	18	32	0
5	0	38	17	28	0
Average	0	39.6	19	32.4	0
SD	0	1.67	1.79	2.97	0

Table 1. Raw data for each of the five trials. The diameters (mm) of the inhibition zones after 18 hours of incubation were recorded. Four different antibiotics disks were tested along with one blank disk for a control. The average diameters for each disk and the standard deviation across all trials were also calculated.

RESULTS

Rationale for Interpretation

To interpret our results, we compared the recorded data (**Table 1**) to interpretive standards for antibiotic susceptibility (**Table 2**). Health professionals create interpretive standards to indicate the sensitivity of bacteria to an antibiotic based on the size of their zone diameter. We obtained values for the interpretive standards of each antibiotic from a study by Sarker *et al.* (16) which used the disk diffusion method and swabbed bacteria from similar locations. There are different acceptable diameters for each antibiotic depending on the concentration used, however, **Table 2** corresponds with the standardized concentrations determined to be most effective. The antibiotic disks we used in this study were of the standard concentrations of erythromycin (15 µg/disk), tetracycline (30 µg/disk), streptomycin (10 µg/disk), and neomycin (30 µg/disk). By comparing the values recorded in **Table 1** to the standards presented in **Table 2**, we were able to interpret the ability of each antibiotic to inhibit the growth of the subject bacteria. For measurements that fell within the range of the "sensitive" column for the respective antibiotic, we determined that the bacteria responded normally. Additionally, we assumed that a normal response indicated that there were no significant changes in resistance as a result of the treatment. For measurements that fell within the range of values in the "resistant" column, we concluded that the subject bacteria developed resistance mechanisms to that antibiotic at the effective concentrations. No measurements in the present study fell within the "moderately sensitive" range.

Resistance to Erythromycin

We exposed oral bacteria collected from the subject to erythromycin, neomycin, streptomycin, and tetracycline. After each trial, we assessed the bacterial growth on the agar plates visually. We assumed that, if the bacteria tested were sensitive to an antibiotic disk, they would not grow around it. In contrast, if the bacteria were resistant to the antibiotic, they would grow closer to the disk. We also evaluated the difference in bacterial growth by measuring the diameter of

Name of Antibiotic (Dose)	Sensitive (mm)	Moderately Sensitive (mm)	Resistant (mm)
Erythromycin (15 µg/disk)	≥23	14-22	≤13
Tetracycline (30 µg/disk)	≥15	12-14	≤11
Streptomycin (10 µg/disk)	≥15	12-14	≤11
Neomycin (30 µg/disk)	≥17	13-16	≤12

Table 2. Zone diameter (mm) interpretive standards for the determination of antibiotic sensitivity and resistance status. Values were obtained from Ref. 16. Susceptibility can be approximated by comparing raw data in Table 1 to the ranges in the table.

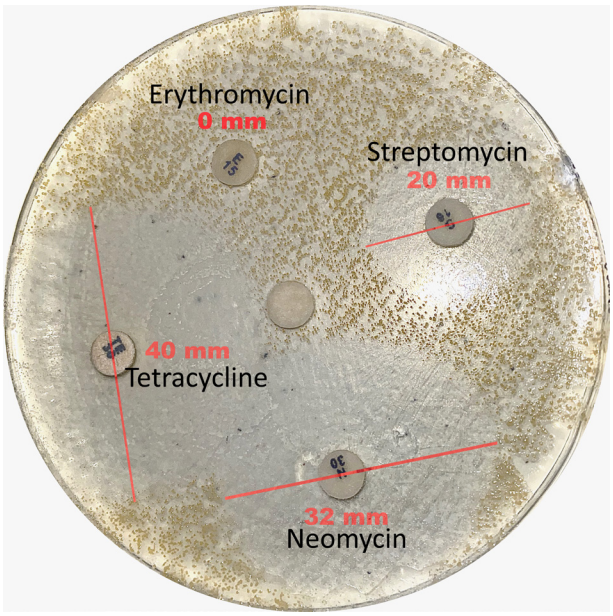

Figure 2. Image of the bacterial growth after trial one. Clockwise: (0 mm) inhibitory zone for erythromycin, (20 mm) inhibitory zone for streptomycin, (32 mm) inhibitory zone for neomycin, (40 mm) inhibitory zone for tetracycline. Note the variation in growth between the blank control and the antibiotic diffusion disks.

the circular zone where no bacteria had grown. If the zone expanded beyond the boundaries of the plate, we doubled the distance between the center of the disk to the nearest colony. Colonies of bacteria appeared to grow consistently outside of a certain range of the antibiotic disks, excluding the control and erythromycin, which had no visual signs of growth inhibition (**Figure 2**). After recording these observations over five trials, we concluded that the subject bacteria had developed resistance to erythromycin.

Susceptibility to Functional Analogs

The raw data for the five subject trials (**Table 1**) showed that on average, neomycin, streptomycin, and tetracycline exceeded the interpretive standard for sensitivity by varying amounts. We visually represented the data by calculating the average points for each disk and plotting them graphically in comparison to the standard sensitivity (**Figure 3**). We noted that the average inhibitory zones of tetracycline and neomycin were significantly higher than the interpretive standard for sensitivity. There was a less significant difference between the average diameter and the standard for streptomycin. Based on these results, we concluded that the subject bacteria were susceptible to the other three antibiotics. Additionally, we calculated the average fold-change to determine the difference between the interpretive standards and the experimental values for each antibiotic. As seen in **Figure 4**, there was a significant difference in zone diameter from the standard for sensitivity in neomycin and tetracycline. We consider the validity of this result in more detail in the Discussion section.

DISCUSSION

In this study, we investigated a subject who has been receiving prolonged azithromycin antibiotic therapy for a neuropsychiatric condition related to chronic GAS infections (10). We had one major finding based on the data collected, as well as inferences that could be supported by further experiments. We concluded that the subject bacteria were completely resistant to erythromycin, an antibiotic belonging to the same class as the azithromycin used in therapy. This resistance is most likely a result of chemical-specific defensive mechanisms since azithromycin and erythromycin are structural analogs with only a few variations in their molecular compositions. As seen in **Figure 1**, the majority of the structure remains the same, as azithromycin is a derivative of erythromycin (15). We hypothesized that the differences in these molecules may affect how they distribute throughout the body and into cells; however, our study has shown they do not affect the mechanism of inhibition.

Tetracycline, streptomycin, and neomycin are considered functional analogs to azithromycin. These antibiotics inhibit bacterial growth in similar ways by affecting mRNA translation (12-14), but their molecular compositions vary quite significantly (**Figure 1**). If our conditional hypothesis was correct, resistance to these three other antibiotics would indicate the presence of bacteria that have mutated nonspecific defense mechanisms. However, this was not the case and suggests that the previously mentioned mutations were absent. We speculated that the mechanisms found in the tested bacteria were specific to the location the antibiotics bind to, as both erythromycin and azithromycin bind to the 50S subunit of bacterial ribosomes (11, 15). In the case that these nonspecific mutations were present, we expected that they would affect processes such as material intake through the cell wall or the pathway in which proteins are assembled. This would limit the access of antibiotics to parts of the cells that must be shut down to stop bacterial growth. In a future study, we could determine the correlation between metabolic changes and susceptibility by evaluating these two factors separately.

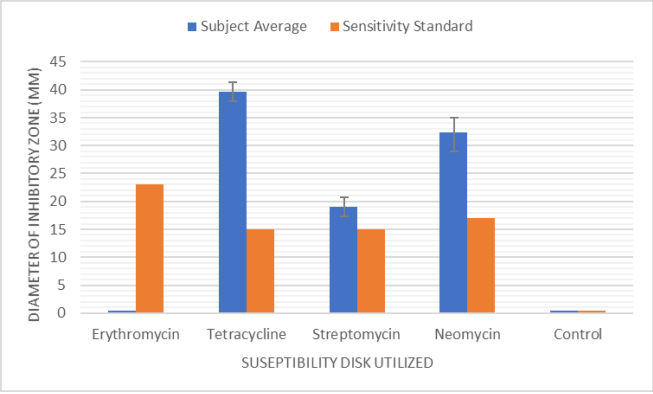

Figure 3. Comparison of subject average zone diameters (blue) with the interpretive standard for sensitivity (orange). Bacterial growth inhibition occurred for every disk except erythromycin and the control. Error bars represent standard deviation.

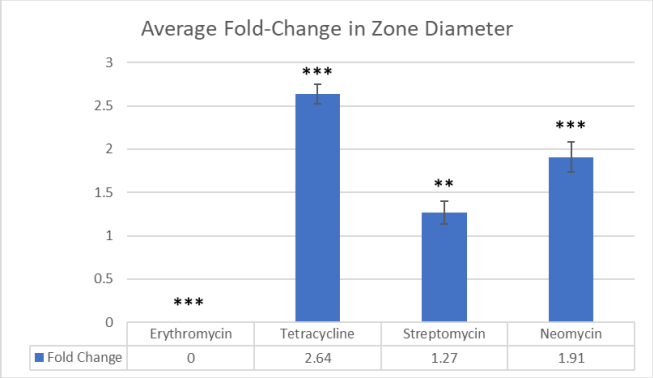

Figure 4. Average fold-change in diameter relative to the minimum sensitivity standard for each antibiotic. Values greater than one indicate an increase, while values less than one indicate a decrease. Error bars represent standard deviation. Asterisks indicate significance of the changes (**p-value<0.01, ***p-value<0.001).

Though zone diameter can vary above the standard depending on the subject, we questioned the significance of the results in **Figure 4**. The basis behind another treatment method, combination antibiotic therapy, is that resistance to one antibiotic may increase susceptibility to another (17). The chances of resistance to one or more antibiotics utilized are significantly lower compared to the use of a single antibiotic (17). Although we speculated that the susceptibility of the subject's sampled bacteria could be influenced by the factors making combination therapy successful, we did not identify the specific strain or mixture of strains we isolated. In future studies, we could accomplish this by observation of the bacteria under a microscope, or by Gram staining to classify.

We determined the concentration of any infection before the procedure by measurement through blood work. The subject patient had recently been tested and confirmed to have insignificant levels of the pathogen in their system, suggesting the absence of erythromycin-resistant streptococcus. Based on the health of the subject at the time of the study, it is unlikely there were any other pathogenic strains to interfere with the results obtained. Though the presence of foreign, non-pathogenic, erythromycin-resistant strains was a possibility, we concluded that while not a result of selective evolution in the subject, this could still act as an expression of the risk of prolonged treatment.

There were two sources of error in our experimental process. Firstly, we lacked control over air contaminants due to the inaccessibility of lab equipment during the time we conducted the study. We followed sterilization protocol rigorously during the preparation of the plates and before incubation using isopropyl alcohol and flame sterilization of tools used to minimize the risk of contamination. We attempted to make this source of error more negligible by testing environmental bacteria in the proximity of where we completed the procedure. The samples we collected proved to be sensitive to the antibiotics, implying that the only bacteria within the resistant ranges could be from the subject. Secondly, the bias in the collection of raw data using a ruler was a source of error during the procedure; however, we completed multiple trials and calculated the standard deviation between results calculated to make this more negligible.

There are also revisions to our experimental process that would improve the viability of the results we obtained. Although we based the experiment on the assumption that the subject bacteria were resistant to azithromycin, the addition of an azithromycin disk to the susceptibility test could confirm or deny any speculations about erythromycin-resistant strains. The procedure also lacked the presence of a non-resistant control to compare results with. Although the interpretive standards act as a reliable baseline, we were not able to obtain precise results with the procedure here. In future studies, the presence of a control subject could solidify our findings.

Lastly, characterizing the effect of prolonged exposure to antibiotics on specific species of bacteria could have a wider-reaching impact in this field. In the context of PANDAS, many patients would benefit from research on specifically Group A streptococcus infection and its response to prolonged antibiotic exposure. Although we considered the changes expressed in **Figure 4** statistically significant, they lack meaning in the context of this study as the bacteria tested were not identified. We could address the biological significance in a future study, where the development of resistance may vary depending on the species and their properties.

The results from this study are meaningful in the context of illnesses associated with chronic bacterial infections, such as PANDAS, a recurring infection, and Mycobacterium, which are highly difficult to kill. Treatment options for these conditions demand extended durations of many months to even years. With knowledge of the rapid spread and dangers associated with microbial resistance mechanisms, prospective patients may be hesitant to undergo such therapy. The results of this case study should aid prospective patients in identifying the risks associated with antibiotic treatment significantly longer than the standard duration.

MATERIALS AND METHODS

Collecting the Samples

Bacterial samples were collected from the teeth, gums, and throat of the subject using a sterile swab, then directly streaked onto a plate containing nutrient agar and incubated at 35°C for 24 hours. After colonies had formed, a single colony was isolated with an inoculating loop and transferred to a tube containing 10 mL of LB liquid broth medium (American Bio Innovations). The tube was incubated at 35°C for 18 hours, shaken regularly until turbidity was visible. SRC/IRB approval for human subject research was not required since the contributor of the samples was the author.

Preparing the Plates

The bacteria were collected from the tube by dipping a sterile swab into the medium, then rotating it against the side

to remove excess fluid. The bacteria were streaked onto five different plates containing 15 mL of Mueller Hinton nutrient agar (Carolina Biological). To ensure even distribution, bacteria were swabbed three times over the entire agar surface, rotating the plate approximately 60° each time. For the details of these methods, the Kirby-Bauer disk diffusion susceptibility test protocol was referenced (18).

Applying the Antibiotic Disks

Antibiotic susceptibility testing disks (Carolina Biological) were kept frozen at -18°C in a desiccated container until the day of use to ensure the validity of the results. The antibiotic disks were set out to equilibrate with room temperature for two hours before the procedure began. Plates were divided into four different sections, one for each antibiotic and a blank control disk in the center (Carolina Biological). The disks were placed in the center of their sections and pressed down lightly to ensure contact with the agar. The plates were then flipped upside down and incubated at 35°C for 18 hours. Before the study, a plate with bacteria collected from the environment was incubated to verify the efficacy of each antibiotic disk.

Measuring Inhibitory Zones

The diameter of the inhibition zones was measured to the nearest millimeter using a ruler. If the edge of the inhibitory zone fell beyond the edge of the plate and could not be measured, the distance from the center of the antibiotic disk to the edge of the zone was taken and multiplied by two to find the diameter.

Statistical Analysis

The susceptibility tests were repeated for a total of five trials. The standard deviations and means of the collected data were calculated for each type of antibiotic disk used based on the data presented in **Table 1**.

For **Figure 4**, the fold-changes for five trials of each antibiotic were calculated and then averaged. To determine the fold-change of each trial, the formula B/A was used, where B was the measurement from that trial, and A was the interpretive standard minimum for sensitivity. We also used an unpaired t-test to determine the *p*-values for each comparison. Due to the polarity of our results, performing additional tests was unlikely to change our conclusions.

Received: August 27, 2020
Accepted: November 23, 2020
Published: December 4, 2020

REFERENCES

1. Barker, Keith F. "Antibiotic resistance: a current perspective." *British journal of clinical pharmacology,* vol. 48, no. 2, Aug. 1999, pp. 109-24, doi:10.1046/j.1365-2125.1999.00997.x.
2. "Antibiotic Resistance." *World Health Organization,* 31 July 2020, who.int/news-room/fact-sheets/detail/antibiotic-resistance.
3. Langdon, Amy, *et al*. "The effects of antibiotics on the microbiome throughout development and alternative approaches for therapeutic modulation." *Genome medicine,* vol. 8, no. 1, 13 Apr. 2016, doi:10.1186/s13073-016-0294-z.
4. Shaw, Liam P., *et al*. "Modelling Microbiome Recovery after Antibiotics Using a Stability Landscape Framework." *Nature News*, Nature Publishing Group, vol. 13, 15 Mar. 2019, pp. 1845-1856, doi: 10.1038/s41396-019-0392-1.
5. Giedraitienė, Agnė, *et al*. "Antibiotic Resistance Mechanisms of Clinically Important Bacteria." *Medicina*, vo. 47, no. 19, 22 Mar. 2011, doi: 10.3390/medicina47030019.
6. McCoy, Lisa S., *et al*. "Antibiotics That Target Protein Synthesis." *WIREs RNA*, vol. 2, no. 2, 22 Nov. 2010, pp. 209-232, doi: 10.1002/wrna.60.
7. Périchon, Bruno, and Patrice Courvalin. "Antibiotic Resistance." *Encyclopedia of Microbiology*, by Moselio Schaechter, 3rd ed., Elsevier/Academic Press, 2009, pp. 193–204.
8. Szybalski, Waclaw, and Vernon Bryson. "Genetic studies on microbial cross resistance to toxic agents. I. Cross resistance of Escherichia coli to fifteen antibiotics." *Journal of Bacteriology*, vol. 64, no. 4, Oct. 1952, p. 497, doi: 10.1128/JB.64.4.489-499.1952.
9. Gutmann, Laurent, *et al*. "Mutation of Salmonella Paratyphi A Conferring Cross-Resistance to Several Groups of Antibiotics by Decreased Permeability and Loss of Invasiveness." *Antimicrobial Agents and Chemotherapy*, vol. 32, no. 2, 1 Feb. 1988, pp. 195-201, doi: 10.1128/AAC.32.2.195.
10. "PANDAS/PANS Treatment Option: Antibiotics." *PPN*, 2 Dec. 2019, pandasppn.org/antibiotics/.
11. Farzam, Khashayar, *et al*. "Erythromycin." *StatPearls*, U.S. National Library of Medicine, 19 June 2020, ncbi.nlm.nih.gov/books/NBK532249/.
12. "Neomycin." *LiverTox*, U.S. National Library of Medicine, 12 Apr. 2019, ncbi.nlm.nih.gov/books/NBK547874/.
13. Shutter, Mollie C., and Hossein Akhondi. "Tetracycline." *StatPearls*, U.S. National Library of Medicine, 6 July 2020, ncbi.nlm.nih.gov/books/NBK549905/.
14. Waters, Mitchell, and Prasanna Tadi. "Streptomycin." *StatPearls*, U.S. National Library of Medicine, 9 Mar. 2020, ncbi.nlm.nih.gov/books/NBK555886/.
15. Sandman, Zachary, and Omar A. Iqbal. "Azithromycin." *StatPearls*, U.S. National Library of Medicine, 30 May 2020, ncbi.nlm.nih.gov/books/NBK557766/.
16. Sarker, M.M.R, *et al*. "Studies of the Impact of Occupational Exposure of Pharmaceutical Workers on the Development of Antimicrobial Drug Resistance." *Journal of Occupational Health*, vol. 56, no. 4, 3 Oct. 2014, pp. 260-270, doi: 10.1539/joh.14-0012-OA.
17. Ahmed, Armin, *et al*. "Current Concepts in Combination Antibiotic Therapy for Critically Ill Patients." *Indian*

Journal of Critical Care Medicine, vol. 18, no. 5, May 2014, pp. 310-314, doi: 10.4103/0972-5229.132495.
18. Hudzicki, Jan. "Kirby-Bauer disk diffusion susceptibility test protocol." 8 December 2009, asmscience.org/content/education/protocol/protocol.3189.

JOURNAL OF
EMERGING INVESTIGATORS

Article

Dune flora can emerge from seed islands (Concon, Chile)

Josefa Farías Giusti-Bilz[1], Mr. Sergio Elórtegui Francioli[2]
[1]Sagrada Familia School, Viña del Mar, Chile.
[2]Department of Biology, Epistemologist, Sagrada Familia School, Viña del Mar, Chile. Proyecto Anillos ANID PIA SOC 180040.

SUMMARY

The study of species within natural communities, which has progressed remarkably in recent decades, is of great interest in the field of ecology. Through the process of characterizing dunes, mounds of sand formed by the wind, and their plant communities we can get to know the physiognomy and floristic composition of the territory. However, little is known about how these plant communities originate. Based on the hypothesis that dune flora can emerge from seed islands: holes in the sand 6 cm deep containing a mixture of seeds, broken branches of shrubbery, and rabbit feces, during spring, we determined the composition of 20 seed islands in the sand dunes of Concon, Chile and measured how many seeds germinated in each one. In support of our hypothesis, we found that, on average, four seeds germinated in each seed island.

INTRODUCTION

Among the many types of dunes that exist, this study advocates to sand dunes, defined as mounds of sand formed by the wind. Dunes are created by accumulations of sand carried by the wind to wide open spaces such as deserts and seashores. Coastal dunes form downwind of a small obstacle around which sand accumulates. Within coastal dunes, plant species adapt to the sandy substrate, wind, and action of the waves, growing in topographically favorable places such as the horizontal surface of marine terraces (1). These dunes are located near sandy beaches in places above high tide level, where winds that blow from the sea transport sand to South America. They contribute to the landscape diversity of the coastal area, constituting a natural heritage of the coastlines. Although dunes span most of the coastlines of South America, Chilean dunes are scarce because rocky shores and cliffs predominate. The dunes account for about 3% of the country's surface (2).

The sand dunes of Chile are located in the three cities of Iquique, San Pedro de Atacama, and Concon, where the climate is Mediterranean-like with warm, dry summers and mild winters (3). The dunes of Concon are a well-developed system in Valparaíso, covering an area of roughly 21 hectares of Chile's fifth region. Due to their location between the towns of Ritoque and Viña del Mar (about 30 km north of Valparaíso city), they are designated as urban to peri-urban. The Concon dune system is mainly fed by fine-grained sands from the Aconcagua River Basin, to a lesser extent from weathering material of coastal rocks, and potentially from sediment of the Aconcagua Estuary (2).

The dunes of Concon are unique in that they are not being fed by sands from the beach because they are separated by a cliff, making them fossil dunes, or ancient desert dunes **(Figure 1)** (4). More than 120 endemic species belong to the region of the dunes, unlike other dunes that exhibit less biodiversity (5). However, it is not immediately clear how these species emerge in the Concon dunes. Our exploration of the dunes by foot led to the discovery of seed islands **(Figure 2A)**, which are holes in the sand 6 cm deep containing a mixture of seeds, broken branches of shrubbery, and rabbit feces. Seeds are fundamental for plant propagation, especially for the dune vegetation in Concon, as there is scarce fauna that can propagate the seeds by ingesting and then defecating them as organic matter (1). Therefore, we hypothesized that dune flora can emerge from seed islands.

To test our hypothesis, we determined the composition of 20 seed islands and how many seeds germinated in each one. We concluded that seeds account for only 30% of the total content of seed islands, and the majority consists of branches and rabbit feces. Despite this, on average, four seeds germinated in each seed island. This outcome supports our hypothesis **(Figure 2B).**

Figure 1: Sand dune from Concon. Coordinates 32 ° 54 '30" and 32 ° 58'50" south latitude and 71 ° 30' 40" and 71 ° 34 '46" west longitude. Nearby cities: Viña del Mar

RESULTS

The rationale of the experiment lies on the idea that if we can prove that flora can emerge from seed islands, seeds islands must be ecologically preserved. We chose 20 seed islands for analysis. Then, we separated the seeds from

each seed island from branches and rabbit feces by flotation to determine each component's percentage. Each seed island had a different percentage of seeds, branches, and rabbit feces, but on average; we considered quantification as units of seeds, broken branches, and rabbit feces; 30% corresponded to seeds, 18.7% to broken branches, and 51.3% to rabbit feces **(Table 1)**.

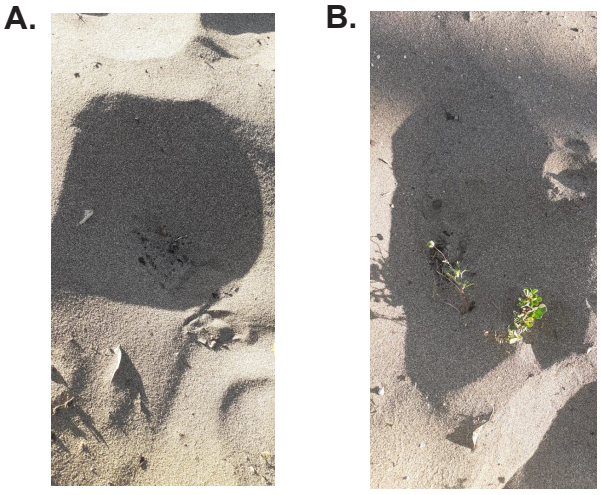

Figure 2: Seed island from Concon. A. Found at coordinates 32 ° 54 '30" and 32 ° 58'50" south latitude and 71 ° 30' 40" and 71 ° 34 '46" west longitude. Nearby cities: Viña del Mar. B. Found between coordinates 32 ° 54 '30" and 32 ° 58'50" south latitude and 71 ° 30' 40" and 71 ° 34 '46" west longitude, showing seeds that germinated.

Later on, we observed seed islands daily over a 12-day period under ideal temperature, humidity, and substrate during spring. We chose spring because it is when seeds from dune flora usually germinate (1).

We established a concept to determine how we we consider germination: germination was defined as the hatching of a seed or sprout of a seed. Our observations demonstrated that seeds do germinate from seed islands but in different quantities; on average, four seeds germinated per island, with an average percent germination of 12% (**Table 2)**. The seed island that experienced the highest percent germination was number six with a percent germination of 26%. Furthermore, the seed island that experienced the lowest percent germination was number eight with a percent germination of 4.88%.

The variance of the Nº of seeds that germinated indicates that the data is not spread out and numbers are close to each other, which means that the number of seeds that germinated are similar in amounts. On the other hand, the variance of the total of seeds and the variance of the percent of seeds that germinated are higher with values of 37 and 23.16 respectively, which means that they do not tend to homogeneity.

DISCUSSION

Regardless of the geographical or climatic zone where dune systems develop, they present a set of environmental characteristics. Coastal dunes exhibit highly dynamic characteristics and interactions, including influence from wind, accumulation or erosion of sand, mobility of the substrate, presence of water, sea spray, saline soils, floods, water stress, very permeable and coarse-grained substrates with low capacity, and nutrient poverty. These characteristics affect the composition and abundance of dune vegetation and the characters of the plants that form it, the latter referring to different processes in their life cycle: germination, implantation, growth, development, dispersal, and senescence (6).

A.

Seed Island	% of seeds	% of branches	% of rabbit feces
1	41	10	49
2	35	14	51
3	37	19	44
4	21	23	56
5	18	25	57
6	21	12	67
7	27	9	64
8	38	30	32
9	31	11	58
10	24	24	52
11	34	15	51
12	26	22	52
13	30	13	57
14	24	17	59
15	32	23	45
16	29	19	52
17	41	17	42
18	23	22	55
19	35	23	42
20	33	26	41
Average	29,4	18,7	51,3
Variance	46,2	32,5	65,9

B.

SUMMARY

Groups	*Count*	*Sum*	*Average*	*Variance*
% of seeds	20	559	29,4	46,2
% of branches	20	364	18,7	32,5
% of rabbit feces	20	977	51,3	65,9

C.

ANOVA

Source of Variation	*SS*	*df*	*MS*	*F*	*P-value*	*F crit*
Between Groups	10324,8772	2	5162,4386	102,724138	3,93786E-19	3,16824597
Within Groups	2713,78947	54	50,2553606			
Total	13038,6667	56				

Table 1: A. Percent composition of seeds, branches, and rabbit feces in seed islands. B. Summary of the above data. C. Statistical analysis using ANOVA.

Germination is essential to all plant life cycles in dunes; this leads us to center the investigation in the number of seeds that germinated per seed island. The experimental results showed that seeds germinated from each seed island with an average percent germination of 23.7%. It supports the hypothesis that dune flora can emerge from seed islands; because out of 20 seed islands that were studied, seeds germinated from each one of them in different proportions. Based on the findings we concluded that because dune flora can emerge from seeds islands, their preservation is essential for the dune ecosystem. The results of our research impact what is known about how seeds from the dunes of Concon germinate, bringing up the idea that seeds germinate in seed islands in the company of broken branches and rabbit feces. Rabbit feces have a high amount of nutrients, including

nitrogen, phosphorus, potassium, calcium, magnesium, and zinc (6). Therefore, it is highly probable that the rabbit feces within the seed islands provide necessary nutrients that help the germination process and future proliferation of dune flora.

Seed island	Nº of seeds that germinated	Total of seeds	% of seeds that germinated
1	6	35	17,14
2	3	29	10,34
3	4	44	9,09
4	5	37	13,51
5	3	31	9,68
6	7	26	26,92
7	3	38	7,89
8	2	41	4,88
9	4	33	12,12
10	5	26	19,23
11	5	34	14,71
12	4	43	9,3
13	2	31	6,45
14	4	29	13,79
15	3	37	8,11
16	4	31	12,9
17	3	29	10,34
18	4	27	14,81
19	6	44	13,64
20	3	24	12,5
Average	4	33,5	12
Variance	1,7	37	23,16
Total	80	669	11,96

Table 2: Number of seeds that germinated in each seed island in a 12-day period, including the total number of seeds and proportion of seeds that germinated.

Factors that could have influenced our research can be classified into two major categories: biological and non-biological factors. First, a living factor that was not considered was the presence of predators like humans, who perform sports such as sandboarding in sand dunes. Sandboarding is a sport that consists of descending dunes with special boards. It is considered an extreme sport that damages the dune flora because sliding the board on the sand alters its composition and changes the location of the seeds and other elements necessary for dune flora proliferation (3). Next, the manipulation of seeds islands for the purpose of this research could have led to the loss or inactivation of some of the seeds during the flotation process. Third, regarding non-living factors, the large number of commercial constructions that are invading the Concon dunes may have a great impact on how the dune flora develops. Lastly, another non-living factor to consider is the wind. Because of its altitude of 80 m above sea level, the dune field receives strong winds all year long (5). Wind is a driving force behind the dynamics of the dune field, transporting sand, saline spray, debris, and burying vegetation. For that reason, wind could have carried seeds to or from other environments and altered the characteristics of the seed islands, which may have influenced our results.

Based on the information mentioned previously, it is necessary to emphasize the negative impact of human intervention on the dune field, which involves both the construction of commercial buildings and sports like sandboarding. Commercial buildings are invading the dune field, leaving construction debris in the sanctuary. Additionally, tourists do not take necessary environmental precautions when visiting this sanctuary. These events can eventually lead to an extinction of the seed islands and a reduction in the amount of dune flora, thus modifying the environment and altering the habitat of many animal species. Further research on seed islands can corroborate the importance of their conservation. Experiments we would like to complete in the future would involve determining the genus and species of the seeds found in sand dunes as well as analyzing the specific mechanism of reproduction of each species. Since flora emerges from seed islands, if seeds islands become extinct because of the factors mentioned above, species of seeds that require seed islands may also become extinct.

MATERIALS AND METHODS

The dunes of Concon are located at coordinates 32º56´30´´S 71º32´57´´W and the seed islands were found in the tip of the sand dune between coordinates 32°56'26.3"S 71°32'51.7"W and 32°56'24.4"S 71°32'51.7"W. We selected 20 seed islands, all approximately 6 cm deep. First, each seed island was fenced in a circular way with pieces of wood, at a height of 10 cm. Subsequently, each wood fence was marked with a number between 0–20 to identify the seed islands, after which twenty 2.3 L plastic containers were brought to the sand dune. Each container was marked with the seed island identifier. Later on, each seed island was carefully taken from its hole using a shovel before being put in the matching plastic box filled with 1 L of mineral water. By flotation, the seeds were separated from the branches and the rabbits' feces. This procedure was repeated with each seed island, taking an average of 72 hours per box. Lids were placed on the plastic boxes to prevent wind from altering the results.

The seeds that floated in each plastic container were transported to a 100 mL metallic box marked with the corresponding seed island number. In the new container, the seeds were counted individually, after which the information was collected. We quantified composition by counting each of the elements; seeds, branches and rabbit feces. Then we calculated the percent using the rule of three simples considering seeds, branches and rabbit feces as independent units. Seeds were put back into their respective holes. Then, the branches and rabbit feces were strained with a strainer that matched their seed island number, to separate them from water. Later on, the branches and rabbits feces were put back into their respective seed island to maintain the original composition. The reconstituted seed islands were covered using 1 L translucent glass boxes with tiny holes to prevent seeds from blowing away and to allow air flow. The seed islands were observed with binoculars for a 12-day period to assess the number of seeds germinating, hatching of a seed, in each seed island once daily at 9 a.m.

Received: August 21, 2020
Accepted: November 5, 2020
Published: December 7, 2020

REFERENCES

1. Serey, I., et al. “Diversidad de La Vegetación de Las Dunas de Concon.” *Ciren*, vol. 53, no. 9, 2013, pp. 1689–99, doi:10.1017/CBO9781107415324.004.

2. Avaria, Consuelo Castro. Geografía de Las Dunas Costeras de Chile. 1st ed., *Ediciones UC*, 2015, www.jstor.org/stable/j.ctt1bhkqg8.

3. Nehren, Udo, et al. “Ecosystem-Based Disaster Risk Reduction and Adaptation in Practice.” Springer International Publishing, vol. 42, no.1 , 2016, doi:10.1007/978-3-319-43633-3.

4. Martínez, Carolina. “Shoreline Changes in Concón and Algarrobo Bays, Central Chile, Using an Adjustment Model.” Scielo, vol. 35, no. 2, 2007, pp. 99–112, doi:10.4067/S0717-71782007000200010.

5. Kuncar, Felipe, et al. “Estudio Experimental de La Interacción Bulbo-Suelo En Anclajes Postensados Inyectados En Arenas Eólicas Del Sector Reñaca-Concón Resumen.” Sochige, vol. 50, no. 4, 2018, p. 13

6. Vega de Seoane, Carlos Ley. Manual de Restauración de Dunas Costeras. Edited by Paola Gomez Lobato, 1st ed., Gobierno de España, 2007.

ACKNOWLEDGEMENTS

I would like to thank my beloved mother for motivating me to study the environment and our ecosystem. I would also like to thank Harvard’s Journal of Emerging Investigators for giving me the incredible opportunity to publish this research.

JOURNAL OF
EMERGING INVESTIGATORS

Article

Comparing Virulence of Three T4 Bacteriophage Strains on Ampicillin-Resistant and Sensitive *E. coli* Bacteria

Lillian Hudanich[1], Christian Hudanich[1], James Carey, PhD[1]
[1] Norwell High School, Norwell, Massachusetts

SUMMARY

While bacteria have demonstrated antibiotic resistance since the advent of antibiotics, the threat that these resistant microbes pose has recently gained much more attention in scientific and public communities. Antibiotics work by disrupting functions and structures in bacteria that animal cells lack. Bacteria acquire resistance to these drugs through genetic mutations that allow them to sidestep the effects of the antibiotic. When this occurs, antibiotics may not be able to treat an illness caused by resistant bacteria. An alternative therapy is the use of bacteriophages, or viruses that infect bacteria.

In this experiment, we grew cultures of ampicillin-resistant and ampicillin-sensitive K12 strain *E. coli* and applied three strains of T4 bacteriophage, T4r+, T4r, and T4rIIA, to different cultures of the resistant and sensitive *E. coli*. After the bacteriophages had time to infect and lyse the bacteria, we determined the lysed percentage of each culture.

The results of this work showed that the wild type T4r+ caused the greatest amount of lysis of *E. coli*. There was not a significant difference in percentage lysed between cultures containing resistant and sensitive *E. coli* infected with the same strain of bacteriophage. These results suggest that the T4r+ bacteriophage may be the most effective in treating an *E. coli* infection, regardless of the ampicillin resistance of the *E. coli*.

INTRODUCTION

Over the last several years, bacterial resistance to antibiotics has risen as a critical threat to global health. In 2013, the Centers for Disease Control and Prevention (CDC) stated that the world had entered the "post-antibiotic era" and organizations such as the World Health Organization (WHO) have expressed concerns about the future of infectious disease treatment (1). In just the United States, 99,000 deaths are caused by hospital-acquired resistant infections annually, resulting in billions of dollars lost in the United States economy (2). Solutions to this growing problem of antibiotic resistance are an active area of research worldwide, and we explored the use of bacteriophages as an alternative germicide for antibiotic-resistant bacteria.

Antibiotics often work by targeting structures unique to bacteria that animal cells lack. Some of these features include bacterial membranes, bacterial DNA, and organelles used in bacterial protein synthesis, such as ribosomes (3). Each class of antibiotics targets a different component of bacterial cells by inhibiting or interfering with a function. For example, penicillin prevents bacteria from building cell walls. As a part of the beta-lactam class, penicillin works best on gram-positive bacteria, as it interferes with peptidoglycan production. In order to assemble their walls, bacteria link peptidoglycan molecules together with various proteins and lipids. The beta-lactam antibiotics interfere with this process. Without support from a cell wall, internal pressure causes the bacterial cell to lyse (3). In general, bacteria develop resistance to these antibiotics through genetic mutations that bypass the function of the drug. Mutations randomly occur in the DNA and can occasionally benefit the bacterial organism. If by chance the mutation helps the bacteria resist the effects of the antibiotic, then that bacteria will survive to pass on its genes, while sensitive bacteria will die (4). Genes can be transferred in several different ways, including binary fission and horizontal gene transfer. Binary fission is how a bacterial cell asexually reproduces to become two separate bacteria, thus the genetic information is passed from the parent cell to the two daughter cells (4). Horizontal gene transfer includes conjugation, transformation, and transduction. In conjugation, bacterial cells exchange nucleic acids through direct contact. Transformation is where a bacterial cell takes up extracellular DNA and incorporates this genetic material into its genome. In transduction, a bacteriophage will transfer genetic material from one bacterium to another. Through horizontal gene transfer, resistance can spread from one bacterium to a whole colony of bacteria (4). Therefore, when an ill patient takes antibiotics, if even one bacterium develops resistance and does not die, this resistance can spread and cause an entirely resistant infection. When this resistance occurs, alternative methods of treatment must be used.

One alternative method is the use of bacteriophages to kill the bacteria causing the infection. Phages infect bacteria through six general steps of the lytic cycle (5). The first step, adsorption, is how a virion uses specific receptors on the host membrane or wall to attach to the cell. After adsorption, the virion must penetrate the cell. T4 bacteriophages complete this process by first using tail fibers to attach to the bacterium. Then using enzymes on its tail, the virion will create a hole in the wall or membrane. The virion's tail sheath contracts, causing the DNA to leave the protein coat and enter the host cell. The DNA then travels to the nucleus and is used as a template by the cell to create viral mRNA. This mRNA travels to the host cell's ribosomes and is used to make viral proteins. Once viral protein subunits, also known as capsomeres, form in the cell, they spontaneously self-assemble into a complete protein coat. Viral DNA is also replicated by the cell, and it combines with the protein coat to create a new intact virus.

	R T4r	S T4r	R T4r+	S T4r+	R T4rIIA	S T4rIIA
Plate 1	34	28	45	40	22	26
Plate 2	38	36	51	60	34	27
Plate 3	30	31	49	40	7.5	49

Table 1: Percentage of Resistant (R) and Sensitive (S) Bacteria Lysed for Each Trial of Each T4 Strain. T4r+ phage appears to have the highest percent lysis.

Finally, lysosome-like viral enzymes break down the cell wall and the host cell lyses as the new viruses leave the cell (5). Although bacteria can become resistant to phages through genetic mutations, phages can mutate in response. This coevolution allows phages to remain generally effective (5). Previous studies have also indicated that as bacteria develop resistance to phage infections, they may become more susceptible to antibiotic treatment, as the bacterial host must proverbially trade-off between resistant genes for antibiotics or phages (6).

In this experiment, we infected ampicillin-resistant and ampicillin-sensitive K12 strain *Escherichia coli* bacteria samples with three different strains of T4 bacteriophages. Ampicillin, an antibiotic of the beta-lactam class similar to penicillin, is often used in clinical settings to fight bacterial infections, and resistance to common drugs of the beta-lactam class is increasing in prevalence (6). By exposing the K12 *E. coli* cultures to ampicillin, the *E. coli* cultures developed ampicillin resistance and the surviving bacteria grew into their own cultures. The three strains of virus used were T4r+ wild type, T4rIIA, and T4r bacteriophage. These strains of T4 bacteriophages reproduce by the lytic cycle when infecting the *E. coli*. The "r" in T4r denotes a mutation that leads to rapid lysis of the bacterial host (7). In T4rIIA, mutations have occurred in the rII genes, specifically the A:5 section of these genes, that modify the proteins responsible for interacting with the host cell membrane (7). Previous experiments have indicated that the T4rIIA strain has reduced ability to infect K12 *E. coli* bacteria due to its modified proteins (8). The other mutant strain, T4r, differs from the wild type T4r+ in its size. T4r is physically larger than its wild type counterpart, and therefore diffuses through a bacterial culture more slowly (8). This slower diffusion rate of T4r would indicate that the wild type T4r+ may be most effective at infecting K12 *E. coli*.

The hypothesis of this research project was that the wild type T4r+ would cause the greatest percent lysis of the K12 *E. coli* bacteria, as compared to the T4r and the T4rIIA mutant strains. Additionally, we hypothesized that the antibiotic resistant bacteria would be more sensitive to bacteriophage infection. The results of the research demonstrate that the wild type viral strain caused the greatest amount of bacterial lysis and that there was not a significant difference in lysis between resistant and sensitive bacterial plates when infected with the same bacteriophage strain. These results indicate that the T4r+ phage may be the best of the three strains to treat an *E. coli* infection, and that ampicillin resistance may not affect T4 virulence.

RESULTS

To investigate the virulence of the bacteriophage strains, we added each strain to six petri dishes, three of which contained ampicillin-resistant *E. coli* and three of which contained sensitive *E. coli*. All of the petri dishes had bacterial confluent lawns. We calculated the percentage of the bacterial confluent lawn that lysed to determine which strain had caused the most lysis. For each of the resistant and sensitive petri dish sets, we used one petri dish as a negative control for lysis despite not being inoculated with bacteriophage. The wild type T4r+ bacteriophage demonstrated the highest percentages of lysis for both resistant and sensitive bacteria (**Table 1**). On average, the T4r+ strain had a higher percentage of lysis than the other strains (**Table 2**).

DISCUSSION

Based on the data, the three different strains of T4 bacteriophage induced statistically significant different percentages of lysis in the host *E. coli* bacteria. We found that for both the resistant and sensitive bacteria, the T4r+ strain had the highest rate of lysis, while the T4rIIA strain had the lowest rate of lysis, with the T4r strain in between. This result supports the hypothesis that the T4r+ strain would cause the greatest amount of bacterial lysis. The results also showed that whether the bacteria were resistant or sensitive to ampicillin had no significant effect on phage susceptibility, disputing the hypothesis that the resistant bacteria would be more susceptible to phage infection. This result suggests that the mechanisms behind antibiotic resistance and phage resistance in *E. coli* bacteria are not the same.

The average lysis percentage for the wild-type T4r+ strain was 48%. This strain was the smallest in size of the three and did not have any mutations affecting its ability to interact with the cell wall of the bacteria (7, 8). Therefore, it was best suited to quickly spread, infect, and lyse the *E. coli* host cells. The T4rIIA strain of bacteriophage did have mutations that affected its adsorption capabilities (7). Since the bacteriophage was not as effective at attaching to the cell wall, the infection rate decreased. Thus, the lysis rate decreased as well, compared to the wild-type strain. The average lysis percentage for the T4rIIA strain was 28%. The T4r strain did not have these mutations, but was much larger than the T4r+ wild type (8). This larger size decreased the rate of diffusion for the bacteriophage through a bacterial culture. Therefore, the bacteriophage came into contact with less host bacteria, and did not infect as many cells as the wild type strain. The average lysis percentage for the T4r strain was 33%.

	T4r	T4r+	T4rIIA
R Average	34 ± 3.6[1]	48 ± 2.7[1]	21 ± 12[1]
S Average	32 ± 3.6[2]	47 ± 10.[2]	34 ± 12

Table 2: Average Percentage of Resistant (R) and Sensitive (S) Bacteria Lysed for each Strain of T4. T4r+ phage lyses *E. coli* most efficiently and is non-discriminate on ampicillin sensitivity.
[1] There was a statistically significant difference between the three resistant groups as determined by a one-way ANOVA ($F(2,15) = 20.632$, $p = 0.000049$ at $\alpha = 0.05$) and a post-hoc Tukey's Honest Significant Difference (HSD) test.
[2] There was a statistically significant difference between the T4r and T4r+ sensitive groups as determined by a one-way ANOVA ($F(2,15) = 4.600$, $p = 0.028$ at $\alpha = 0.05$) and a post-hoc Tukey's HSD test.

Although we took many steps to maintain constants and controls and ensure the accuracy of the data, there is always some level of error. We chose the drug ampicillin because it is a common choice to treat bacterial infections, and resistance can be common (6). However, the ampicillin-resistant bacteria in this experiment may not have truly been resistant to ampicillin. In all cultures of the resistant bacteria, a small percentage (less than 7%) of the bacteria did die, and we did not perform genetic analysis to check that the bacteria were in fact resistant. If this potential source of error occurred, assessing whether the reported lysis percentages for resistant bacteria were too high or too low would be difficult. Another source of possible error is if the cultures of bacteria were contaminated by something in the laboratory setting. The contamination may have killed some of the *E. coli*, leading the lysis percentages reported to be too high. There was a low chance of a contaminant in this experiment, as the negative controls showed no plaques, or clear-looking areas in the confluent lawn of bacteria where cells were lysed due to infection. A final potential source of error is if we did not properly dilute the bacteriophages of each strain. The original dilution of the T4rIIA strain was $1.0 \cdot 10^9$/mL, the T4r strain was $2.8 \cdot 10^9$/mL, and the T4r+ strain was $2.5 \cdot 10^9$/mL. In order to make these even dilutions, we added deionized water accordingly. If error was present in this process, the concentration of virus particles could have been different. If the liquids applied to the bacteria cultures had different concentrations of virus particles, the lysis percentages reported could have been anomalously low or high in some cases.

The results of this experiment indicated that the T4r+ strain was the most effective of the three tested strains in causing lysis of K12 *E. coli* bacteria. This indication could present pathways for further research into the most promising bacteriophages for phage therapy. To delve deeper into this topic, different classes of antibiotics could be used on the *E. coli* to examine their effect on the bacteriophage rate of lysis. Also, other strains of bacteriophage, rather than T4, could be used on various species of bacteria to determine their rate of lysis. Furthermore, research could be done into why the state of the bacteria being antibiotic resistant did not seem to affect susceptibility to phage infection.

MATERIALS AND METHODS

Petri Dish Preparation

To create each petri dish, 8g of LB nutrient agar powder (Bio-Rad) were first measured out on a spring scale and added to an Erlenmeyer flask with 200mL of deionized water in a manner that prevented clumps. The flask was covered with cling wrap with a small hole punched in the top and was placed in a microwave. The flask was heated in intervals to prevent the broth from bubbling over until the broth appeared clear. After the broth had cooled to about 60°C, a medium-sized petri dish was filled about half way and the broth was allowed to cool and congeal. Once solid, the plate was inverted and dried overnight.

Ampicillin-Resistant Bacteria Preparation

To create the ampicillin-resistant *E. coli* bacteria, 2 g of LB broth powder (BD Difco) were measured out on a spring scale and added to a flask with 100mL of deionized water in a manner that prevented clumps. The flask was covered with cling wrap with a hole and was heated in intervals in a microwave until the broth appeared clear. After the broth had cooled to 60°C, the broth was evenly poured into 4 separate test tubes, about 8 mL each. For each test tube, an inoculation loop was used to swab a small amount of *E. coli* from the original dish (Carolina Biological Supply Company) and was shaken inside the tube to loosen the bacteria. The caps were loosely put on and the test tubes were incubated for 24 hours at 37°C. Using a micropipette, the liquid from the test tubes was transferred to 16 microcentrifuge tubes and was spun at 1200 rpm for 3 minutes. Then, the bacterial pellet in each microcentrifuge tube was resuspended and all of the broth was combined. Using a micropipette, 500µL of broth was dispensed onto a petri dish and spread around via gentle shaking. Three ampicillin antibiotic disks (Carolina Biological Supply Company) were placed in the petri dish, equidistant from each other and the edges of the dish. Each disk had an ampicillin concentration of approximately 0.012 mg/mL, or about 10 mcg. After the liquid had solidified, the petri dish was inverted and incubated at 37°C for 24 hours. After the bacteria had grown, an inoculation loop was used to swab bacteria from the edge of the zone of inhibition. The same steps were repeated three times with the *E. coli* from the zone of inhibition to help ensure the bacteria were resistant to the antibiotic.

Exposing Bacteria to Bacteriophages

For the main part of the experiment, an ampicillin-resistant bacterial broth and an ampicillin-sensitive bacterial broth were created using the method for ampicillin-resistant bacterial broth preparation as listed above (using K12 *E. coli* from the original Carolina Biological Supply Company dish for the sensitive broth). Then, 10 petri dishes received 500µL of resistant broth and 10 petri dishes received 500µL of sensitive broth. The petri dish was shaken gently in circles on the lab bench in order to spread the broth evenly across the whole dish. Once dried and inverted, the petri dishes were incubated at 37°C for 24 hours.

To prepare the bacteriophages, the T4r, T4r+, and T4rIIA supply stocks (Carolina Biological Supply Company) were diluted with deionized water to create equal concentrations of $1.0 \cdot 10^9$/mL for each strain. One milliliter of each phage strain was dispensed on each of three resistant and three sensitive petri dishes. The last two petri dishes were left with no bacteriophage. After the plates had dried and been inverted, all of the plates were incubated at 37°C for 24 hours.

Data Recording

To record the data, a ruler was used to make a grid of 0.5 cm by 0.5 cm squares on the petri dishes. Using these squares, the area of the zones of inhibition was found for each petri dish and divided by the total area of the petri dish to determine a percentage.

Statistical Tests

To test the differences in percent lysis between viral strains, a one-way ANOVA Test was carried out at a confidence level of 0.95 by inputting the percent lysis for each plate within each strain. If the results were significant, a Tukey's Honest Significant Difference (HSD) Test was performed to determine where the significant differences were. The same process was carried out to compare differences between percent lysis of the same strain on resistant versus sensitive plates. To carry out these calculations, the Social Science Statistics website was used for the ANOVA Test (9), and the iCalcu website was used for the HSD Test (10).

ACKNOWLEDGEMENTS

We would like to thank our parents for supporting us throughout the process and Dr. Stephen Marsh for his insights and assistance.

Received: July 11, 2020
Accepted: September 14, 2020
Published: December 9, 2020

REFERENCES

1. Ventola, C Lee. "The antibiotic resistance crisis: part 1: causes and threats." *Pharmacy and Therapeutics*, vol. 40, no. 4, 2015, pp. 277-83. PubMed Central, PMC4378521
2. Aslam, B., *et al*. "Antibiotic resistance: a rundown of a global crisis." *Infect Drug Resist*, vol. 2018, no. 11, 2018, pp. 1645-58. Dovepress, doi.org/10.2147/IDR.S173867.
3. Fitch, Chris. "The Path of Least Resistance: Antimicrobial Resistance Threatens to Become the World's Largest Health Hazard as Antibiotics Become Ineffective through Overuse, Potentially Reversing Years of Development Progress." *Geographical. Science in Context*, link.galegroup.com/apps/doc/A556230364/SCIC?u=mlin_s_norhs&sid=SCIC&xid=68c98f94. Originally published in Geographical, 2018.
4. Burmeister, Alita R. "Horizontal Gene Transfer." *Evolution, Medicine, and Public Health*, vol. 2015, no. 1, 2015, pp. 193-94. Oxford Academic, doi.org/10.1093/emph/eov018.
5. Brock, Thomas D. *Biology of Microorganisms*. 2nd ed., Englewood Cliffs, Prentice-Hall, 1974.
6. Burmeister, Alita R., *et al*. "Pleiotropy complicates a trade-off between phage resistance and antibiotic resistance." *Proceedings of the National Academy of Sciences*, vol. 117, no. 21, 2020, pp. 11207-16. Researchgate, doi.org/10.1073/pnas.1919888117.
7. *Bacteriophage (Coliphage)*. Ward's Science, 2008, www.wardsci.com/www.wardsci.com/images/Bacteriopha_Coliphage.pdf.
8. Burch, Lauranell H., *et al*. "The Bacteriophage T4 Rapid-Lysis Genes and Their Mutational Proclivities." *John W. Drake Journal of Bacteriology*, vol. 193, no. 14, 2011, pp. 3537-45. American Society for Microbiology, doi.org/10.1128/JB.00138-11.
9. "One-Way ANOVA Calculator." *Social Science Statistics*, Jeremy Stangroom, www.socscistatistics.com/tests/anova/default2.aspx.
10. "One-way ANOVA and Tukey's HSD Calculator." *iCalcu*, www.icalcu.com/stat/anova-tukey-hsd-calculator.html.

JOURNAL OF
EMERGING INVESTIGATORS

Article

Alterations of the [Fe/H] Values Modulate Light Curves by Absolute Magnitude in non-Blazhko RRab Lyraes

Michelle Park[1], Dustin Schroeder[2]
[1] Solon High School, Solon, Ohio, US
[2] Stanford University, Stanford, California, US

SUMMARY

RR Lyraes are a type of variable star known for their short periods and their periodicity can be used as standard candles to determine the distances of interstellar objects they reside in. The correlation between the composition of RR Lyraes and their light curves is not well understood. This study investigated the relationship between the metallicity and resulting changes in the light curves of non-Blazhko RRab Lyraes. We analyzed 135 images of the 15 RR Lyraes throughout nine periods of the day by remotely accessing the Canary 2 telescope at the Slooh Canary Islands Observatory. We examined the images using multiple image analysis software programs to find locator stars, determine the apparent magnitudes of the RR Lyraes, and create light curves. We observed a negative exponential relationship between the [Fe/H] and the light curve amplitudes of the RR Lyraes, and a negative linear relationship between the [Fe/H] and the periods of the RR Lyraes. These results demonstrate that we can obtain a better idea of an RR Lyrae's composition based on solely its light curve and that characteristics of a light curve can be predicted based off of metallicity without time-consuming visual observations being required. These conclusions will assist in applying metallicity corrections to obtain more precise absolute magnitudes of the RR Lyraes so that they may be more effective standard candles.

INTRODUCTION

Variable stars are stars that change in luminosity over time (1). Approximately 200,000 of them have been discovered, and many of them have been placed into more than 20 different categories (2). Known to be old Population II stars, RR Lyraes are one of the most common types of variable stars, classified as intrinsic and pulsating (3). They are named after RR Lyrae, the brightest example and prototype star of the RR Lyrae variable star class. They are most prevalent in globular clusters, near the disk and halo of galaxies (4, 5). Located near the instability strip of the Hertzsprung–Russell diagram, the stars that demonstrate RR Lyrae variability are limited to those with specific physical properties (6). Their short pulsation periods make them the best candidates for variable star analysis, lasting from 0.1 to 2 days and ranging from 0.3 to 2 magnitudes in brightness (7-9). RR Lyraes are further divided into three subtypes based on the shape of their light curve – RRab (91% of all RR Lyraes), RRc (9%), and RRd (< 1%) (9, 10).

RR Lyraes are used as standard candles to calculate distances to interstellar objects (5, 7, 11, 12). The period-luminosity relation can calculate the luminosity of any variable star through information on its period (13, 14). The luminosity is expressed as $L = 4\pi d^2 m$, where L is the luminosity in solar units, d is the distance in parsecs, and m is the apparent magnitude (15).

Metallicity is defined as the fraction of a star's composition that is not hydrogen or helium – the crucial ingredients for stellar fusion (16). The iron-hydrogen ratio, or indicated by [Fe/H], measures metallicity by comparing the iron content of a star to its hydrogen content (16). This logarithmic unit is dependent on the Sun as shown by the following equation (where the asterisk represents the target star):

$$[Fe/H] = log \frac{(Fe/H)_*}{(Fe/H)_{Sun}}$$

This ratio can quantitatively measure the composition of a star and define if it is metal-rich or metal-poor. In the study by Nemec *et al*., the [Fe/H] values were determined by analyzing the Fe I and Fe II in the spectra of the target RR Lyraes (19).

A significant property of RR Lyraes is the Blazhko effect, defined as a long-term, periodic fluctuation in period and amplitude of an RR Lyrae light curve that occurs in 30% of all RR Lyraes (**Figure 1**) (17). Without the Blazhko effect, RR Lyraes experience the same maximum and minimum flux values throughout multiple periods. The additional Blazhko effect periodicity produces noise in a data sample; thus, we

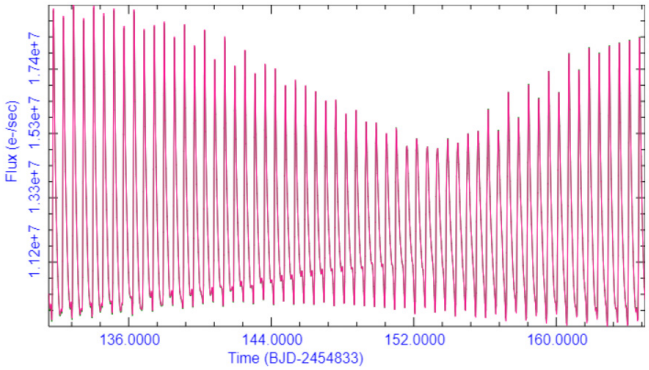

Figure 1: The RR Lyrae star demonstrating the Blazhko effect. The flux (directly correlated to luminosity) of the light curve's maxima and minima fluctuate over a long period of time (17). The figure is a screenshot from Kepler data (18).

RR Lyraes	Time (EST)								
	5:30 PM	6:30 PM	7:30 PM	8:30 PM	9:30 PM	10:30 PM	11:30 PM	12:30 AM	1:30 AM
NR Lyr	-2.4407	-2.6225	-2.7155	-2.6553	-2.8285	-2.7386	-3.0625	-4.3038	-2.7724
V782 Cyg	-0.5177	-1.0191	-1.0046	-0.8359	-0.7089	-0.4619	-1.1652	-0.3714	-0.2403
V784 Cyg	-0.1393	-0.1600	-0.6537	-0.7417	-0.5915	-0.3210	-0.1462	-0.1824	-0.4299
KIC 6100702	-4.1788	-4.3702	-4.5138	-4.6071	-4.2762	-4.2791	-4.2811	-3.9266	-3.7975
NQ Lyr	-2.4662	-3.1488	-3.0829	-3.5614	-3.2828	-3.1270	-3.2581	-3.9761	-3.8990
FN Lyr	-2.5064	-2.8878	-3.4605	-3.4975	-3.5534	-3.5439	-3.4425	-3.6199	-4.0223
KIC 7021124	-6.7220	-7.9242	-8.2350	-7.9687	-6.6598	-6.1535	-6.8909	-8.2090	-8.3501
KIC 7030715	-2.4142	-2.6743	-2.9465	-2.8180	-2.8512	-2.4074	-2.9916	-3.1295	-2.3096
V1510 Cyg	-1.9835	-2.6573	-2.4545	-2.3518	-3.2043	-3.1653	-2.6127	-2.5619	-3.5011
V350 Lyr	-8.0375	-8.7083	-8.4939	-8.4995	-8.4324	-8.1985	-8.1737	-8.0784	-8.2484
V894 Cyg	-5.1432	-4.8776	-4.8990	-4.7510	-4.7053	-4.7510	-4.7703	-4.9842	-5.0746
V2470 Cyg	-4.1512	-4.8740	-4.3359	-4.4442	-4.3696	-4.6481	-4.6973	-4.7677	-4.5483
V1107 Cyg	-0.2045	-2.5409	-2.0754	-1.2271	-1.2011	0.4527	-1.6672	-0.5812	-1.4576
V838 Cyg	-5.4219	-6.0141	-5.8607	-4.6875	-5.8335	-5.6845	-5.8842	-5.5810	-5.7519
AW Dra	-3.8583	-3.9051	-4.9322	-4.7302	-4.8139	-4.9149	-4.0427	-4.3134	-3.9249

Table 1: The absolute magnitudes of the 15 RR Lyraes found by running the Slooh images using AstroImageJ and using a locator star to compare magnitude.

investigated non-Blazhko RR Lyraes to refine our analysis and produce consistent results. We selected these non-Blazhko RRab Lyraes from a 2011 study by Nemec *et al.* (19).

The purpose of this analysis was to examine how the light curves of non-Blazhko RRab Lyraes would vary based on their metallicity. We hypothesized that the fluctuations of the absolute magnitude of the light curve will decrease as the iron content of the RR Lyrae increases. Based on the data, as the [Fe/H] values increased, the fluctuations of the absolute magnitude (as represented by the amplitude of the phase plot) of these variable stars decreased in a negative exponential relationship. Thus, the hypothesis was accepted. The rationale for this negative exponential trend may be because as the metallicity of a star increases, there is less room for hydrogen and helium as that room is taken up by metals. As that space is taken up, this results in less fusion so the RR Lyrae will have less energy for its light curve to fluctuate.

RESULTS

We investigated 15 non-Blazhko RRab Lyraes to analyze how [Fe/H] values of non-Blazhko RRab Lyrae variable stars affected their light curves. We took multiple images of each variable star via remote access and analyzed them using locator stars to calculate their apparent and absolute magnitude. We plotted the absolute magnitude data into light curves and compared by amplitude with other RR Lyraes in the study to examine the relationship between metallicity and the shape and amplitude of the graph. We hypothesized that the fluctuations of the absolute magnitude of the light curve will decrease as the iron content of the RR Lyrae increases because less fusion occurs with a decreased presence of hydrogen and helium, thus providing less energy for the light curve to produce a larger amplitude.

The analysis involved a total of 135 absolute magnitude values and 15 stars across nine different time slots from September to October 2018 (**Table 1**). These data points were plotted to produce light curves, and their amplitudes were calculated and compared to known [Fe/H] values by Nemec *et al.* (**Table 2**) (19). The amplitude of the light curves, or phase plots, represents the extent of the fluctuation of the RR Lyraes. The period of the RR Lyraes was determined by finding where the absolute magnitude returns to the same value as the first data point.

RR Lyrae Name	[Fe/H]	Amplitude of Phase Plot
NR Lyr	-2.34	0.48
V782 Cyg	-0.47	0.35
V784 Cyg	-0.14	0.285
KIC 6100702	-0.35	0.325
NQ Lyr	-1.83	0.57
FN Lyr	-1.9	0.675
KIC 7021124	-2.08	0.88
KIC 7030715	-1.66	0.1725
V1510 Cyg	-1.83	0.3625
V350 Lyr	-1.84	0.3375
V894 Cyg	-1.79	0.15
V2470 Cyg	-0.71	0.14
V1107 Cyg	-1.56	0.645
V838 Cyg	-1.56	0.305
AW Dra	-1.74	0.485

Table 2: [Fe/H] and amplitudes of the phase plots of the 15 RR Lyraes found using VStar.

In **Figure 2**, the correlation between [Fe/H] and amplitude of the phase plots using a linear scale was a power law relationship with an equation of $y = 0.2268x^{-0.138}$, with an r^2 value of 0.1570 and $X^2 = 3.493$, p = 0.9978 with 14 degrees

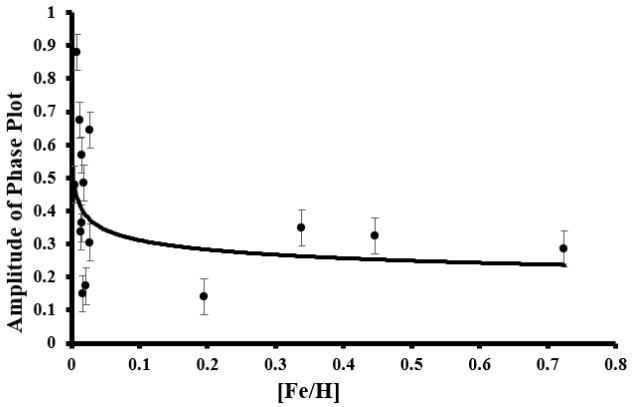

Figure 2: The relationship between [Fe/H] and the amplitude of the phase plots produced. Stars with a higher metallicity (less hydrogen and helium) showed less dramatic fluctuations in their light curves (smaller amplitude). Mean ± SD (n=15).

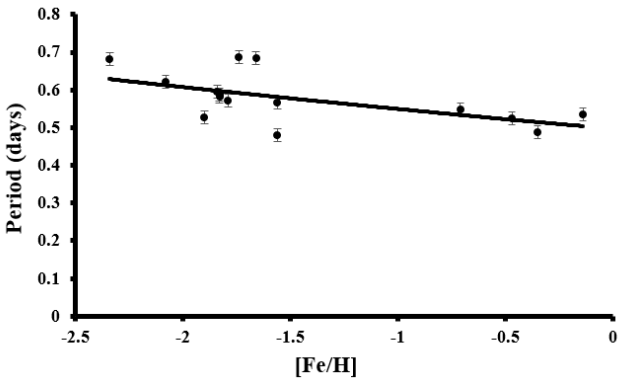

Figure 3: The relationship between [Fe/H] and the period of non-Blazhko RRab Lyraes. Stars with a higher metallicity were found to maintain shorter periods in their light curves. Mean ± SD (n=15).

of freedom. After removing outliers, the determined r^2 was 0.5584. When a logarithmic scale was applied, the line of best fit was $y = 0.2268e^{-0.318x}$, with an r^2 value of 0.2011 and $X^2 = 8.3835$, p = 0.8684 with 14 degrees of freedom. The conclusions of other studies are strongly connected to the correlation found in our study between [Fe/H] and absolute magnitude light curve amplitude. The concentration of data points on the left side of **Figure 2** was due to the RR Lyraes selected.

In **Figure 3**, the relationship between [Fe/H] and the period was a negative linear relationship modelled with the equation $y = -0.0582x + 0.494$ and an r^2 value of 0.3543. After removing outliers, the determined r^2 was 0.6013. The justification for this relationship is because RR Lyraes with fewer fusing elements are affected less by the natural process of atomic diffusion that can elongate a period in this type of variable star, as explained by Sandage *et al.* (20). This additional relationship proves how composition has a significant impact on an RR Lyrae's light curve. By being able to predict both the amplitude and the period of a RR Lyrae using just its [Fe/H] values, these relationships prove how metallicity can be a useful tool in predicting the light curves of RR Lyraes without extensive visual observation.

DISCUSSION

Through this study, the relationship between metallicity and the light curves of non-Blazhko RRab Lyraes was determined. We observed a negative exponential relationship between the [Fe/H] and the light curve amplitudes, and a negative linear relationship between the [Fe/H] and the light curve periods. These relationships prove how the composition of an RR Lyrae variable star has an impact on its light curve and thus can be utilized to provide better approximations of its light curve for use as a standard candle tool. The RR Lyraes used in this study were examined to be non-Blazhko RRab Lyraes in a 2011 study using the Kepler Space Telescope by Nemec *et al.* (19). Additionally, their [Fe/H] values were utilized in this analysis. The findings of Nemec *et al.* identified that non-Blazhko RRab Lyraes with lower [Fe/H]

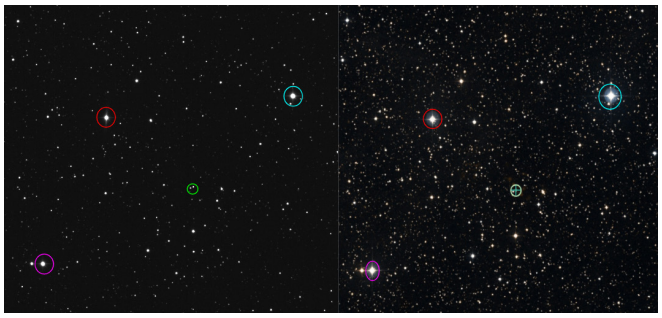

Figure 4: Comparison of Slooh image to SIMBAD image for identifying locator stars. To determine nearby locator stars of the RR Lyrae, we compared the image taken from Slooh and identified its location using the AladinLite View on SIMBAD. We then determined the coordinates and the apparent magnitude of locator star to find the apparent magnitude of the RR Lyrae.

values tended to have longer periods (19). This relationship matched with a secondary analysis in this study, where the correlation between [Fe/H] and period was represented as a negative exponential trend. Although not exactly the [Fe/H] to amplitude relationship found in this study, Nemec *et al.* identified a negative linear relationship between [Fe/H] to [B–V] color index (19). As the [B–V] color index is closely related to absolute magnitude, this negative trend found by Nemec *et al.* likely is tied to the negative exponential trend found in the present analysis.

Multiple previous studies support the trend found in **Figure 2** regarding metallicity and RR Lyrae light curve amplitudes. In the findings of Fernley *et al.* in 1990, the [Fe/H] value of –1.52 corresponds to a visual absolute magnitude (MV) of 0.72 ± –0.10 (21). This point is approximately the midpoint of V1107 Cyg, one of the RR Lyraes in the present study, with a [Fe/H] of –1.56. Fernley *et al.* also identified a positive linear slope of 0.18 ± 0.03 when comparing [Fe/H] and visual absolute magnitude (21). Furthermore, a study by Demarque *et al.*

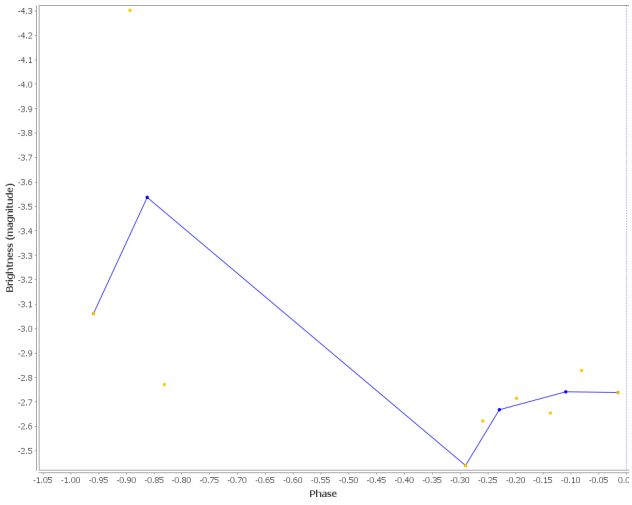

Figure 5: Resulting light curve of NR Lyr, one of the RR Lyraes analyzed. As the light curves produced by VStar display two periods (duplicates of the same data), only one period is shown here for clarity. The blue line represents the means of the data points from the analysis of the Slooh images. The x-axis is the phase while the y-axis is the brightness (in absolute magnitude).

looked into the use of horizontal branch models and the main sequence to further develop RR Lyraes as standard candles to globular clusters rather than using the period-luminosity relationship (22). By gathering data from the Hipparcos satellite, they concluded that the slope when depicting the relationship between visual absolute magnitude and [Fe/H] increased as [Fe/H] produced greater values. This provided evidence of a positive exponential relationship and supporting the study by Fernley *et al*. (21). These conclusions also verify the present study, since a larger absolute magnitude on a light curve's lower bound would produce smaller amplitudes with greater [Fe/H]. However, this draws discussions about a light curve's upper bound and how it would affect a phase plot's amplitude. A relationship identified by Fernley *et al*. was for Cepheids – the slope when comparing [Fe/H] and visual absolute magnitude was negative and linear at –2.15 ± 0.44, coming to show the variance amongst a wide spectrum of variable stars (21). A study on the specific Fourier components of RR Lyrae light curves by Norman R. Simon found that the particular Fourier phase parameter Φ_{21}, which shapes an RR Lyrae's light curve, decreases regularly with decreasing metallicity in short period stars but does not show this characteristic in long period stars (23).

In addition to the focus of our research in **Figure 2**, other papers support the additional relationship found in **Figure 3** regarding $10^{[Fe/H]}$ and period. In the findings by Sandage in 2004, a correlation across 140 stars between period *P*, metallicity, and amplitude range *AV* of RR Lyraes was found to be *[Fe/H] = -1.453 AV - 7.990 log P - 2.145*, a power law relationship written as a linear equation as the data were plotted with a logarithmic scale (24). This distinctly supports the current study as a negative relationship between [Fe/H] and both amplitude and period were observed in the 15 non-Blazhko RRab Lyraes analyzed.

In the future, increasing the sample size and diversifying the [Fe/H] values of the RR Lyraes would allow this correlation to be analyzed further. The large scatter in Fe abundance, which is typical in astronomical observations, certainly played a role in the determined r^2 value. Some additional errors may have resulted from the averaging procedure to calculate amplitude, the possible lack of data points to accurately determine period, and from varying weather conditions as the photos were taken across multiple days, which would have impacted the apparent magnitudes of the RR Lyraes in the images significantly.

One application of our conclusion would be to further utilize RR Lyraes as standard candles. Variable stars are often used to calculate distances because the period-luminosity relation facilitates the comparison between apparent magnitude and luminosity (13, 14). By analyzing the characteristics and light curves of RR Lyraes, scientists can better employ these variable stars as tools to find distances to galaxies, clusters, and other interstellar objects. Another application would be in research for stellar properties. Variable stars, especially RR Lyraes, contain quite extraordinary stellar properties that give them their characteristic light curve. In the future, further research on these variable stars such as analyzing the connection between composition and light curves for other variable star types or investigating the connection between composition and specific Fourier components of the light curve will provide a better comparison with normal stars and develop understanding of these unique stars.

MATERIALS AND METHODS

Obtaining Slooh Images

To gather data of 15 non-Blazhko RRab Lyraes, 135 images were taken via remote access by the 432 mm aperture Slooh Canary Two telescope located at the Institute of Astrophysics of the Canary Islands (IAC) in Tenerife, Canary Islands. Reservations were made for nine times during the day (eastern standard time): at 5:30 pm, 6:30 pm, 7:30 pm, 8:30 pm, 9:30 pm, 10:30 pm, 11:30 pm, 12:30 am, and 1:30 am. The 15 non-Blazhko RRab Lyraes include NR Lyr, V782 Cyg, V784 Cyg, KIC 6100702, NQ Lyr, FN Lyr, KIC 7021124, KIC 7030715, V1510 Cyg, V350 Lyr, V894 Cyg, V2470 Cyg, V1107 Cyg, V838 Cyg, and AW Dra. These variable stars were identified as non-Blazhko RRab Lyraes in a 2011 study by the Kepler Space Telescope by Nemec *et al*. (19).

Using AstroImageJ to Find Apparent Magnitude

By accessing the SIMBAD database, the AladinLite View provides information such as the apparent magnitude of the locator star (**Figure 4**). Using AstroImageJ (University of Louisville), the apparent magnitude of the variable star in the images can be found by comparing it to the given apparent magnitude of the locator star.

Parallax angles are offered on SIMBAD, which can help calculate the distance of the star in parsecs by using the equation:

$$d = 1/p$$

where *p* is the parallax angle in arcseconds and *d* is the distance in parsecs.

The apparent magnitude found in the collected images can be combined with the distance calculated to find the absolute magnitude via the distance modulus.

$$M = m + 5 - 5\log d$$

where *M* is the absolute magnitude, *m* is the apparent magnitude, and *d* is the distance in parsecs.

Using VStar to Create and Analyze Light Curves

Data were put into a .txt file, with the Julian date in decimal format separated by a comma with the absolute magnitude, with each new line signifying a different time. Using VStar, a plotting program by the AAVSO, light curves (also known as phase plots) were created with means to display lines for the graph's shape (**Figure 5**). The light curve's amplitude was defined as the average of the absolute value of the difference between the maximum and minimum of the apparent magnitude values from **Table 1**.

Data Analysis

Data were plotted using Microsoft Excel. The line of best fit was calculated using the method of least squares which was also automatically calculated by Excel. The r^2 statistical test was implemented through Excel by using the RSQ formula on the dataset. The X^2 statistical test was also implemented through Excel by first producing a spreadsheet with the original data and the expected data (calculated using the line of best fit for the correlation) then using the CHISQ. TEST formula to find p (probability of independence). X^2 was calculated manually by using the formula (*observed value* - *expected value*)^2/(*expected value*) for each data point then adding up all the calculated results together. The degrees of freedom were calculated using (*rows* - 1) × (*columns* - 1). The correlating statistical tests were also calculated after removing outliers visually. The calculation for the error bars used the standard error method which is indicative of the data's standard deviation (n = 15 for **Figure 2** and **Figure 3**).

In **Figure 2**, the correlation between [Fe/H] and amplitude of the phase plots was determined by testing both a linear scale and a logarithmic scale. Since [Fe/H] is a logarithmic unit, the linear scale was determined by calculating $10^{[Fe/H]}$ for each RR Lyrae. The linear scale was implemented on the graph by placing $10^{[Fe/H]}$ on the x-axis and amplitude on the y-axis. After comparing different relationship types for the line of best fit on Excel, a power law relationship was found to visually be the best fit for the data. For a logarithmic scale, [Fe/H] was placed on the x-axis and amplitude on the y-axis.

Received: May 16, 2020
Accepted: October 27, 2020
Published: December 13, 2020

REFERENCES

1. Space.com Staff. "Types of Variable Stars: Cepheid, Pulsating and Cataclysmic." *Space*, 29 Jan. 2015, www.space.com/15396-variable-stars.html. Accessed 11 Aug. 2018.
2. "Variables: What Are They and Why Observe Them?" *Aavso.Org*, www.aavso.org/variables-what-are-they-why-observe-them. Accessed 2 Aug. 2018.
3. CSIRO Australia Telescope National Facility. "Types of Variable Stars." *Csiro.Au*, www.atnf.csiro.au/outreach/education/senior/astrophysics/variable_types.html. Accessed 2 Aug. 2018.
4. Kiess, C. "The Importance of Variable Stars in Modern Astronomy." *Publication of the Pomona College Astronomical Society*, vol. 5, Jan. 1916, pp. 48–53. Accessed 16 Oct. 2020. Accessed 2 Aug. 2018.
5. CSIRO Australia Telescope National Facility. "Pulsating Variable Stars." *Csiro.Au*, www.atnf.csiro.au/outreach/education/senior/astrophysics/variable_pulsating.html. Accessed 2 Aug. 2018.
6. "RR Lyrae." *Aavso.Org*, www.aavso.org/vsots_rrlyr. Accessed 9 Aug. 2018.
7. "Distance Modulus." *Unl.Edu*, www.astro.unl.edu/naap/distance/distance_modulus.html. Accessed 9 Aug. 2018.
8. Fernie, John Donald. *Britannica.Com*, www.britannica.com/science/RR-Lyrae-star. Accessed 2 Aug. 2018.
9. CSIRO Australia Telescope National Facility. "Pulsating Variable Stars." *Csiro.Au*, www.atnf.csiro.au/outreach/education/senior/astrophysics/variable_pulsating.html. Accessed 2 Aug. 2018.
10. Smith, Horace A. Cambridge Astrophysics: RR Lyrae Stars Series Number 27. *Cambridge University Press*, 2004.
11. "Apparent and Absolute Magnitudes." *Ksu.Edu*, www.phys.ksu.edu/personal/wysin/astro/magnitudes.html. Accessed 16 Oct. 2020. Accessed 9 Aug. 2018.
12. "Cepheid Variable Stars, Supernovae and Distance Measurement." *Lco.Global*, www.lco.global/spacebook/distance/cepheid-variable-stars-supernovae-and-distance-measurement/. Accessed 5 Aug. 2018.
13. Willick, Jeffrey A. Measurement of Galaxy Distances. 1996, www.ned.ipac.caltech.edu/level5/Willick/Willick2.html. Accessed 11 Aug. 2018.
14. CSIRO Australia Telescope National Facility. "Cepheid Variable Stars & Distance." *Csiro.Au*, www.atnf.csiro.au/outreach/education/senior/astrophysics/variable_cepheids.html. Accessed 10 Aug. 2018.
15. Ryden, Barbara. "Lecture 16: Pulsating Stars." *Ohio-State.Edu*, 28 Jan. 2003, www.astronomy.ohio-state.edu/~ryden/ast162_4/notes16.html. Accessed 9 Aug. 2018.
16. Mihos, Chris. "Metallicities and Stellar Populations." *Case.Edu*, www.burro.case.edu/Academics/Astr222/Galaxy/Structure/metals.html. Accessed 4 Aug. 2018.
17. Smolec, R. "The Blazhko Effect." *ArXiv [Astro-Ph.SR]*, 2016, www.arxiv.org/abs/1603.01252.
18. "Kepler Data Search & Retrieval." *KEPLER Search*, Mikulski Archive for Space Telescopes, www.archive.stsci.edu/kepler/data_search/search.php.
19. Nemec, J. M., *et al.* "Non-Blazhko RR Lyrae Stars Observed with the KEPLER Space Telescope." *ArXiv [Astro-Ph.SR]*, Aug. 2011, www.arxiv.org/abs/1108.5683.
20. Sandage, Allan. "The Oosterhoff Period-Metallicity Relation for RR Lyrae Stars at the Blue Fundamental Edge of the Instability Strip." *The Astronomical Journal*, vol. 106, 1993, p. 687.
21. Fernley, J. A., *et al.* "The Absolute Magnitudes of RR Lyrae Stars – III. DH Peg *." *Monthly Notices of the Royal Astronomical Society*, vol. 242, no. 4, 1990, pp. 685–691.
22. Demarque, Pierre, *et al.* "The Metallicity Dependence of RR Lyrae Absolute Magnitudes from Synthetic Horizontal-Branch Models." *The Astronomical Journal*, vol. 119, no. 3, 2000, pp. 1398–1404.
23. Simon, Norman R. "On Metallicity and RR Lyrae Light Curves." *The Astrophysical Journal*, vol. 328, 1988, p. 747.
24. Sandage, Allan. "The Metallicity Dependence of the

Fourier Components of RR Lyrae Light Curves Is the Oosterhoff-Arp-Preston Period Ratio Effect in Disguise." *The Astronomical Journal*, vol. 128, no. 2, 2004, pp. 858–868.

JOURNAL OF
EMERGING INVESTIGATORS

Article

Impact of soil productivity on the growth of two Meyer lemon trees

Aniyah Shen and Shiqin Xu
University High School, Irvine, California

SUMMARY

Home gardening is one of the most popular activities in the United States. As participation increases, more homeowners are turning to home testing to solve gardening problems. We aimed to apply home soil testing to one such problem: identifying the cause of the growth differences between two lemon trees in our backyard. Since the two lemon trees are of the same species, were planted at the same time side-by-side, and given similar amounts of water and fertilizer, we hypothesized that differences in physical and chemical soil characteristics were influencing differences in soil productivity and plant growth. We tested five factors that affect soil productivity: soil composition, permeability, water-holding capacity (WHC), pH and free ions, and ion exchange capacity. We analyzed five soil samples with three trials each from the root spread perimeter of each tree, then analyzed variance of the results. We found that the soil samples from the lemon tree with higher growth had significantly higher WHC and permeability due to higher humus content and better anion exchange capacity (AEC) due to higher clay content. High sand content and low humus content reduced WHC, permeability, and AEC in the poor soil. All samples had sufficient nutrients and ideal pH, so the two soils did not differ obviously in the tested chemical characteristics. A clay and humus mixture can be added to improve soil productivity for the lower-performing tree. Overall, our study demonstrated the effectiveness of home soil testing to characterize soils and help homeowners solve common gardening problems.

INTRODUCTION

Home gardening has increased by 200% since 2008, with 35% of households in the United States growing food at home or in a community garden (1). During the COVID-19 pandemic, even more people have begun home gardening and crowdfunding community gardens (2). This may be attributed to the higher emotional wellbeing and sense of connectivity that is associated with vegetable gardening in urban settings (3). In fact, more than half of all California residences have a citrus tree (4). By using two lemon trees as our experimental subjects, we studied the most popular crop category in California residences.

The major factor affecting plant growth is soil productivity, defined as a soil's capacity to produce a certain crop yield under certain inputs of water and nutrients. Soil productivity is influenced primarily by the physical and chemical composition of soil (5). Physical soil composition consists of soil texture and structure; the former describes the amounts of sand, clay, and silt that make up a specific soil, while the latter refers to the arrangement of these particles to form distinctive geometries (6-7). In each soil sample, 40 – 80% of soil is made of sand, clay, and silt; different combinations result in different properties (8). Soils with a nearly equal balance of all three particles are described as loam soils (6). Prior studies have shown that soil water content decreases gradually as particle size increases and texture becomes coarser (9). Sand, the largest particle, increases permeability, water infiltration, capillarity, and density but does not retain water for long-term use. Silt, the second largest, increases aeration and water retention. Clay, the smallest, is critical for ion exchange and increases water retention but resists water infiltration.

Soil organic matter (SOM) is another important component of physical soil composition. SOM makes up only 1 - 6% of soil but has significant effects on physical properties and chemical composition (8). SOM contains live organisms, fresh residue, and stable, clay-bound matter called humus that contributes nutrients and increases water-holding capacity (WHC), permeability, and ion exchange capacity. WHC measures water absorption and retention, while permeability measures water infiltration and the speed of water movement through soil. Both are critical for plant growth in the dry, sunny Southern California climate. In fact, lemon trees grown in soils with low silt, clay, and SOM have lower WHC, permeability, and ion exchange capacity, resulting in significantly lower fruit yield (10).

Ion exchange capacity is a chemical property that refers to a soil's ability to hold onto cationic (positively charged) and anionic (negatively charged) nutrients. Ion exchange capacity is an indicator of soil fertility; soils with poor ion exchange capacity suffer from leaching (9). Leaching then decreases WHC, as shown by a decrease in soil water content after leaching under consistent air pressure and water pressure of soil pores (11). Ion exchange capacity can be improved by clay and SOM because negatively charged sites on the surfaces of clay and SOM particles attract cations. Anions, however, travel with water and run out more frequently.

Chemical soil properties are influenced by a soil's chemical composition, including pH and nutrient levels. pH indicates the acidity of a soil and affects solubility and availability of nutrients, microorganism activity, and crop yield (12-13). Lemon trees have an ideal pH range of 5.5 – 6.5. To maintain this pH range, the mixture of soil components can be altered. Clay and SOM increase the buffering capacity of soils, which is important because soil pH fluctuates as environments inevitably change. In contrast, sandy soils often have low SOM and are more vulnerable to acidification (13).

Nitrogen, potassium, and phosphorus are the three macronutrients most critical for productive soils. They are needed in large quantities and found in soil as mobile nitrate (NO_3^-), immobile phosphate (PO_4^{3-}), and immobile potassium ions (K^+) (14). Nitrogen, which is not retained long in the root zone, is a component of chlorophyll and nucleic acids (15). Sufficient nitrogen is vital for high rates of photosynthesis, vigorous plant growth, and dark green leaf color (8). Potassium plays a key role in osmoregulation, enzyme activation, pH neutralization, and energy production. Phosphorus is a component of nucleic acids and is important for cell division, tissue development, and regulation of protein synthesis (16). Lemon trees require double the amount of nitrogen needed by other citrus species, potassium for high-quality fruit, and phosphorus for flowers to bloom (16-17).

We purchased two Meyer lemon tree seedlings about ten years ago and planted them side by side at the same time. One lemon tree consistently produces more fruit and visibly has higher biomass, while the other tree has lower fruit yield **(Figure 1)**. We conducted this project to find why these two trees differ so significantly in growth despite growing in similar environments and receiving similar amounts of water and fertilizer. Access to and retention of water and nutrients play critical roles in soil productivity and, consequently, plant growth. Thus, we hypothesized that the growth differences between the two lemon trees in our backyard were due to differences in soil productivity. We specifically hypothesized that differences in soil productivity resulted from differences in physical and chemical soil composition. Our results show that higher clay and humus levels in the good soil led to higher permeability, WHC, and ion exchange capacity. However, the two soils did not differ obviously in pH and macronutrient content. Like my family, many homeowners are amateur gardeners who encounter problems that they do not know how to characterize and address. The methods and results from this study can serve as an accessible example.

Figure 1. The two Meyer lemon trees in the Southern California backyard of this study. The left tree exhibits improved growth, as evident from the higher leaf density and number of fruits.

RESULTS

We took five evenly spaced soil samples from around the root spread of each lemon tree. We conducted three trials per sample for a total of 15 trials per tree for soil composition, WHC, soil permeability, and ion exchange capacity. The soil samples from the lemon tree with good growth were labelled G1, G2, G3, G4, and G5 for "good" growth. The samples from the lemon tree with poor growth were labelled B1, B2, B3, B4, and B5 for "bad" growth. We extended this labelling system to include trial numbers during the experiments (i.e. G1.1, G1.2, G1.3 for the 3 trials of sample 1 with good growth, B1.1, B1.2, B1.3 for sample 1 with bad growth, etc.).

We analyzed the results from each experiment by comparing the B and G samples to the controls to determine the specific factors influencing each property. Overall, the two soils showed significant differences in physical characteristics but no obvious differences in the tested chemical characteristics. Results are summarized in **Table 1.**

We tested soil composition to analyze particle distribution. The B samples contained 51% sand, 22% clay, and 27% silt. The G samples contained 45% sand, 24% clay, and 31% silt (**Table 1**, **Figure 2**). According to the USDA Soil Texture Triangle, the B samples are on the border between sandy clay loam and loam, and the G samples are loam (8). While preparing the soil samples, we noticed that the G samples were darker in color and had a chunkier texture. Then, in the WHC experiment, we observed that the control sample of humus (9.33 g) weighed less than the same volumes of sand (20.36 g) and clay (14.93 g). Likewise, the ANOVA analysis showed that the G samples (average weight 14.56 g) weighed significantly less ($p < 0.001$) than the B samples of the same volume (average weight 16.41 g) (**Table 2**). Together, these

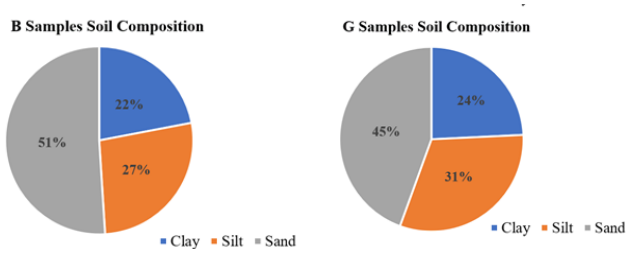

Figure 2. Physical composition of soil samples. The B samples (n = 15) were between sandy clay loam and loam and contained more sand than the G samples (n = 15). The G samples were loam and contained higher levels of clay and silt than the B samples.

Table 1. Summary of results from the five main experiments.

Sample	Soil Composition			WHC***	Soil Permeability		pH	N	P	K	Ion Exchange Capacity	
	% Sand	% Clay	% Silt		Dry Samples (s)**	Wet Samples (s)*					CEC	AEC
B1	51	19	30	0.36	334	1379	6	4	3	3	High	Low
B2	48	25	27	0.31	340	3190	6	4	4	2	High	Medium
B3	46	22	32	0.35	309	1483	6	3	3	3	High	Low
B4	53	26	21	0.36	244	1312	6	3	3	3	High	Low
B5	57	17	26	0.38	609	2198	6	4	2	2	High	Low
B Mean	**51**	**22**	**27**	**0.35**	**367**	**1912**	**6**	**3.6**	**3**	**2.6**	**High**	**Low**
Standard Deviation (SD)	**6**	**6**	**4**	**0.12**	**175**	**774**	**0**	**0.5**	**0.7**	**0.5**	**N/A**	**N/A**
G1	49	22	29	0.47	145	1354	6.5	4	4	2	High	Medium
G2	47	20	33	0.49	70	644	6.5	4	4	2	High	Medium
G3	41	29	30	0.46	160	1036	6.5	4	4	3	High	Medium
G4	42	25	33	0.47	112	1102	6.5	4	4	3	High	Medium
G5	44	25	31	0.47	70	911	6.5	4	4	3	High	Medium
G Mean	**45**	**24**	**31**	**0.47**	**112**	**1009**	**6.5**	**4**	**4**	**2.6**	**High**	**Medium**
SD	**4**	**4**	**2**	**0.01**	**51**	**296**	**0**	**0**	**0**	**0.5**	**N/A**	**N/A**
p-value (ANOVA)	**N/A**			**1.21e-05**	**0.00455**	**0.04280**	**N/A**					

*Note: Nutrient levels: 4 = surplus, 3 = sufficient, 2 = adequate, 1 = deficient, 0 = depleted. Significance: *** = 0.001, ** = 0.01, * = 0.05.*

factors indicated higher humus content in the G samples.

We calculated the mean WHC for the 15 B samples and the 15 G samples **(Table 2)**. B samples had low average WHC (0.35) and G samples had medium average WHC (0.47) according to the WHC classification in the *Carolina Physical and Chemical Properties of Soil* kit manual. A mixed model ANOVA indicated that such a difference in WHC between B samples and G samples was statistically significant ($p < 0.001$). Among the control samples of humus, clay, and sand in this experiment, humus had the highest WHC (0.47), followed by clay (0.37) and sand (0.24). Therefore, higher humus levels in the G samples appear to associate strongly with higher WHC.

We tested permeability in both wet and dry conditions. The mean time for the 15 dry B samples was 367 s, which was significantly longer than the average 112 s for the 15 dry G samples ($p = 0.00455$ from the ANOVA analysis). The mean time for the 15 wet B samples was 1,912 s, which was significantly longer than the average 1,009 s for the 15 wet G samples ($p = 0.0428$ from the ANOVA analysis) **(Figure 3)**. For controls, water traveled slowest through clay (dry: 365 s, wet: 6,965 s) and fastest through humus (dry: 37 s, wet: 239 s).

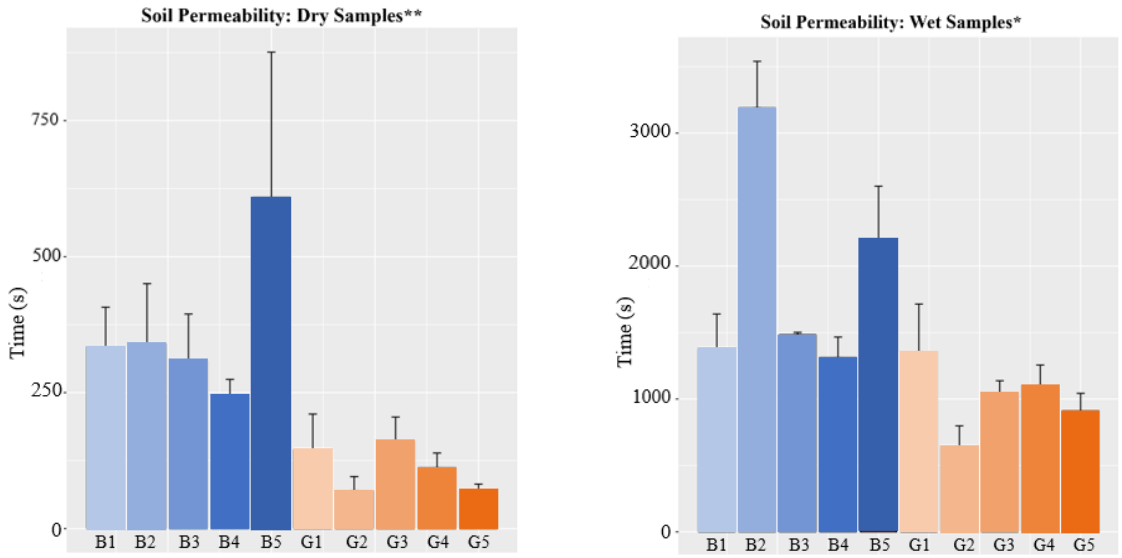

Figure 3. Soil permeability of samples. In both experiments, G samples ($n = 15$) took significantly less time than B samples ($n = 15$) and thus had higher permeability. The larger SD of the B samples indicates less uniformity within the poorer soil. Significance: *** = 0.001, ** = 0.01, * = 0.05.

The permeability of sand was between clay and humus (dry: 190 s, wet: 327 s). Humus was the most permeable, followed by sand and clay. Although the G samples had 2% more clay, the decrease in permeability from this small amount of clay was insignificant compared to the increase in permeability from the large amount of humus.

We analyzed the pH and nitrogen, phosphorus, and potassium levels of the soil samples using the color comparators of the *Rapitest* soil test kit included in the *Carolina* kit. B samples had mean pH = 6 and G samples had mean pH = 6.5, both in the ideal range for a lemon tree. All samples had adequate potassium and surplus or sufficient nitrogen and phosphorus **(Figure 4)**. Thus, there was no obvious difference between the two soils in pH and macronutrient levels.

While the pH and free ions analysis measured the availability of essential nutrients, ion exchange capacity was tested to determine the ability of the samples to hold onto those nutrients. Both B and G samples had high cation exchange capacity (CEC) for Crystal Violet. For Eosin Y, G samples had medium anion exchange capacity (AEC) and B samples had low AEC **(Table 3)**. The movement of positively

Table 2. Water Holding Capacity (WHC) of the soil samples.

Sample		Weight of Empty Column (g)	Weight of Column + Dry Soil (g)	Weight of Column + Saturated Soil (g)	Weight of Water (g)	Weight of Soil (g)***	WHC***	
Control	Clay	3.25	18.18	23.66	5.48	14.93	0.37	Low
	Sand	3.14	23.50	28.34	4.84	20.36	0.24	Low
	Humus	3.20	12.53	16.90	4.37	9.33	0.47	Medium
B1	B1.1	2.88	19.74	25.64	5.90	16.86	0.35	Low
	B1.2	2.90	19.16	25.16	6.00	16.26	0.37	Low
	B1.3	2.92	19.54	25.45	5.91	16.62	0.36	Low
B2	B2.1	2.93	19.00	24.85	5.85	16.07	0.36	Low
	B2.2	2.90	19.55	24.43	4.88	16.65	0.29	Low
	B2.3	2.93	19.50	24.18	4.68	16.57	0.28	Low
B3	B3.1	2.91	18.67	24.78	6.11	15.76	0.39	Low
	B3.2	2.87	18.97	24.08	5.11	16.10	0.32	Low
	B3.3	2.88	18.52	24.03	5.51	15.64	0.35	Low
B4	B4.1	2.92	19.08	24.73	5.65	16.16	0.35	Low
	B4.2	2.88	18.98	24.77	5.79	16.10	0.36	Low
	B4.3	2.87	19.28	25.26	5.98	16.41	0.36	Low
B5	B5.1	2.94	20.60	26.50	5.90	17.66	0.33	Low
	B5.2	2.96	19.72	27.54	7.82	16.76	0.47	Medium
	B5.3	2.89	19.41	25.14	5.73	16.52	0.35	Low
B Mean		**2.91**	**19.31**	**25.10**	**5.79**	**16.41**	**0.35**	**LOW**
SD		**0.11**	**1.94**	**2.24**	**1.08**	**1.98**	**0.12**	**N/A**
G1	G1.1	2.94	17.44	24.38	6.94	14.50	0.48	Medium
	G1.2	2.90	17.50	24.21	6.71	14.60	0.46	Medium
	G1.3	2.90	18.16	25.55	7.39	15.26	0.48	Medium
G2	G2.1	2.89	17.16	23.96	6.80	14.27	0.48	Medium
	G2.2	2.90	17.76	25.03	7.27	14.86	0.49	Medium
	G2.3	2.92	17.52	25.00	7.48	14.60	0.51	Medium
G3	G3.1	2.93	16.70	24.46	7.76	13.77	0.46	Medium
	G3.2	2.89	16.94	24.89	7.95	14.05	0.47	Medium
	G3.3	2.92	17.54	25.56	8.02	14.62	0.46	Medium
G4	G4.1	2.92	17.10	25.32	8.22	14.18	0.48	Medium
	G4.2	2.93	17.39	25.67	8.28	14.46	0.48	Medium
	G4.3	2.92	17.30	25.33	8.03	14.38	0.46	Medium
G5	G5.1	2.90	18.26	25.35	7.09	15.36	0.46	Medium
	G5.2	2.93	17.76	24.84	7.08	14.83	0.48	Medium
	G5.3	2.91	17.53	24.62	7.09	14.62	0.48	Medium
G Mean		**2.92**	**17.47**	**24.94**	**7.47**	**14.56**	**0.47**	**MEDIUM**
SD		**0.02**	**0.42**	**0.53**	**0.53**	**0.42**	**0.01**	**N/A**
p-value (ANOVA)		**N/A**				**5.35e-05**	**1.21e-05**	**N/A**

*Note: WHC less than 0.4 is classified as low capacity, and WHC between 0.4 and 0.6 is classified as medium capacity according to the kit manual. Significance: *** = 0.001, ** = 0.01, * = 0.05.*

charged Crystal Violet and negatively charged Eosin Y mimicked the movement of cationic and anionic nutrients through soil, respectively. For Eosin Y, the controls sand and sand + humus had low AEC, while sand + clay had medium AEC. This displays the negative effects of sand on AEC and how clay increases AEC. The G samples contained 2% more clay and 6% less sand than the B samples **(Figure 1)**. Therefore, the higher AEC of the G samples was consistent with its higher clay levels, and the low AEC of the B samples was consistent with its higher sand content and lower clay content.

DISCUSSION

The higher permeability and WHC of the G samples mean that water travels to the roots significantly faster in the G soil and is retained significantly better. The G soil also provides better aeration and resists nutrient leaching due to its more compact, fine texture. The organic matter in the humus balances the effects of higher clay and silt levels by increasing drainage speed and binding particles into stable clumps. In contrast, the sandy texture of the B soil means that while water drainage is efficient, water retention and AEC are low. Thus, while both soils hold onto cation nutrients well, the good soil retains mobile anion nutrients like NO_3^- more effectively.

An unexpected result was that the soils did not differ obviously in the measured chemical characteristics. Nutrient deficiencies were expected for the poor soil, but both soils had an ideal pH for lemon trees and contained sufficient nitrogen, phosphorus, and potassium. Even the difference in ion exchange capacity, a chemical property, was likely due to differences in physical composition. Thus, our hypothesis that the growth differences between the two lemon trees was being caused by differences in both physical and chemical soil composition was partially supported. The soil productivity of the poor soil can be improved by the addition of a clay and humus mixture.

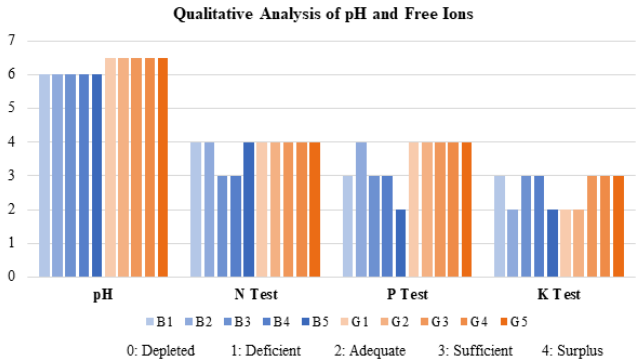

Figure 4. pH, nitrogen (N), phosphorous (P), and potassium (K) levels of soil samples. Both B samples (n = 5) and G samples (n = 5) had an ideal pH for lemon trees, adequate potassium, and sufficient or surplus amounts of nitrogen and phosphorus. All three ions are dimensionless.

In addition, the B samples had a larger standard deviation (SD) in physical characteristics compared to the G samples, suggesting an uneven distribution of soil composition, permeability, and WHC in the poor soil **(Table 1)**. Likewise, the B samples had more variation in nitrogen and phosphorus levels **(Figure 4)**. The relative chemical inconsistency of the B samples could be impactful despite the B and G samples showing little differences in pH and free ions. Overall, such

Table 3. Ion Exchange Capacity of the soil samples.

Sample		Crystal Violet			Eosin Y		
		Average Amount of Water (mL)	Color Intensity	CEC	Average Amount of Water (mL)	Color Intensity	AEC
Controls	Sand	6	Dark	Low	5	Dark	Low
	Sand + Clay	15	Light	High	6	Light	Medium
	Sand + Humus	18	Light	High	6	Medium	Low
B	B1	10	Light	High	6	Medium	Low
	B2	13	Light	High	6.3	Light	Medium
	B3	14	Light	High	6	Medium	Low
	B4	15	Light	High	6	Medium	Low
	B5	15	Light	High	6.3	Medium	Low
B Mean		**13.40**	**Light**	**High**	**6.12**	**Light**	**Low**
SD		**3.2**	**N/A**		**0.4**	**N/A**	
G	G1	17	Light	High	7.7	Light	Medium
	G2	17	Light	High	6.7	Light	Medium
	G3	17	Light	High	5	Light	Medium
	G4	16	Light	High	6.7	Light	Medium
	G5	16	Light	High	7	Light	Medium
G Mean		**16.60**	**Light**	**High**	**6.62**	**Light**	**Medium**
SD		**3.2**	**N/A**		**1.1**	**N/A**	

Note: AEC = anion exchange capacity, CEC = cation exchange capacity.

uneven physical and chemical distribution may have been another factor negatively affecting lemon tree growth.

In conclusion, there are few differences in the measured chemical characteristics but several significant differences in the tested physical characteristics, especially those related to water retention. Considering California's particularly dry climate, poor water retention was likely the most influential factor behind one lemon tree's poorer growth.

In addition, one confounding factor that could have influenced the growth differences was differing amounts of reflected sunlight due to different physical backgrounds. Though the two lemon trees were planted side by side, the tree with poor growth is located closer to the corner and in front of a white wall, while the tree with better growth is in front of a brown brick wall **(Figure 1)**. The former's shaded corner location may prevent it from attaining sunlight for photosynthesis during dimmer days, while its white background reflects more heat and light during the hot summers compared to the brown brick background of the other tree. This may exacerbate the water burden already placed on the lemon tree with poor growth due to its soil composition. In the future, we can measure the amount of reflected light and the average temperature near the two trees during different times of the day to better characterize this potential factor.

Limitations that could have affected the results include imprecise timing and subjective color assessment. During the permeability experiment, five samples had to be observed simultaneously, so timing precision may have been compromised. In the ion exchange capacity experiment, color intensity of filtered water was assessed through comparison to surrounding samples. These aspects can be improved by incorporating slow-motion recordings and color references into the experimental design. Slow-motion video could be used for rewind purposes to determine more precisely when specific moments occurred. Ideally, a colorimeter would be used to determine color intensity of the filtered water. From a realistic homeowner perspective, however, a color scale or examples of what should be considered light, medium, and dark water would improve the color assessment.

Further research on soil structure, porosity, and nutrient distribution would also contribute to this study by addressing the variability in the B samples and the effects of WHC and permeability on soil aeration and nutrient availability. Testing soil uniformity would enable more concrete conclusions to be drawn about soil consistency. Testing micronutrients such as iron, zinc, and manganese would also contribute to the comprehensiveness of the chemical analysis.

In total, our results provide valuable insight to homeowners and gardeners who are having difficulties raising healthy plants. Applying these experiments to home soils can pinpoint problems and determine what specific particles, nutrients, or fertilizers to add to improve soil productivity. Potential applications of this study include soil testing for gardens, backyards, and parks to characterize and study soil quality at the household, community, and city levels. An increased accessibility to soil testing would help people correct common errors like overwatering and using the wrong fertilizer.

MATERIALS AND METHODS

Preparing the soil samples

500 g of soil from 8 in below the ground was retrieved from each of five evenly spaced sites around the perimeter of each lemon tree's root spread. Each sample was placed on separate 18" x 20" sheets of Nalgene Versi-Dry surface protectors from ThermoFisher Scientific. Rocks, stones, and branches were taken out, clumps of soil crushed, and soil spread out evenly. Samples were placed in an open area and dried under natural sunlight for 1 day before being transferred into labelled 10" x 14" Ziploc bags for storage.

The *Carolina Physical and Chemical Properties of Soil* kit and accompanying manual were adapted for use in the following experiments:

Soil composition

Thirty-three plastic jars (30 samples, 3 controls: clay, silt, and sand) were labelled and marked at the halfway line with a black china marker pencil. Each jar was filled with the corresponding sample to the halfway mark. Tap water was added to the lower rim of the jar before each jar was shaken for 30 seconds. 1 drop of dish detergent was added to each jar to help the layers settle clearly overnight. Settled layers were labelled (from top to bottom): humus, clay, silt, and sand. The thickness of every layer except humus, an organic component, was measured and recorded. The thickness percentages of clay, silt, and sand for the samples were then calculated, averaged, and compared to the USDA Soil Texture Triangle in the *Carolina* kit manual to determine soil composition.

WHC and capillary action

Thirty-three plastic columns (30 samples, 3 controls: sand, clay, humus) were used. A black china marker pencil was used to mark a line 7 cm from the bottom end of each column. Two 1" x 1" cheesecloth pieces were secured over each bottom end using a rubber band. A balance scale was used to determine the weight in grams of each column before and after filling to the 7 cm mark with soil. The weight of soil was calculated by subtracting the weight of the empty column from the weight of the column and dry soil. A plastic bin was filled with water to the 1 cm mark and all 33 columns were secured into a holder and placed into the bin overnight with the cheesecloth ends submerged. The following day, the weight of absorbed water was calculated by subtracting the weight of the saturated column from the weight of the unsaturated column. The weight of absorbed water was divided by the weight of soil and the resulting value compared to the manual's standards to determine WHC.

Soil permeability

Each saturated column from the WHC experiment was

suspended using 2 twist ties above a vial. 10 mL of water was poured into each wet sample using a measuring cup. A timer was used to record when the first drop of water passed out of the bottom of each column and when all the water above each sample was absorbed. 30 dry soil samples and 3 control samples were prepared using the same procedure from the WHC experiment and the timing process was repeated. The time it took for 10 mL of water to travel through each wet and dry saturated column was used to measure soil permeability.

Analysis of pH and free ions

For pH, soil samples were filled to the bottom tester line and chemical reagents from a pH indicator capsule were added. Water was added using a pipet to the top tester line. The tester was shaken vigorously by hand for 1 minute and allowed to settle for another 1 minute. The color of the solution was compared with the pH chart and pH was recorded.

For nitrogen, phosphorus, and potassium, the 30 jars from the soil composition experiment were used. For each sample, 10 mL of soiled water was pipetted from the top of the 3 trial jars and mixed in a cup. The mixed water was added to each tester to the marked line and shaken for 1 minute with the powder from 1 corresponding indicator capsule. Testers settled for 5 minutes before colors of the solutions were compared to the corresponding charts.

Qualitative analysis of Ion Exchange Capacity

Thirty-three centrifuge tubes (30 samples, 3 controls: sand, sand + clay, sand + humus) were labelled. A line 15 cm from the bottom of each tube was marked with a black china marker pencil. Two rubber bands were bound at the line to help secure the centrifuge tube above the vial. Corresponding soil samples were filled to the 15 cm mark and 20 drops of 1% Crystal Violet were added evenly across the top of each sample. Water was pipetted in increments of 1 mL into each sample until water began to pass out the bottom of the centrifuge tube. The amount of water added and the color intensity of the filtered water relative to the other samples was recorded. Tubes and vials were rinsed and dried before the entire process was repeated with Eosin Y. Results were compared to the manual's Exchange Capacity Chart.

Statistical Analysis

Charts from the kit were used to analyze the data for WHC, analysis of pH and free ions, and qualitative analysis of ion exchange capacity. The linear mixed model of $y_{ijk} = \mu + \alpha_i + \beta_{ij} + \varepsilon_{ijk}$ was used in the statistical analysis, where y_{ijk} is the observed response variable, such as WHC, μ is the grand mean, α_i is the fix effect for tree location with i = 1 or 2, β_{ij} is the random effect for the jth sample collected from the ith tree location with j = 1, 2, 3, 4, or 5, and ε_{ijk} is the random error of the kth measurement for the jth sample from the ith tree location with k = 1, 2 or 3. The ANOVA for the linear mixed effects model was performed using R package 'lmerTest' (18).

ACKNOWLEDGEMENTS

I would like to acknowledge Wanqi Jia (University High School, Irvine) for helping me complete the ANOVA tests. Special thanks also go to Dr. Francesco Palomba (University of California, Irvine) and Professor Michelle Digman (University of California, Irvine) for giving me valuable advice on how to communicate my scientific findings clearly. Lastly, I would like to thank the reviewers and editors of the Journal of Emerging Investigators for all their constructive feedback and for giving students like me an opportunity to practice writing and publishing our findings.

Received: August 9, 2020
Accepted: December 7, 2020
Published: December 14, 2020

REFERENCES

1. Lissy, Marin. "Gardening Boom: 1 in 3 American Households Grow Food." Farmer Foodshare, *Farmer Foodshare*, 15 June 2017, farmerfoodshare.org/farmer-foodshare/2017/6/15/gardening-boom-1-in-3-american-households-grow-food
2. Yu, Alan. "Fearing Shortages, People Are Planting More Vegetable Gardens." *NPR*, National Public Radio, 27 Mar. 2020, npr.org/sections/coronavirus-live-updates/2020/03/27/822514756/fearing-shortages-people-are-planting-more-vegetable-gardens.
3. Ambrose G, Das K, Fan Y, Ramaswami A. "Is gardening associated with greater happiness of urban residents? A multi-activity, dynamic assessment in the Twin-Cities region, USA." *Landscape and Urban Planning*, vol. 198, June 2020, pp. 4-9, doi.org/10.1016/j.landurbplan.2020.103776.
4. "California Citrus." California Citrus Threat, *Citrus Pest & Disease Prevention Program*, 2018, californiacitrusthreat.org/california-citrus/.
5. Karlen, DL. "PRODUCTIVITY." *Encyclopedia of Soils in the Environment*, 2005, pp. 330-336, doi.org/10.1016/B0-12-348530-4/00241-1.
6. Ball, Jeff. "Soil and Water Relationships." *Noble News and Views*, Noble Research Institute, 1 Sept. 2001, noble.org/news/publications/ag-news-and-views/2001/september/soil-and-water-relationships/.
7. "Soil Management in Home Gardens and Landscapes." *PennState Extension*, Penn State University, 12 Sept. 2017, extension.psu.edu/soil-management-in-home-gardens-and-landscapes.
8. Physical and Chemical Properties of Soil Student Guide. *Physical and Chemical Properties of Soil Kit*, 2007 pp. 12-13, 16, Carolina.
9. Efretuei, Arit. "The Soils Cation Exchange Capacity and its Effect on Soil Fertility." *Permaculture News*, Permaculture Research Institute, 19 Oct. 2016, permaculturenews.

org/2016/10/19/soils-cation-exchange-capacity-effect-soil-fertility/.
10. Mann KK, Schumann AW, Obreza TA, Harris WG. "Response of Citrus Productivity to the Root Zone Soil Properties in Variable Sandy Soils." *Soil Science*, vol. 176, no. 11, July 2011, pp. 611-624, doi: 10.1097/SS.0b013e31822f069a.
11. Guo, ZQ *et al*. "Effect of Particle Size and Solution Leaching on Water Retention Behavior of Ion-Absorbed Rare Earth." *Geofluids*, vol. 2020, doi.org/10.1155/2020/4921807.
12. Carter, M.R., and E.G. Gregorich. *Soil Sampling and Methods of Analysis*. Second ed., Canadian Society of Soil Science, 2006.
13. "Soil pH." *Soil Quality Kit - Guides for Educators*, pp. 1-5, United States Department of Agriculture, nrcs.usda.gov/Internet/FSE_DOCUMENTS/nrcs142p2_053293.pdf.
14. Goldy, Ron. "Knowing nutrient mobility is helpful in diagnosing plant nutrient deficiencies." *Michigan State University Extension*, Michigan State University, 14 Nov. 2013, canr.msu.edu/news/knowing_nutrient_mobility_is_helpful_in_diagnosing_plant_nutrient_deficienc.
15. "Testing Your Soil: Why and How to Take a Soil-Test Sample." *Agronomy and Soils*. USDA NRCS, College of Tropical Agriculture & Human Resources, Nov. 1997, nrcs.usda.gov/Internet/FSE_DOCUMENTS/nrcs142p2_037208.pdf.
16. "Introduction." *Nutrient Management*, Cornell University, nrcca.cals.cornell.edu/soilFertilityCA/CA1/CA1_print.html.
17. Hansen, Jolene. "Fertilizing Lemon Trees." *SF Gate*, Home Guides, 7 Oct. 2016, homeguides.sfgate.com/fertilizing-lemon-trees-100018.html.
18. Alexandra K, Per BB, Rune HBC. "lmerTest Package: Tests in Linear Mixed Effects Models." *Journal of Statistical Software*, vol 82, no. 13, 2017 pp: 1–26. doi:10.18637/jss.v082.i13.

JOURNAL OF
EMERGING INVESTIGATORS

Article

Discovery of the heart in mathematics: Modeling the chaotic behaviors of quantized periods in the Mandelbrot Set

Anudeep Golla, Paul K. Strode
Fairview High School, Boulder, Colorado

SUMMARY

The phenomenon of small changes leading to drastic effects is fundamental to Chaos Theory. Understanding the chaos in our world could provide more control over the systems that govern the universe. Therefore, this study aimed to predict and explain chaotic behavior in the Mandelbrot Set, one of the world's most popular models of fractals and exhibitors of Chaos Theory. We hypothesized that repeatedly iterating the Mandelbrot Set's characteristic function would give rise to a more intricate layout of the fractal and elliptical models that predict and highlight "hotspots" of chaos through their overlaps. While a novel method of discovering miniature versions of the Mandelbrot fractal was discovered and a statistically significant transformation function was developed, overlaps of the elliptical models were not supported to exhibit higher levels of chaos. Many biological and natural phenomena such as the heartbeat, lung vessels, neurons, weather, the stock market, and more, are both chaotic in nature and can be described using fractal-based models. The positive and negative results from this study may provide a new perspective on fractals and their chaotic nature, helping to solve problems involving chaotic phenomena.

INTRODUCTION

Chaos Theory

Chaos Theory attempts to explain completely unpredictable systems such as the stock market, weather, turbulence, and human organs including the heart, lungs, and brain (1). Chaos theory has numerous principles that have varied as more information about chaos was discovered, but there are six significant principles that effectively explain the fundamentals of Chaos Theory. The first principle is the phenomenon of slight changes in the initial state leading to drastic changes in the final state. The Butterfly Effect, which is the assertion that a butterfly flapping its wings in one place guarantees the occurrence of a hurricane in a place across the world, is the most used example to explain this phenomenon (2). While there are 5 other principles, this study and the rest of the principles heavily rely on this first principle.

The second principle is unpredictability: the impossibility of knowing how to control the output of a system as it is impossible to know all the initial parameters of the system. Thus, it becomes entirely possible for this output to exhibit chaotic characteristics even if a slight change is made in the initial conditions (2).

The third principle is that chaos connects order and disorder. Order comes from an established operation for which, when an input is provided to the operation, the exact output can be confidently paired with the input. On the other hand, disorder arises when a slight alteration is made to a known input-output pairing. Namely, when that input is slightly altered, it is impossible to use the established operation to determine how the corresponding output will change. The entity that is connecting this order and disorder to enable the system to continue functioning is chaos (2).

The fourth principle is mixing. Given a system with an established operation, two similar inputs can produce very different outputs, similar to a group of balloons ending up in very different places after being released from the same location (2).

The fifth principle is the fractal, or the geometric representation of chaos and one of the most prominent phenomena that appears in chaos. Fractals are infinite and intricate figures that are self-repeating at every scale, and are present at every scale in the universe, whether it be entire landscapes, biological structures, or leaves on a plant (3). Therefore, the Mandelbrot Set, one of the world's most popular models of fractals, was investigated to gain insight into the chaos of fractal nature in our world.

The sixth principle is feedback. Specifically, chaos can be amplified when there is a response to the chaos itself (3). With fractals, feedback can be understood as the process of a simple operation (Mandelbrot function) being carried out on data (points in the complex plane) and then feeding the output back into the operation.

While these six principles are the core of Chaos Theory, it is important to understand that the phenomenon of slight changes in the initial state leading to drastic changes in the final state of a system is the foundational characteristic of chaos and what much of the work in this study relies on.

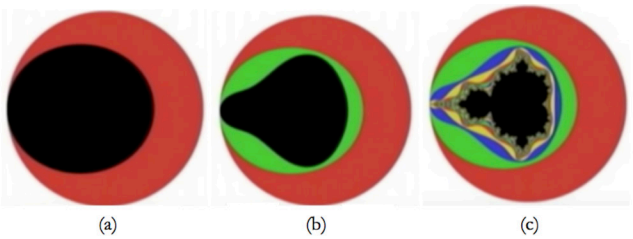

Figure 1. Stages of Mandelbrot Set iterations. a) The red and black regions combine to make up a circle with radius 2, centered at the origin of the complex plane. The red region indicates all complex numbers excluded during the first iteration, while the black region indicates all points that are in the Mandelbrot Set after the first iteration. **b)** The green region indicates all complex numbers excluded during the second iteration. The black region indicates all points that could possibly be in the Mandelbrot Set after the second iteration. **c)** The Mandelbrot Set formed by infinitely removing regions that prove to have an unbounded path after each iteration.

Mandelbrot Set

The Mandelbrot Set contains the set of complex numbers 'c' for which the function $F(z) = z^2 + c$ remains bounded for the orbit of 0, the path a function takes when iterated over 0 (**Figure 1**). The main cardioid is the main heart-shaped region of the Mandelbrot Fractal. This part of the Mandelbrot Fractal is in the section between -0.75 and 0.25 on the real axis and between approximately -0.637 and 0.637 on the imaginary axis. The approximate circles surrounding and attached to the cardioid are called primary bulbs. Any of the approximate circles not directly attached to the cardioid are simply called bulbs. For each bulb, all the points inside it approach a cycle of period n (4). Therefore, each bulb is assigned a period n. Additionally, "Minibrots" are defined as smaller figures similar in shape to the Mandelbrot itself. Minibrots are found when zooming into certain regions of the Mandelbrot Fractal (**Figure 2**) and consist of a cardioid and bulbs themselves. In other words, Minibrots are self-similar cardioid-bulb pairings emanating from all bulbs around the Mandelbrot Fractal.

Significant Points

The Mandelbrot Set contains an infinite number of points for which $z = 0$ orbits with a finite period when iterated over the function $F(z) = z^2 + c$, and every one of these points resides inside a cardioid and bulb. Furthermore, these points are denoted "center points" due to their location at the approximate center of the cardioids and bulbs (**Figure 3**).

The point where the largest primary bulb meets the main cardioid of the Mandelbrot Set (**Figure 3**) signifies a period doubling; the transition from points inside the cardioid to points inside the largest primary bulb parallels the transition from approaching a period of 1 to a period of 2. As this point is a representation of bifurcation, or the division of something into two branches, they are referred to as "bifurcation points" in this study (5). Specifically, the main cardioid's bifurcation point resides at -0.75 (**Figure 3**, red marker). The period doubling characteristic of bifurcation points leads to the fact that the derivative of the Mandelbrot function where 'c'

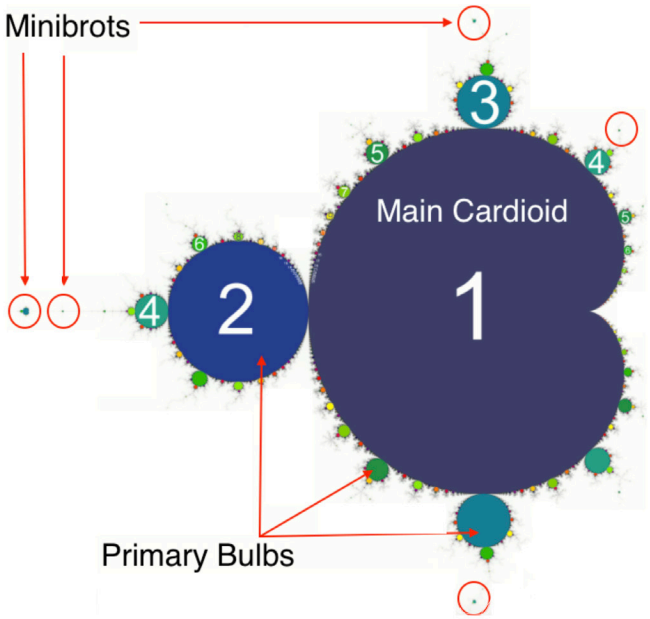

Figure 2. Mandelbrot Set components. The main cardioid and three primary bulbs are labeled. Four Minibrots are emphasized with red circles. The numbers indicate the period of each bulb.

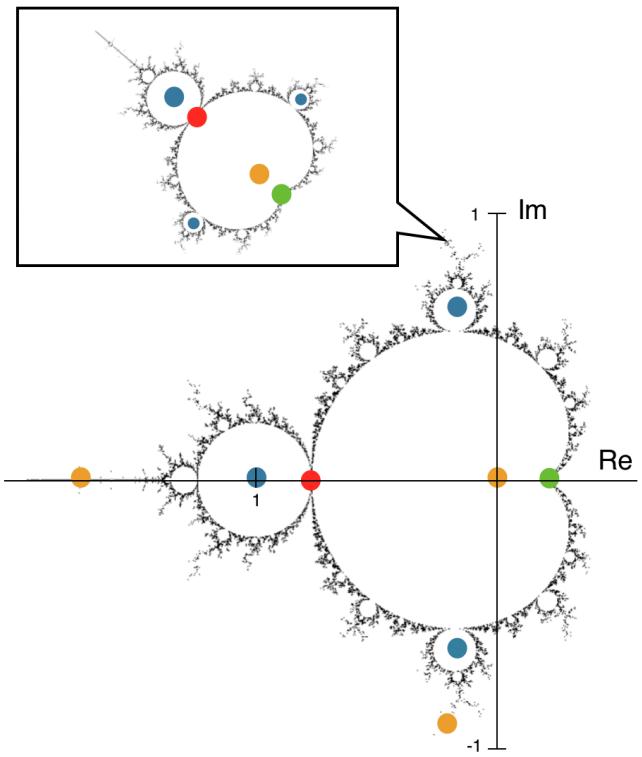

Figure 3. Significant points. Examples of center points for bulbs are shown in blue. The orange point inside the main cardioid is the center point for the main cardioid. Other orange points represent the center points for cardioids of Minibrots. Green points represent saddle points and red points represent bifurcation points. One Minibrot is enlarged to show all four of these points on a specific Minibrot.

equals the bifurcation point is greater than 1 for any input. This is because the rate of change of the approximate period increases at a factor of 2 at bifurcation points and other points along the real axis.

The point 0.25 on the Mandelbrot Set (**Figure 3**, green marker) carries significance for the opposite reason as that for the bifurcation point; this point is where, rather than the period doubling, the period simply ceases to exist. Due to the Mandelbrot Set resembling a saddle at this point, it will be referred to as the "saddle point" in this study. Contrasting bifurcation points, the derivative of the Mandelbrot function where 'c' equals the saddle point is equal to 1 for any input.

Bifurcation points and saddle points provide helpful insight into the nature of the structures they are a part of. Specifically, while bifurcation points are part of both the largest primary bulb and the cardioid, saddle points are only part of the cardioid. These properties can provide important information when locating Minibrots. Namely, once a set of center points is discovered, one can determine whether each center point resides in a bulb or cardioid by calculating whether the derivative of the Mandelbrot function where 'c' equals the center point is equal to 1 for any input. If so, then that center point is not associated with a bulb but with a cardioid, and thus, a Minibrot.

Entropy

The Kolmogorov entropy, an important measure of the degree of chaos in systems such as fractals, gives the average rate of information loss about a position of the phase point on the attractor (6). In this case, the phase point is any given point in the complex plane and the attractor is a set of values toward which a system tends to approach given many starting conditions of the system. In the Mandelbrot Set, this attribute converts nicely to the number of Minibrots in a specified region of the fractal. Specifically, the higher number of Minibrots in the region, the larger range of possible periods of inputs for which 'c' equals each point in the region; thus, this larger range is associated with a loss of information about the period. Furthermore, because the Kolmogorov entropy measures chaos, a higher number of Minibrots in a region is associated with higher entropy, which in turn is associated with more chaos.

The overlap of period states creates a region which could contain Minibrots that could have multiple possible periods, creating unpredictability and chaos (**Figure 4**). A higher level of Minibrots incidence in these regions would support these overlapping regions display a more intense chaotic nature.

RESULTS

In this study, the primary goal was to predict and explain chaotic behavior in the Mandelbrot Set. This was approached by repeatedly iterating the Mandelbrot Set's characteristic function, using an elliptical model to characterize the results from the iterations, and applying a logistical regression test to these data. The regression was employed to engender

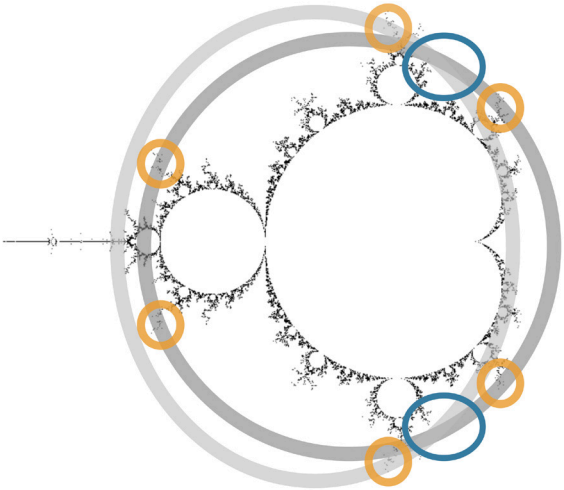

Figure 4. Examples of period states and overlaps. The two gray ellipses are the states that traverse the Mandelbrot Set, with a certain thickness due to the error margin, with intersections with Minibrots circled in orange and the overlap of states circled in blue.

statistically significant parameters of a function that predicts the layout of the Mandelbrot Set and insight into relationships between chaos intensity and fractal locations. We hypothesized that repeatedly iterating the Mandelbrot Set's characteristic function would give rise to a more intricate layout of the fractal and elliptical models that predict and highlight "hotspots" of chaos through their overlaps. While a novel method of discovering miniature versions of the Mandelbrot fractal was discovered and a statistically significant transformation function was developed, overlaps of the elliptical models were not supported to exhibit higher levels of chaos.

Solving the Mandelbrot iteration function resulted in both center points of cardioids and bulbs that may be attached to cardioids (**Figure 5**). The Python program developed to fit an ellipse to each cardioid center set resulted in five diagrams (**Figure 6**, panels i–v). For each plot, the parameters that describe the ellipse are also given. Each parameter is relative to the period that the curve is being fit upon. To develop a transformation of a period that results in a function mapping

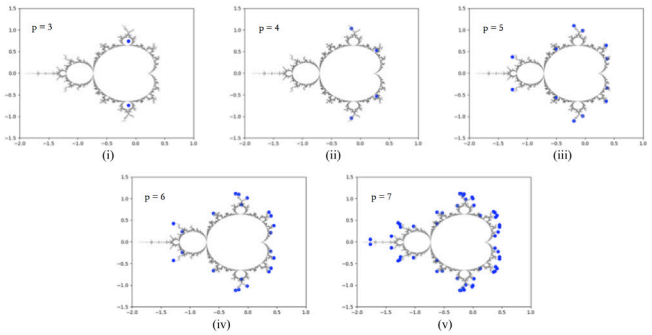

Figure 5. Calculated center points. Plot data of center points for Mandelbrot cardioids and bulbs of a certain period. Periods 3 to 7 correspond with panels (**a**) to (**e**) respectively.

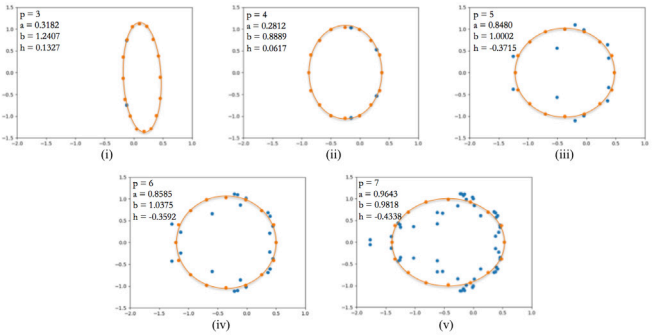

Figure 6. Calculated period states. Best fit ellipse for set of center points (blue points) for each period. Each ellipse is associated with a, b, and h values that are derived from the equation (III). Orange points are example points on the calculated ellipses spaced at equal intervals.

Table 1. Minibrot incidence and differences by period state.

Period of First State (P1)	Period of Second State (P2)	P1 Minibrot Incidence	P2 Minibrot Incidence	Difference Between Average and P1 Minibrot Incidence	Difference Between Average and P2 Minibrot Incidence
4	5	1	2	0.1100936	0.0735924
4	5	1	2	0.0677731	0.0735924
4	5	1	1	0.0677731	0.1100924
4	5	1	1	0.0677731	0.1100924
4	6	1	2	0.0677731	0.0123936
4	6	1	2	0.0677731	0.0123936
4	6	1	4	0.0677731	0.0748936
4	6	1	4	0.0677731	0.0748936
4	7	1	5	0.0677731	0.0293101
4	7	1	5	0.0677731	0.0293101
4	7	1	7	0.0677731	0.0605601
4	7	1	7	0.0677731	0.0605601
5	6	1	2	0.1100924	0.0123936
5	6	1	2	0.1100924	0.0123936
5	7	2	0	0.0735924	-0.0488150
5	7	1	0	0.1100924	-0.0488150
5	7	1	4	0.1100924	0.0136851
5	7	1	4	0.1100924	0.0136851
6	7	2	2	0.0123936	-0.0175650
6	7	2	1	0.0123936	-0.0331900
6	7	2	4	0.0123936	0.0136851
6	7	2	4	0.0123936	0.0136851

the best fit curve for that period, a relation must exist between the period and the parameters (**Figures 7-9**).

The linear regression test used to generate functions for the parameters of an elliptical curve function resulted in the following equations:

$$a = 1.137 * \ln(p) - 1.175 \quad (1)$$
$$b = -0.6400 * \ln(p) - 2.175 \quad (2)$$
$$c = -0.7530 * \ln(p) - 0.9812 \quad (3)$$

Embedded into the general elliptical curve equation symmetric about the real axis ($(x-c)^2/a^2 - y^2/b^2$), the parameters give rise to final transformation model with a relationship with the period:

$$T(p) = \frac{(x + (0.7530 * \ln(p) + 0.9812))^2}{(1.137 * \ln(p) - 1.175)^2} + \frac{y^2}{(0.6400 * \ln(p) + 2.175)^2} \quad (4)$$

The resulting incidence of Minibrots inside of overlapping period states and difference between the average Minibrot incidence and the actual Minibrot incidence of each period within each ellipse-pairing overlap show an insignificant change (**Table 1**). The various calculated ellipses for each period imposed on the same plane show the similarities for ellipses of higher periods (**Figure 10**).

DISCUSSION

The current study resulted in the development of a novel method that traverses the Mandelbrot Set to locate all Minibrots throughout the Mandelbrot Fractal. In addition, a significant transformation model was developed to predict the positions of all Minibrots of a certain period altogether. However, when ellipses were widened and overlaps of these period states were analyzed, there was no significant difference between the average Minibrot incidence and the incidence of Minibrots within the overlaps. The difference between the period state overlaps' Minibrot incidence and the average Minibrot incidence is almost negligible, with some overlaps even consisting of less Minibrots than the average number of Minibrots in a similarly sized region (**Table 1**). This result did not align with the initial intuition. Namely, since an overlap of states indicates that the main cardioid of a Minibrot found in that region does not have a predetermined period, its period has as many possibilities as the number of states that have overlapped to create that region and should produce

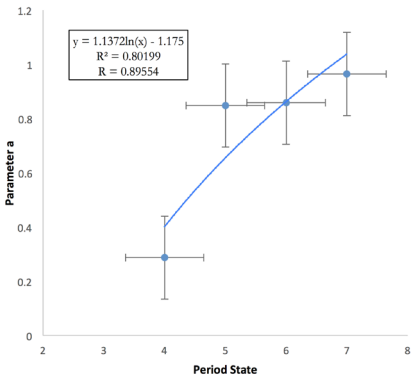

Figure 7. A parameter. Regression analysis results with 95% confidence intervals for a parameter of the transformation function. (R = 0.896 > R_crit = 0.811; $p < 0.05$, df = 4)

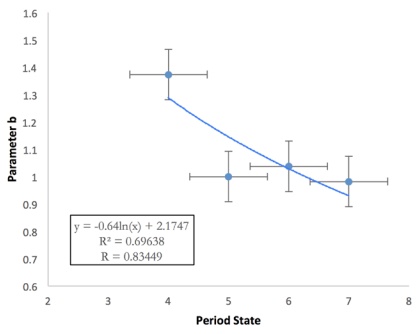

Figure 8. B parameter. Regression analysis results with 95% confidence intervals for b parameter of the transformation function. (R = 0.834 > R_crit = 0.811; $p < 0.05$, df = 4)

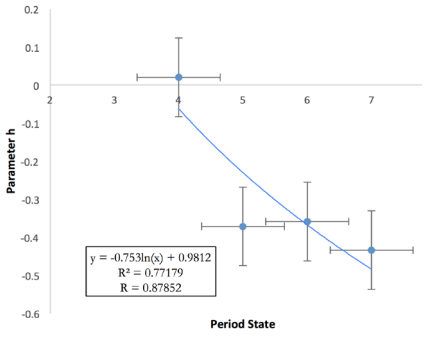

Figure 9. H parameter. Regression analysis results with 95% confidence intervals for h parameter of the transformation function. (R = 0.879 > R_crit = 0.811; $p < 0.05$, df = 4)

higher Minibrot incidence. Therefore, instead of discovering areas associated with elevated chaos, analysis of the overlapping period states revealed that these areas exhibit as much chaos as the rest of the Mandelbrot Fractal. In fact, this result inevitably inspires the possibility that chaos (or entropy) is evenly "distributed" among the fractal space. Despite the negative result, taken together, this study did partially predict and explain chaos in the Mandelbrot Set. Looking forward, the newfound possibility of uniform chaotic behavior throughout the Mandelbrot Fractal provides numerous interesting new avenues of research if a substantial relationship between the specific Mandelbrot Fractal and the fractal nature of the universe can be established.

Based on our results, there are three major recommendations to improve future directions from this study. The first would be to use a larger sample size with not only the period state-parings for overlaps, but also with the Minibrots used to calculate the average Minibrot incidence in a certain area. By including Minibrots for which the center points cycle with higher periods, it would be possible to increase the sample size and use a similar strategy as used in this study to uncover a significant difference between the period state overlaps' Minibrot incidence and the average Minibrot incidence. The second direction to further this study would be to model the states using a figure more versatile than an ellipse to capture slight variations in the state's curve. This would then allow for less of an error margin as the state would prove a more accurate method of locating Minibrots in the Mandelbrot Set. Finally, the third direction would be to introduce more diversity by applying the same study to various fractals. This would potentially provide more insight into the purpose of chaos in dynamical systems which could then be applied to the following areas.

The Mandelbrot Fractal and Chaos Theory in general are at the core of how the universe functions (7). Furthermore, numerous significant fields, such as biology, physics, chemistry, cosmology, meteorology, and even the stock market, have been shown to follow fractal laws and exhibit chaotic behavior (8). This study provides valuable insight into three inherent mechanisms of the human body: the heart, lungs, and brain. The rate of the human heartbeat, the firing of neural clusters and the network of arteries, lung vessels, and neurons are all both chaotic in nature and can be described using fractal-based models. Intersections of certain muscles, which are essential to human biology and resilience, very closely resemble the regions of overlapping states in this study (9). If the future directions outlined above were proven more successful in confirming the entire hypothesis of this study, it may be possible to support that cardiac malfunctions, lung alveoli blockages, and neuron damage cases are associated with overlapping period state regions and can be efficiently reduced and predicted in the future using correspondences between the Mandelbrot Set and human organs (9). Therefore, the intersections of period states from this study could prove useful for diagnosis and

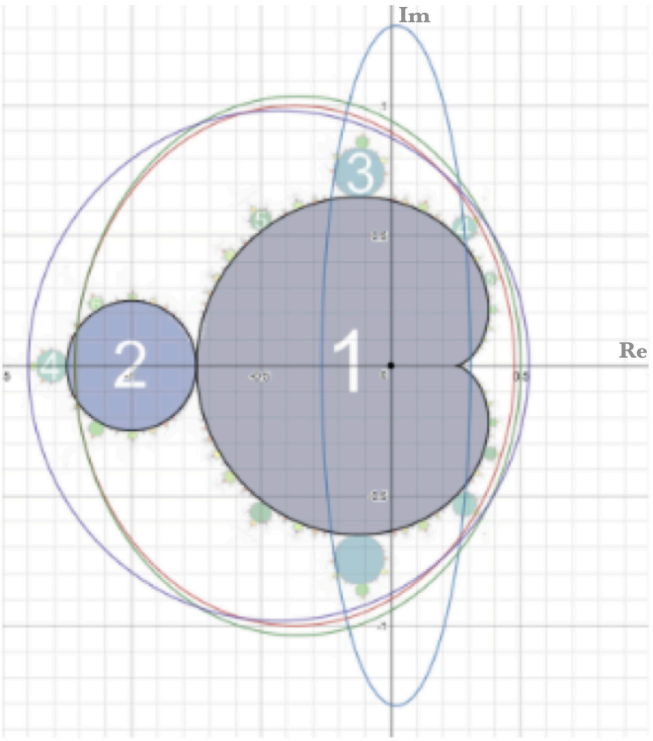

Figure 10. Calculated ellipses together. Various resulting period states, calculated using the transformation model. Figure created using Desmos.

therapeutic treatment for various diseases, development of artificial intelligence, and overall advancement of efficient technology in the future.

METHODS

Phase 1: Locating Minibrots

To find the points 'c' for which *F(0)* cycles exactly with period n, it is necessary to find the solution to the equation value, that, when plugged into the n-times-iterated Mandelbrot function, equals itself. Therefore, for varying values of n, the equation $F^n(c) = c$ was solved using a program developed in Python (3.6.3). Since the solutions to this equation are in both cardioids and bulbs, it is required to find only those located in cardioids to locate the Minibrots containing those cardioids. As explained in the introduction, the equation $d/dc(F^n(c) = 1)$ was tested for each center point to determine whether each center point corresponded to a bulb or cardioid. After eliminating the solutions that correspond to center points in bulbs, the set of points that correspond to each Minibrot was established.

Phase 2: Constructing Period States

The set of solutions to $F^n(c) = c$ becomes very tedious to calculate after the first few periods. Therefore, as the portion of the Mandelbrot Fractal on the right side of the imaginary axis represents a nearly elliptical figure, and the majority of Minibrots reside on the perimeter of this "ellipse," ellipses are an ideal model for predicting the locations of all Minibrots in

a certain period state. A Python program was developed to compute the best fit elliptical regression curve for all Minibrots in a given state. This was done by applying the OpenCV fitEllipse function to all the center points of the Minibrots in the respective state. After gathering the equations for these ellipses for various states, a linear regression test was used to generate functions for the parameters of an elliptical curve function with an error margin that outlines a regional state where the Minibrot could possibly be located. Note that k = 0 due to fractal symmetry. The parameter equations were then plugged into the general equation for an ellipse symmetrical over the real axis to develop the final transformation model. Finally, error margins for each ellipse were set equal to the average uncertainty in each parameter's regressions.

Phase 3: Testing Overlaps of Period States

The ellipses calculated in phase 2 combined with their error margins are referred to as period states in this study. The overlap of period states (**Figure 5**) creates a region that could contain a significantly higher number of Minibrots and thus more chaos. To determine whether overlaps truly do exhibit higher levels of chaos, each overlap was analyzed by calculating the incidence of Minibrots that it enclosed. After executing this for multiple pairs of period states that intersect, it was determined whether there is a significantly higher density of Minibrots in these overlapping regions than the average Minibrot incidence density throughout the entire Mandelbrot Set (determined by averaging the number of Minibrots inside multiple areas across the perimeter of the Mandelbrot Set roughly equal in size to the overlaps of period states).

Received: April 27, 2020
Accepted: December 14, 2020
Published: December --, 2020

REFERENCES

1. Levy, David. "Chaos theory and strategy: Theory, application, and managerial implications." *Strategic Management Journal,* Vol 15, Issue S2, Summer 1994, pp. 167-178.
2. Ghys, Étienne. "The butterfly effect." *The Proceedings of the 12th International Congress on Mathematical Education*. Springer, Cham, 2015.
3. Devaney, Robert L. "The complex geometry of the Mandelbrot set." *ISCS 2013: Interdisciplinary Symposium on Complex Systems*, 2014.
4. Devaney, Robert L. "Unveiling the Mandelbrot Set." *Unveiling the Mandelbrot Set*. N.p., 31 Aug. 2006. Web. 26 Nov. 2015.
5. Agiza, H.n. "On the Analysis of Stability, Bifurcation, Chaos and Chaos Control of Kopel Map." *Chaos, Solitons and Fractals*, Vol. 10, no. 11, 1999, pp. 1909–1916.
6. Zmeskal, Oldrich, Petr Dzik, and Michal Vesely. "Entropy of fractal systems." *Computers and Mathematics with Applications,* 2013, pp. 135-146.
7. Li, J., and Ye, X. D. "Recent development of chaos theory in topological dynamics." *Acta Mathematica Sinica, English Series*, 2016, pp. 83-114
8. Richardson, M. J., Kuznetsov, N. A., and Paxton, A. "Nonlinear Methods for Understanding Complex Dynamical Phenomena in Psychological Science." *American Psychological Association-Psychological Science Agenda,* 2017
9. Klonowski, Wlodzmierz. "Applications of Chaos Theory Methods in Clinical Digital Pathology." *Handbook of Applications of Chaos Theory*, 2016, pp. 681–690.
10. Mcmullen, Chris T. "The Mandelbrot set is universal." *The Mandelbrot Set, Theme and Variations*, 24 Feb. 1997, pp. 1–18.
11. Shaw, William T. "The Mandelbrot set." *Complex Analysis with MATHEMATICA*, April 20, 2006, pp. 105-37.
12. Douady, Adrien. "Julia sets and the Mandelbrot set." *The beauty of fractals*, 1986, pp. 161-174.
13. Álvarez, G., Romera, M., Pastor, G., and Montoya, F. "Determination of Mandelbrot Sets Hyperbolic Component Centres." *Chaos, Solitons and Fractals*, (1998): 1997-2005.
14. Liang, X. S. "Local predictability and information flow in complex dynamical systems." *Physica D: Nonlinear Phenomena*, 2013, pp. 1-15.
15. Richardson, M., Alexandra Paxton, and N. Kuznetsov. "Nonlinear methods for understanding complex dynamical phenomena in psychological science." *American Psychological Association-Psychological Science Agenda*, 2017.
16. Bums, J. S. "Chaos Theory and Leadership Studies: Exploring Uncharted Seas." *Journal of Leadership and Organizational Studie*s, 2002, pp. 42-56.

JOURNAL OF
EMERGING INVESTIGATORS

Article

The Effect of School Climate and Parenting Style on Academic Achievement

Quinn Myers[1], Jason Scott[1]
[1] The Neighborhood Academy, Pittsburgh, PA

SUMMARY

Previous research suggests that there are positive and negative relationships between parenting style and academic achievement and that school climate can potentially mediate the effects of parenting style. Research suggests that less effective styles of parenting tend to negatively affect grades, and more effective styles tend to produce higher grades. The purpose of this study is to verify previous research and confirm those relationships in a sample of African American students in a college preparatory program. We obtained students' perception of their school's climate and parent's parenting styles by conducting a Parental Authority Questionnaire and school climate survey on a sample of freshmen, sophomores, and junior high school students. We then correlated these perceptions to student grades. We found no significant relationship between school climate and academic achievement. However, permissive parenting, which is characterized by low responsiveness and demandingness, exhibited a negative relationship with academic achievement. Authoritarian parenting, a style high in demandingness and low in responsiveness, exhibited a positive relationship to academic achievement. These results suggest that while school climate has little relation to academic achievement, parenting style has a significant impact. The cultural implications for parenting styles and academic achievement are explored more in depth.

INTRODUCTION

A positive home and school environment can have a powerful impact on students' academic performance (1). In this study, we examine the relationship between parenting style, school climate, and academic achievement. This relationship is especially important for schools which try to mitigate the effects of negative parenting styles and/or low socioeconomic status on academic achievement. This study focuses on a school in which 58.3 % of students qualify for free and reduced lunch. The results of this study could have a powerful impact on how that school and others like it function.

School Climate & Academic Achievement

School climate influences a student's emotions, sociability, and academic performance in many ways (1). Freiburg and Stein define school climate as, "the heart and soul of the school. It is about the essence of a school that leads a child, a teacher, and an administrator to love the school and look forward to being there each school day" (2).

School climate has four components — community, safety, institutional environment, and academics — which are then broken down into three to four components of their own. School climate is associated with academic performance in primary and secondary school. Wang and Degol claim that schools that set high academic standards, stress commitment to students, exhibit effective leadership, and emphasize mastery goals tend to have higher-performing students (3). Warm teacher-student relationships, frequent communication between parents and schools, and appreciation for diversity, cultivate an environment that is conducive to learning and promotes optimal achievement and motivation among students. School environment and safety seem to be less significant when other factors are controlled for (3).

Davis and Warner conducted a study in New York City in which they study the effects of school climate on academic achievement. They analyzed surveys about school climate taken by teachers, students, and parents. Results demonstrated that parents, students, and teachers having positive perceptions of the school climate was positively associated with academic achievement (1). It was found that being eligible for free or reduced lunch was negatively associated with academic achievement. However school climate explained more of the variance in academic achievement than did background characteristics such as race and poverty. This is significant because being African American or Hispanic was negatively associated with academic achievement (1).

Parenting Style and Academic Achievement

Raul and Ahmed claimed there was a predictive association between parenting and academic performance in school students (4). Parental involvement is separated into seven variables: parent-child discussions about school, parental aspirations and expectations, parenting style, reading at home, checking homework, school involvement, and house rules and supervision (5). Parenting style was found to be the greatest predictor amongst the seven (5).

Parenting style is compartmentalized into three types: authoritative, authoritarian, and permissive. Each different type is specified based on the amount of responsiveness and demandingness from the parent (5). Responsiveness refers to how much a parent caters to their child's needs and feelings. However, demandingness refers to the amount of expectations and restrictions that a parent places on their child. Permissive parents are predominantly responsive. Singh's

study of parenting styles' relation to mental health and self-esteem concluded that permissive parents tend to produce low self-esteemed children (6). Low self-efficacy was also negatively correlated with academic achievement (7). Therefore, drawing a direct connection between permissiveness and lower academic performance.

Authoritarian parents are predominantly demanding (5). Raul and Ahmed organized a study in Pakistan strictly focusing on the impact that authoritarian parenting had on a student's academic achievement. Through the study, some significant conclusions were drawn. Authoritarian parenting style was associated with lower academic performance. The dominating nature of authoritarian parenting practices demands children to strictly follow rules and regulations as the basis of their decisions. In the study, authoritarian parenting contributed significantly to the students' academic performance (38%), but in a negative way (4).

Previous research found that authoritative parents were equally demanding and responsive (5). A 2011 meta-analysis on parental involvement concluded that authoritative parenting was positively related to achievement (5). Raul and Amhed, although studying authoritarianism, found that firm and supportive parenting practices are associated with academic success (4). Other studies have also shown that authoritative parenting is correlated with higher student motivation in school (7).

School Climate, Parenting Style, and Academic Achievement

From 2008 to 2010, 1.5 million high school students from 92 public high schools were surveyed about their family structure, school climate, and grades. For single-parent and homeless children, school climate provided the greatest boost in GPA (8). For students in foster care, the effect was promotive but not protective (8). School climate boosted their GPAs, but the benefit they received was not as great as students in other groups.

Hopson and Weldon conducted another study investigating the impact of parental expectations on academic success in the context of school climate. Parental expectations had no effect on students with no connection to their school (9). Parental expectations are most impactful on students with a connection to their school. More than anything else, family income and gender had the greatest effect on grades (9). They concluded that school climate is a factor between parental expectations and grades, which magnifies the effect of "good" parenting, but does not help or negate the bad.

Berkowitz et. al ran another study seeking to determine the relationship between socioeconomic background, inequality, school climate, and academic achievement. A meta-analysis of 78 studies concluded that positive school climate contributes to higher academic performance and decreases the effects of poor socioeconomic status and other negative predetermining factors (10). The effect of school climate is mitigating, not eliminating. Also, they state that schools would improve academic achievement if funding was directed towards school climate and not towards educational purposes (10).

In the current study, we investigated how school climate and parenting styles impact academic achievement. Overall, research suggests that there are connections between how students are parented, how they feel about their school, and how they perform academically. However, there is limited research on the connection between the three. Our study focused on African American students from a private college-preparatory high school called The Neighborhood Academy. We had all students, ninth through eleventh grade, take a survey about the school climate and a survey about the way they are parented. With consent, their grades were also pulled from the school information system.

We hypothesized that there is an association between GPA and parenting style. Research suggests that authoritative parenting styles are associated with higher performance (5). Second, we hypothesized there is a significant positive relationship between school climate and GPA. This is because students, parents, and teachers' perceptions of school climate positively affect academic progress (1). Finally, we hypothesized that there is a greater benefit of positive school climate on academic performance for less effective parenting styles. Research suggests students parented in less effective styles receive the greatest aid from a positive school climate (8).

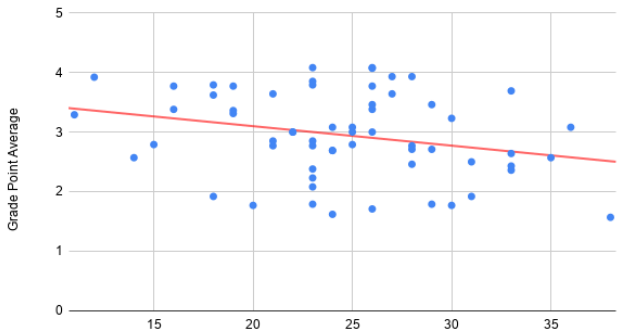

Figure 1. Permissive Parenting vs. GPA. Parenting style survey results were correlated to student GPA. Data were analyzed using a Pearson's correlation test (r (59)=-0.26, p=0.02) enzyme inhibition.

RESULTS

We surveyed students to determine what style of parenting best fits that of their caregiver and to obtain their perception of their school's climate. Parenting styles include authoritarian (high demandingness and low responsiveness), authoritative (high demandingness and high responsiveness) and permissive (low demandingness and high responsiveness). We then correlated each student's GPA to the survey results.

Our first hypothesis was that parenting styles would be associated with students' GPA. We used all respondents' scores on the Parental Authority Questionnaire to investigate the parenting score with GPA. When we looked at the correlation between the parenting score and GPA there was a significant negative relationship between permissive parenting and GPA (Pearson correlation, r(59) = -0.26, p =

0.02) **(Figure 1).** Students who had more permissive parents seemed to have lower GPAs. There was a nonsignificant negative relationship between authoritative parenting and GPA (Pearson correlation, r(59) = -0.009, p = 0.5). However, there was a significant positive correlation between authoritarian parenting and GPA (Pearson correlation, r(59) = 0.21, p = 0.049) **(Figure 2).**

To further explore the connection between parenting style and GPA, we assigned each student a parenting style, based on the highest scoring style category. A one-way ANOVA test revealed that there was no significant difference in GPA between the three parenting styles (F(2,56) = 0.64, p = 0.53). Students who are parented by authoritarian (3.02 ± 0.71) or authoritative (2.97 ± 0.70) parents have similar GPAs, but students who are parented by permissive (2.53 ± 0.86) parents have a much lower GPA.

Regarding school climate and GPA, we found that there was an nonsignificant positive relationship between perception of school climate and GPA (Pearson correlation, r(59) = 0.1, p = 0.22) **(Figure 3)**. Having a higher perception of the school climate did not necessarily mean a student also had a higher GPA.

To investigate how school climate and GPA interact within each parenting style, a linear regression was calculated for each parenting style. For students with authoritarian parents, there was a nonsignificant linear relationship (p = 0.19, R^2=0.025). GPA was predicted by the function GPA = 0.19(C) + 2.3, where C is the climate score. For every 1-point increase in school climate, there was on average a 0.19 increase in GPA. For students with authoritative parents, there was also a nonsignificant linear relationship (p=0.4, R^2=0.002). GPA was predicted by the function GPA = -0.04(C) + 3.1. For every 1 point in school increase in school climate, there was essentially no effect on GPA. Due to the low number of students with permissive parents in the sample (n=5), no regression was calculated.

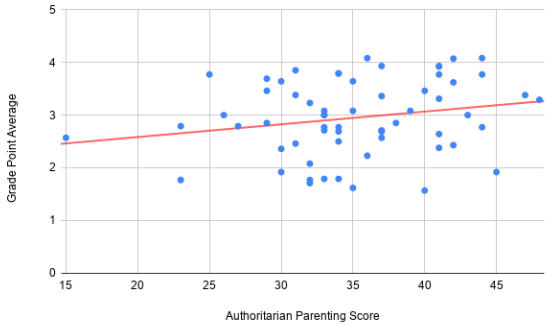

Figure 2. Authoritarian Parenting vs. GPA. Parenting style survey results were correlated to student GPA. Data were analyzed using a Pearson's correlation test (r (59)=0.21, p=0.049).

DISCUSSION

Our first hypothesis was that all parenting styles would influence GPA This was partially supported with our data **(Figures 1 and 2)**. Two of the three styles had significant relationships with GPA — permissive (negative) and authoritarian (positive). We also hypothesized that school climate had a direct correlation to GPA, and we hypothesized that worse parenting styles would receive the greatest boost from school climate. Both these hypotheses were unsupported by our results **(Figure 3).**

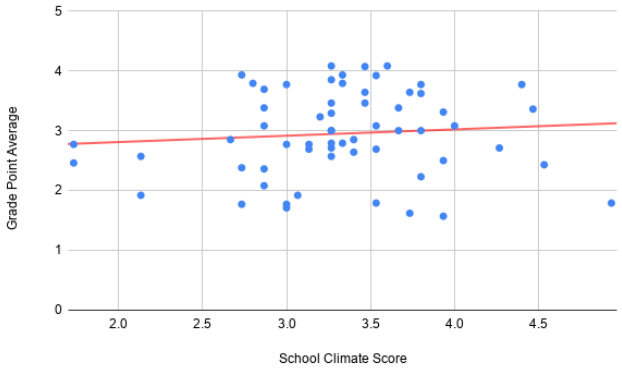

Figure 3. School Climate vs. GPA. Survey results for school climate scores were correlated with GPA. Data was analyzed using a Pearson's correlation test (r (59)=0.1, p=0.22).

Our results concerning the relationship between parenting style and GPA are partially consistent with previous research. Prior research found a negative relationship between authoritarian grade point average (4, 5), while we found a positive relationship. For permissive parenting style scores, our results were consistent with prior studies and found a negative relationship (6). Contrary to our findings, prior research says authoritative is the better parenting style as it balances demandingness and responsiveness (5). Culture may play a role in which parenting style is considered better. White middle-class families might value an even mixture of being demanding and responsive, but in a 100% black sample (mix of low and middle income), the values might be different. In a study of black and white parents conducted from 2008 to 2010, 47% of Caucasians prefer obedient children to self-reliant children, whereas 74% of African Americans do (11). Therefore, we argue that authoritarianism may be more valued amongst African Americans. Black parents averaged a score of 0.78 in authoritarianism, while white parents averaged a score of 0.60 (11). Nearly a 20% gap in the value placed in authoritarianism leads to culture seeming to be relevant in which parenting style is most effective. Black families may tend to value authoritarianism and whites may tend to value authoritativeness, which is consistent with our data.

Our results concerning the lack of relationship between school climate and GPA are inconsistent with previous research. According to prior research, school climate tends to be positively correlated to grade point average (1). The discrepancy between our results and others might result from the fact that the extreme scores in our school climate produced lower grades, and higher performers had a middling school

climate. If a student likes school too much, he or she might not be there to learn, while those who hate it may not work. High performers might feel stress and therefore view teachers and school differently. This difference may stem from the college preparatory agenda that the school has, which may be unlike the public schools that were used in the other studies.

Although we did not directly find a connection between school climate and academic achievement, we did notice an interesting trend in how the students responded to questions. Participants had a mean score of 3.3 for perception of school climate (scale 1–5), with a standard deviation of 0.7. We also found the average score of each question and identified the scores that fell outside of one standard deviation as outliers. Questions 8, 9, and 15 fell below and questions 2, 4, and 6 were above.

Statement 8, which had an average score of 2.2, reads "At school, I help decide things like class activities or rules." Statement 9, which averaged a score of 2.5, reads, "At school, I do things to make a difference." Averaging a score of 2.2, statement 15 says, "The teachers at this school treat students fairly." These statements mostly directly related to the student's personal involvement at school.

Statement 2, which averaged a score of 4.0, says, "At my school, there is an adult who tells me when I do a good job." Statement 4, which averaged a 4.3, reads, "At my school, there is an adult who always wants me to do my best." Averaging a score of 4.2, statement 6 says, "At my school, there is an adult who believes I will be a success." All these statements are related to their interactions with an individual adult in the building. This suggests that school climate may be made up of different smaller concepts, some of which might be more relevant to student success in this sample.

Our results relating the proposed relationships between parenting styles and GPA are not consistent with prior research. The values of the slopes of the regressions +0.19 (authoritarian) and -0.04 (permissive) are consistent with the directions found in previous research (4, 5, 7), although the relationships were not significant. Authoritarian parenting is positive and permissive parenting is negative, as research suggests they should be, but the lack of significance means it is hard to draw any conclusions. Parents might have less influence due to the sample school's extended (9-hour) school day, and the school's authoritarian rule structure, which we already know is associated with improved grade point average. Our small sample for permissive students (n=5) makes it impossible to reflect on the effects of the parenting style. In a private, competitive school such as this sample, there may be selection pressure that forces out permissively parented students.

One limitation is that parenting styles have overlapping characteristics, since they all consist of different proportions of the same factors — demandingness and responsiveness Despite these overlapping characteristics, students are assigned to only one parenting style. For example, a student scoring only one point higher on the authoritative parenting style would still be assigned to only that category, despite scoring very highly on the other two parenting styles as well.. Twenty-five of sixty-one students were placed in a category, while another parenting was within 5 points of the score. Another limitation would be the lack of parenting style variation. Nearly all students viewed their parents as authoritative and authoritarian, but there were only three students who viewed their parents as predominately permissive. This may be because permissively parented children are not commonly admitted to the school in this study, or it could be because permissiveness is so normal that it goes unnoticed by the students. Also, the demographics of the school could be a factor. The study school is 100% African American and a mix of middle- and lower-class students, and other studies were typically middle-class white students. These limiting factors may have led to some of the observed differences from prior research.

For future research, we would study a group with more variation in socioeconomic class and races so that if parenting is culturally based, there can be a more accurate comparison between the effects of parenting styles of different cultural groups. We would also survey the parents to see if how they view their parenting differs from how the students view the parenting. This will potentially give two lenses into how the child is parented therefore providing more accurate results.

Having a higher perception of school climate does not necessarily mean there will be a higher GPA in a school environment, particularly in a school which has its own strong culture, extended hours, and stress. However, our data suggest authoritarian parenting may be beneficial to a student's academic achievement in an environment and permissive parenting may be detrimental. In our study, authoritative parenting did not have a significant relationship to students' academic achievement, in contrast to other studies which found that authoritative parenting is associated with better grades. Due to culture seeming to be a significant factor, results may vary as environments change. While GPA is important for future opportunities, such as college, it is not the only measure of parenting quality. Therefore, we suggest parenting decisions should not be decided based solely on GPA, as it is not necessarily the most important aspect of a child's development.

MATERIALS AND METHODS

The participants were students from 9th through 11th grade from The Neighborhood Academy, a college preparatory, private high school. There were 61 students requested to participate, 24% male and 76% female. All 61 students accepted and completed the surveys. The materials were the Parental Authority Questionnaire (PAQ) and a school climate survey. The PAQ is a survey used to identify the parenting style of an individual's caregiver (12). The school climate survey was used to identify the way an individual perceives their relationships, opportunities, school safety, and school connectedness (8). We modified the PAQ to be

comprehensive to all students and applicable to all family situations. The word "mother" was replaced with "caregiver" so that students who are not parented by their mother can apply the questions to their life.

After modifying the PAQ, both the PAQ and the school climate survey were given to the 61 study participants over a one-week period. On the PAQ, those surveyed were to rate how much the question related to their caregiver on a scale of one to five. The participants were categorized by summing up their scores on specific questions. All questions were associated with either authoritative, authoritarian, or permissive parenting. For the school climate survey, participants were to score each statement relating to school climate on a scale of one through five based on their agreement of the statement. The score of the school climate survey was evaluated by averaging their scores. The surveys were completed during class and participants were not given any incentives.

Students' grade point averages were gathered and used as data as well. The anonymized grades were directly obtained from the school's grading system to avoid potential inaccuracy of self-reported grade point averages. Permission to view anonymized participants' grade point averages was granted by the school on the condition of individual student consent, which was obtained at the time of the survey was given.

Received: April 9, 2020
Acccepted: November 21, 2020
Published: December 16, 2020

REFERENCES

1. Davis, Jonathan Ryan, and Nathan Warner. "Schools Matter: The Positive Relationship Between New York City High Schools' Student Academic Progress and School Climate." *Urban Education,* vol. 53, no. 8, 2015, pp. 959-980.
2. Freiberg, H J. & Stein, T.A. School Climate: Measuring, Improving, and Sustaining Healthy Learning Environments. New York: *Routledge Falmer*, 1999.
3. Wang, Ming-Te, and Jessica L. Degol. "School Climate: A Review of the Construct, Measurement, and Impact on Student Outcomes." *Educational Psychological Review*, vol. 28, 2015, pp. 315-352.
4. Rauf, Junaid, and Khalida Ahmed. "The Relationship of Authoritarian Parenting and Academic Performance in School Students." *Pakistan Journal of Psychology,* vol. 48, no. 2, 2017, pp. 61-71.
5. Shute, Valerie J, et al. "A Review of the Relationship between Parental Involvement and Secondary Students' Academic Achievement." *Education Research International,* 2011.
6. Singh, Shweta. "Parenting Style in Relation to Children's Mental Health and Self-Esteem: A Review of Literature." *Indian Journal of Health and Well-being*, vol. 8, no. 12, 2017, pp. 1522-1527.
7. Rivers, Jewrell, et al. "Relationships Between Parenting Styles and the Academic Performance of Adolescents." *Journal of Family Social Work*, vol. 15, no. 3, 2012, pp. 202-216.
8. O'Malley, Meagan, et al. "School Climate, Family Structure, and Academic Achievement: A Study of Moderation Effects." *School Psychology Quarterly,* vol. 30, no. 1, 2015, pp. 142-157.
9. Hopson, Laura, and Patricia Weldon. "Parental Expectations and Academic Success in the Context of School Climate Effects." *Families in Society: Journal of Contemporary Human Services*, vol. 94, no. 1, 2013, pp. 45-52.
10. Berkowitz, Ruth, et al. "A Research Synthesis of the Associations Between Socioeconomic Background, Inequality, School Climate, and Academic Achievement." *Review of Educational Research,* vol. 87, no. 2, 2017, pp. 425-469.
11. Perez, Efren O. and Marc J. Hetherington. "Authoritarianism in Black and White: Testing the Cross-Racial Validity of the Child Rearing Scale." *Political Analysis*, vol. 22, no. 3, 2014, pp. 398-412.
12. Buri, John R. "Parental Authority Questionnaire." *Journal of Personality Assessment*, vol. 57, no. 1, 1991, pp. 11110-119.

JOURNAL OF
EMERGING INVESTIGATORS

Article

Computational structure-activity relationship (SAR) of berberine analogs in double-stranded and G-quadruplex DNA binding reveals both position and target dependence

Stephanie Sun[1], Bhavesh Ashok[2], Andrew Su[3], Saira Hamid[4], Karthikha Sri Indran[4], Aashi Shah[2], Sarah Su[5], Simrun Sakhrani[6], Edward Njoo[7]

[1]BASIS Independent Silicon Valley, San Jose, California
[2]Amador Valley High School, Pleasanton, California
[3]Foothill High School, Pleasanton, California
[4]Mission San Jose High School, Fremont, California
[5]Los Altos High School, Los Altos, California
[6]The College Preparatory School, Oakland, California
[7]Department of Chemistry, Biochemistry, & Physical Science, Fremont, California

SUMMARY

Berberine, a natural product alkaloid, and its analogs have a wide range of medicinal properties, including antibacterial and anticancer effects. Previous studies showed that berberine and its analogs intercalate into DNA, thereby inhibiting DNA replication. Berberine has also been studied as a photosensitizer and was shown to generate reactive singlet oxygen *in situ*, and this has applications in photodynamic therapy. Various groups have synthesized berberine analogs that have comparable or improved biological activity; however, an exhaustive structure-activity relationship of the free energy of binding of berberine analogs with substitution at C-8, C-12, and C-13 to DNA have not been previously reported. High-throughput virtual screening (HTVS) allows for efficient analysis of compound libraries to identify lead compounds as possible pharmaceutical agents. Here, we employed HTVS towards a library of alkyl or aryl berberine analogs on C-8, C-12, and C-13 to probe binding to double-stranded and G-quadruplex DNA. Predicted free energies of binding to double-stranded DNA and G-quadruplex DNA were generated via molecular docking. The excited state electronic structure calculations were conducted via time-dependent density functional theory to probe the potential photosensitizing activity of each compound, and the potential G-quadruplex stabilizing abilities of key berberine analogs were probed through molecular dynamics simulations on a 4.0 nanosecond timescale. We determined that the nature of the substituent, the position of the substituent, and the nucleic acid target affect the free energy of binding of berberine analogs to DNA and G-quadruplex DNA, however berberine analogs did not result in net stabilization of G-quadruplex DNA.

INTRODUCTION

Berberine **(Figure 1**), a naturally occurring isoquinoline alkaloid extracted from the roots and stem of plants from the genus *Berberis,* has been of great medicinal interest due to its wide range of reported biological activities, including antimicrobial, antidiabetic, and anticancer activity (1-5). Berberine-containing extracts have been used as a medicinal agent in many traditional cultures dating back to 3000 BC (6).

The mechanism of action of berberine is believed to be intercalation with DNA, where it acts as a photosensitizer. Berberine was previously found to intercalate in DNA with a high free energy of binding (ΔG), driven by electrostatic attractions and pi-stack interactions between the compound and nucleotide base pairs in DNA secondary structures (7). Upon photoirradiation of the berberine-DNA complex, berberine acts as a photosensitizer and generates singlet oxygen, a reactive oxygen species, which oxidizes guanines and results in DNA damage, thereby inhibiting DNA replication and halting cell division (8). This was previously studied in application to photodynamic therapy as a potential treatment of various types of cancers and antimicrobial agents (9-10). Berberine has also been reported to stabilize G-quadruplex DNA (G4DNA), a four-stranded, noncanonical secondary structure of DNA consisting of guanine-rich DNA sequences

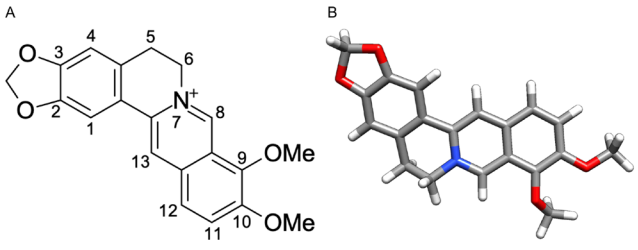

Figure 1. Background and introduction of Berberine 1.
(a) Chemical structure of berberine with the carbons numbered.
(b) 3D structure of berberine (DFT optimized, B3LYP, def2-SVP).

(11). Stabilization of G4DNA inhibits telomerase, an enzyme that is overexpressed in cancers; this inhibition of telomerase results in the inhibition of cancer activity (12).

Several semisynthetic analogs and derivatives of berberine have previously been prepared and evaluated for biological activities; some of these are reported to have comparable or superior antibacterial, antifungal, or anticancer activity compared to the natural product, and some have been reported to possess improved free energies of binding to DNA and G4DNA. Addition of an alkyl or aryl chain to C-8 of berberine can be achieved via nucleophilic addition of alkyl or aryl Grignard; such compounds have been reported to have more potent antimicrobial activity (13), but the possible role of the stereogenic center at C-8 in DNA binding is not yet known (**Figure 2a**). Wang *et al*. previously reported a library of 12-amine-berberine derivates that demonstrate increased anticancer activity compared to berberine (14). The synthesis and biological screening of 13-alkylberberine analogs revealed that the addition of alkyl chains of various lengths improves the anticancer, anti-inflammatory, and antioxidant activity of berberine (15-16). It has also been reported that a borohydride reduction at the C-8 iminium to yield dihydroberberine generally results in a loss of antimicrobial efficacy (17). While many have studied the biological activities of berberine and its analogs, less than 20 percent of studies reported in the last 10 years quantify the DNA free energy of binding of such analogs, and even fewer have produced crystal structures of berberine bound to a DNA target.

Here, we report an extensive *in silico* virtual screen of a representative library of 8-, 12-, and 13-alkyl and aryl berberine analogs (**Figure 2b**). The use of HTVS, which screens small molecule libraries against potential drug targets, has enabled the rapid and efficient screening of large libraries of chemical entities (18-20). We employed molecular docking to determine the predicted free energy of binding of each analog to each of the two DNA targets and we performed molecular dynamics (MD) simulations on berberine and selected analogs to simulate potential ligand-mediated stabilization

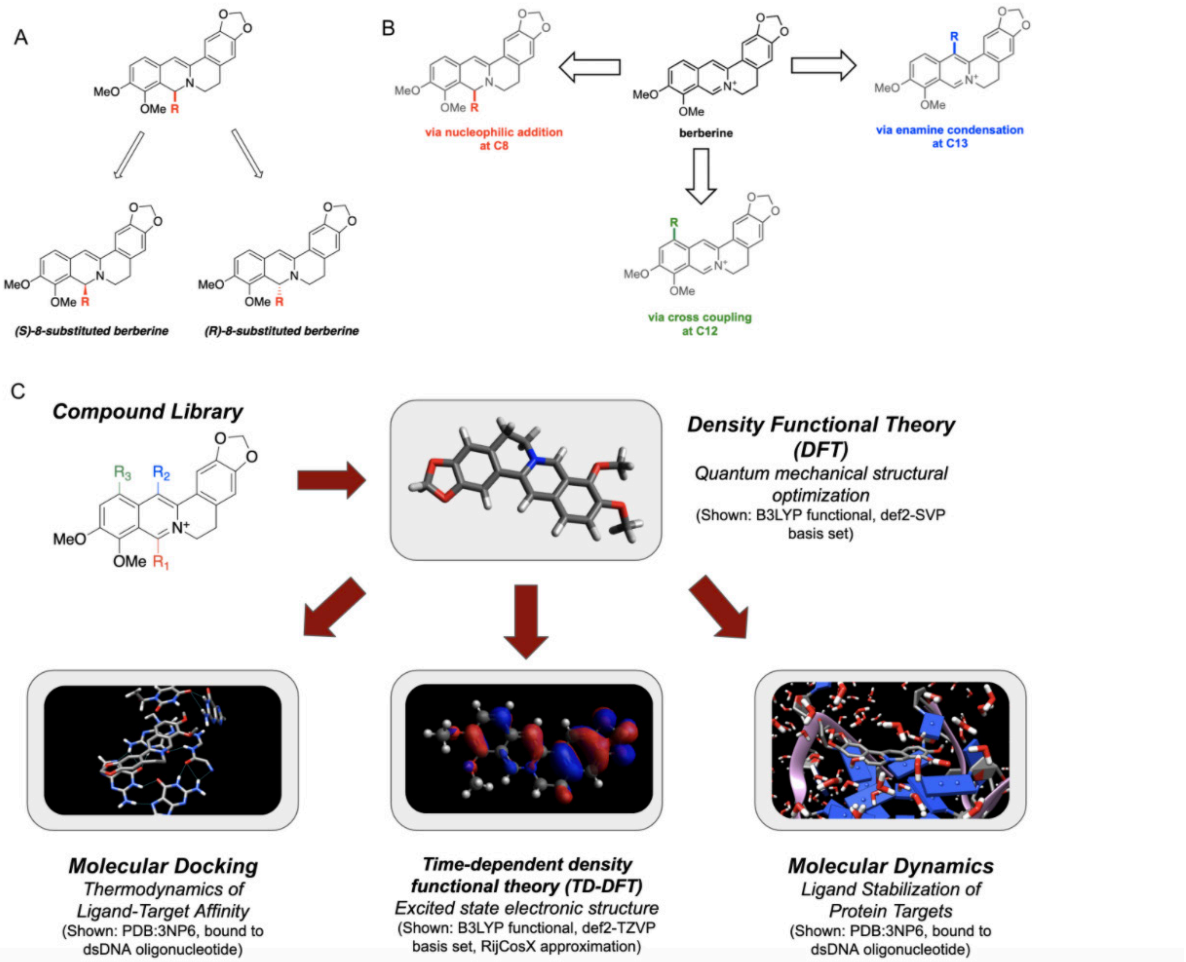

Figure 2. Design of the library of berberine analogs and our methodology in this study. (a) A stereocenter is formed when alkyl and aryl chains are added to C-8 of berberine, resulting in R and S enantiomers. Both R and S enantiomers of all C-8 analogs were studied. **(b)** Possible reactions for the synthesis of C-8, C-12, and C-13 analogs that inspired the design of the library. Possible reactions include a nucleophilic addition to C-8 with Grignard reagents, treatment of berberine with elemental bromine yields 12-bromoberberine, which can serve as a handle for cross coupling reactions, and enamine condensations to C-13. **(c)** Workflow and methodology in our work.

of the G4DNA complex. We implemented time-dependent density functional theory (TD-DFT) calculations to predict the wavelength of maximal absorbance and the relative energies of the singlet and triplet excited states of each analog. The energetic ordering of these excited states affects whether the berberine analogs can generate singlet oxygen, the process of which can result in DNA damage (**Figure 2c**). Since many DNA intercalators rely on pi-stack interactions or electrostatic attractions, we initially hypothesized that the addition of aromatic systems to C-8, C-12, or C-13 would provide an increase in ΔG, and that loss of the cationic iminium at C-8 would diminish the free energy of binding (21).

In this work, we screened a library of 31 berberine analogs against 2 biological targets, double-stranded DNA (dsDNA) d(CGTACG) and G4DNA, based on previously-reported crystal structures (PDB codes 3NP6 for dsDNA and 6JWD for G4DNA) (22-23). The results of the HTVS, MD simulations, and TD-DFT calculations indicate that the impact of aryl and aliphatic substitution on DNA free energy of binding is both position-dependent and target-dependent. We determined that the binding affinity of berberine analogs to dsDNA and G4DNA is affected by the nature and carbon position of the substituent, and these compounds have no net stabilizing effect on G4DNA complexes.

RESULTS

Molecular docking of the library of berberine analogs with dsDNA d(CGTACG) and G4DNA was completed using Autodock Vina (24-25). Docking parameters were determined from previously reported crystal structures, and the high degree of similarity in ligand positioning achieved between docked poses and the crystal structure demonstrates the predictivity of the docking parameters used (22-23). Results were quantified based on the ΔG in kcal/mol (**Figure 3**).

dsDNA Binding

Docking results for analogs with bromo-, phenyl-, and naphthyl- substitutions at the C-12 position had greater ΔG to dsDNA than analogs with substitutions at C-8 and C-13, and some of these compounds exhibited greater ΔG values than berberine itself. A lower ΔG value indicates stronger binding affinity to target proteins, and a negative ΔG indicates that the interaction between the compound and target is thermodynamically stable. Compounds with naphthyl groups on C-12 had a ΔG of -6.0 and -6.8 kcal/mol (**Figure 4c**), compound **12c** and **12d**, respectively. Interestingly, naphthyl additions to the C-8 position yielded lower ΔG values than berberine, with ΔG values of -2.1 and -3.3 kcal/mol for the R and S enantiomers of compound **8h**, respectively. The same trend was seen in the R and S enantiomers of compound **8i**, whose ΔG increased to -1.0 kcal/mol and -2.2 kcal/mol, respectively.

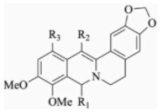

Compound 2, 8a-h

Compound	R_1	R_2	R_3	ΔG - dsDNA	ΔG - G4DNA
2	H	H	H	-6.2	2.5
8a	CH_3	H	H	R = -4.0, S = -4.1	R = -0.1, S = 2.3
8b	C_2H_5	H	H	R = -4.2, S = -3.8	R = 0.8, S = 1.4
8c	C_4H_9	H	H	R = -4.5, S = -4.3	R = 3.3, S = 5.0
8d	C_6H_{13}	H	H	R = -3.8, S = -3.6	R = 3.0, S = 2.5
8e	C_8H_{17}	H	H	R = -3.7, S = -3.6	R = 6.3, S = 1.5
8f	$C_{10}H_{21}$	H	H	R = -3.0, S = -3.2	R = 9.1, S = 3.4
8g		H	H	R = -4.4, S = -3.4	R = 6.1, S = 9.8
8h		H	H	R = -2.1, S = -3.3	R = 9.3, S = 9.2
8i		H	H	R = -1.0, S = -2.2	R = 65.9, S = N/A

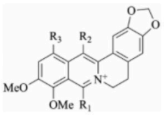

Compound 1, 12a-d, 13a-g

Compound	R_1	R_2	R_3	ΔG - dsDNA	ΔG - G4DNA
1	H	H	H	-5.6	2.6
12a	H	H	Br	-5.8	4.0
12b	H	H		-5.9	25.7
12c	H	H		-6.0	35.5
12d	H	H		-6.8	N/A
13a	H	C_4H_9	H	-4.8	3.2
13b	H	C_6H_{11}	H	-4.8	7.4
13c	H	C_8H_{17}	H	-4.6	4.1
13d	H	$C_{10}H_{21}$	H	-4.3	8.2
13e	H		H	-4.4	10.4
13f	H		H	-4.9	4.9
13g	H		H	-4.2	11.1

Figure 3. Thermodynamics of the binding of the library berberine analogs to dsDNA and G4DNA. Free energies of binding (ΔG) are reported in kcal/mol and represent the ΔG of the most thermodynamically-stable predicted binding pose.

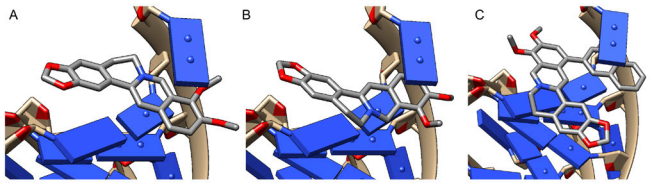

Figure 4. Most thermodynamically stable binding pose of representative compounds in our library to dsDNA. (a) Berberine 1 (ΔG = -5.6 kcal/mol) **(b)** Dihydroberberine 2 (ΔG = -6.2 kcal/mol) **(c)** Compound 12d, the berberine analog with the best free energy of binding to dsDNA (ΔG = -6.8 kcal/mol).

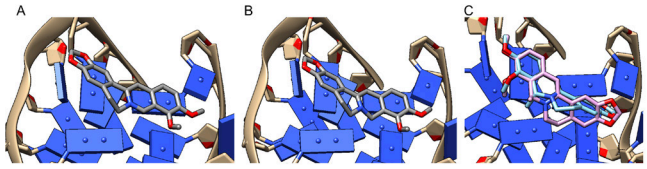

Figure 5. Binding poses of berberine and berberine analogs to G4DNA. (a) Berberine 1 (ΔG = 2.6 kcal/mol) **(b)** Dihydroberberine 2 (ΔG = 2.5 kcal/mol) **(c)** Both enantiomers of compound 8a. The structure in blue is the R enantiomer (ΔG = -0.1 kcal/mol), and the structure in purple is the S enantiomer (ΔG = 2.3 kcal/mol).

G4DNA Binding

Berberine analogs had lower free energies of binding to G4DNA than dsDNA. Unlike dsDNA, aliphatic chains on the C-8 positions demonstrated the best binding affinity to G4DNA. The R enantiomer of compound **8a** had the lowest ΔG value of all analogs screened at -0.1 kcal/mol (**Figure 5c**). Additions of naphthyl groups at both C-8 and C-12 greatly decreased the ΔG values of analogs **8h**, **8i**, **12c**, and **12d** to G4DNA. Compounds **8i** and **12d** were not able to dock to G4DNA. It is unclear why AutoDock Vina returned positive ΔG values for the DNA-berberine binding interaction.

The lengthening of the alkyl chain on the C-8 analogs also resulted in decreased free energy of binding of the compound to G4DNA. This could be attributed to steric clashes, in which members of the alkyl chain past the fourth carbon overlap with atoms of the receptor without taking part in the binding interactions. This is thermodynamically unfavorable due to repulsive electron interactions between these clashing atoms, increasing the ΔG value. Differences were also observed between the R and S enantiomers of these analogs, with thermodynamic favorability of the R enantiomer for alkyl chains four carbons and shorter. This trend seems to be reversed for alkyl chains longer than four carbons, with the S enantiomer having lower ΔG values.

Time-Dependent Density Functional Theory

TD-DFT was utilized to study the excited state electronic structure of each compound. Moreover, the molecular orbital energies that resulted allowed us to probe whether berberine analogs could undergo electronic transitions that can effectively produce singlet oxygen (**Figure 6**).

Here, we found that the energy gap generated by berberine and all analogs screened was sufficient for the production of singlet oxygen species. The energy emitted through phosphorescence, the transition from the triplet excited state back to ground state, is transferred to oxygen for the production of singlet oxygen (**Figure 7**). The energy gap necessary for the production of the singlet oxygen is 0.98 eV, which all of our compounds are able to undergo (26). The absorbance maximum wavelengths of the analogs of berberine undergo a blueshift. The C-8 compounds, which contain the reduced isoquinoline chromophore, undergo a larger blueshift than analogs with the same isoquinolinium chromophore as berberine. The rate of intersystem crossing

Compound	E_{S0} (eV)	E_{S1} (eV)	E_{T1} (eV)	$\Delta E_{S0\rightarrow S1}$ (H → L)	$\Delta E_{T1\rightarrow S0}$ (H → L)	λ_{max} (nm)
1	-5.645	-2.701	-3.854	2.944	1.791	421
2	-4.735	-1.119	-2.447	3.616	2.288	343
8a	-4.775	-1.069	-2.400	3.706	2.375	335
8b	-4.768	-1.048	-2.382	3.720	2.396	334
8c	-4.688	-1.123	-2.447	3.565	2.241	348
8d	-4.685	-1.112	-2.430	3.573	2.255	347
8e	-4.861	-1.117	-2.436	3.744	2.425	331
8f	-4.620	-1.030	-2.343	3.590	2.277	346
8g	-4.766	-1.219	-2.506	3.547	2.260	350
8h	-4.771	-1.568	-2.563	3.203	2.208	387
8i	-4.699	-1.487	-2.419	3.212	2.280	386

Compound	E_{S0} (eV)	E_{S1} (eV)	E_{T1} (eV)	$\Delta E_{S0\rightarrow S1}$ (H → L)	$\Delta E_{T1\rightarrow S0}$ (H → L)	λ_{max} (nm)
12a	-5.976	-2.851	-4.063	3.125	1.913	397
12b	-5.837	-2.700	-3.953	3.137	1.884	396
12c	-5.822	-2.710	-3.942	3.112	1.880	399
12d	-5.718	-2.699	-3.962	3.019	1.756	411
13a	-5.720	-2.610	-3.892	3.110	1.828	399
13b	-5.719	-2.608	-3.892	3.111	1.827	399
13c	-5.725	-2.610	-3.880	3.115	1.845	398
13d	-5.814	-2.584	-3.876	3.230	1.938	384
13e	-5.724	-2.609	-3.893	3.115	1.831	398
13f	-5.814	-2.584	-3.876	3.230	1.938	384
13g	-5.761	-2.665	-3.940	3.096	1.821	401

Figure 6. Energy of the ground state, singlet excited state, and triplet excited state of berberine and its analogs from TD-DFT calculations. Electronic transitions are reported in eV, and the wavelength of maximal absorbance is reported in nanometers. Calculations were performed using the B3LYP/def2-TZVP level of theory.

can be effectively calculated from Fermi's golden rule based on the spin-orbit coupling matrix elements, but this is not easily implemented in TD-DFT calculations in ORCA (27).

MD simulations were used to probe the potential stabilizing effects and stabilization timescale of the binary complexes between G4DNA and berberine, dihydroberberine, and 8-methylberberine. Specifically, stabilization over time of the G4DNA by berberine and the two analogs were calculated in GROMACS (**Figure 8a**), and the average RMSD was calculated over the same time interval (**Figure 8b**). G4DNA with berberine had a lower maximum RMSD value than G4DNA with dihydroberberine and 8-methylberberine. RMSD is a measure of the change in atom position from an initial point to a final point, and a lower RMSD value indicates that an atom or system has moved less from its initial position. A lower RMSD value over time indicates that the complex has been relatively stable. Unpaired t-testing revealed that the differences in RMSD between 8-methylberberine (2-tail unpaired *t*-test, *p*-value 0.10), dihydroberberine (2-tail unpaired *t*-test, *p*-value 0.087), and G4DNA were insignificant at a 95% confidence interval. However, the difference between the RMSD of G4DNA and berberine was statistically significant (2-tail unpaired *t*-test, *p*-value 0.00003), suggesting a destabilization of G4DNA by berberine.

DISCUSSION

Molecular docking, TD-DFT excited state calculations, and molecular dynamics simulations were performed to investigate the SAR in berberine analogs on the impact of aliphatic and aromatic side chains at C-8, 12, and 13 in the free energy of binding towards dsDNA and G4DNA. While the ΔG values of G4DNA appear positive, the results were predictive because the most thermodynamically favorable binding pose was accurately predicted. Analogs with the best free energy of binding to dsDNA were the 12-substituted analogs, which had ΔG values of -5.8 to -6.8 kcal/mol compared to a ΔG of -5.6 kcal/mol for berberine. The aromatic 12-substituted analogs performed the best overall with ΔG values comparable to berberine, likely due to the increased number of pi-stacking interactions.

Contrary to our initial hypothesis, berberine analogs with aromatic substitution did not always have the highest free energy of binding to either dsDNA or G4DNA targets. Rather, the effect of aryl versus aliphatic substitution on DNA binding appears to be dependent on not only the nature of the substituted group, but also the substituted carbon position (C-8, C-12, C-13) and the nucleic acid target, as different trends were observed in ΔG to dsDNA and G4DNA. Moreover, it appears that a loss of the persistent cation in the isoquinolinium core of berberine, as in the case of dihydroberberine and any 8-alkyl or 8-aryl analog, is not necessarily detrimental to DNA binding. Additionally, against initial expectations, MD simulations do not seem to indicate net stabilization of the G-quadruplex-ligand binary complex.

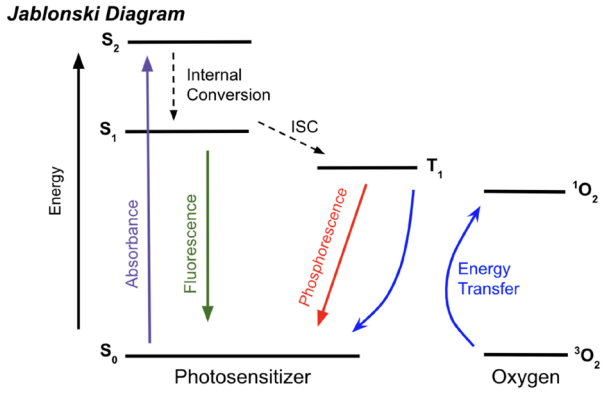

Figure 7. Jablonski Diagram depicting electronic transitions that occur as photosensitizers excite oxygen into singlet oxygen. Initial absorbance of a photon excites the ground state photosensitizer (S_0) to the second excited state (S_2), which undergoes rapid internal conversion to the first excited state (S_1). This undergoes intersystem crossing (ISC) to the first excited triplet state (T_1), which can excite ground state triplet oxygen ($^3O_2$) to an excited singlet state ($^1O_2$).

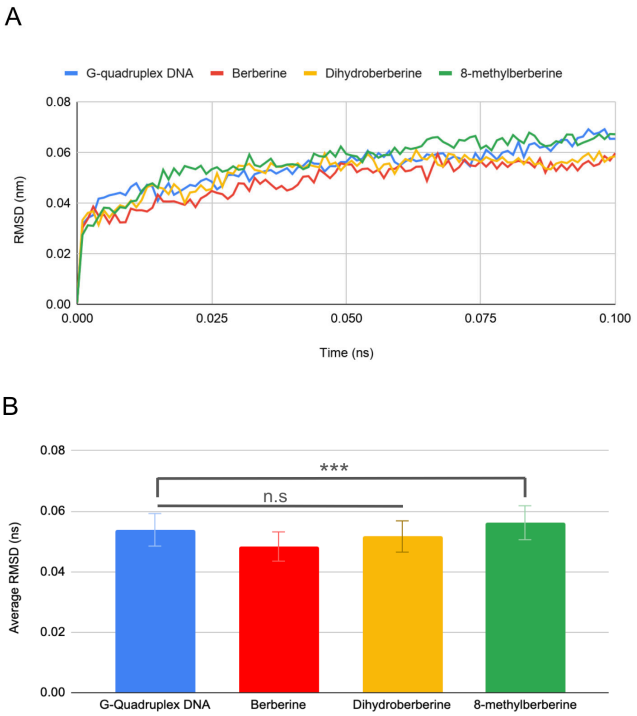

Figure 8. Root-mean-square deviation (RMSD) of atomic position calculations from molecular mechanisms. (a) Average RMSD of G4DNA, G4DNA with berberine, G4DNA with dihydroberberine, and G4DNA with 8-methylberberine over 0.1 nanosecond in water **(b)** Net Destabilization of G4DNA by berberine, dihydroberberine, and 8-methylberberine. 2-tail unpaired t-testing was completed to determine statistical significance between the average RMSD values of G4DNA compared to G4DNA with berberine, G4DNA with dihydroberberine, and G4DNA with 8-methylberberine. "n.s." indicates that the difference in average RMSD values are not statistically significant (*p*-value >0.05). "***" indicates that the difference in average RMSD values are statistically significant (*p*-value = 0.0001).

Visual analysis of the docked poses suggest that steric effects are operative in the superior ΔG of 8-alkyl berberine analogs in G4DNA (**Figure 3**, compounds **8a**-**8d**). The crystal structure positions the compound in a manner where C-8 directly faces the DNA, forcing a substituent on C-8 to have more interactions with the G4DNA. However, the relatively poor ΔG value of a larger substituent such as the aromatic compound **8g** is potentially caused by greater steric encumbrance to intercalate in G4DNA. Aliphatic 8-substituted analogs in the R enantiomers of G4DNA are more thermodynamically favorable than S enantiomers for four carbons and shorter, which can be explained by reduced steric hindrance in the direction of the S enantiomers.

The analogs with the lowest ΔG to G4DNA and the best ΔG to dsDNA were the aromatic substituents. The lower affinity for aromatic chains in G4DNA can be attributed to the G4DNA complex folding, exacerbating the problems of steric hindrance (28). The larger variation in free energies of binding with G4DNA can be attributed to the smaller binding since bigger molecules, like compound **12b**, are too sterically hindered to bind in more thermodynamically favorable conformer poses.

Compound 8a had the highest ΔG to G4DNA; however, MD simulations revealed that this compound destabilized G4DNA with an average RMSD value of 0.0562 ns while G4DNA has an average RMSD value of 0.0538 ns. Comparatively, berberine and dihydroberberine had much higher stabilization capabilities with average RMSD values of 0.0483 and 0.0516 ns respectively, which are lower than the average G4DNA's RMSD value.

Through TD-DFT calculations, we were able to determine that the berberine analogs can undergo an electronic transition that is sufficient for the production of singlet oxygen. This is deemed to be beyond the current scope of the study. Further studies on the lifetime of the triplet state of the berberine analogs are necessary to accurately understand the photosensitizing ability of berberine. One limitation with the use of berberine analogs is the blueshift observed in the maximum wavelength of absorbance. Many biomolecular entities, such as DNA and aromatic amino acids, have absorbance in the ultraviolet range, and photodynamic therapy with berberine analogs could possibly result in undesired side effects (29).

Through molecular docking, TD-DFT, and MD simulations we present an exhaustive SAR of berberine and its C-8, C-12, and C-13 analogs with respect to their free energy of binding to both dsDNA and G4DNA. While this study primarily focused on computational work and rapid *in silico* screening of such compounds, it provides the basis for future work in the chemical synthesis and *in vitro* evaluation of hit structures and their DNA-binding efficacy.

MATERIALS AND METHODS

Molecular Mechanics Pre-Optimization

Avogadro, a cross-platform molecular editor, was used to create three-dimensional computational models of berberine and each of the studied analogs (30). Prior to density functional theory (DFT) geometry optimization, each model was initially optimized by molecular mechanics using the Merck Molecular Force Field (MMFF94) to 10,000 steps. Input files for DFT structural optimizations were created on Avogadro.

DFT Structural Optimization

Density functional theory (DFT) is a quantum mechanical modelling method based on electron density that is used to calculate the ground state energies of molecules and solids (31). Here, DFT was used to calculate the most quantum mechanically minimized molecular geometries of berberine analogs. ORCA, an *ab initio* quantum mechanical molecular modeling software, was used in tandem with Avogadro to generate ORCA input files to compute the DFT optimized structure of berberine and each analog (32-33). An implicit conductor-like polarizable continuum (CPCM) solvation model of water was used to simulate the conditions of an aqueous environment. B3LYP, a hybrid functional, was chosen for the calculation due to its low computational cost compared to other traditional functionals, as well as its acceptance in the scientific community for creating low parameter, accurate results (34). The def2-SVP basis set was used as the compounds are comprised of light main group elements. All DFT calculations were carried out to default convergence thresholds. Additionally, TD-DFT, with the B3LYP hybrid functional, was used to model and calculate the excited singlet and triplet energies of berberine and its analogs, which is instrumental to understanding the photosensitizing ability of berberine analogs. The def2-TZVP basis set was used in conjunction with the RIJCOSX approximation method to greatly accelerate the calculation with negligible decrease in accuracy and significant reduction of computational expense.

AutoDockTools

AutoDockTools (ADT), a part of the MGLTools suite, is a graphical user interface that allows for the preparation and generation of coordinate files for use in AutoDock Vina (34). To prepare the dsDNA d(CGTACG) and G4DNA moieties for the docking procedure, ADT was used to identify the receptors as a macromolecule, which adds Gasteiger charges to the molecule and merges non-polar hydrogens. The search space for the ligand was also chosen at this stage, modelled after 3NP6 for dsDNA and 6JWD for G4DNA. Each ligand was prepared by importing the coordinate file into ADT as a ligand, upon which the Gasteiger charges were computed and applied to the molecule. The identification of the torsion tree root allowed the number of rotatable bonds to be set, allowing for maximum conformity of the ligand to induce fit into the specified search grid.

AutoDock Vina

AutoDock Vina is an open source molecular docking program, allowing us to understand and model the

thermodynamics of ligand-protein interactions (36). Configuration of Vina included the definition of the search grid from ADT. Additionally, Vina was queried to generate 15 conformers of each ligand rather than the default 9 binding modes in order to avoid omission of possible conformers. The exhaustiveness value of the search was doubled from the default 8 to 16 in order to generate models from more computationally exhaustive methods. The validity of the docking parameters used was first assessed by comparing the predicted highest-affinity binding pose of berberine to dsDNA d(CGTACG) with that which was previously reported in its crystal structure (PDB 3NP6), and these were found to be consistent.

UCSF Chimera/ChimeraX

Visual analysis to determine the accuracy of the computationally determined binding mode of the berberine molecule relative to that of the crystal structure shown in 3NP6 and 6JWD was done in UCSF Chimera and UCSF ChimeraX molecular visualization programs (37-38).

GROMACS

GROMACS, or the GROningen MAchine for Chemical Simulations, is a molecular dynamics (MD) package that simulates interactions between proteins and ligands using Newton's laws of motion (39). GROMACS was used to carry out high-level molecular dynamics simulations to computationally model the interactions between atoms in the most thermodynamically favorable conformers of berberine, dihydroberberine, and G4DNA. The AMBER99SB force field and an explicit TIP3 water solvation model were used. Energy minimization was conducted in order to minimize the structure and remove clashes within the system. An equilibration step was conducted to meet temperature and pressure constraints imposed by the MD simulation. Configuration of the force field using AMBER99SB parametrics and bond-charge correction (BCC) charges on the ligand level was carried out on the ACPYPE Web Server (40). Additional time-dependent RMSD calculations to determine net stabilization of the DNA were also carried out using GROMACS. MDWeb was used to generate the structure of each MD simulated system in the PDB format with GROMACS trajectories for visualization in Chimera (41).

DFT, TD-DFT, molecular docking, and molecular dynamics calculations were performed on a Dell PowerEdge 710 server with a 24 core Intel Xeon X5660 processor at 2.80GHz and 32GB RAM.

Wavelength of Excitation

The minimum energy in electron-volts (eV) to excite berberine and its analogs was found by determining the energy difference between the lowest unoccupied molecular orbital (LUMO) by the highest occupied molecular orbital (HOMO). The wavelength corresponding to the HOMO-LUMO gap was determined according to the following equation:

$$\lambda = \frac{hc}{E} = \frac{(6.626*10^{-34}Js)(3.00*10^{8}m/s)*10^{9}nm/m}{(LUMO-HOMO)*1.602*10^{-19}J/eV}$$

HOMO and LUMO orbitals were visualized on Avogadro. Orbital energies were calculated through time-dependent density functional theory (TD-DFT) calculations in ORCA.

ACKNOWLEDGEMENTS

We would like to acknowledge the Scripps Research Institute and Olson Laboratory for generously providing Autodock Vina for use in academic research. DFT and TD-DFT calculations were performed on ORCA, an *ab-initio*, DFT, and semi-empirical electronic structure package developed by Frank Neese at the Max Planck Institute for Chemical Energy Conservation, and the authors are grateful for open source access to the software in academic research. Molecular visualizations were produced using the UCSF Chimera package from the Resource for Biocomputing, Visualization, and Informatics at the University of California, San Francisco (supported by NIH P41 RR-01081). Molecular graphics and analyses were performed with UCSF ChimeraX, developed by the Resource for Biocomputing, Visualization, and Informatics at the University of California, San Francisco, with support from National Institutes of Health R01-GM129325 and the Office of Cyber Infrastructure and Computational Biology, National Institute of Allergy and Infectious Diseases.

The authors declare no competing conflicts of interests in the work presented. The authors gratefully acknowledge Prof. Robert Downing from the Department of Computer Science & Engineering at ASDRP for his guidance with initial setup and remote access to the server.

Received: June 11, 2020
Accepted: November 16, 2020
Published: December 18, 2020

REFERENCES

1. Grycová, Lenka, *et al.* "Quaternary Protoberberine Alkaloids." *Phytochemistry*, vol. 68, no. 2, 2007, pp. 150–175., doi:10.1016/j.phytochem.2006.10.004.
2. Wang, Ye, *et al.* "The Anti-Cancer Mechanisms of Berberine: A Review." *Cancer Management and Research*, Volume 12, 2020, pp. 695–702., doi:10.2147/cmar.s242329.
3. Stermitz, F. R., *et al.* "Synergy in a Medicinal Plant: Antimicrobial Action of Berberine Potentiated by 5'-Methoxyhydnocarpin, a Multidrug Pump Inhibitor." *Proceedings of the National Academy of Sciences*, vol. 97, no. 4, 2000, pp. 1433–1437., doi:10.1073/pnas.030540597.
4. Wang, Haoran, *et al.* "Metformin and Berberine, Two Versatile Drugs in Treatment of Common Metabolic Diseases." *Oncotarget*, vol. 9, no. 11, 2017, pp. 10135–10146., doi:10.18632/oncotarget.20807.

5. Lau, Chi-Wai, *et al*. "Cardiovascular Actions of Berberine." *Cardiovascular Drug Reviews*, vol. 19, no. 3, 2006, pp. 234–244., doi:10.1111/j.1527-3466.2001.tb00068.x.
6. Tillhon, Micol, *et al*. "Berberine: New Perspectives for Old Remedies." *Biochemical Pharmacology*, vol. 84, no. 10, 2012, pp. 1260–1267., doi:10.1016/j.bcp.2012.07.018.
7. Krey, A. K., and F. E. Hahn. "Berberine: Complex with DNA." *Science*, vol. 166, no. 3906, 1969, pp. 755–757., doi:10.1126/science.166.3906.755.
8. Hirakawa, Kazutaka, *et al*. "The Mechanism of Guanine Specific Photooxidation in the Presence of Berberine and Palmatine: Activation of Photosensitized Singlet Oxygen Generation through DNA-Binding Interaction." *Chemical Research in Toxicology*, vol. 18, no. 10, 2005, pp. 1545–1552., doi:10.1021/tx0501740.
9. Callaghan, Susan, and Mathias O. Senge. "The Good, the Bad, and the Ugly – Controlling Singlet Oxygen through Design of Photosensitizers and Delivery Systems for Photodynamic Therapy." *Photochemical & Photobiological Sciences*, vol. 17, no. 11, 2018, pp. 1490–1514., doi:10.1039/c8pp00008e.
10. Ragàs, Xavier, *et al*. "Singlet Oxygen in Antimicrobial Photodynamic Therapy: Photosensitizer-Dependent Production and Decay in E. Coli." *Molecules*, vol. 18, no. 3, 2013, pp. 2712–2725., doi:10.3390/molecules18032712.
11. Moraca, Federica, *et al*. "Ligand Binding to Telomeric G-Quadruplex DNA Investigated by Funnel-Metadynamics Simulations." *Proceedings of the National Academy of Sciences*, vol. 114, no. 11, 2017, doi:10.1073/pnas.1612627114.
12. Spiegel, Jochen, *et al*. "The Structure and Function of DNA G-Quadruplexes." *Trends in Chemistry*, vol. 2, no. 2, 2020, pp. 123–136., doi:10.1016/j.trechm.2019.07.002.
13. Iwasa, Kinuko, *et al*. "Antimicrobial Activity of 8-Alkyl- and 8-Phenyl-Substituted Berberines and Their 12-Bromo Derivatives." *Journal of Natural Products*, vol. 61, no. 9, 1998, pp. 1150–1153., doi:10.1021/np980044+.
14. Wang, Bo, *et al*. "Syntheses and Structure–Activity Relationships in Growth Inhibition Activity against Human Cancer Cell Lines of 12 Substituted Berberine Derivatives." *Molecules*, vol. 25, no. 8, 2020, p. 1871., doi:10.3390/molecules25081871.
15. Lee, Dong-Ung, *et al*. "Effects of 13-Alkyl-Substituted Berberine Alkaloids on the Expression of COX-II, TNF-α, INOS, and IL-12 Production in LPS-Stimulated Macrophages." *Life Sciences*, vol. 73, no. 11, 2003, pp. 1401–1412., doi:10.1016/s0024-3205(03)00435-1.
16. Zhang, Lei, *et al*. "Synthesis and Cytotoxicity Evaluation of 13-n-Alkyl Berberine and Palmatine Analogues as Anticancer Agents." *Molecules*, vol. 17, no. 10, 2012, pp. 11294–11302., doi:10.3390/molecules171011294.
17. Rodrigues, Catarina A. B., *et al*. "Synthesizing a Berberine Derivative and Evaluating Antimicrobial Activity To Reinforce with Students the Potential Significance of Small Chemical Structure Changes for Biological Systems." *Journal of Chemical Education*, vol. 95, no. 3, 2018, pp. 492–495., doi:10.1021/acs.jchemed.7b00458.
18. Dhasmana, Anupam, *et al*. "High-Throughput Virtual Screening (HTVS) of Natural Compounds and Exploration of Their Biomolecular Mechanisms." *New Look to Phytomedicine*, 2019, pp. 523–548., doi:10.1016/b978-0-12-814619-4.00020-3.
19. Kumari, Madhulata, *et al*. "High Throughput Virtual Screening to Identify Novel Natural Product Inhibitors for MethionyltRNA-Synthetase of Brucella Melitensis." *Bioinformation*, vol. 13, no. 1, 2017, pp. 8–16., doi:10.6026/97320630013008.
20. Kontoyianni, Maria. "Docking and Virtual Screening in Drug Discovery." *Methods in Molecular Biology Proteomics for Drug Discovery*, 2017, pp. 255–266., doi:10.1007/978-1-4939-7201-2_18.
21. Mignon, P. "Influence of the π-π Interaction on the Hydrogen Bonding Capacity of Stacked DNA/RNA Bases." *Nucleic Acids Research*, vol. 33, no. 6, 2005, pp. 1779–1789., doi:10.1093/nar/gki317.
22. Ferraroni, Marta, *et al*. "X-Ray Diffraction Analyses of the Natural Isoquinoline Alkaloids Berberine and Sanguinarine Complexed with Double Helix DNA d(CGTACG)." *Chemical Communications*, vol. 47, no. 17, 2011, p. 4917., doi:10.1039/c1cc10971e.
23. Wang, Fei, *et al*. "Colchicine Selective Interaction with Oncogene RET G-Quadruplex Revealed by NMR." *Chemical Communications*, vol. 56, no. 14, 2020, pp. 2099–2102., doi:10.1039/d0cc00221f.
24. Morris, Garrett M., *et al*. "AutoDock4 And AutoDockTools4: Automated Docking with Selective Receptor Flexibility." *Journal of Computational Chemistry*, vol. 30, no. 16, 2009, pp. 2785–2791., doi:10.1002/jcc.21256.
25. Trott, Oleg, and Arthur J. Olson. "AutoDock Vina: Improving the Speed and Accuracy of Docking with a New Scoring Function, Efficient Optimization, and Multithreading." *Journal of Computational Chemistry*, 2009, doi:10.1002/jcc.21334.
26. Derosa, M. "Photosensitized Singlet Oxygen and Its Applications." *Coordination Chemistry Reviews*, vol. 233-234, 2002, pp. 351–371., doi:10.1016/s0010-8545(02)00034-6.
27. Alberto, Marta Erminia, *et al*. "Rational Design of Modified Oxobacteriochlorins as Potential Photodynamic Therapy Photosensitizers." *International Journal of Molecular Sciences*, vol. 20, no. 8, 2019, p. 2002., doi:10.3390/ijms20082002.
28. Ida, Jeunice, *et al*. "G-Quadruplexes as An Alternative Recognition Element in Disease-Related Target Sensing." *Molecules*, vol. 24, no. 6, 2019, p. 1079., doi:10.3390/molecules24061079.
29. Schmid, Franz-Xaver. "Biological Macromolecules: UV-Visible Spectrophotometry." *Encyclopedia of Life Sciences*, 2001, doi:10.1038/npg.els.0003142.
30. Hanwell, Marcus D, *et al*. "Avogadro: an Advanced

Semantic Chemical Editor, Visualization, and Analysis Platform." *Journal of Cheminformatics*, vol. 4, no. 1, 2012, doi:10.1186/1758-2946-4-17.
31. Neese, Frank. "The ORCA Program System." *WIREs Computational Molecular Science*, vol. 2, no. 1, 2011, pp. 73–78., doi:10.1002/wcms.81.
32. Lee, Chengteh, *et al.* "Development of the Colle-Salvetti Correlation-Energy Formula into a Functional of the Electron Density." *Physical Review B*, vol. 37, no. 2, 1988, pp. 785–789., doi:10.1103/physrevb.37.785.
33. Kohn, W., *et al.* "Density Functional Theory of Electronic Structure." *The Journal of Physical Chemistry*, vol. 100, no. 31, 1996, pp. 12974–12980., doi:10.1021/jp960669l.
34. Becke, Axel D. "Density-Functional Thermochemistry. III. The Role of Exact Exchange." *The Journal of Chemical Physics*, vol. 98, no. 7, 1993, pp. 5648–5652., doi:10.1063/1.464913.
35. Morris, Garrett M., *et al.* "AutoDock4 And AutoDockTools4: Automated Docking with Selective Receptor Flexibility." *Journal of Computational Chemistry*, vol. 30, no. 16, 2009, pp. 2785–2791., doi:10.1002/jcc.21256.
36. Trott, Oleg, and Arthur J. Olson. "AutoDock Vina: Improving the Speed and Accuracy of Docking with a New Scoring Function, Efficient Optimization, and Multithreading." *Journal of Computational Chemistry*, 2009, doi:10.1002/jcc.21334.
37. Pettersen, Eric F., *et al.* "UCSF Chimera - A Visualization System for Exploratory Research and Analysis." *Journal of Computational Chemistry*, vol. 25, no. 13, 2004, pp. 1605–1612., doi:10.1002/jcc.20084.
38. Goddard, Thomas D., *et al.* "UCSF ChimeraX: Meeting Modern Challenges in Visualization and Analysis." *Protein Science*, vol. 27, no. 1, 2017, pp. 14–25., doi:10.1002/pro.3235.
39. "GROMACS." *Gromacs*, www.gromacs.org/.
40. Silva, Alan W Sousa Da, and Wim F Vranken. "ACPYPE - AnteChamber PYthon Parser InterfacE." *BMC Research Notes*, vol. 5, no. 1, 2012, p. 367., doi:10.1186/1756-0500-5-367.
41. Hospital, Adam, *et al.* "MDWeb and MDMoby: an Integrated Web-Based Platform for Molecular Dynamics Simulations." *Bioinformatics*, vol. 28, no. 9, 2012, pp. 1278–1279., doi:10.1093/bioinformatics/bts139.

JOURNAL OF
EMERGING INVESTIGATORS

Article

Comparing the dietary preference of *Caenorhabditis elegans* for bacterial probiotics vs. *Escherichia coli*.

Shraddha Lulla, Christine Chiodo
Weston High School, Weston, Massachusetts

SUMMARY

The use of probiotics is on the rise as more people are learning about their possible health benefits. In this experiment, we used *C. elegans* as a simple model organism to observe the impact of probiotics on the human digestive system. In this investigation the dietary preference of *C. elegans* was tested using three different bacterial probiotics (Chobani, siggi's and Stonyfield) and the control nutrient source, *E. coli*. The results of the experiment showed that the *C. elegans* were, on average, most present in Chobani cultures. At the end of the observation period, there were, on average, about 1,207 *C. elegans* present in the *E. coli* quadrants, and about 1,314 *C. elegans* present in the Chobani quadrants, as compared to 1,133 *C. elegans* in the siggi's quadrants and 981 in the Stonyfield quadrants. There were about 8.9% more *C. elegans* present in the Chobani quadrants than in the *E. coli* quadrants. Additionally, the Chobani quadrants grew, on average, by 188 *C. elegans*/day, 9.3% more than the 172 *C. elegans*/day growth in the *E. coli* quadrants. While not statistically significant, these results still demonstrated that *C. elegans* might prefer Chobani cultures over other probiotic yogurts, which may also indicate greater gut benefits from Chobani over the other yogurt brands tested.

INTRODUCTION

For decades, the yogurt aisle in American supermarkets had been dominated by corporations like General Mills and Kraft (1). Against all odds, a Turkish immigrant named Hamdi Ulukaya brought his Greek yogurt, Chobani, to the United States in 2007 (2). Detractors were skeptic that a yogurt with live bacteria cultures would sell due to public discomfort around eating bacteria (3). However, the public was convinced with Chobani's health benefits - twice as much protein as regular yogurts, no artificial sweeteners, and 3 probiotics (4). Today, Chobani pulls over $1.5 billion in annual revenue is the second largest yogurt titan in the US and has inspired other companies to increase the nutritional value of their own yogurts (5). Like Greek yogurt, Icelandic yogurt ("skyr"), including the brand siggi's, is strained and provides a similar protein content, low sugar level, and number of probiotics (6).

Probiotics are microorganisms that are present in Greek and Icelandic yogurts, as well as in American yogurts like Stonyfield today (7). The concept behind probiotics was introduced in the early 20th century, when Nobel Laureate Elie Metchnikoff, known as the "father of probiotics," proposed that consuming beneficial microorganisms could improve people's health (8). Researchers continued to investigate this idea, and the term "probiotics" - meaning "for life" - eventually came into use. Probiotics can have various health benefits, such as enhanced digestion and immune function in humans (9-10). Products with probiotics include foods like yogurt, dietary supplements, and even skin creams. The use of probiotics has been on the rise in the last decade, as more people are learning about their health benefits (11). The probiotic market globally is worth over $15B USD due to increasing research of their health benefits and efficacy in treating certain diseases (12). While Chobani, siggi's, and Stonyfield share some strains of probiotic bacteria, they also have probiotics unique to their preparations (**Table 1**) (7, 13-14).

In this experiment, we aimed to see the impact of these different yogurt preparations on humans by using the model organism *Caenorhabditis elegans,* a nematode roundworm that is around 1 mm long (15). Our goal was to see whether probiotics have a positive effect on the growth of *C. elegan s*, which normally feed off and grow in decomposing plants which are rich in bacteria (16). In the lab, *C. elegans* are often fed *Escherichia coli*, so we chose it as our control food source (16). Even though they are much smaller than humans, many of their organ systems are like those of humans and other mammals, making *C. elegans* a good model organism for our study (17). Since both *C. elegans* and humans share similar digestive tissue, we aimed to determine the effect of probiotics on the growth of *C. elegans* to possibly infer outcomes within the human gut, although we cannot determine exact outcomes unless specifically tested on humans (17). In addition, *C. elegans* was chosen as the model organism because they are easy to culture and use, which made them well suited for this type of independent study.

Table 1. Number and strains of probiotic cultures in each yogurt.

Yogurt	Probiotics and Active Cultures	Number of Cultures
Y1 (Chobani)	*S. thermophilus, L. bulgaricus, L. acidophilus, Bifidus, L. casei*	5
Y2 (siggi's)	*S. thermophilus, L. delbrueckii subsp. bulgaricus, B. lactis, L. acidophilus, L. delbrueckii subsp. lactis*	5
Y3 (Stonyfield)	*S. thermophilus, L. bulgaricus, L. acidophilus, Bifidus, L. paracasei, L. rhamnosus*	6

Note: Cultures identified from the nutrition facts provided by each company (7, 13-14).

A culture of probiotics was grown for each of the three yogurt brands to become a food source for the *C. elegans*. To limit sources of variability, each of the three yogurts were plain with 0% milkfat. By seeing which probiotic or *E. coli* the *C. elegans* population grows most in, we inferred which culture might be most beneficial for growth.

Since Stonyfield yogurt has the largest variety of active cultures, we hypothesized that *C. elegans* would migrate to areas with Stonyfield as there would be a greater chance that *C. elegans* would prefer eating at least one of the various active cultures and potentially display the best growth. We also hypothesized that all the probiotic yogurts would promote *C. elegans* growth more than the control group, *E. coli,* due to the availability of additional active cultures. Ultimately, we found that the Chobani fed *C. elegans* had the highest population increase, differing from what we had hypothesized. After Chobani, the control food source (*E. coli*) had the most *C. elegans* growth followed by the siggi's. The areas with Stonyfield yogurt ended up with the least amount of *C. elegans*, on average.

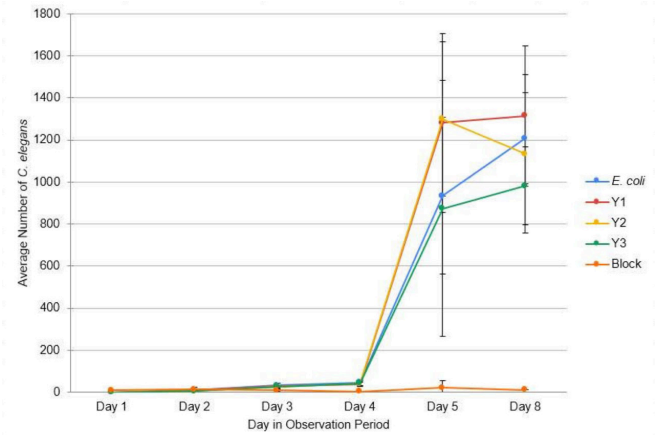

Figure 1. Average number of *C. elegans* each day by food source. Data represent the *C. elegans* population in all quadrants and the central block, as well as the overall population growth. Graph shows the average number of *C. elegans* by food source each day, where different colors represent the food sources. Data was measured daily for 5 days and again on Day 8. The data values are the average number of *C. elegans* in all 8 petri dishes. Error bars represent standard deviation.

RESULTS

The goal of this experiment was to learn more about the effect of probiotics on human nutrition. Today, *C. elegans* is widely used as a model organism to study humans and other mammals (17). We compared *C. elegans*'s growth in their typical laboratory food source, *E. coli*, versus three probiotic yogurts (16).

To study the dietary preferences of *C. elegans*, eight petri dishes were partitioned into four quadrants. The four quadrants were then labeled as E, for *E. coli*, Y1 for Chobani, Y2 for siggi's, and Y3 for Stonyfield. The *C. elegans* were added to the center of each petri dish and were observed daily for 5 days and once more on day 8 of the experiment.

Y1 (Chobani yogurt) had the most *C. elegans* at the end of the observation period, followed by *E. coli* (which acted as the control food source environment), Y2 (siggi's), and finally Y3 (Stonyfield) (**Table 2**). On Day 8, there was an average (across all 8 petri dishes) of 1314 *C. elegans* in the Y1 quadrants, 1207 *C. elegans* in the *E. coli* quadrants, 1133 *C. elegans* in the Y2 quadrants, and 981 *C. elegans* in the Y3 quadrants. The block at the center of each petri dish, where the *C. elegans* were initially placed, contained Luria broth and agar. Since the block is not as nutrient rich as the other food sources, *C. elegans* numbers are consistently low in the block, with an ending average of 12 *C. elegans*, almost identical to its starting value of 10 *C. elegans*.

Table 2. Average number of *C. elegans* per day.

	Day 1	Day 2	Day 3	Day 4	Day 5	Day 8
Average in *E. Coli*	0 ± 0	10 ± 5.6	32 ± 11	46 ± 13	934 ± 370	1207 ± 220
Average in Y1	0 ± 0	10 ± 6.0	29 ± 13	38 ± 8.3	1281 ± 420	1314 ± 330
Average in Y2	0 ± 0	6 ± 3.6	26 ± 9.7	40 ± 11	1230 ± 370	1133 ± 380
Average in Y3	0 ± 0	6 ± 1.5	27 ± 17	43 ± 13	874 ± 610	981 ± 190
Average in Block	10 ± 2.1	14 ± 10	9 ± 5.8	3 ± 2.0	21 ± 34	12 ± 0
Average Total Number of *C. elegans* (per plate)	10 ± 2.1	45 ± 16	123 ± 48	170 ± 29	4411 ± 1200	4646 ± 740

Note: Data were measured daily for 5 days, with an extra measurement on Day 8. Values represent the average number of C. elegans *in all 8 petri dishes ± standard deviation. Data not recorded on Day 6 and 7.*

Up until Day 4, the growth of the *C. elegans* population in all quadrants was relatively low (**Figure 1**). While some individual petri dishes had large *C. elegans* population increases before Day 4, others even had decreases in their *C. elegans* population, so the average *C. elegans* population growth was rather low as compared to after Day 4. In the period after Day 4, *C. elegans* population in all quadrants grew rapidly each day. One exception was the average *C. elegans* population change from Day 5 to Day 8 in the Y2 quadrant, where the *C. elegans* population decreased. The average daily increase in the *C. elegans* population was calculated for all quadrants in each petri dish (**Figure 2**).

The quadrant with the highest average daily increase in number of *C. elegans* was the Y1 quadrant, which increased, on average, 188 *C. elegans*/day. This was followed by the *E. coli* quadrant, which increased by an average of 172 *C. elegans*/day. Next was the Y2 quadrant, which increased an average of 162 *C. elegans*/day. The Y3 quadrant had the lowest daily increase of the quadrants at 140 *C. elegans*/day. Finally, the block had the lowest average daily increase, with an increase of 0 *C. elegans*/day, because of its low nutrient levels compared to the quadrants' food sources.

Three paired one-tailed *t*-tests were performed between *E. coli* and each of Y1, Y2, and Y3. However, only Y1 had a higher average daily increase in *C. elegans* than *E. coli*, and Y2 and Y3 had lower increases in *C. elegans* than *E. coli* on average. *E. coli* was compared to Y1, and the result was not statistically significant using a significance cutoff of $\alpha < 0.05$ (*p*-value = 0.19). Since the other quadrants (Y2 and Y3) had lower increases in *C. elegans* than Y1 and even *E. coli*, their results were also not statistically significant (with the alternate

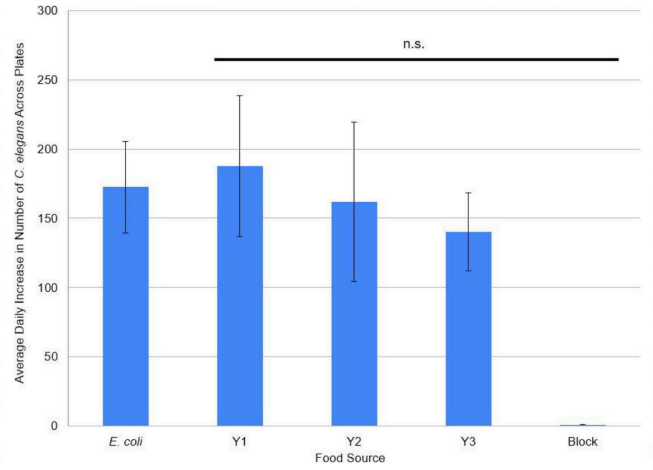

Figure 2. Average daily increase in number of *C. elegans* by food source. Data represent the average daily increase in number of *C. elegans* in each quadrant of the petri dishes/plates. Data was measured daily for 5 days and an extra measurement was done on Day 8. The average was calculated across all eight petri dishes. Error bars represent standard deviation. Not significant, compared to the control group (*E. coli*), is denoted by n.s. (n = 6, paired t-test, $\alpha = 0.05$).

hypothesis that the probiotic quadrants would perform better than the *E. coli* quadrants.

DISCUSSION

Our initial hypothesis was that overall, all probiotic yogurts tested would have a greater increase in number of *C. elegans* than the *E. coli* quadrants. The specific hypothesis was that since Stonyfield (Y3) has the largest variety of active cultures, it would promote the highest population increase in *C. elegans*. Therefore, we hypothesized that the *C. elegans* would consume most of the Stonyfield active cultures and that they would be found the most often in this quadrant compared to the others. However, the experiment did not support the original hypothesis. By the end of the experiment, *C. elegans* had the highest population increase in the Chobani (Y1) quadrants. Therefore, our specific hypothesis that *C. elegans* population would increase the most in Stonyfield quadrants was not observed in this experiment. Our general hypothesis that probiotic yogurt quadrants would promote *C. elegans* growth more than *E. coli* quadrants was also not observed, as we could not reject the null hypothesis.

Although the average daily increase in number of *C. elegans* in Y1 was not statistically significant compared to the *E. coli* quadrants, the Y1 quadrants still had a higher average and overall increase in their *C. elegans* population. The Y1 quadrants increased, on average, by 188 *C. elegans*/day, which is 9.3% more than the 172 *C. elegans*/day increase in the *E. coli* quadrants. Additionally, on Day 8, there was an average of 1314 *C. elegans* in the Y1 quadrants: 8.9% more than the average of 1207 *C. elegans* in the *E. coli* quadrants. This shows that Y1 (Chobani) is still an effective food source for *C. elegans* and could still be more effective than *E. coli*. Further study could validate this result. Additionally, *C. elegans* did not prefer the most diverse food source in terms of active cultures (Stonyfield, Y3). This may indicate that *C. elegans* do not necessarily favor diverse food sources.

Many individual petri dishes indicated a possible food cycle in some quadrants because their numbers of *C. elegans* per day fluctuated, instead of constantly increasing. For example, in the Y2 quadrant of the 6th petri dish, the *C. elegans* population was growing rapidly since the initial observation up until Day 2. There were around 1200 *C. elegans* observed on Day 2, but the population dramatically decreased to 200 *C. elegans* on Day 3, and 20 *C. elegans* on Day 4. This could be because of a food shortage in the 6th petri dish's Y2 quadrant. Since the *C. elegans* population was growing so rapidly, the *C. elegans* population could have reached its carrying capacity in that quadrant, so no food was left, and many *C. elegans* could have died or migrated. Once the probiotic bacteria in Y2 replenished itself due to a low *C. elegans* population on Day 4, the *C. elegans* had enough food to grow once again, so the *C. elegans* population grew to around 2213 on Day 5. Most petri dishes showed patterns that might indicate a food cycle on similar days and, on average, reflected the same trends.

There were several possible sources of error that could have influenced the outcome of this experiment. Some environmental factors could not be controlled. Each petri dish was wrapped with Parafilm because otherwise the *C. elegans* might have left the dishes, since they move so fast and easily. Despite re-wrapping after every data collection, the humidity and the temperature of the room could not be controlled uniformly. This inconsistency could have been a potential cause of variability of *C. elegans* thriving on certain days more than others. Although all the plates were in the same environment, they could have been affected in other ways. Another likely source of error was that the microscope had some limitations. The microscope was not powerful enough to magnify the *C. elegans* enough to see their embryonic and larval stages, possibly giving an inaccurate count of *C. elegans*. An additional factor that could not be controlled was how fast the three yogurt cultures grew and how much of it was eaten. There was no way to tell how much of each nutrient source was available at each time. In addition, each of the three yogurts were a mix of multiple active cultures, meaning that the relative growth of each bacterial strain in the cultures could have impacted the available food sources and reduced the diversity of those cultures. Also, when the *C. elegans* were being placed in each of the 8 petri dishes, they may not have been exactly centered, so the *C. elegans* might have been more inclined to go to a quadrant closest to them. Another source of error could have occurred while counting the *C. elegans* on the petri dishes. Some of the *C. elegans* were clumped together, making it difficult to count them. As a result, this likely caused the numbers of *C. elegans* that were counted to differ slightly from the actual number. *C. elegans* were growing and moving at an accelerated rate, possibly making the counts marginally inaccurate.

This experiment raised multiple questions for further

investigation. One of these questions is testing out other food sources to find out *C. elegans*'s preferences. *C. elegans* 's diet has been studied in other experiments, including a study testing *C. elegans*'preference for two different strains of *E. coli* (18). To continue studying *C. elegans*'s diet, one expansion of this experiment could study how varying amounts of probiotic cultures could affect the growth of *C. elegans*. In this experiment, each yogurt had some of the same active cultures as other yogurts, but mostly differed in their selection of probiotics. It would be interesting to see if preferences change with other probiotic cultures not tested in this experiment. It would also be interesting to see if a higher concentration of probiotic cultures could increase the overall population growth of *C. elegans*. Another area of deeper and further examination would be to grow each culture in its own petri dish and then allow *C. elegans* to consume it individually as opposed to having multiple food sources share a petri dish.

In conclusion, this experiment demonstrated that *C. elegans*' population size grew most effectively in Chobani, possibly indicating that the cultures Chobani contained were the preferred source of nutrition compared to that of other probiotic yogurts and *E. coli*. This result may apply to humans as well due to the shared similarities in the gut with *C. elegans*.

MATERIALS AND METHODS

Culture growth and maintenance

A sterile plastic milliliter pipette was used to transfer four drops of each yogurt sample and the control - Y1 (Chobani), Y2 (siggi's), Y3 (Stonyfield), and *E. coli* (Carolina Biological Supply) - into 6 mL Luria broth (Carolina Biological Supply). A sterile inoculation loop was used to mix each yogurt and *E. coli* with Luria broth until evenly distributed into each test tube. This mixture formed the culture of probiotics for each yogurt brand and for *E. coli*. The test tubes were placed in a room overnight (70°F), and later in the biology classroom (70°F).

Eight petri dishes were then filled with agar. One bottle of agar was melted using a microwave and poured equally into each of the eight petri dishes. They were kept solidifying for the length of the school day (approximately eight hours), before turning them upside down to prevent too much condensation. The petri dishes were then wrapped in Parafilm and stored in the fridge overnight.

The next day, the petri dishes were split into four quadrants (on the outside of the petri dish) by using a marker to equally separate the dishes into four parts. The four quadrants were the three yogurt cultures and one control food source (*E. coli*). Each of the four parts was labeled as E for *E. coli*, Y1 for Chobani, Y2 for siggi's, and Y3 for Stonyfield. Using a micropipette, 200 ul of *E. coli* and each of the three probiotic yogurt cultures from the test tubes were aliquoted and spread with an inoculation loop into their respective quadrants in the eight petri dishes. They were then left to sit for five hours at room temperature (70°F).

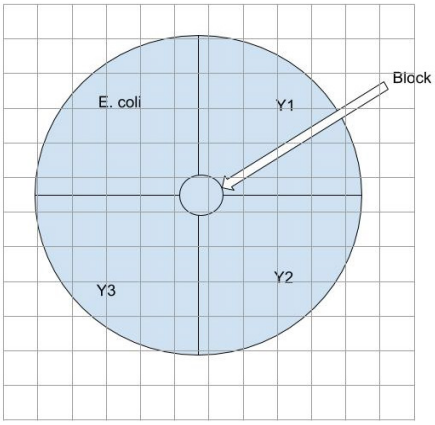

Figure 3. Petri dish setup. Each dish was divided into quadrants and, and graph paper was placed under each dish to approximate the count in each quadrant. *C. elegans* were counted in one square at the center of each quadrant and multiplied by the number of squares per quadrant to estimate the total *C. elegans* in each quadrant.

C. elegans maintenance and observation

The *C. elegans* used in the experiment (Carolina Biological Supply Company) came in a petri dish of agar and Luria broth, and a 1 cm^2 block of *C. elegans* was cut out and placed in the center of each of the eight experimental petri dishes. Each 1 cm^2 block of agar had an average of ten *C. elegans*. The *C. elegans* were first observed 2.5 hours after their initial placement in the center of the experimental petri dishes.

During the first observation, the *C. elegans* were counted once again in each quadrant as well as in the block. We used a microscope with 100-400x magnification to count the number of *C. elegans* throughout the observation period. The *C. elegans* were counted daily for 5 days and once more on day 8 to see the population growth in each of the 4 different food sources, as well as the block.

On Day 3 of the observation, there were too many *C. elegans* in each quadrant for them to be accurately counted, so a piece of graph paper was placed under each petri dish. The *C. elegans* were then counted in one square in the center of each quadrant. These numbers were then multiplied by the number of squares per quadrant to calculate an estimate of how many *C. elegans* were in each quadrant (**Figure 3**). After data collection, daily averages of the number of *C. elegans* in each quadrant (of all dishes) were calculated (**Figure 1**).

Average daily increase calculation

Average daily increases in the *C. elegans* population were then calculated to see which food source *C. elegans* consume most over time and to see in which of the 4 food sources their population grew fastest (**Figure 2**).

For example, in the Y3 quadrant of the second petri dish, the initial observation on Day 1 had 0 *C. elegans,* and the final observation on Day 8 had about 1406 *C. elegans*. Therefore, the average daily increase in *C. elegans* in the Y3 quadrant of the second petri dish was:

$$\frac{Day\ 8\ Population - Day\ 1\ Population}{7\ Days} = \frac{1406 - 0}{7} = 201\ C.elegans/\text{day}.$$

Then, the average across all petri dishes was taken, so the average daily increase for Y3 became 140 *C. elegans*/day (shown in **Figure 2**), because other petri dishes' Y3 quadrants had lower daily increases in *C. elegans* population.

Statistical analysis

Three paired one-tailed *t*-tests were performed between *E. coli* and each of Y1, Y2, and Y3 with a significance cutoff of $p < 0.05$. In this test, the alternate hypothesis was that the probiotic quadrants would perform better than the *E. coli* quadrants, and the null hypothesis was that *E. coli* and probiotic yogurt quadrants would have the same *C. elegans* population increase.

ACKNOWLEDGEMENTS

I would like to thank my family for their constant support and advice and Ms. Liu for her feedback and help.

Received: April 20, 2020
Accepted: December 5, 2020
Published: December 18, 2020

REFERENCES

1. Schactman, Brian. "Want Greek Growth? Eat Some Yogurt." *CNBC*, CNBC, 14 July 2011, www.cnbc.com/2011/07/14/want-greek-growth-eat-some-yogurt.html.
2. Wang, Hansi Lo. "Greek Yogurt Sales Rise in U.S. Dairy Aisles." *NPR*, NPR, 22 Aug. 2011, www.npr.org/2011/08/22/139847892/greek-yogurt-sales-rise-in-u-s-dairy-aisles.
3. Mourdoukoutas, Panos. "How Greek Yogurt Captured the American Market: The Other Half of The CNBC Story." *Forbes*, Forbes Magazine, 22 Apr. 2013, www.forbes.com/sites/panosmourdoukoutas/2011/07/22/how-greek-yogurt-captured-the-american-market-the-other-half-of-the-cnbc-story/.
4. "The Chobani Story." *DairyHerd,* DairyHerd Management, 2013. https://dairyherd.com/sites/default/files/Chobani-Media-Kit-2013.pdf
5. Gelles, David. "Chobani, the Greek Yogurt Maker, Reclaims Control of Its Finances." *The New York Times* , The New York Times, 28 June 2018, www.nytimes.com/2018/06/28/business/chobani-tpg-healthcare-ontario-pension-plan.ht ml.
6. Sportelli, Natalie. "The Founder Behind Siggi's Dairy, The Fastest-Growing Yogurt Brand in America." *Forbes* , Forbes Magazine, 2 Mar. 2016, www.forbes.com/sites/nataliesportelli/2016/02/25/the-founder-behind-siggis-dairy-the-fastest-growing-yogurt-brand-in-america/.
7. "Smooth & Creamy - Fat Free Plain (5.3oz)." *Stonyfield*, 29 July 2020, www.stonyfield.com/products/yogurt/smooth-creamy/fat-free-plain.
8. Cooper, Edwin L. "ECAM: Darwin and Metchnikoff." *Evidence-Based Complementary and Alternative Medicine* , vol. 6, no. 4, 6 Dec. 2009, pp. 421–422., doi:10.1093/ecam/nep194.
9. Roselli, Marianna, *et al*. "Caenorhabditis Elegans and Probiotics Interactions from a Prolongevity Perspective." *International Journal of Molecular Sciences*, vol. 20, no. 20, 10 Oct. 2019, p. 5020., doi:10.3390/ijms20205020.
10. Jäger, Ralf, *et al*. "International Society of Sports Nutrition Position Stand: Probiotics." *Journal of the International Society of Sports Nutrition*, vol. 16, no. 1, 21 Dec. 2019, doi:10.1186/s12970-019-0329-0.
11. Kechagia, Maria, *et al*. "Health Benefits of Probiotics: A Review." *ISRN Nutrition*, vol. 2013, 2 Jan. 2013, pp. 1–7., doi:10.5402/2013/481651.
12. Day, Richard Lj, *et al*. "Probiotics: Current Landscape and Future Horizons." *Future Science OA*, vol. 5, no. 4, 3 May 2019, doi:10.4155/fsoa-2019-0004.
13. "Non-Fat Plain." *Chobani*, www.chobani.com/products/plain/cup/non-fat-plain/.
14. "Plain Non-Fat." *Siggi's Dairy*,9 Jan. 2020, siggis.com/product/plain-non-fat.
15. Apfeld, Javier, and Scott Alper. "What Can We Learn About Human Disease from the Nematode C. Elegans?" *Methods in Molecular Biology Disease Gene Identification* , 2018, pp. 53–75., doi:10.1007/978-1-4939-7471-9_4.
16. Gómez-Orte, Eva, *et al*. "Effect of the Diet Type and Temperature on the C. Elegans Transcriptome." *Oncotarget*, vol. 9, no. 11, 21 Dec. 2017, pp. 9556–9571., doi:10.18632/oncotarget.23563.
17. Haag, Eric S., *et al*. "From 'the Worm' to 'the Worms' and Back Again: The Evolutionary Developmental Biology of Nematodes." *Genetics*, vol. 210, no. 2, 1 Oct. 2018, pp. 397–433., doi:10.1534/genetics.118.300243.
18. Shtonda, Boris Borisovich. "Dietary Choice Behavior in Caenorhabditis Elegans." *Journal of Experimental Biology*, vol. 209, no. 1, Jan. 2006, pp. 89–102., doi:10.1242/jeb.01955.

JOURNAL OF
EMERGING INVESTIGATORS

Article

The long-term effect of CBD crystals and CBD oil on depressive-associated rat behaviors

Jiarui Yang, Siyu Liu
The Affiliated High School of Peking University, Beijing, China

SUMMARY

Cannabidiol (CBD) is a chemical extracted from cannabis and shown by some studies to alleviate the symptoms of many mental disorders, especially major depressive disorder. Many researchers have explored how acute CBD treatment impacts the attitude of depressive patients, but few researchers have examined how chronic CBD consumption influences the mood of people without depression. To simulate the effect of CBD on people, we used male Wistar Rats as experimental models, divided into three groups: the control group received peanut oil (vehicle), the CBD oil group received CBD oil and vehicle, and the CBD crystal group received CBD crystals and vehicle. We hypothesized that chronic treatments with purified CBD through oral administration would relieve depression-associated behaviors in normal healthy rats under adverse conditions. The CBD oil used in this study was made from crude oil of hemp by molecular distillation, and the CBD crystals were further processed from CBD oil by crystallization. We used forced swimming test and sucrose preference test to assess the characters associated with the diagnosis of depression: despair-like behavior and anhedonia. Furthermore, we used the weight of the rats to assess appetite. A statistical analysis of the experimental data suggested that long-term consumption of CBD could elicit depression associated symptoms in normal rats without depression. The results imply that people should consume CBD-containing products with extreme caution and highlight the need to carefully monitor the use of CBD in health care products.

INTRODUCTION

There are at least 66 kinds of cannabinoids in the cannabis sativa plant. Within those cannabinoids, Δ9-tetrahydrocannabinol (THC) is the main psychoactive chemical, while cannabidiol (CBD) is non-psychoactive (1).

The activation of the endocannabinoid system (ECS) accounts for most of the effects of cannabinoids. The ECS is a highly conserved endocrine network in the process of evolution, and it is a neuroregulatory system that regulates mood, cognition, autonomic nervous system and movement. The ECS is composed of the cannabinoid receptor 1 (CB1) and cannabinoid receptor 2 (CB2) as well as endogenous ligands (mainly arachidonoyl ethanolamide, 2-arachidonoyl glycerol, and 2-arachidonyl glyceryl ether) (2). Different from THC, CBD has a low affinity for cannabinoid receptors and acts as an antagonist on both the CB1 and CB2 receptors (3). Clinical and preclinical evidence suggests CBD could ameliorate or reverse some of detrimental effects induced by THC, but the mechanism of this effect is unclear (3). CBD shows promising effects in treating various diseases, including psychosis, substance use disorder, anxiety disorder, cognitive impairment, and epilepsy (4-8). In 2010, the anti-depressant effects of acute CBD administration in mice were first reported by Zanelati *et al*. (9). Many studies have demonstrated the effectiveness of acute CBD preclinical treatment through rodent behavioral tests, including the forced swimming test (FST), sucrose preference test (SPT), tail suspension test (TST), and open field test (OFT), raising the possibility that CBD could be used for treating depression (8). Studies reported that CBD might possess agonist properties at serotonin 1A (5-HT1A) receptors and regulate the brain-derived neurotrophic factor (BDNF). The 5-HT1A receptors and BDNF levels have been consistently related to the neurobiology of depression and the mechanism of antidepressant drugs (9, 10). However, the exact cause for the effects of CBD on the brain is not yet fully understood.

Under federal law, CBD has not yet been approved to be added to dietary supplements, food ingredients, or animal food. Cosmetics can contain CBD as long as the THC content is lower than 0.3% (11). Still, because of the wide therapeutic effects of CBD, in the past few years, CBD had seen a surge in popularity and many CBD products have emerged in United States and Europe with widespread use. Health care products, pet products, skincare products, drinks, food, and e-cigarettes containing CBD have been sold in the market, but the market is chaotic, and the quality of the products is mixed (12, 13). According to a study by University of Michigan's Institute for Social Research, in the past year, 38% of high school seniors had used CBD at least one time (14). This popularity has led to healthy people consuming CBD in addition to those using it for potential therapeutic effects.

Although the acute antidepressant properties of CBD have been reported in several preclinical experiments (9), only a few researchers put emphasis on studying the chronic impact of CBD on depressive-associated behaviors in preclinical tests (15). Also, only rodents that had shown depressive-

associated behaviors, not healthy rodents, were included in the few chronic tests (16). In order to assess the potential of CBD in mood improvement and the safety of CBD as a health care product, it is necessary to monitor the impacts of CBD after repeated administration on healthy rodents. Therefore, the aim of the present study is to evaluate how chronic CBD treatment could affect the mood of healthy rats and compare the effects of purified CBD crystals and impure CBD oil in chronic treatments. We hypothesize that chronic treatments with purified CBD through oral administration would relieve depression-associated behaviors in normal healthy rats under adverse conditions and that impure CBD oil would not change the behaviors of rats. Our results from FST indicated that the chronic administration of both CBD crystals and CBD oil elicited depression-associated behaviors compared to the control group. We also observed that other ingredients in CBD oil affected the weight gain of the rats.

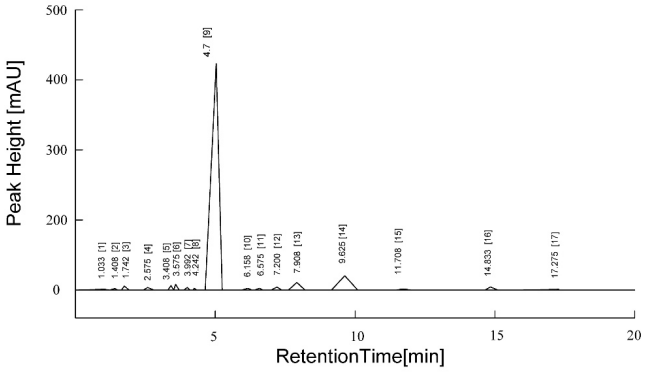

	Retention Time[min]	Peak Area [mAU]	Peak Height [mAU]	Area [%]	Height[%]	WOS[min]	Compound Name
1	1.033	35.683	1.208	0.5	0.2	0.79	
2	1.408	34.157	2.604	0.5	0.5	0.18	
3	1.742	140.865	7.015	2.2	1.4	0.19	
4	2.575	141.734	4.543	2.2	0.9	0.67	
5	3.408	138.208	7.900	2.1	1.6	0.24	
6	3.575	127.592	10.062	2.0	2.0	0.21	
7	3.992	60.287	4.561	0.9	0.9	0.29	
8	4.242	42.958	3.272	0.7	0.7	0.25	
9	4.700	4785.036	404.056	73.2	81.3	0.18	Cannabidiol
10	6.158	60.340	2.238	0.9	0.4	0.58	
11	6.575	46.883	2.373	0.7	0.5	0.35	
12	7.200	98.753	4.514	1.5	0.9	0.26	
13	7.908	211.591	12.419	3.2	2.5	0.23	Tetrahydrocannabinol
14	9.625	470.410	24.395	7.2	4.9	0.28	
15	11.708	26.178	1.112	0.4	0.2	0.34	
16	14.833	111.293	4.746	1.7	1.0	0.35	
17	17.275	8.725	0.271	0.1	0.1	0.56	
	SUM	6540.693	497.289	100	100		

Figure 1. The composition of the CBD oil. The chromatogram and composition of the CBD oil were determined by high-performance liquid chromatography. The result of the chromatography showed that there were 17 kinds of chemicals presented in the CBD oil. The retention time for CBD was 4.700 mins, while the retention time for THC was 7.908 mins. The content of each substance is equal to the percentage of each peak area. The CBD content was 73.2%, and the THC content was 3.2%.

RESULTS

This study compared the influence of oral intragastric administration of CBD crystals and CBD oil on 6-8 week-old male Wistar rats once a day for 21 days at a dose of 30mg/kg body weight. The CBD oil was made from crude oil of hemp by molecular distillation, and the CBD crystals were further processed from CBD oil by crystallization. Chromatography showed that there were 17 kinds of chemicals presented in the CBD oil, with CBD and THC comprising 73.2%, and 3.2%, respectively (**Figure 1**). The result of the chromatography showed that after crystallization, there were only six substances present in the CBD crystals, and the percentage of CBD was 98.8% and THC was 0.2% (**Figure 2**).

Forced swimming test (FST) is used to model hopelessness and helplessness of the rats by putting them in extreme conditions. Rodents are placed into large graduated cylinders filled with water. In the beginning, rodents display active movements trying to escape. As time goes on, rodents tend to be less active and be more motionless. The rodents only exhibit minimal movement essential to keep their head above water. Immobility of the rodents is regarded as an indicator of despair (17).

In the forced swimming test, both CBD crystal and CBD oil treatments significantly shortened the active periods of the rats before they showed immobility as compared to the vehicle treatment ($p = 0.00019$ and $p = 0.00021$, respectively).

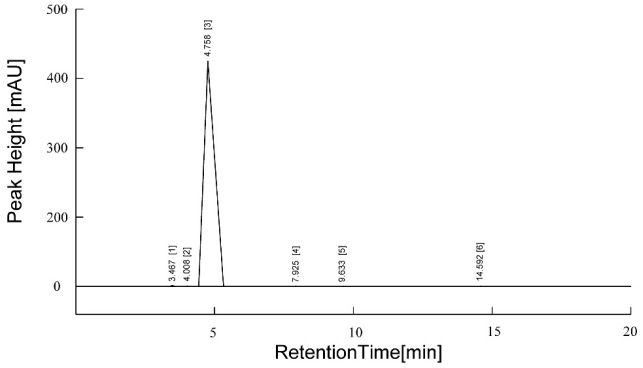

	Retention Time[min]	Peak Area [mAU]	Peak Height [mAU]	Area [%]	Height[%]	WOS[min]	Compound Name
1	3.467	25.705	1.892	0.5	0.5	0.18	
2	4.008	10.495	0.992	0.2	0.2	0.17	
3	4.758	4683.473	405.755	98.8	98.9	0.19	Cannabidiol
4	7.925	7.957	0.639	0.2	0.2	0.19	tetrahydrocannabinol
5	9.633	7.405	0.463	0.2	0.1	0.26	
6	14.592	7.565	0.378	0.2	0.1	0.33	
	SUM	4742.601	410.120	100	100		

Figure 2. The composition of the CBD crystals. The chromatogram and composition of the CBD crystals were determined by high-performance liquid chromatography. The result of the chromatography showed that after crystallization, there were only six substances present in the CBD crystals. The retention time for CBD was 4.758 mins, while the retention time for THC was 7.925 mins. The content of each substance is equal to the percentage of each peak area. The CBD content was 98.8%, and the THC content was only 0.2%.

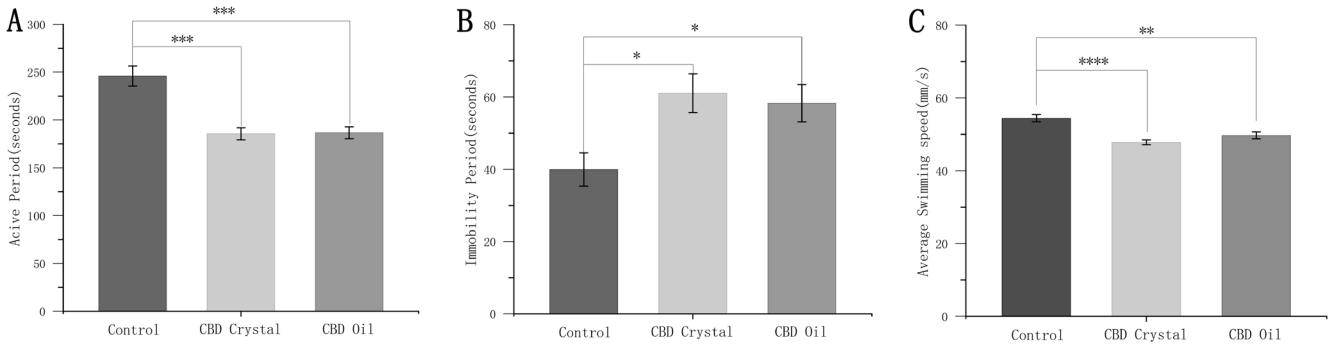

Figure 3. Effect of chronic administration of CBD on forced swimming test. CBD shortens the active periods (A), increases the immobility periods (B), and slows down the average swimming speeds of rats (C) in the forced swimming test regardless of the purity of CBD. The active periods before showing immobility, the immobility periods, and the average swimming speeds were recorded or calculated for three groups. The means were calculated. Data are presented as means, and error bars represent standard error of the mean (n = 10). * indicates $p < 0.05$, ** indicates $p < 0.01$, *** indicates $p < 0.001$, and **** indicates $p < 0.0001$.

However, no significant difference was observed between the CBD crystal and CBD oil groups (p = 0.93, **Figure 3A**). Additionally, both CBD crystal and CBD oil treatments significantly increased the immobility periods as compared to the vehicle treatment (p = 0.011 and p = 0.016 respectively). However, no significant difference is observed between CBD crystal and CBD oil groups (p = 0.82, **Figure 3B**).

Both CBD crystal and CBD oil treatments significantly slowed down the average swimming speeds of the rats as compared to the vehicle treatment (p = 0.00005 and p = 0.0043, respectively). However, no significant difference was observed between the CBD crystal and CBD oil groups (p = 0.13, **Figure 3C**). Overall, compared with rats only treated with vehicle, rats treated with CBD crystals and rats treated with CBD oil spent less time swimming and were more immobile.

The sucrose preference test (SPT) is used to measure whether rats show anhedonia-like behavior. Anhedonia is the inability to experience pleasure from normally pleasurable activities and is a core symptom of depression in humans (18). This test assesses the animals' preference for sweet-tasting sucrose solution relative to plain water. Studies have shown that sucrose solution with 1-2% (wt/vol) would be the optimal concentration to distinguish whether or not animals have anhedonia syndromes (19).

Rats in the same treatment group (n =10/group) were placed into a single cage and the preference for sucrose against water was measured. The consumption of CBD, either oil or crystal, decreased the sucrose preference as compared to the control group (**Figure 4**). The sucrose preference of the control group, the CBD crystal group, and the CBD oil group were respectively 73.57%, 67.74%, and 57.29%. Also, compared with the CBD crystal group, the CBD oil group showed even less sucrose preference. The total volumes of water consumed by the control group, the CBD crystal group, and the CBD oil group were respectively 439 mL, 589 mL, and 391 mL **(Figure 5**).

Animals' weight can be used to assess appetite and food consumption, which can reflect the influence of CBD. Rats were weighed on the first and seventh day after purchase, and then every four days after that. Intragastric administration of CBD began on the tenth day. At the initial time point, the mean weight of the rats in the control group, CBD crystal group, or CBD oil groups was respectively 287.7, 283.7, and 284.2 grams. On the seventh day, the mean weights of the rats in the control group, CBD crystal group, or CBD oil groups were respectively 314.7, 317, and 314.4 grams. There were no significant differences in mean weight between the groups, during these two weighing sessions before CBD intragastric administration. To rule out the effect of original weight, the ratio of daily weight to original weight of each group was calculated (**Figure 6**). After 21 days of chronic treatments, the mean weight ratios of the control group and the CBD crystal group showed significant differences compared with that of the CBD oil group (p = 0.0039 and p = 0.03, respectively). The CBD oil group had a significantly lower body weight compared to the vehicle control and CBD crystal groups.

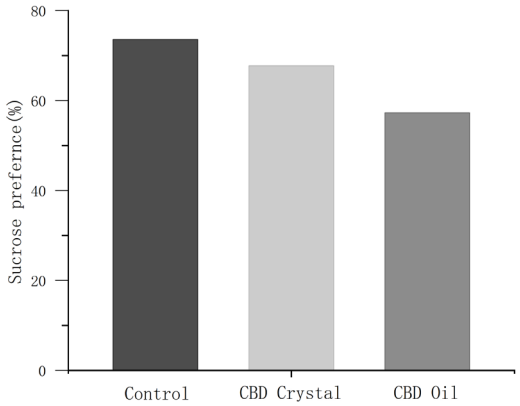

Figure 4. CBD decreases the sucrose preference of the group. As 10 rats were placed in the same cage and the sucrose preference was not individually recorded, therefor there are no statistics. The sucrose preference of the control group, CBD crystal group, and CBD oil group are respectively 73.57 %, 67.74 %, and 57.2 9%. Both the CBD crystal group and CBD oil group showed lower sucrose preference than the control group. The sucrose preference is calculated using the equation: sucrose solution intake/(sucrose solution intake + tap water intake). There were 10 rats in each cage.

There was no significant difference in the mean weight ratio between the CBD crystal group and the control group. These data indicated that the impurities in the CBD oil affected the weight gain of the rats compared with CBD crystals.

DISCUSSION

In the present study, we hypothesized that that chronic administration of purified CBD products would be able to relieve depression-associated behaviors in normal healthy rats under adverse conditions, but the results from FST did not confirm this hypothesis. On the contrary, the chronic administration of both CBD crystals and CBD oil elicited depression-associated behaviors compared to the control group.

The consumption of CBD shortened the active periods during swimming for rats in the CBD crystal group and CBD oil group as compared to the control group ($p < 0.001$, **Figure 3A**). An active period accounts for the rats' persistence when they are trying to escape and is defined as the period between when a rat is first put into water and when the rat starts to show immobility. The shortened active period implied that under adverse conditions, rats revealed less persistence when treated with CBD crystals, or CBD oil. This result indicates that after taking CBD products for a long period, the rats had behavioral patterns associated with anxiety and pessimism under adverse conditions.

Compared to the control group, repeated CBD treatments using CBD crystals and CBD oil increased the immobility period for normal rats ($p = 0.011$ and $p = 0.016$, respectively; **Figure 3B**). As the passive immobility period is considered representative of behavioral hopelessness and helplessness in human depression, rats that exhibit more immobility are thought to have behavioral patterns associated with depression (20). The results of the tests showed that male Wistar rats treated with CBD crystals, or CBD oil demonstrated more behavioral patterns associated with depression than rats treated only with vehicle. This result demonstrates potential of CBD consumption to elicit depression-associated symptoms in normal people.

The consumption of CBD slowed down the average swimming speed, a measure of activity level, of rats in the CBD crystal and CBD oil groups as compared to the control group (**Figure 3C**). The swimming speed differences induced by the CBD crystal group and the CBD oil group were statistically significant compared with the control group, as both p values are less than 0.01. These results showed that the consumption of CBD reduced the active level of the rats.

The consumption of CBD also decreased sucrose preference. Lower sugar preference is thought to reflect the anhedonia condition present in human depression. The CBD crystal group and the CBD oil group had lower sucrose preferences than the control group. Although the lower sucrose preference may suggest that the rats treated with CBD exhibited anhedonia-like behavior, but we could not draw any strong conclusions for this SPT experiment, because the sucrose preference was not individually recorded.

After chronic treatments, both the CBD oil group and CBD crystal group had apparently shorter active periods, significantly longer immobility periods, and obviously slower swimming speeds compared to the control group (**Figure 3**). These results showed that the consumption of CBD elicited depression-associated behaviors in the rats. However, some

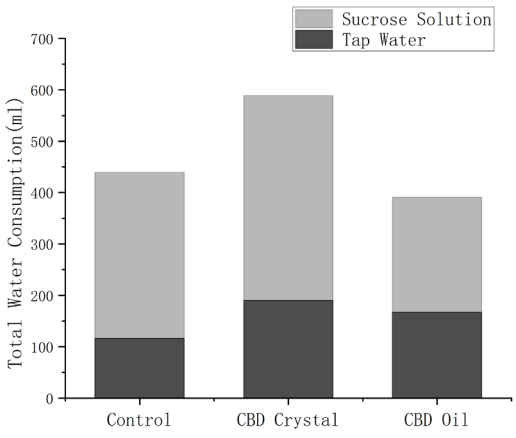

Figure 5. Total water consumption for the three groups. The total volumes of water consumed by the control group, the CBD crystal group, and the CBD oil group were respectively 439 ml, 589 ml, and 391 ml. There were 10 rats in each cage.

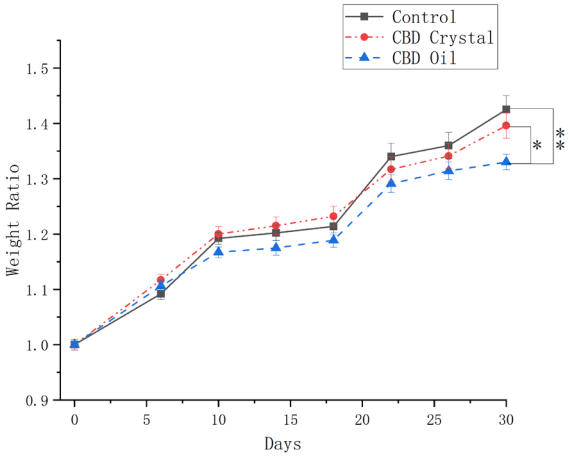

Figure 6. Change in the weight ratio of daily weight to original weight of rats for a month. The impurities in the CBD product had an effect on the weight of the rats. The weight of the rats was measured, and the weight ratio of daily weight to original weight of each group is shown on the Y-axis. The number of days from the beginning of feeding is indicated on the X-axis. At the start of the experiment, the weight ratios showed no significant difference among the groups. At the end of the experiment, after three weeks of the intragastric administration, the mean weight ratio of the control and the CBD crystal groups was significantly greater than that of the CBD oil group. However, the weight ratio of the control group showed no significant difference with that of the CBD crystal group throughout the experiment. Data are given as mean ratio, and error bars represent standard error of the mean ratio ($n = 10$). * indicates $p < 0.05$, ** indicates $p < 0.01$. There is no significant difference between the points without asterisks plotted for the same day.

studies have reported that CBD showed an antidepressant-like property, as acute CBD administration (30 mg/kg body weight) significantly reduced the immobility time compared to the vehicle group, without changing locomotor activity in the open field test or altering hippocampal BDNF levels (9-10). Even though there are some minor differences in methodology, such as total swimming period, it is unlikely that the difference in results between acute and chronic administration of CBD could be explained by these factors. The treatment time period of our study is very short, so future studies could treat normal healthy rats for longer periods of time and examine more behavioral and physical indicators of depression-like symptoms.

Only a few long-term studies conducted using depressive rat models showed that CBD has an antidepressant-like property. Campos *et al*. claimed that CBD administration (30 mg/kg of body weight) for 14 days prevented the anxiogenic-like effect of chronic unpredictable stress (CUS) in wild type mice in the novelty suppressed feeding test and elevated plus maze (21). Linge *et al*. reported that chronic CBD treatment provided both fast-acting and sustained antidepressant-like effects for an olfactory bulbectomy mouse model of depression (OBX) in open field and sucrose preference tests (16). That these two studies present results that are different from our study's findings may be related to animal species, behavior tests, or the health conditions of animal models. Both of the chronic tests used animal models, CUS and OBX, which displayed depressive behaviors before the CBD treatment, while our long-term experiment used healthy rats as subjects.

Similar to our findings, another study using normal healthy Lister-hooded rats showed that chronic administration of CBD produced an anxiogenic-like effect (22). The results of that study further showed that chronic administration of CBD significantly decreased BDNF expression in the hippocampus and frontal cortex (22). The neurotrophic hypothesis of depression suggests that BDNF is reduced in depression and increased after antidepressant treatments. The decrease in BDNF level could represent depression in rats. These results suggest that chronic administration of CBD has the potential of eliciting depressive-like behaviors in healthy rats, but this speculation needs to be thoroughly tested in the future.

Other ingredients in CBD oil affected the weight gain of the rats. At the end of the experiments, there were apparent differences between the mean weight ratio of the oil group and those of the control group and the CBD crystal group (p = 0.0039 and p = 0.03, respectively) (**Figure 6**). The presence of other cannabinoids in the CBD oil could be the cause for the slow weight gain rate. This suggests that the effect of CBD purity on human health should also be taken into account in licensing for market sales (12-13, 23).

Many researchers have already studied the effects of CBD on the human body. For healthy people, some studies used the dose of 10 mg/day or 3 mg/kg body weight, which is a much smaller dose than the dose in this study (24-25). For patients with psychotic symptoms, the therapeutic doses were 600-1500 mg/day (26-29). This higher therapeutic dose is more comparable to the dose of 30 mg/kg used in this study. Although a lower dose maybe yields less distinct behavioral effects, but the effect of a long-time administration should be further studied. Therefore, additional long-term multi-dose studies are needed to determine the optimal dose for healthy individuals.

For humans, acute and chronic CBD administrations may have different effects. The mechanism of action underlying the effects of CBD seems to be complex. However, chronic CBD studies on humans are still scarce. Our study provides evidence for the possibility that CBD could elicit depression when consumed by normal people for a long period. Our experiments also highlight the need for carefully monitoring CBD dose and its effects when used in health care and medicine.

METHODS

CBD preparation

In this study, crude hemp oil (supplied by Beijing Beihua Engineering Co., China) was used as the raw material. Using an operating temperature of around 110°C and an operating pressure (absolute) of approximately 40 Pa, the crude oil went through the first distillation step to remove the volatile components, comprising about 15-20% of the total weight. The residue from the first distillation went through a second distillation at the operating temperature of approximately 160°C and operating pressure of approximately 5Pa. The distillate was the middle product, which was called CBD oil. In order to obtain a CBD product of higher purity, the CBD oil was further crystallized. First, CBD oil was heated to approximately 60°C. As the CBD oil cooled down slowly, the CBD started to crystallize out. Under the final temperature of around 5°C for several days, CBD crystals could be obtained after filtering, washing, and drying. The composition of the CBD oil and the CBD crystals were determined by high performance liquid chromatography with C18 column (Shimadzu, Japan).

Animals

Male Wistar rats weighing 270-300 g were used as the experimental subjects. Thirty male Wistar rats (between six and eight weeks old) were purchased from the Medical Discovery Leader Company (Beijing, China). Rats were housed in stainless steel cages (535x390x200 mm), with ten rats per cage under a 12h-12h dark, light cycle (dawn at 7 am). Humidity maintained between 20% and 40%, and room temperature was between 20–23°C (30). Food and water was provided ad libitum. Rats were allowed to acclimate to the living environment for nine days prior to the beginning of the test. Rats were weighed on the first day and the seventh day after purchase, and then they were weighed every four days.

CBD administration

Thirty mg/kg of purified CBD crystals or CBD oil dissolved

in peanut oil (vehicle) as a dose (8). CBD crystals, CBD oil, and vehicle solution were prepared immediately before use. The solution was prepared together for thirty rats at a ratio 3:1 (mg solute / mL vehicle). Thirty Wistar male rats were randomly separated into three groups (10 rats per group). The three groups were fed with CBD crystal solution, CBD oil solution, or only peanut oil (vehicle), through intragastric administration using a 10 mL syringe (Jiangsu Zhiyu Medical Equipment Co. Ltd.) and a 10 cm gavage needle (HL-GWQ-16, Beijing Heli Science and Technology Development Co. Ltd.). The rats consumed these solutions at about 10 o'clock every morning once a day for 21 days. The volume of the solution which a rat consumed was calculated according to the weight of the rat.

Forced swimming test

The forced swimming test began the day after the rats had finished their 21 days of intragastric gavage, between 10 am and 3 pm in an experimental room. Rats were placed in a cylinder (45 x 20 x 30 cm) and water at a temperature of 24°C ± 2°C was added. The water was so deep that the rat could not reach the bottom with its feet or tail. The rat was immersed in the cylinder for six minutes. The total immobility time was measured based on how long it took the rat to stay afloat without a struggle and keep its head above water using only a minimum amount of movement (31). The test also monitored the active period before showing immobility, the amount of time between when the rat was first placed into the cylinder and when despair-like behaviors started. Swimming was a non-stationary activity and the swimming time was calculated by subtracting the total immobility time from the total test period. At the beginning of each trail, rats were initially placed in the same position to avoid environmental effects. When the experiment was over, the animal was dried with a towel. Between test animals, cylinders were cleaned and water was replaced to prevent the effects of water pollution (21)

The whole experiment was recorded by a video analysis system (Model number: ZS-001, Beijing Zhongshi Dichuang Technology Development Co., Ltd.). This avoided the subjective error and interference to experimental rodents by manual observation. Thus, the objectivity and reliability of the experimental results could be ensured. It could display indicators in various ways: exporting a trajectory diagram, trajectory coordinates, and average swimming speed. The behavior of the rats was recorded during the experiment and the experimenter could play back the recording for manual calibration. The active period before showing immobility, the immobility period, and the swimming distance were recorded. Swimming speed was calculated by dividing the distance by the swimming time.

Sucrose preference test

The sucrose preference test began one day after the forced swimming test's last day. Sucrose water was prepared by dissolving sucrose in pure water to form a 1% weight/volume sucrose solution. Forty-eight hours before the actual experiment, the mice were given adaptive training, which reduced their anxiety about the sucrose solution (18). Rats in the same treatment group were placed in the same cage (10 in each cage) to adapt to the SPT condition by placing sucrose and water bottles in the cages at the same time. Water or food was still available during the adaptive training and the actual experimental period. On the test day, each group was given two identical 500 mL bottles: one contained sucrose solution (1%) and one contained drinking water. Over the next 24 hours, the animals were given the opportunity to drink at their will (18). To minimize the influence of water bottles' positions, the positions of the two bottles were turned every 8 hours. The volumes of the sucrose solution, drinking water, and total liquid consumption were recorded before and after the experiment. The ratio of sucrose solution intake to total liquid intake is defined as the sucrose preference. The following formula was used to determine sucrose preference: sucrose preference = sucrose solution intake / (sucrose solution intake + water intake) × 100%.

Statistical analysis

For statistical analysis, the mean and standard deviation of the data was calculated. The sample fulfilled the following criteria: first, the sample was randomly selected from the population and randomly assigned to three different groups; second, although the sample did not reach the standard threshold (sample size ≥ 30), there were no major outliers or skewness in the three groups. Thus, the distribution of the sample could be assumed as approximately normal distribution. The data of the forced swimming test and the data of the weight ratios for the three groups were analyzed using one-way ANOVA. If the calculated *p*-value was less than 0.05, the difference was considered statistically significant between the two groups.

Received: August 4, 2020
Accepted: December 12, 2020
Published: December 18, 2020

REFERENCES

1. Ross, Hamish Redmond, *et al.* "Inhibition of Recombinant Human T-Type Calcium Channels by Δ9-Tetrahydrocannabinol and Cannabidiol." *Journal of Biological Chemistry*, vol. 283, no. 23, 2008, pp. 16124–16134.
2. Pertwee, R.G., Ross, R.A. Cannabinoid receptors and their endogenous ligands. *Prostaglandins, Leukot. Essent. Fat. Acids,* vol. 66, 2002, pp. 101–121.
3. Boggs, Douglas L, *et al.* "Clinical and Preclinical Evidence for Functional Interactions of Cannabidiol and Δ9-Tetrahydrocannabinol." *Neuropsychopharmacology*, vol. 43, no. 1, 2017, pp. 142–154.
4. Mandolini, G. M., *et al.* "Pharmacological Properties of

Cannabidiol in the Treatment of Psychiatric Disorders: A Critical Overview." *Epidemiology and Psychiatric Sciences*, vol. 27, no. 4, 2018, pp. 327–335.
5. Stith, Sarah S., *et al.* "The Association between Cannabis Product Characteristics and Symptom Relief." *Scientific Reports*, vol. 9, no. 1, 2019.
6. Sales, A.J., *et al*. Antidepressant-like effect induced by Cannabidiol is dependent on brain serotonin levels. *Prog. Neuro-Psychopharmacol. Biol. Psychiatry* 86, 2018, pp. 255–261.
7. Morgan, Celia J. A., et al. "Impact of Cannabidiol on the Acute Memory and Psychotomimetic Effects of Smoked Cannabis: Naturalistic Study." *British Journal of Psychiatry*, vol. 197, no. 4, 2010, pp. 285–290.
8. Silote, Gabriela Pandini, *et al.* "Emerging Evidence for the Antidepressant Effect of Cannabidiol and the Underlying Molecular Mechanisms." *Journal of Chemical Neuroanatomy*, vol. 98, 2019, pp. 104–116.
9. Zanelati TV, *et al.* Antidepressant-like effects of cannabidiol in mice: possible involvement of 5-HT1A receptors. *Br J Pharmacol* vol. 159, no. 1, 2010, pp. 122–128.
10. Sartim, A.G., *et al*. "Antidepressant-like Effect of Cannabidiol Injection into the Ventral Medial Prefrontal Cortex—Possible Involvement of 5-HT1A and CB1 Receptors." *Behavioural Brain Research*, vol. 303, 2016, pp. 218–227.
11. Mead, Alice. "The Legal Status of Cannabis (Marijuana) and Cannabidiol (CBD) under U.S. Law." *Epilepsy & Behavior*, vol. 70, 2017, pp. 288–291.
12. Lauren Singer et al. "The cannabidiol conundrum: Potential benefits and risks of cannabidiol products for children." Curr Opin Pediatr, vol. 32, no. 1, 2019.
13. Dirk W. Lachenmeier, Stephan G. Walch. Cannabidiol (CBD): "a strong plea for mandatory pre-marketing approval of food supplements." Journal of Consumer Protection and Food Safety (2020) 15:97–98
14. Johnston LD, *et al.*, Monitoring the Future National Results on Drug Use: 2012 Overview, Key Findings on Adolescent Drug Use. *Ann Arbor: Institute for Social Research, The University of Michigan;* 2013.
15. Zsolt Gáll *et al*. "Effects of Chronic Cannabidiol Treatment in the Rat Chronic Unpredictable Mild Stress Model of Depression." Biomolecules 2020, 10, 801.
16. Linge, R., *et al.* Cannabidiol induces rapid-acting antidepressant-like effects and enhances cortical 5-HT/glutamate neurotransmission: role of 5-HT1A receptors. Neuropharmacology vol. 103, 2016, pp. 16–26.
17. Carter, M and Shieh, JC. *Guide to Research Techniques in Neuroscience.* Academic Press, 2015.
18. Liu, Meng-Ying, *et al.*, "Sucrose Preference Test for Measurement of Stress-Induced Anhedonia in Mice." *Nature Protocols*, vol. 13, no. 7, 1 2018, pp. 1686–1698.
19. Seong, Eunju, *et al.* "Mouse Models for Psychiatric Disorders." *Trends in Genetics*, vol. 18, no. 12, 2002, pp. 643–650.
20. Monti, Jaime M. "Hypnotic like Effects of Cannabidiol in the Rat." *Psychopharmacology*, vol. 55, no. 3, 1977, pp. 263–265.
21. Campos, A.C., *et al.*, 2013. The anxiolytic effect of cannabidiol on chronically stressed mice depends on hippocampal neurogenesis: involvement of the endocannabinoid system. *Int. J. Neuropsychopharmacol.* vol. 16, 2013, pp. 1407–1419.
22. ElBatsh, Maha M., *et al*. "Anxiogenic-like Effects of Chronic Cannabidiol Administration in Rats." *Psychopharmacology*, vol. 221, no. 2, 2011, pp. 239–247.
23. Busse F, Omidi L, Leichtle A, *et al*. "Lead poisoning due to adulterated marijuana." N Engl J Med 2008; 358:1641–1642.
24. Mincis M, *et al*. Chronic administration of cannabidiol in man. Pilot study. *AMB Rev Assoc Med Bras* vol. 19, no. 5, 1973, pp. 185-90.
25. Cunha JM, *et al*. Chronic administration of cannabidiol to healthy volunteers and epileptic patients. *Pharmacology* vol. 21, 1980, pp. 175-85.
26. Zuardi AW, *et al.*, Antipsychotic effect of cannabidiol. *J Clin Psychiatry* vol. 56, no. 10,1995, pp. 485-6.
27. Zuardi AW, *et al.*, Cannabidiol monotherapy for treatment-resistant schizophrenia. *J Psychopharmacol.* vol. 20, no. 5 2006, pp. 683-6.
28. Zuardi AW, *et al.*, Cannabidiol was ineffective for manic episode of bipolar affective disorder. *J Psychopharmacol,* vol. 24, no. 1, 2010, pp. 135-7.
29. Leweke FM, *et al.*, Cannabidiol as an antipsychotic. A double-blind, controlled clinical trial on cannabidiol vs amisulpride in acute schizophrenia. *Eur Psychiatry*, vol. 22, 2007.
30. Comelli F, *et al.*, Antihyperalgesic effect of a Cannabis sativa extract in a rat model of neuropathic pain: mechanisms involved. *Phytother. Res.* vol. 22, no. 8, 2008; pp. 1017-24.
31. Shbiro, Liat, *et al*. "Effects of Cannabidiol in Males and Females in Two Different Rat Models of Depression." *Physiology & Behavior*, vol. 201, 2019, pp. 59–63.

JOURNAL OF
EMERGING INVESTIGATORS

Article

Caffeine: Does Drinking Coffee Alter Performance and RPE Levels of a Teenage Athlete in both Aerobic and Anaerobic Exercises?

Srinidhi Gopalan[1] and Jaysree Gopalan[1]
[1]South Brunswick High School, Dayton, New Jersey

SUMMARY

The purpose of the study is to determine if ingesting caffeine in the form of coffee prior to workouts can enhance performance and alter Borg Rating of Perceived Exertion (RPE) of teenage athletes for both endurance (aerobic) and strength (anaerobic) exercises. Our hypotheses are that caffeine lowers RPE for both endurance and strength exercises and that it enhances performance in endurance, but not strength, exercises.To answer this question, we analyzed a 16-year-old high school athlete (myself) for a total of 12 days: 3 days consuming a cup of coffee prior to running, 3 days consuming a cup of coffee 1 hour prior to performing strength exercises, and 3 days without consuming a cup of coffee prior to exercise for each exercise type. For the endurance test, the athlete ran two miles as fast as they could. Average heart rate and total time of the run were analyzed for three days with coffee and three days without, as well as RPE levels. For the strength test, the athlete performed as many push-ups as possible in a one-minute time frame. The results showed that caffeine ingestion prior to exercise enhanced endurance, but had no impact on strength. Additionally, though RPE was lower for the endurance test, RPE remained unchanged for the strength test. Thus, the effect of drinking coffee in aerobic and anaerobic exercises were evaluated through several measures in this study, providing support that caffeine has an effect on aerobic exercises as opposed to anaerobic exercises.

INTRODUCTION

Caffeine, a substance commonly found in coffee, sports drinks, soft beverages, and energy supplements, is a stimulant. This is the world's most consumed psychoactive drug and it is legal for consumption. Caffeine stimulates the central nervous system as it is a part of the methylxanthine class (2). Many athletes consume cups of coffee prior to workouts, races, or games. Recent research has shown that caffeine can compete with adenosine for adenosine receptors in the brain to specifically affect endurance performance. Due to this mechanism, caffeine can modulate perceived exertion, pain, and other levels of vigor and exhaustion. Additionally, caffeine may have a greater impact on endurance, as caffeine may have more significant neural effects than muscular effects due to the ability to cross nerve cell membranes (4). Studies have supported an increase in endurance performances with caffeine as there is an increase in secretion of β-endorphins after caffeine consumption (4). For example, research has shown that in two groups of cyclists, the one that ingested caffeine had an increase in plasma β-endorphins during a two-hour period of cycling as opposed to the placebo group. An increase in these endorphins is highly significant in that it leads to a decrease in pain perception, thus being a vital force in improving endurance(5). Studies have shown that caffeine improves performance in endurance exercises since a majority of the energy is produced through aerobic pathways. Conversely, in short-term exercise at a high intensity, energy is produced through anaerobic pathways. After about three minutes of exercise, most energy is produced through aerobic pathways, and thus, becomes classified as endurance exercise. When energy is produced through aerobic pathways, for example, during the runs, it is independent of exercise mode. Aerobic performance is most likely enhanced far more than anaerobic performance as studies have noted, through increased fat oxidation and muscle glycogen sparing. Additionally, as previously mentioned by other studies, central nervous system stimulation through adenosine antagonism is also a mechanism for enhanced aerobic performance (6–8). Although studies involving caffeine have been performed, these studies were done on adults and athletes who were professionally trained. There are few studies done on teenagers, specifically, the teenage athlete.

RPE is the Borg Rating of Perceived Exertion and a way of measuring physical activity intensity level. RPE is primarily based on how the individual feels during the exercise, through analysis of heart rate, breathing, perspiration, and muscle fatigue. The scale goes from a 6 with no exertion at all, to 20, being maximum exertion. Furthermore, by using RPE levels, one's heart rate during the exercise can be estimated by multiplying the level by ten (3). Research about caffeine's competition with adenosine was done to see if RPE levels decreased only in aerobic activities. The antagonism at the adenosine receptors leads to several mechanisms which are crucial in caffeine's more significant effect on aerobic exercise. Caffeine increases energy metabolism throughout the brain and activates noradrenaline neurons, affecting the local release of dopamine. This release of dopamine increases adrenaline, leading to an overall better mood and increased energy (11).

In this study, the effects of caffeine on teenage athletic performance and RPE were investigated. We hypothesized that caffeine would lower RPE for both endurance and strength exercises. We also hypothesized that caffeine would enhance performance in endurance exercise but not strength

Variables Analyzed	Measurements
Endurance HR with Caffeine	144 bpm
Endurance HR without Caffeine	147 bpm
Strength HR without caffeine	106 bpm
Strength HR with caffeine	106 bpm
Number of Push-ups performed with Caffeine	13
Number of Push-ups performed without Caffeine	14
Total Time With Caffeine	12.27 minutes (12:16)
Total Time Without Caffeine	12.80 minutes (12:48)
Strength RPE Without Caffeine	12
Strength RPE With Caffeine	12
Endurance RPE With Caffeine	13
Endurance RPE Without Caffeine	17

Table 1. Average values for each variable measured during experimentation. (*Right*) List of conditions measured in each experiment. (*Left*) Average values for each condition (3 trials). The variables included heart rate during the endurance and strength exercises, RPE levels for strength and endurance exercises, and the performance being analyzed (total time and number of push-ups). Each variable was analyzed with and without caffeine consumption and the averages of all data analyzed show the general differences with and without caffeine intake.

Percent Decrease	Measurements-Aerobic Test Only
4%	Total Time
16%	HR
23.5%	RPE Levels

Table 2. Percent decrease for each variable significantly affected by caffeine consumption. (*Right*) Percent decrease of the conditions that were measured and affected by caffeine intake (endurance test only). (*Left*) List of the conditions analyzed. The variables include the aerobic test only-- heart rate, RPE levels, and performance being analyzed (total time). This indicates by what percent each variable was affected by caffeine consumption in the endurance test only.

exercises. To test the hypotheses, a teenage athlete (myself) was analyzed for a total of 12 days. During the first three days, aerobic endurance exercise (2-mile run) was performed one hour after caffeine consumption. The next three days consisted of strength exercises performed one hour after caffeine consumption.

A week later, the same exercises were performed in the three-day periods, except no coffee/caffeine drinks were consumed an hour before, only water. The teenage athlete in this study trains 15 hours a week, and is more physically fit than most teenagers, however, not to the level of a professional athlete. This study analyzed a teenage athlete to see if the similar benefits of a professional athlete or adult can be reciprocated in both endurance and strength fields

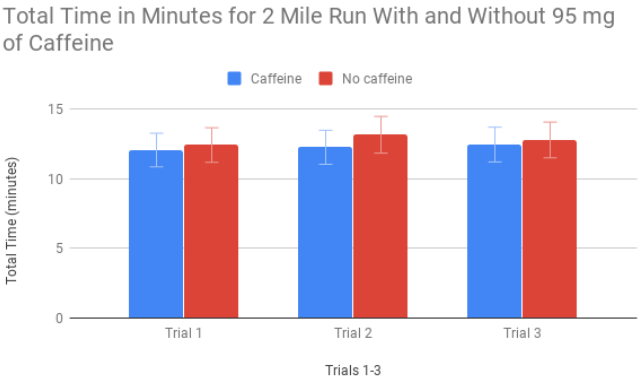

Figure 1. Lower total run time in the presence of caffeine. The total run time in the presence (blue) or absence (red) of 95 mg of caffeine was measured after a 2-mile run (*n*=3)

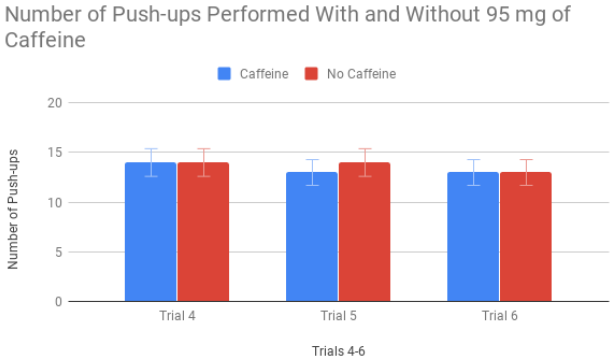

Figure 2. No observable differences in number of push-ups performed in the presence or absence of caffeine . The number of push-ups performed in the presence (blue) or absence(red) of 95 mg of caffeine was measured in one minute (*n*=3)

despite being younger and not as highly trained. Additionally, few studies have been done on caffeine's impact on strength exercises. The exercises performed in this experiment vary from traditional ones, as the athlete is not running to "exhaustion" as other studies have done and the athlete is performing push-ups as a form of anaerobic activity, not lifting weights (9–10). By running to exhaustion, it would be difficult to gauge caffeine's effect clearly as there is no clear data for comparison. By performing a timed trial, data is more effective to compare. Finally, we directly compared and contrasted both aerobic and anaerobic activity's changes after caffeine consumption which has a lack of evidence. Little research has been done analyzing a single trained teenage athlete for a long period of time, 12 days in this case, and this study seeks to see if by performing this experiment for a longer duration, caffeine's effect may change. Previous research led us to hypothesize that there could be lower RPE levels in both strength and endurance training, however, no performance advantage in strength workouts. The findings supported the hypothesis that caffeine enhanced aerobic performance and lowered aerobic RPE levels. The findings also supported the hypothesis that caffeine did not enhance anaerobic performance. However, the findings did not support the hypothesis that RPE levels were lowered in anaerobic

Variables Analyzed	Standard Deviation
Endurance HR with Caffeine	5.86 bpm
Endurance HR Without Caffeine	3.06 bpm
Strength HR With Caffeine	5.69 bpm
Strength HR Without Caffeine	3.21bpm
Number of Push-ups Performed With Caffeine	0.56 push-ups
Number of Push-ups Performed Without Caffeine	0.58 push-ups
Total Time With Caffeine	0.20 minutes
Total Time Without Caffeine	.37 minutes
Strength RPE With Caffeine	0.00
Strength RPE Without Caffeine	0.00
Endurance RPE With Caffeine	.58
Endurance RPE Without Caffeine	1.00

Table 3. Standard Deviations for each variable measured during experimentation. (*Right*) List of conditions measured in each experiment. (*Left*) standard deviations for each condition (3 trials). Each variable was analyzed with and without caffeine consumption and the standard deviations of all data analyzed show general differences in the data spread with and without caffeine intake.

Variables Analyzed	Coefficient of Variation
Endurance HR with Caffeine	0.04
Endurance HR Without Caffeine	0.02
Strength HR With Caffeine	0.05
Strength HR Without Caffeine	0.03
Number of Push-ups Performed With Caffeine	0.04
Number of Push-ups Performed Without Caffeine	0.04
Total Time With Caffeine	0.02
Total Time Without Caffeine	0.03
Strength RPE With Caffeine	0.00
Strength RPE Without Caffeine	0.00
Endurance RPE With Caffeine	0.04
Endurance RPE Without Caffeine	0.06

Table 4. Coefficient of variation for each variable measured during experimentation. (*Right*) List of conditions measured in each experiment. (*Left*) coefficient of variations for each condition (3 trials). Each variable was analyzed with and without caffeine consumption and the coefficient of variations of all data analyzed show general differences in the data spread with and without caffeine intake.

exercises. There could be broader implications that caffeine may be more beneficial to an endurance athlete as opposed to a strength athlete based on the evidence of this study only,

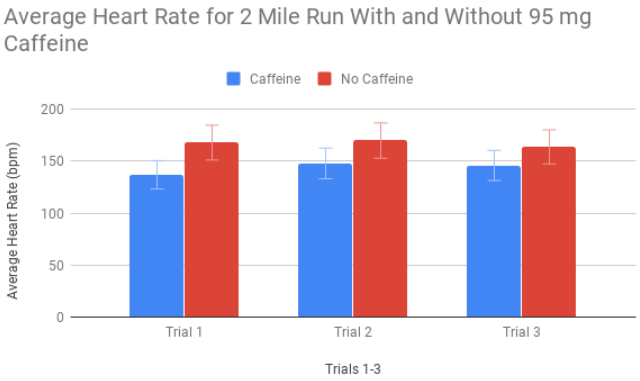

Figure 3. Lower average heart rate for 2-mile run in the presence of caffeine in the presence of caffeine. The average heart rate for the 2-mile run in the presence (blue) or absence (red) of 95 mg of caffeine was measured (*n*=3)

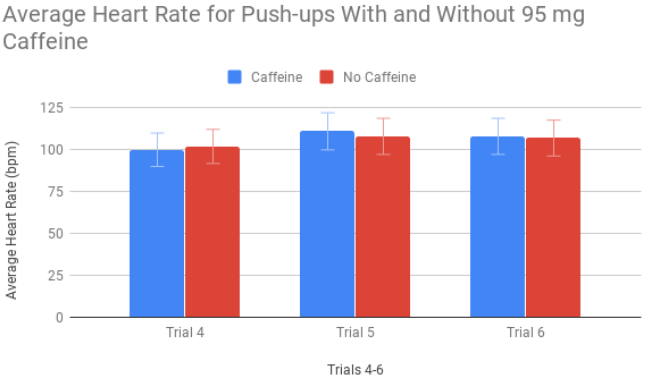

Figure 4. No observable differences in the average heart rate in presence or absence of caffeine for push-ups. The average heart rate in the presence (blue) or absence (red) of 95 mg of caffeine was measured during the push-ups performed in one minute (*n*=3).

but much further research needs to be done.

RESULTS

This experiment examines the effect of caffeine in performance enhancing and RPE levels for both aerobic and anaerobic exercises for the teenage athlete First, to investigate the effects of caffeine on the athlete's performance during aerobic exercise, the athlete performed a 2-mile run 1 hour after caffeine (95 mg) or water consumption. In three separate trials, performance was measured, in total time in minutes of the run. After caffeine consumption, the athlete's total run time was 4% lower on days. (**Table 2**, **Figure 1**). Conversely, caffeine had no observable effects on the athlete's performance in an anaerobic test – performing as many push-ups as possible in a minute (**Table 1**, **Figure 2**).

The effects of caffeine on average heart rate during aerobic exercises and anaerobic exercises were also investigated in the same experiments. In three separate trials, average heart rate was measured during a 2-mile run. After caffeine consumption, the athlete's average heart rate was 16% lower (**Table 2**, **Figure 3**). Meanwhile, caffeine had no observable effects on the athlete's average heart rate when performing

push-ups (**Table 1**, **Figure 4**).

To investigate the effects of caffeine on average RPE levels during aerobic exercise, the athlete performed a 2-mile run 1 hour after caffeine (95 mg) or water consumption. In three separate trials, RPE levels were recorded during the 2-mile run. We observed that the RPE levels were 23.5% lower on average after caffeine consumption (**Table 2**, **Figure 5**). Again, caffeine had no observable effects on the athlete's RPE levels when performing push-ups (**Table 1**, **Figure 6**).

Lastly, for all of the variables analyzed, the standard deviations show a lack of a large spread in data (**Table 3**). The results varied little, especially shown through the coefficients of variation, which were all low – under 0.1 – for all data collected (**Table 4**).

DISCUSSION

The 12 days of the experiment – 3 days of running with caffeine, 3 days of running without caffeine, 3 days of push-ups with caffeine, 3 days of push-ups without caffeine – supported evidence that caffeine had a greater impact on endurance exercises than on strength exercises. The results support the hypothesis stating that caffeine would lower RPE, heart rate, and increase performance for endurance exercises Additionally, the hypothesis that caffeine would not enhance performance for the strength exercises was also supported. However, the hypothesis that caffeine would lower RPE levels and heart rate for the push-up test was not supported by the study. This is perhaps because caffeine's competition with adenosine receptors is most directly associated with aerobic activity. The increase in adrenaline created a decrease in RPE levels as the athlete felt as if they had more energy during the run.

Moreover, the accuracy of using the Borg Rating of Perceived Exertion seems to be fairly accurate as based on the rating, one can multiply the levels by 10 to estimate average heart rate during the period. Obviously, these are just estimations, not extremely accurate representations. However, these estimations seem to coincide with the data and rating the athlete gave themselves in this experiment. For example, the rating of 13 during the running portion with caffeine should lead to a heart rate of 130. This is comparable to a heartrate of 144 bpm. The rating of 17 given on the day of running with caffeine should lead to an estimated heart rate of 170 bpm. This is again comparable to a heartrate of 167 bpm. Thus, the RPE is a reliable indicator of exertion levels.

There are several limitations in this experiment. Firstly, this experiment analyzed one highly trained high school athlete over the course of 12 days. Perhaps if multiple athletes, such as 10 or more, were analyzed, there would be a much wider and varying set of results. People might have differing responses to caffeine, especially in teens, so these results cannot be a standard for every person. Additionally, coffee was used as the source of caffeine here. The coffee also had full fat milk and sugar in it, so it was not drunk as black coffee. The milk and sugar could also play into the factors

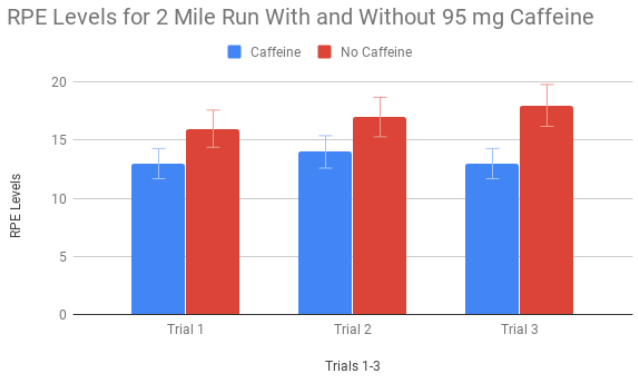

Figure 5. Lower RPE levels for a 2-mile run in the presence of caffeine. The RPE levels in the presence (blue) or absence(red) of 95 mg of caffeine was measured during the 2-mile run (*n*=3).

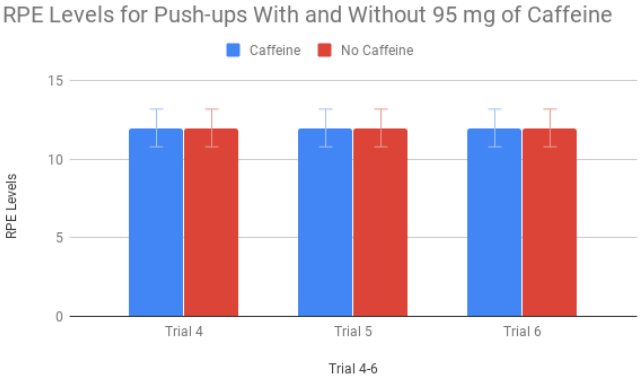

Figure 6. No observable differences in RPE levels for push-ups exercises in the presence of caffeine. The RPE levels in the presence (blue) or absence(red) of 95 mg of caffeine was measured during the push-ups performed in one minute (*n*=3).

analyzed for this athlete, so it is a limitation as it is unclear if the milk and sugar could have enhanced performance along with the caffeine as well. Perhaps caffeine pills or other gels may have different results, but for the sake of this experiment being performed on a teenager and not an adult, coffee was resorted to for safety.

Another note is that this experiment could have an element of bias to it. The experiment has no placebo and the athlete was not blinded, so they knew that they were ingesting caffeine prior to the runs. Perhaps, the athlete would have expected to feel energized, affecting the results, especially in a subjective indicator like RPE levels. As a follow-up to this study, it would be effective to use a decaf coffee in a blinded experiment to compare this with the effect of a caffeinated coffee which tastes the same. This way, there could be a greater elimination of bias that could alter perception of effort, and to see if those results are similar to the ones found in this study. Additionally, as a follow-up, it would be effective to perform this on a group of 10 people around the same age and same athletic capacity. It would be important to test people who are also runners/endurance athletes predominantly to see if the results are the same, and perhaps do another trial with those who are predominantly strength athletes, such as lifters, to see if the results are similar or different. By incorporating a

decaf coffee in a blinded experiment on the same three-day rotation along with a caffeinated coffee, the results may vary, and this could provide much larger implications than the ones studied here.

The order of the experiments could have affected the results as well, but not to a degree as great as the bias element. This is because the athlete was highly trained for years, and the athlete also received a week of complete rest and very easy running between the caffeine and no caffeine sessions. Within the three days of each trial, whether it be strength or endurance, and caffeine or non-caffeine, we observed no significant difference in exertion or difficult levels. Between the caffeine and non-caffeine experiments, we gave a week period of rest so that two continuous weeks of strenuous exercise would not lead to poor performance and skewed results. However, there is a chance that within the three-day periods, the athlete could have felt tired on the third day as opposed to the first, but in this case, we observed no significant difference.

Furthermore, as previous studies have only analyzed caffeine's effect for one or two days, this study analyzed caffeine for a longer period of time. However, the extent of caffeine's impact on aerobic and anaerobic activity did not lessen over the period, indicating that it could potentially be beneficial for an avid, daily, drinker. If this study were performed on someone who does not consider themselves an avid drinker, the results could be different. The effect of the caffeine could perhaps be more potent and lasting as his or her body may not be as accustomed to it, compared to the regular consumer. Another limitation of this study as it was not performed on more people is that each person may have differing reactions to caffeine, with it having a more potent effect on others, so these results can again not be generalized.

Finally, as this study observed an adolescent athlete, there could be differences compared to performing it on adults, as many previous studies have done. This is because adolescents may have a much stronger reaction to coffee or caffeinated substances compared to adults for reasons such as body weight, or that their bodies are still growing (12).There are growing concerns of caffeine overconsumption in teens, as many teens demand busy schedules with social life, school, and extracurriculars, losing sleep. These are indeed addictive substances, and overconsumption in a growing adolescent could lead to damage of their bodies and risks to their health (1). Based on the results in this study, the benefit caffeine seemed to provide may lead to an excuse for overconsumption of teenage athletes; however, since this is just a case of only one athlete, it does not mean the effects are generalizable, but this should be a concern as teenagers could potentially abuse anything that can enhance their performances. As many studies perform studies using caffeine pills or gels, this study used a common household item – coffee. Thus, this study supports evidence that a common household item can have profound effects on an endurance athlete's performance. Thus, the experiment's results are consistent with data from various studies, however, they cannot be the same case for all teenage athletes.

METHODS

The order of the four three-day periods of testing were as follows: three days of running after drinking coffee, three days of strength exercises after drinking coffee, three days of running without coffee and three days of strength exercises without coffee. The experiments performed without coffee happened a week after the experiments that happened with coffee. This was done so that the athlete could have time to recover and reset, so that they would not feel tired or sore, which could affect the results. For the endurance portion of the experiment, the athlete used a Garmin Forerunner 35 watch to monitor heart rate, pace, and distance of runs.

Additionally, the athlete also consumed 95 mg of brewed coffee with 2 tablespoons of full fat milk and 2 teaspoons of sugar exactly 1 hour prior to running. On days when no caffeine was consumed, the athlete consumed no drink besides water 1 hour prior to the run. The time of running was always at the same time each day. The athlete ran at eight in the morning and coffee was consumed at seven in the morning. Similar weather conditions were also picked each day, with close humidity levels and temperatures. This way, the athlete could not feel more tired on a particular day due to higher temperatures or humidity. The athlete ran 2 miles at a tempo pace, or 70% of VO2 max. Thus, the pace should have been in the 6:15-6:25 range ideally for this particular athlete. The pace and average heart rate were recorded during the 2-mile distance.

For the strength portion, the athlete again consumed 95 mg of brewed coffee with 2 tablespoons of full fat milk and 2 teaspoons of sugar exactly 1 hour prior to performing the push-ups test. The athlete also did not consume any drink besides water 1 hour prior to the strength exercises on the days without caffeine. The athlete turned on the watches with a timer for a minute and performed as many pushups as possible during this time period. At the conclusion, heart rate was recorded as well as how many pushups they were able to perform consecutively. Finally, at the conclusion of each session, the athlete recorded their RPE level based on the scale and how they felt based on effort during the session. The Borg Scale used ranged from 6-20.

Received: July 19, 2020
Accepted: November 5, 2020
Published: December 20, 2020

REFERENCES

1. "Energy Drinks | NCCIH." https://www.nccih.nih.gov/health/energy-drinks. Accessed 11 Jul. 2020.
2. Sanchez, Juan M. "Methylxanthine Content in Commonly Consumed Foods in Spain and Determination of Its Intake during Consumption." Foods (Basel, Switzerland), MDPI, 4

Dec. 2017, www.ncbi.nlm.nih.gov/pmc/articles/PMC5742777/.
3. “Perceived Exertion (Borg Rating of Perceived Exertion Scale).” Centers for Disease Control and Prevention, *Centers for Disease Control and Prevention*, 10 Apr. 2020, www.cdc.gov/physicalactivity/basics/measuring/exertion.htm. Accessed June 20th, 2020.
4. Spriet LL. Caffeine and performance. *Int J of Sport Nutr.* 1995 5:S84–99
5.Laurent D, Schneider KE, Prusaczyk WK, Franklin C, Vogel SM, Krssak M, Petersen KF, Goforth HW, Shulman GI. Effects of caffeine on muscle glycogen utilization and the neuroendocrine axis during exercise. J *Clin Endocrinol Metab.* 2000;85:2170–75. doi: 10.1210/jc.85.6.2170.
6.Goldstein ER, Ziegenfuss T, Kalman D, et al. International society of sports nutrition position stand: caffeine and performance. *J Int Soc Sports Nutr.* 2010;7(1):5.
7. Keisler BD, Armsey TD., 2nd Caffeine as an ergogenic aid. *Cur Sports Med Rep*. 2006;5:215-219. [PubMed] [Google Scholar]
8. Paluska SA. Caffeine and exercise. *Cur Sports Med Rep.* 2003;2:213-219.
9. Pickering C., Kiely J. Are the current guidelines on caffeine use in sport optimal for everyone? Inter-individual variation in caffeine ergogenicity, and a move towards personalised sports nutrition. *Sports Med.* 2018;48:7–16. doi: 10.1007/s40279-017-0776-1.
10. Goldstein E.R., Ziegenfuss T., Kalman D., Kreider R., Campbell B., Wilborn C., Taylor L., Willoughby D., Stout J., Graves B.S., *et al.* International society of sports nutrition position stand: caffeine and performance. *J. Int. Soc. Sports Nutr.* 2010;7:5. doi: 10.1186/1550-2783-7-5.
11. Planning Committee for a Workshop on Potential Health Hazards Associatedwith Consumption of Caffeine in Food and Dietary Supplements. “Caffeine Effects on the Central Nervous System and Behavioral Effects Associated with Caffeine Consumption.” Caffeine in Food and Dietary Supplements: Examining Safety: Workshop Summary., *U.S. National Library of Medicine*, 23 Apr. 2014, www.ncbi.nlm.nih.gov/books/NBK202225/. Accessed June 13th, 2020
12. Joy, Kevin. "Parents, Perk Up to the Dangers of Caffeine for Teens". 31 May 2017, healthblog.uofmhealth.org/childrens-health/parents-perk-up-to-dangers-of-caffeine-for-teens.

JOURNAL OF
EMERGING INVESTIGATORS

Article

Spectroscopic Kinetic Monitoring and Molecular Dynamics Simulations of Biocatalytic Ester Hydrolysis in Non-Aqueous Solvent

Allen Chen[1], Ayeeshi Poosarla[1], Karankumar Mageswaran[1], Anushka Rajasekhar[2], Brian Fu[3], Andrew Liang[4], Kara Tran[5], Edward Njoo[6]

[1]Mission San Jose High School, Fremont, CA
[2]Amador Valley High School, Pleasanton, CA
[3]American High School, Fremont, CA
[4]The College Preparatory School, Oakland, CA
[5]Dublin High School, Dublin, CA
[6]Department of Chemistry, Biochemistry, & Physical Science, Aspiring Scholars Directed Research Program, Fremont, California

SUMMARY

The use of enzymes as catalysts is becoming an increasingly important tool in chemical synthesis, given the mild conditions and high chemoselectivity that can be achieved through enzyme-catalyzed reactions. However, a major limitation in the use of enzymatic biocatalysis is the degradation of enzyme structure and activity in non-aqueous media. Lipases are a subclass of esterases found in most, if not all, living organisms that break ester bonds in lipids. In this study, we explored the effects of various concentrations of non-aqueous organic solvents on pancreatic lipase activity and analyzed the relationships between different properties of solvents and the kinetics of enzymatic hydrolysis through spectroscopic monitoring of a synthetic colorimetric substrate, 4-nitrophenyl acetate. The influence of non-aqueous solvent environments on protein stability was further explored with molecular dynamics (MD) simulations on a 1 nanosecond timescale. Our results suggest a general trend of decreasing enzymatic activity with increasing concentrations of non-aqueous solvent; however, lipase activity in low concentrations of methanol, specifically 5% methanol, was 28% higher than lipase activity in water. Lipase activity in methanol also displayed the greatest rate of hydrolysis of the substrate compared to all other non-aqueous solvents. Interestingly, our MD simulations showed that the conformational state and stability of lipase in methanol is similar to that of the enzyme in water. Lipase activity works the best in 5% methanol which can be used in industry for chemical synthesis and enzyme-catalyzed reactions.

INTRODUCTION

Enzymatic biocatalysis has attracted important applications in chemical synthesis due to greater levels of chemoselectivity, increased atom economy, and reduced production of hazardous byproducts produced by common reagents that are found in common reagents in synthesis (1). In particular, biocatalytic cascades—combinations of

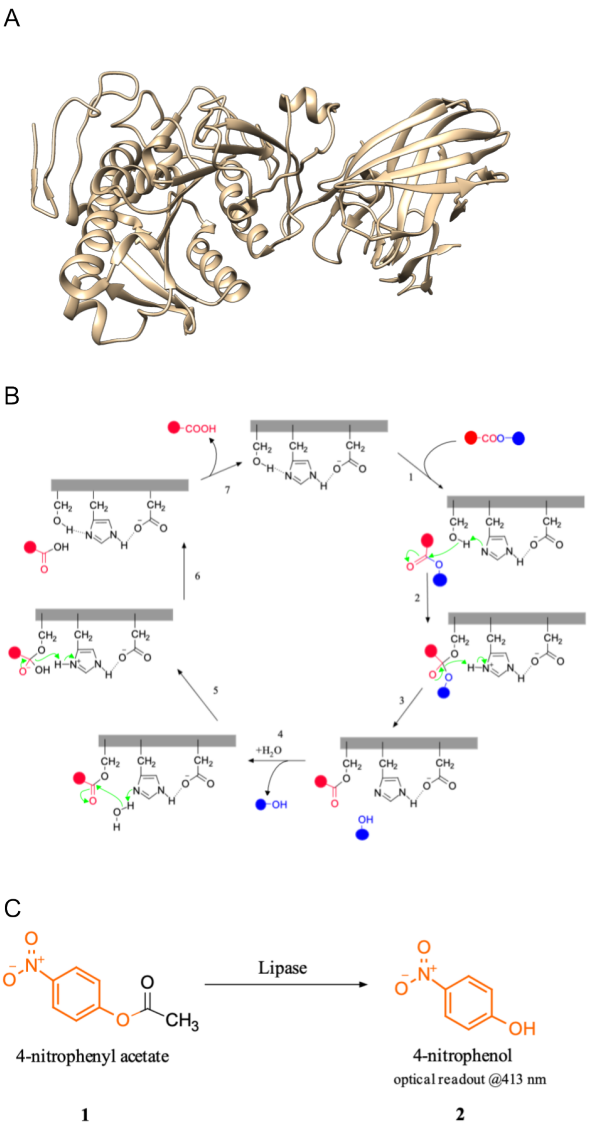

Figure 1. Structure and Mechanism of Lipase. (**A**) Crystal structure of a pancreatic lipase-colipase complex (PDB code: 1N8S). (**B**) Ser-His-Asp catalytic triad coordinated hydrolysis of an ester bond. In the mechanism, the serine nucleophile attacks the carbonyl

carbon of the ester, forming a tetrahedral intermediate, which collapses and releases the alcohol product. Then, a water molecule attacks the carbonyl carbon of the acyl-enzyme intermediate, forming another tetrahedral intermediate, which collapses and releases the carboxylic acid product. Thus, the ester bond has been broken, and the serine nucleophile is free to catalyze another reaction. (**C**) Lipase cleaves the ester bond in 4-nitrophenyl acetate, releasing 4-nitrophenol, which can be tracked spectroscopically at 413 nm. This allows for the quantification of lipase activity.

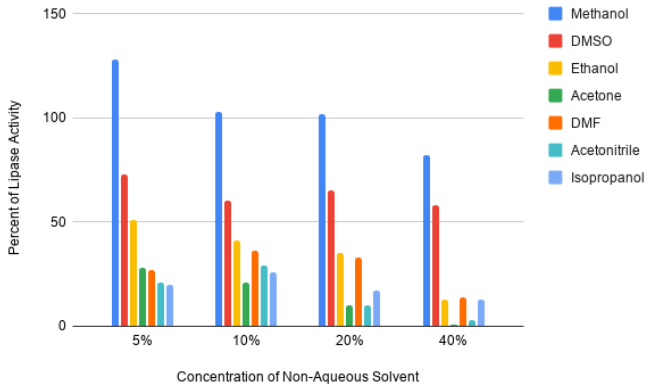

Figure 2. Lipase activity in various concentrations of non-aqueous solvents. Data normalized to percentage of lipase activity in water (100% lipase activity). All the concentrations were prepared in Tris buffer and only one trial was performed.

multiple enzymatic steps—shorten multi-step syntheses by eliminating intermediate steps and reduce hazardous waste (2). Engineered enzymatic biocatalysts have been recently reported in the chemical synthesis of Islatravir (2). *Candida antarctica* lipase B has been reported to catalyze alcoholysis, ammonolysis, and hydrolysis reactions in organic media (3). In addition, biocatalytic processes have been used for the synthesis of chiral intermediates of drugs such as Formoterol and Omapatrilat (4). Deacetylation of phenolic esters can be conducted under acidic or basic conditions, but the utilization of enzymatic catalysis allows the same reaction to be conducted under neutral pH conditions (5).

Lipases—a subclass of esterases—are enzymes that catalyze the hydrolysis of ester bonds in lipids (**Figure 1A**) (6). In addition, lipases have been previously reported to catalyze esterification, interesterification, and transesterification reactions in non-aqueous media (7). For this reason, lipases are used as industrial biocatalysts in the food, detergent, and pharmaceutical sectors, and they also have potential applications in the leather, textile, cosmetic, and paper industries. Given the potential utility of lipase biocatalysis, understanding the effect of different solvent systems on lipase activity is largely applicable.

The digestion of fats in the stomach is catalyzed by three enzymes, one of which being pregastric lipase which originates in the glossoepiglottic area. The active site of pre-gastric lipase consists of a serine nucleophile (Ser152), which is one of the three amino acid residues that make up the catalytic triad (**Figure 1B**), the other two being His263 and Asp176 (8). These residues form a charge-transfer relay network which serves to increase the nucleophilicity of Ser152. This allows the serine nucleophile to cleave an ester bond.

Understanding the effect that different solvents have on the retention of catalytic activity in enzymes is critical in informing the choice of reaction conditions for conducting biocatalytic chemical reactions. The effects of both aqueous and non-aqueous solvents on enzyme activity are well-documented. In aqueous solvents, which are more native to enzymatic processes, water acts as a nucleophile towards enzymes. For example, in serine peptidases, water resolves acyl-enzyme intermediates and reforms the catalytic triad (9). Non-aqueous solvents change the physical properties of the solution, such as dielectric charge, polarity, and hydrophobicity, which would, in turn, affect acyl-enzyme stability and the rate of enzymatic hydrolysis. The impacts of organic solvents on the catalytic activity of enzymes can be attributed to changes in reactive intermediates in the active site or alterations in the noncovalent interactions that define an enzyme's secondary and tertiary structure (10). Macromolecular stability, defined as little-to-no structural changes, can be studied using molecular dynamics—a biophysics tool used to link protein structure and its dynamics—which allows us to determine the stability of lipase in non-aqueous solvents (11, 12).

Over the past decades, numerous colorimetric methods have been used to probe enzymatic activity: peroxidase activity is measured by the reduction of diamines, protease activity is measured using nitroanilide substrates, and esterase activity is measured using nitrophenyl esters (13-15). 4-nitrophenyl acetate is a commonly used substrate to determine lipase activity (16). Enzymatic cleavage of the nitrophenyl ester bond by lipases releases nitrophenol, which can be tracked using UV-visible (UV-vis) spectroscopy, a technique measuring the amount of light that a substance absorbs at a specific wavelength, via absorbance at a wavelength of 413 nanometers (nm) (**Figure 1C**).

Here, we synthesized 4-nitrophenyl acetate from the acylation of 4-nitrophenol and utilize UV-vis spectroscopy to screen and quantify lipase activity in seven organic solvents using 4-nitrophenyl acetate as a colorimetric probe. We hypothesize that the greatest retention of enzymatic activity would be observed in solvent systems whose physical properties most closely mimic water and that higher concentrations of non-aqueous solvent will decrease enzymatic activity. The common organic solvents screened were chosen based on their miscibility with water: methanol, ethanol, isopropanol, acetonitrile, acetone, N,N-dimethylformamide (DMF), and dimethyl sulfoxide (DMSO). Lipase activity was monitored at 5%, 10%, 20%, and 40% concentrations of each organic solvent. While we determined that lipase activity decreased with increasing concentrations of organic solvent, as hypothesized, lipase maintained the highest rate of activity in 5% methanol, suggesting that out of all solvents tested, an aqueous methanol solvent system could be the most favorable in which to perform deacylation reactions involving lipase and organic compounds.

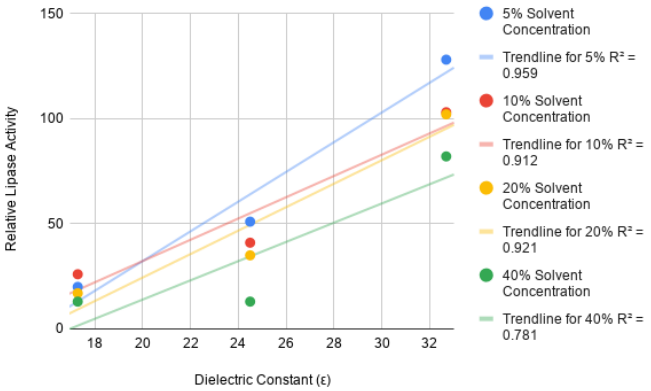

Figure 3. Alcohol polarity impact on lipase activity. Each line represents a different concentration of solvent (blue = 5%; red = 10%; yellow = 20%; green = 40%), and each alcohol is represented by its dielectric constant (ε 17.9 = isopropanol; ε 24.5 = ethanol; ε 32.7 = methanol).

RESULTS

UV-Vis data of several 4-nitrophenol solutions were used to define extinction coefficients, which allowed us to calculate the concentration of nitrophenol as a function of absorbance. In order to measure lipase activities, we measured the accumulation of 4-nitrophenol over time and compared results to those of aqueous lipase. Consistent with our hypothesis, relative lipase activity (compared to lipase activity in water) generally decreased in higher concentrations of organic solvent (**Figure 2**). This loss of enzymatic activity was most apparent in methanol, where an increase in methanol concentration from 5% to 40% caused a decrease of relative enzymatic activity by 46%.

Contrary to our initial expectations, lipase had higher relative levels of activity in lower concentrations of methanol than in water, with 128% lipase activity at 5% methanol, 103% lipase activity at 10% methanol, and 102% enzyme activity at 20% methanol. Lipase activity for all other organic solvents was lower than that of water at all concentrations. A solvent system of 40% acetone resulted in the largest decrease in lipase activity, with only 1% of lipase activity compared to lipase in water. Increasing concentrations of methanol also resulted in the largest decrease in relative lipase activity of 46% between 5% and 40% methanol. On the other hand, increasing concentrations of isopropanol resulted in the smallest decrease in relative lipase activity of 7% between 5% and 40% isopropanol.

We also observed that alcohol solvents (methanol, ethanol, and isopropanol) tend to follow a trend in which a decrease in polarity, or a decrease in the dielectric charge, corresponds to a decrease in lipase activity (**Figure 3**). Methanol, being the most polar of the solvents screened, displayed the highest relative lipase activity, followed by ethanol and isopropanol (least polar). Methanol is the most polar of the three and has properties most similar to water, such as similar dipole properties. Therefore, its dipole interactions with lipase most closely mimic those of water.

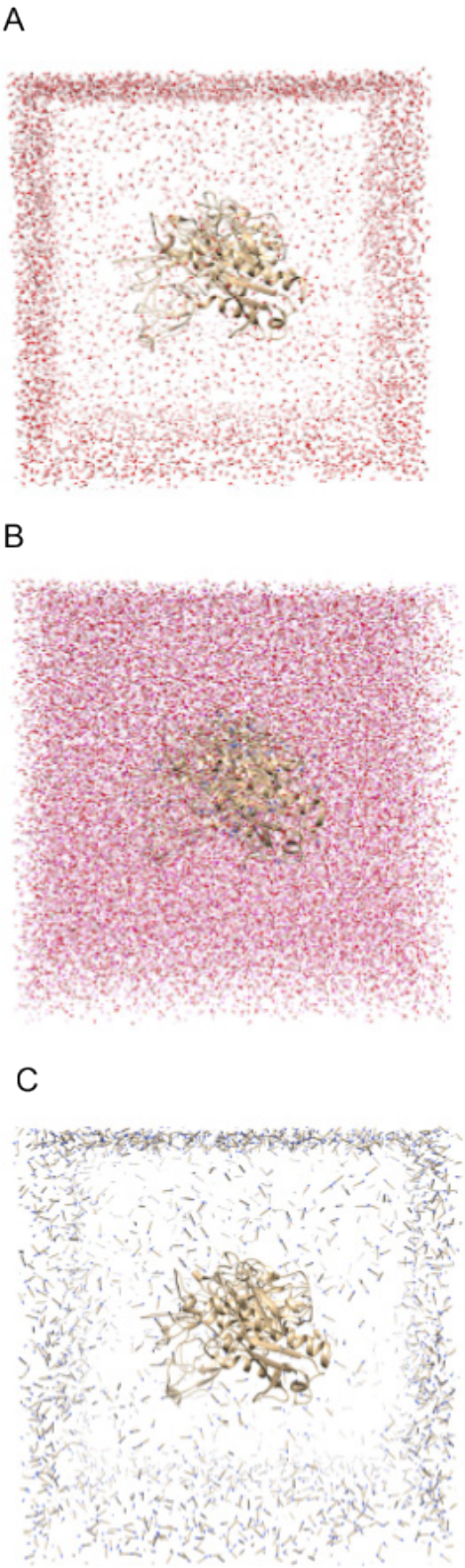

Figure 4. Structures of Lipase in Various Solvents. (**A**) Structure of lipase in water solvation shell. Red represents the solvation shell as water molecules. (**B**) Structure of lipase in methanol solvation shells. The red represen(ts the solvation shell as methanol molecules. (**C**) Structure of lipase in acetonitrile solvation shell. Red represents the solvation shell as acetonitrile molecules.

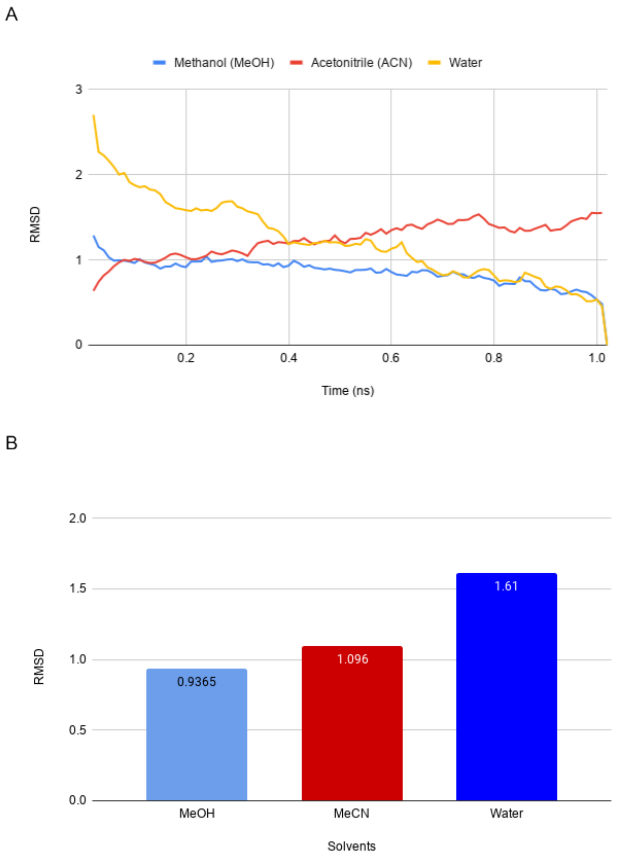

Figure 5. Root mean square deviation (RMSD) Values of Lipase in Various Solvents. RMSD is the deviation of atomic positions between the atoms of the lipase. (**A**) RMSD values of lipase graphed as a function of time in methanol, acetonitrile, and water solvent systems. (**B**) Average RMSD values of lipase in methanol, acetonitrile, and water. Average calculated as the average RMSD values overtime.

Other notable observations are the relatively unchanged rates of lipase activity despite increased concentrations of DMSO. There were also decreases in lipase activity after increases in the concentration of DMF and acetonitrile (**Figure 2**).

Molecular dynamics simulations were also performed using GROningen MAchine for Chemical Simulations (GROMACS) to probe predicted changes in lipase stability in water, methanol, and acetonitrile (**Figure 4**). We were unable to perform these calculations for every solvent because we could not obtain all solvent topology files. Root mean square deviation (RMSD) values for lipase were derived from GROMACS and graphed as a function of time (**Figure 5A**) as well as averages of the time dependent RMSD for each solvent (**Figure 5B**). Lower RMSDs indicate less deviation of atomic positions, between the atoms of the lipase, and analysis of this can suggest protein stability. Over time, the RMSD of lipase in acetonitrile increased, while the RMSD of water and methanol decreased. The average RMSD shows in which solvent lipase is predicted to be most stable versus unstable. Further examination showed lipase in methanol to have the lowest average RMSD of 0.9365 Å, while lipase in water has the highest average RMSD of 1.61 Å.

DISCUSSION

Here, we screened the kinetics of catalytic deacylation of 4-nitrophenyl acetate by a bovine pre-gastric lipase through UV-vis spectroscopy in different organic solvents in efforts to determine the extent of retention of lipase catalytic ability in non-aqueous solvent systems which helps with chemical synthesis under mild conditions. We observed a general decrease in lipase activity with increasing concentrations of non-aqueous solvent, which is consistent with our hypothesis that enzymatic activity would be best retained in solvent systems whose physical properties most closely mimic water and that higher concentrations of non-aqueous solvent will decrease enzymatic activity. However, in low concentrations of methanol, there was a significant increase in lipase activity relative to an aqueous system.

The relative lipase activity in acetone, acetonitrile, and DMF was lower as compared to lipase activity in water as evidenced by the slower increase in absorbance at 413 nm. Lower lipase activity in acetone, acetonitrile, and DMF can likely be attributed to solvent molecules disrupting crucial hydrogen bond interactions with lipase that may otherwise be present with an alcohol solvent. Similar to DMSO, these three solvents lack hydrogen-donor properties that both water and methanol possess, which likely affects the activity of lipase. For example, hydrogen bonds stabilize the tertiary structure of proteins; therefore, without hydrogen bonds, the tertiary structure of lipase may be affected, which would impact its activity. Decreased lipase activity in acetone may also be explained by the lower polarity of acetone compared to water or methanol. Since high catalytic activity in DMSO compared to DMF and acetonitrile cannot be rationalized on the basis of polarity, as DMSO is fairly more polar as compared to DMF and acetonitrile, it seems that loss of enzymatic activity in these solvents is most likely attributed to differences in the degree of disruption in the hydrogen bonding network that defines secondary and tertiary structure in the enzyme. Competition for amide hydrogen-bond networks have been reported with both DMSO and DMF (17).

Our MD simulations suggested that lipase destabilizes in water, as evidenced by lipase's high average RMSD in water. However, the lipase in water RMSD values start at higher values than the lipase in methanol RMSD values, yet they both ended in similar RMSD values. This suggests that the lipase stabilizes faster in methanol than it does in water. Lipase had the lowest average RMSD in methanol, which indicates that lipase experiences the least deviation in atomic positions in methanol compared to water and acetonitrile. Similarly, the time-dependent RMSD behavior of lipase in methanol was lower to that of lipase in water, suggesting that the conformational state and stability of the enzyme in methanol is higher than that of the enzyme in water. This is consistent with our spectroscopic data since lipase displayed higher enzymatic activity in low concentrations of methanol than in water. The RMSD of lipase in acetonitrile increased

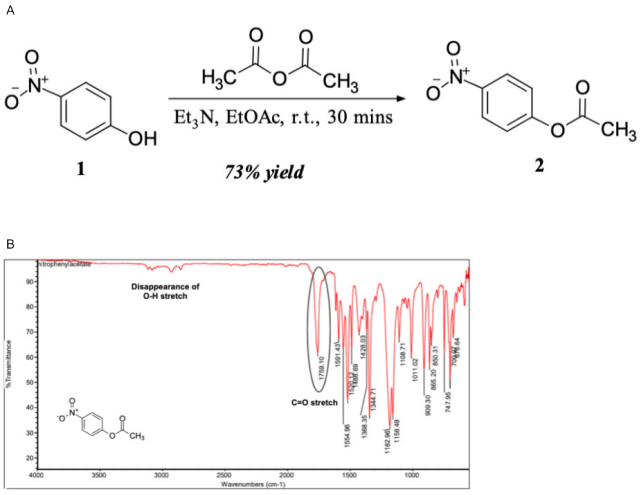

Figure 6. Reaction Schematic and Characterization of 4-nitrophenyl Acetate. (**A**) 4-nitrophenyl acetate [2] was synthesized in 73% yield via acetylation of 4-nitrophenol [1]. (**B**) FT-IR spectrum of 4-nitrophenyl acetate.

over time, which may be attributed to a net destabilization of key noncovalent interactions that define the secondary or tertiary structure of lipase. While further mechanistic studies would be needed to identify whether this translates into greater catalytic activity, these initial MD simulations seem to indicate that the three-dimensional stability of the lipase enzyme in methanol is more similar to its native aqueous environment, in comparison to a solvent such as acetonitrile, and this is consistent with the observation that lipase activity is highest in methanol compared to any other organic solvent.

It was observed that in 5% methanol, lipase activity was 28% higher compared to lipase activity in water. While low concentrations of methanol seem to accelerate the rate of enzymatic hydrolysis of the 4-nitrophenyl acetate ester bond, a trend of decreasing enzymatic activity with increasing concentrations of non-aqueous solvent was still observed. However, across all types and concentrations of organic solvent, enzymatic catalysis in methanol exhibited the greatest rate of substrate deacylation. Therefore, low concentration aqueous methanol solutions may be a desirable solvent system to use when conducting lipase-catalyzed deacylation reactions on organic compounds. Our results inform future efforts involving the optimization of water-methanol co-solvent systems in lipase deacylation reactions.

To further analyze enzymatic activity in non-aqueous organic solvents, future experimentation can be done with other esterases such as acetylcholinesterase, phosphatases, and endonucleases. In doing so, future research can be used to determine whether the trends observed in this study are unique to lipase or whether they represent a general trend for all esterases.

METHODS

Chemical Synthesis

4-nitrophenyl acetate was synthesized via acetylation of 4-nitrophenol. 4-nitrophenol (1.00g, 1 eq., 7.2 mmol) was added to a round-bottom flask equipped with a Teflon stir bar, along with acetic anhydride (11g, 15 eq., 107.8 mmol), triethylamine (0.73g, 1 eq., 7.2 mmol), in ethyl acetate. The progress of the reaction was monitored to completion via thin-layer chromatography. Unreacted acetic anhydride was quenched with methanol, and the crude material was concentrated in a rotary evaporator (Rotovap Buchi R200). The crude product was extracted 3 times in ethyl acetate over saturated sodium bicarbonate to remove excess acetic acid. The combined organic layers were dried over anhydrous magnesium sulfate, concentrated in vacuo and purified on silica gel flash chromatography with a gradient of 0-25% ethyl acetate in hexanes to yield off-white crystals of 4-nitrophenyl acetate with 73% yield (**Figure 6A**). 4-nitrophenyl acetate was characterized via 1H NMR (Nanalysis NMReady 60 MHz 1H NMR spectrometer in chloroform-D), Fourier-transform infrared (FT-IR) spectroscopy (Thermo Scientific iS5 Nicolet FT-IR spectrometer, iD5 ATR assembly) (**Figure 6B**), and UV-vis spectroscopy (BioRad SmartSpec 3000 UV-vis spectrophotometer, quartz cuvette). 4-nitrophenol was characterized via FT-IR and UV-vis spectroscopy. American Chemical Society (ACS) grade 4-nitrophenol was purchased from Reagent Inc. and used without further purification. ACS grade acetic anhydride was purchased from ChemSavers Inc. All solvents used were ACS grade.

4-nitrophenyl acetate: (^{1}H NMR, 60 MHz, CDCl3): δ 7.21-8.34 (dd, 4H, J = 8.3Hz), 2.35 (s, 3H); FT-IR (ATR, cm^{-1}): 2900-3100 (Ar-H), 1759.10 (C=O), 1591.43, 1554.96, 1520.12, 1368.35.
4-nitrophenol: FT-IR (ATR, cm-^{1}): 3317.81 (O-H), 2900-3100 (Ar-H), 1612.64, 1586.58, 1486.66, 1319.95.

Preparation of Enzyme Solutions

Enzyme buffers at pH 8 were prepared with 15 mM Tris base and 100 mM sodium chloride in deionized water. The Tris buffer was used because of its availability and ability to buffer the enzyme solution to pH 8, the optimal pH of lipase. Then, solvent solutions of concentrations 5%, 10%, 20%, and 40% were prepared for each solvent (DMSO, Ethanol, Methanol, Isopropanol, Acetone, DMF, and Acetonitrile) in a buffer. To compare the lipase activity of the lipase in solvents we also monitored the hydrolysis kinetics of the lipase in 100% water. Bovine pre-gastric lipase, obtained as a commercially-available powder from Standing Stone Farms, was then dissolved in each of the solutions to produce a (0.5 mg/mL) solution. To our knowledge, there are no significant differences between human and bovine lipases.

UV-Vis Spectrophotometry

A full UV-vis spectrum of 4-nitrophenol revealed two peaks, one around 413 nm and one at 310 nm, while a UV-Vis spectrum of 4-nitrophenyl acetate revealed a peak at around 300 nm. We chose to track 4-nitrophenol at 413

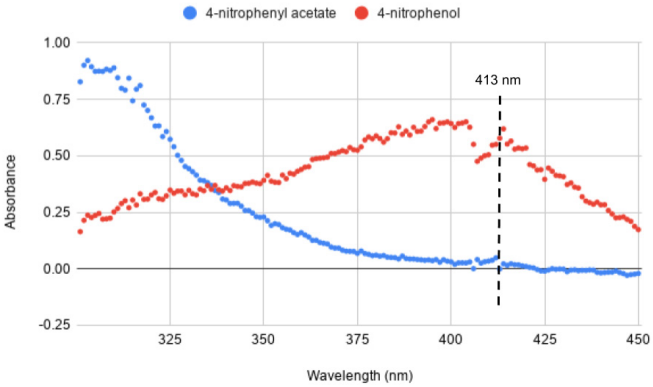

Figure 7. Final average spectrum of overlaid UV-vis spectra of 4-nitrophenol (blue) and 4-nitrophenyl acetate (red).

nm because 4-nitrophenyl acetate does not absorb at that wavelength, which allowed for much simpler calculations when determining the hydrolysis kinetics of lipase (Figure 7). The extinction coefficients of 4-nitrophenol at 413 nm were determined via Beer's Law for each solvent system sampled.

A 1 mM solution of 4-nitrophenyl acetate in 5% DMSO (for the dissolution of nitrophenyl acetate) was prepared. 1 mL of substrate solution and 1 mL of a buffered enzyme solution were mixed in a cuvette. To ensure that observed changes in absorbance during the experiments were a result of enzymatic hydrolysis, separate controls of substrate-only (no-enzyme) and enzyme-only solutions were prepared. The cuvettes were placed in a UV-vis spectrophotometer and tracked at 413 nm every 10 seconds for 3 minutes. All solutions were run immediately after preparation.

We analyzed UV-vis data to determine respective Beer's Law graphs of 4-nitrophenol at 1.00 nM, 10.0 nM, and 50.0 nM. Extinction coefficients were derived from Beer's Law graphs and used to calculate the concentration of nitrophenol as a function of absorbance at 413 nm. The rate of enzymatic hydrolysis is measured using nitrophenyl acetate in each solvent was obtained by determining the initial velocity of lipase, which was calculated using the slope of the line-of-best-fit of the concentration of 4-nitrophenol as a function of time (**Figure 7**).

Molecular Dynamics

To quantify the stability of the enzyme in a non-aqueous environment, molecular dynamics simulations were performed. Molecular dynamics simulations of lipase (PDB: 1N8S) were conducted using GROMACS (18, 19). Solvent models for methanol and acetonitrile were used from the GROMACS molecule topologies website, and the water model was used directly from the software (19). The GROMOS96 43a2 forcefield was used, and the lipase was placed in a cubic solvent box at a distance of 1.0 nm from the solvent molecules. Energy minimization was then run to minimize the structure and clear clashes between the solvent atoms and lipase. Equilibration was run in two parts to reach the thermodynamic requirements of the structure. The final step was run in 50000 steps using Berendsen pressure coupling.

Molecular dynamics simulations were performed on a Dell Poweredge 710 server with a 24 core Intel Xeon X5660 processor @ 2.80GHz and 32GB RAM. Results were analyzed using Visual Molecular Dynamics and MDWeb Server (20, 21).

ACKNOWLEDGMENTS

We would like to thank Neville Bosco, Saly Mamani, and Icela Bernal for ensuring our safety in the lab and for spending countless hours helping us. The authors gratefully acknowledge the Aspiring Scholars Directed Research Program for providing a laboratory and allowing us the opportunity to conduct research as well as providing the funding and supplies for our research.

Received: June 14, 2020
Accepted: November 23, 2020
Published: December 20, 2020

REFERENCES

1. Nestl, Bettina M., *et al*. "New generation of biocatalysts for organic synthesis." *Angewandte Chemie International Edition*, vol. 53, no. 12, 2014, pp. 3070-3095., doi: 10.1002/anie.201302195
2. Huffman, M.A. *et al*. "Design of an in vitro biocatalytic cascade for the manufacture of islatravir." *Science* (New York, N.Y.) vol. 366, no. 6470 2019. pp. 1255-1259., doi: 10.1126/science.aay8484.
3. Madeira Lau R., *et al*. "Lipase-Catalyzed Reactions in Ionic Liquids." *Organic Letters*, vol. 2, no. 26, 2000, pp. 4189–4191., doi: 10.1021/ol006732d
4. Patel R.N., "Biocatalytic Synthesis of Intermediates for the Synthesis of Chiral Drug Substances." *Current Opinion in Biotechnology*, vol. 12, no. 6, 2001, pp. 587–604., doi: 10.1016/s0958-1669(01)00266-x.
5. VanEtten, Robert L., *et al*. "The mechanism of the cycloamylose-accelerated cleavage of phenyl esters." *Journal of the American Chemical Society*, vol. 89, no. 13, 196, pp. 3253-3262., doi: 10.1021/ja00989a028
6. Pirahanchi Y., Sharma S. "Biochemistry, Lipase." [Updated 2019 Feb 2]. In: StatPearls [Internet]. Treasure Island (FL): StatPearls Publishing; 2020 Jan.
7. Houde A., *et al*. "Lipases and Their Industrial Applications: An Overview." *Applied Biochemistry and Biotechnology*, vol. 118, no. 1-3, 2004, pp. 155-170., doi: 10.1385/abab:118:1-3:155.
8. Lüthi-Peng, Qiaoqian, *et al*. "Identification of the Active-Site Serine in Human Pancreatic Lipase by Chemical Modification with Tetrahydrolipstatin." *FEBS Letters*, vol. 299, no. 1,1992, pp. 111–115., doi: 10.1016/0014-5793(92)80112-t.
9. Polgár, László. "The catalytic triad of serine peptidases." *Cellular and molecular life sciences CMLS 62.19-20* (2005): 2161-2172., doi: 10.1007/s00018-005-5160-x
10. Zaks, Aleksey, and Alexander M. Klibanov. "Enzyme-

catalyzed processes in organic solvents." *Proceedings of the National Academy of Sciences*, vol. 82, no.10, 1985, pp. 3192-3196., doi: 10.1111/j.1749-6632.1987.tb45697.x
11. Tsuzuki W., *et al*. "Polar Organic Solvent Added to an Aqueous Solution Changes Hydrolytic Property of Lipase." *Bioscience, Biotechnology, and Biochemistry*, vol. 67, no. 8, 2003, pp. 1660–1666., doi: 10.1271/bbb.67.1660.
12. Mozhaev V.V., *et al*. "Catalytic Activity and Denaturation of Enzymes in Water/Organic Cosolvent Mixtures. Alpha-Chymotrypsin and Laccase in Mixed Water/Alcohol, Water/Glycol and Water/Formamide Solvents." *European Journal of Biochemistry*, vol. 184, no. 3, 1989, pp. 597–602., doi: 10.1111/j.1432-1033.1989.tb15055.x.
13. Gosling, James. "Enzyme immunoassay." Immunoassay. *Academic Press*, 1996. 287-308.
14. Wang, Q. May, *et al*. "A Continuous Colorimetric Assay for Rhinovirus-14 3C Protease Using Peptidep-Nitroanilides as Substrates." *Analytical biochemistry*, vol. 252, no. 2, 1997, pp. 238-245., doi: 10.1006/abio.1997.2315
15. Furutani, Toshiyuki, *et al*. "Simple screening method for lipase for transesterification in organic solvent." *Enzyme and microbial technology*, vol. 17, no. 12, 1995, pp. 1067-1072., doi: 10.1016/0141-0229(95)00035-6
16. Gutfreund, H., and J. M. Sturtevant. "The mechanism of the reaction of chymotrypsin with p-nitrophenyl acetate." *Biochemical Journal*, vol. 63, no. 4, 1956, pp. 656-661., doi: 10.1042/bj0630656
17. Mattos C., Ringe D., "Proteins in organic solvents." *Current Opinion in Structural Biology*, vol. 11, no. 6, 2001, pp. 761-764., doi: 10.1016/S0959-440X(01)00278-0.
18. Lindahl E., *et al*. "GROMACS: High Performance Molecular Simulations through Multi-Level Parallelism from Laptops to Supercomputers." *SoftwareX*, vol. 1-2, 2015, pp. 19–25., doi:10.1016/j.softx.2015.06.001.
19. Baptista A.M, *et al*. "Protein Structure and Dynamics in Nonaqueous Solvents: Insights from Molecular Dynamics Simulation Studies." *Biophysical Journal*, vol. 84, no. 3, 2003, pp. 1628–1641., doi: 10.1016/s0006-3495(03)74972-8.
20. Schulten K., *et al*. "VMD: Visual Molecular Dynamics." *Journal of Molecular Graphics*, vol. 14, no. 1, 1996, pp. 33–38., doi: 10.1016/0263-7855(96)00018-5.
21. Lluís Gelpí J., *et al*. "MDWeb and MDMoby: an Integrated Web-Based Platform for Molecular Dynamics Simulations." *Bioinformatics*, vol. 28, no. 9, 2012, pp. 1278–1279., doi: 10.1093/bioinformatics/bts139.

JOURNAL OF
EMERGING INVESTIGATORS

Article

Alkaloids Detection in Commonly Found Medicinal Plants with Marquis Reagent

Daniel Alejandro Ocampo-Bustos[1] and María Elena Cano-Ruiz[1]
[1] Tecnológico de Monterrey High School, Cuernavaca, Mexico.

SUMMARY

Alkaloids are a class of nitrogenous organic compounds of plant origin that may have important physiological actions on humans. They include many drugs and poisons, but some alkaloids in low doses have health benefits as well. Traditional medicinal plants may contain alkaloids as active ingredients, but this is not well-understood. The Marquis reagent exists as a simple qualitative colorimetric method to determine the presence of alkaloids in medicinal plants. The Marquis reagent test was assayed in medicinal plants by first optimizing the formulation of the reagent using poppy seeds and lavender as the positive and negative controls. Then using the optimized formulation of Marquis reagent in the extracts of 11 medicinal plants with known claims of health benefits. Four medicinal plants tested positive for alkaloids, including a relaxing herbal mix (*Tilia cordata*, *Valeriana officinalis*, *Passiflora incarnata*, and *Melissa officinalis*), *Turnera diffusa*, *Brickellia cavanillesii*, and *Verbascum thapsus*. These findings demonstrate the value of the Marquis reagent test to provide a rapid and simple method for screening for potentially medicinal alkaloids of natural origin.

INTRODUCTION

Alkaloids are a class of nitrogenous organic compounds, usually with aromatic rings, that are widely known for their effects on organisms. These effects are put to use in many kinds of medications, such as analgesics, relaxants, and even antiarrhythmics. They are also naturally present in some plants like *Papaver somniferum*, or poppy, from which several opium alkaloids are extracted; for example, morphine is the most abundant alkaloid in the poppy plant (1, 2).

Alkaloids, in their vast majority, can cause addiction problems or toxicity when consumed by humans, which is why most alkaloids are either prohibited, restricted, or, preferably, controlled by governments globally for availability only with a medical prescription (3). On the other hand, in very low doses, alkaloids seem to have therapeutic effects on certain conditions, such as different kinds of pain, stress, hyperactivity, or nervous system-related illnesses (4).

Phytotherapy is the use of medicinal plants or extracts of natural origin used to prevent and treat different diseases, which is also called folk medicine. In Mexico, this represents a system rooted in the deepest part of the cosmovision and identity of social groups. Many of the medicinal plants have their healing properties known by empirical use through time, but these medicinal plants may contain active ingredients with tested pharmacological properties. One possibility is that some of the active ingredients in medicinal plants belong to the group of alkaloids, which can be determined by a colorimetric chemical reaction with the Marquis reagent. The reagent is dripped onto the substance being tested, and if an alkaloid is present, a color change appears (5). The Marquis reagent is traditionally composed of a mixture of formaldehyde and concentrated sulfuric acid.

Originally, the Marquis reagent was used for testing many different alkaloids, and the results from those studies were the base for developing the color scales that are used as a reference to determine the specific alkaloid that is present in a solution (5, 6). The Marquis reagent can give different color changes to hundreds of drugs (7). Purple-dark or blue-dark colors are observed with methylenedioxylphenyl groups in alkaloids, which is present in methylenedioxymethamphetamine (i.e., MDMA, ecstasy); orange is observed with amphetamines; blue-black to yellow colors are observed with methylenedioxy-substituted analogs; and red-violet is observed with methylenedioxyphenyl amphetamine-type compounds (8, 9).

In this study, a possible explanation for the medicinal properties of some plants was elicited by determining the presence of alkaloids in 11 common medicinal plants that are found in local markets of Mexico. We hypothesized that plants with relaxing effects or claims of better sleep would contain alkaloids, as many medications available in pharmacies for these purposes (e.g., clonazepam) are alkaloids. Using the Marquis reagent qualitative colorimetric test, we tested the 11 common medicinal plants for the presence of alkaloids. Four medicinal plants tested positive for alkaloids indicating the value of the Marquis reagent test as a rapid and economical method for screening for potentially medicinal alkaloids of natural origin.

RESULTS

Marquis reagent is a colorimetric test commonly used for the detection of alkaloids. To obtain the best preparation for the Marquis reagent, we tested several formulations in triplicate varying the concentrations and amount of formaldehyde, acetic acid, and sulfuric acid (10).

Comparing the different color tones that the mixture took

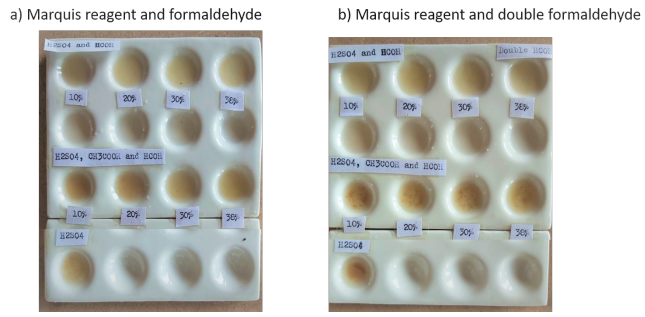

Figure 1: Optimization of Marquis reagent preparation using poppy seed macerate as a positive control. A) (left). Poppy seed macerate was tested after 45 s with the different preparations and concentrations of the Marquis reagent. First line, no acetic acid added; second line, no samples; third line, acetic acid added; bottom-left sample, control sample with sulfuric acid only. First and third lines from left to right: 10%, 20%, 30%, and 38% of formaldehyde. All preparations include 1 mL concentrated sulfuric acid and 0.1 mL formaldehyde. B) (right). Poppy seed macerate was tested after 45 s with the different preparations and concentrations of the Marquis reagent (double formaldehyde). First line, no acetic acid added; second line, no samples; third line, acetic acid added; bottom-left sample, control sample with sulfuric acid only. First and third lines from left to right: 10%, 20%, 30%, and 38% of formaldehyde. All preparations include concentrated 1 mL sulfuric acid and 0.2 mL formaldehyde.

with the poppy seed macerate when different formulations of the Marquis reagent were added, we determined that there was an alkaloid present (morphine) in the poppy seed macerate when the color changed from white to different tones of light orange-brown. All poppy seed samples originated from the same macerate, so the different tones observed are resultant of the different reagent formulations rather than variances in the samples (**Figure 1A & B**).

Reaction time must be measured during the colorimetric tests because sulfuric acid in the reagent will continue reacting with organic compounds, producing a dark color; therefore, the test must be completed in less than 60 seconds. The most sensitive formulation of the Marquis reagent for color development contained 10% formaldehyde in 99% acetic acid and 98% sulfuric acid (**Figure 1A**). We selected and used this formulation for determining the presence of alkaloids in the 11 common Mexican medicinal plants.

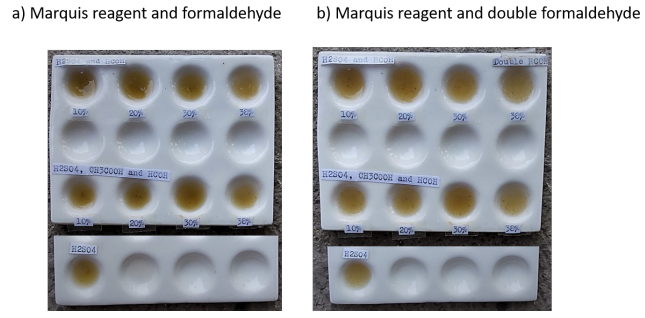

Figure 2: Optimization of Marquis reagent preparation using lavender macerate as a negative control. A) (left). Dry lavender macerate after 45 s with the different preparations and concentrations of the Marquis reagent. First line: no acetic acid added, second line, no samples; third line: acetic acid added; bottom left sample, control sample with sulfuric acid only. First and third lines from left to right: 10%, 20%, 30%, and 38% of formaldehyde. All preparations include 1 mL concentrated sulfuric acid and 0.1 mL formaldehyde. B) (right). Dry lavender macerate after 45 s with the different preparations and concentrations of the Marquis reagent (double formaldehyde). First line: no acetic acid added; second line, no samples; third line: acetic acid added; bottom left sample, control sample with sulfuric acid only. First and third lines from left to right: 10%, 20%, 30%, and 38% of formaldehyde. All preparations include 1 mL concentrated sulfuric acid and 0.2 mL formaldehyde.

Figure 3: Representative images of tea preparations. From left to right, tea preparations of *Tilia cordata*, *Turnera diffusa*, and the relaxing herb mix, using 2 g of dried plant in 100 mL of water at 90°C.

Dry lavender was used as a negative control in this experiment because it does not contain alkaloids (11). The Marquis reagent did not present a change of color with lavender with any of the triplicate tests, where the color of the macerate extract was dark-greenish-brown and remained the same color in all Marquis formulation tests (**Figure 2A & B**).

We prepared teas from 11 common medicinal plants by three different procedures: a standard preparation using 2 g dried herbs in 100 mL of hot water, a concentrated preparation using 2 g dried herbs in 50 mL of hot water, and a macerated preparation with the 2 g of dried herbs blended in 100 mL of hot water (**Figure 3**). We added equal volumes of each tea preparation to porcelain trays (**Figures 4A, 5A, and 6A**). A sulfuric acid only control was used to control for any color changes due to the sulfuric acid and not the Marquis reagent with the macerated preparations (**Figure 7A**). We used the macerated preparation for the sulfuric acid control because,

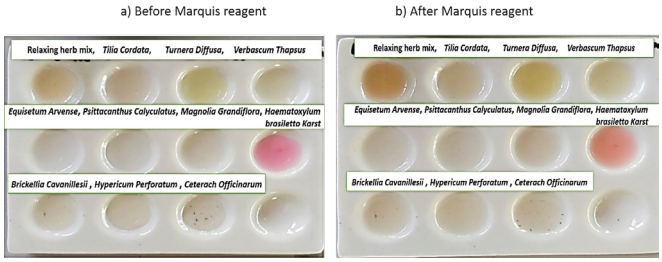

Figure 4: Marquis reagent test for medicinal plants using a standard tea preparation. A) (left). Tea samples of each of the 11 medicinal plants before the Marquis reagent test. Standard preparation, with 2 g of tea in 100 mL of water at 95°C and letting it rest for 5 min. B) (right). Tea samples of each of the 11 medicinal plants after the Marquis reagent test. Positive change in color was observed for the relaxing herbs mix (first line, position one), *Turnera diffusa* (first line, position three), and *Verbascum thapsus* (first line, position four).

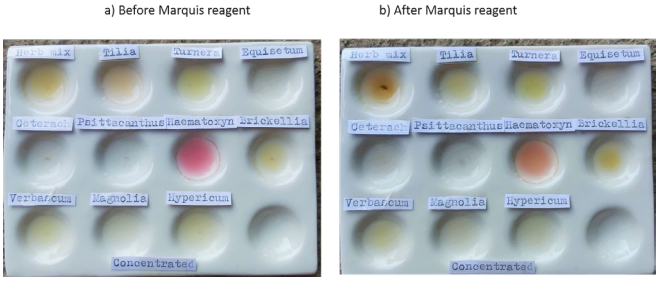

Figure 5: Marquis reagent test for medicinal plants using a concentrated tea preparation. A) (left). Tea samples of each of the 11 medicinal plants before the Marquis reagent test. Concentrated preparation, with 2 g of tea in 50 mL of water at 95°C and letting it rest for 5 min. B) (right). Tea samples of each of the 11 medicinal plants after the Marquis reagent test. Positive change in color was observed for the relaxing herbs mix (first line, position one), *Tilia cordata* (first line, position two), *Turnera diffusa* (first line, position three), *Haematoxylum brasiletto karst* (second line, position three), Brickellia cavanillesii (second line, position four) and *Verbascum thapsus* (third line, position one).

even though they were strained, they could have had very small organic residues from the leaves of the plants which may react with the sulfuric acid in the reagent and change the color of the test. Therefore, with this control, we were certain that the color obtained in the test was not due to the sulfuric acid reacting with confounding organic residues.

For color development, we added the Marquis reagent to all herbal samples (standard, concentrated, and macerated) and for sulfuric acid control, we added sulfuric acid instead of Marquis reagent (**Figures 4B, 5B, 6B, and 7B**). After the reaction time passed, any color changes were observed (**Figures 4–7**). After comparing with the color development in the sulfuric acid control tray, any color change in a sample after Marquis reactant addition was considered a positive result for the presence of alkaloids, independent of the tone or intensity of the color. Different preparations (standard, concentrated, and macerated) gave similar results for all

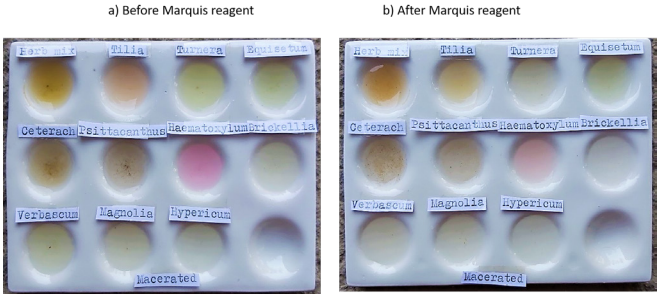

Figure 6: Marquis reagent test for medicinal plants using a macerated tea preparation. A) (left). Tea samples of each of the 11 medicinal plants before the Marquis reagent test. Macerated preparation with 2 g of tea in 100 mL of water at 95°C was added to the blender at medium speed for 30 s and allowed to rest for 60 s. B) (right). Tea samples of each of the 11 medicinal plants after the Marquis reagent test. Positive color change was observed for the relaxing herbs mix (first line, position one), *Tilia cordata* (first line, position two), *Turnera diffusa* (first line, position three), *Haematoxylum brasiletto karst* (second line, position three), and *Verbascum thapsus* (third line, position one).

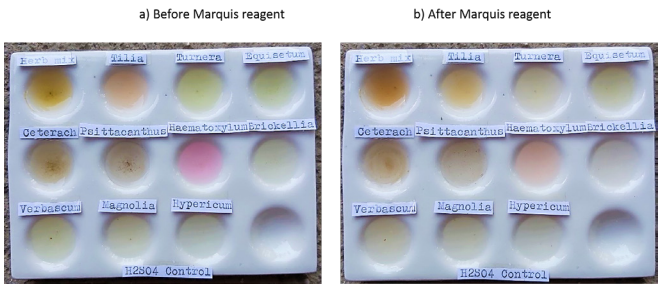

Figure 7: Control test for medicinal plants using a macerated tea preparation and sulfuric acid. A) (left). Tea samples of each of the 11 medicinal plants before adding sulfuric acid. Macerated preparation with 2 g of tea in 100 mL of water at 95°C was added to the blender at medium speed for 30 s and allowed to rest for 60 s. B) (right). Tea samples of each of the 11 medicinal plants after adding sulfuric acid. Positive color change was observed for the relaxing herbs mix (first line, position one), *Tilia cordata* (first line, position two), *Turnera diffusa* (first line, position three), *Haematoxylum brasiletto karst* (second line, position three), and *Verbascum thapsus* (third line, position one).

herbal samples tested. The results from the color changes and possible alkaloids present in the 11 medicinal plants assayed were recorded (**Table 1**).

After adding the Marquis reagent to the standard preparation of the medicinal plants, the relaxing herbs mix changed color from light orange to dark-reddish-brown, *T. diffusa* changed color from light green to orange-yellow, and *V. thapsus* had a color change from pale green to light orange-brown (**Figure 4A & B**). The concentrated preparation after adding the Marquis reagent also had color changes in the relaxing herbs mix from light orange to dark-reddish-brown, in *T. cordata* from pink-orange to yellow-orange, in *T. diffusa*

Plant	Color before test	Color after test	Possible Alkaloid present
Tilia cordata	Pink-orange	Orange (In concentrated and macerated tests only)	Possible, although the color change may be due to a reaction with sulfuric acid only
Turnera diffusa	Light green	Orange-yellowish	YES
Equisetum arvense	Transparent	Transparent	-
Ceterach officinarum	Transparent	Transparent	-
Psittacanthus calyculatus	Transparent	Transparent	-
Haematoxylum brasiletto karst	Pink	Pink-orange (In the concentrated and macerated tests only)	None, the color change was due to the sulfuric acid in the reagent.
Brickellia cavanillesii	Very light pale greenish-yellow	Light orange (in the concentrated)	YES
Verbascum thapsus	Pale green	Light orange-brown	YES
Magnolia grandiflora	Transparent	Transparent	-
Hypericum perforatum	Transparent	Transparent	-
Relaxing herbs mix *(Tilia cordata, Valeriana officinalis, Passiflora incarnata,* and *Melissa officinalis)*	Light orange	Dark reddish-brown	YES

Table 1: Results from the Marquis reagent colorimetric tests with 11 medicinal plant tea extracts

from light green to yellow, in *H. brasiletto karst* from pink to pink-orange, in *B. cavanillesii* from a light green-yellow to light orange, and *V. thapsus* from pale green to a light orange-brown (**Figure 5A & B**). The macerated preparation had also color changes after the addition of Marquis reagent in the samples of the relaxing herbs mix, *T. cordata*, *T. diffusa*, *H. brasiletto karst*, and *V. thapsus* very similar to the color changes in the concentrated preparations. (**Figure 6A & B**). Finally, the sulfuric acid control had color changes in the relaxing herbs mix (from light orange to dark orange), *T. cordata* (from pink-orange to yellow-orange), *T. diffusa* (from light green to light brown), *H. brasiletto karst* (from pink to pink-orange), *B. cavanillesii* (light green-yellow to a light brown) and *V. thapsus* (from pale green to pale orange) (**Figure 7A & B**), but these color changes with only sulfuric acid were different from the color changes observed with the Marquis reagent for the relaxing herbs mix, T. diffussa, B. cavanillessii, and *V. thapsus*, (**Figures 4, 5 and 6A &B**) indicating the presence of alkaloids for these four plants.

DISCUSSION

In this study, the Marquis reagent tested with the poppy seeds macerate (white color) was the positive control due to its morphine content to determine which formulation of Marquis reagent was more sensitive (**Figure 1**). The formulation composed of 98% sulfuric acid, 99% acetic acid, and 10% formaldehyde gave the strongest color change and was used for testing the medicinal plants for the presence of alkaloids (**Figure 1A**). We anticipated that increasing the concentration of formaldehyde would result in darker color development (10). However, increasing formaldehyde concentration did not increase color intensity, and these results were consistent for the three trials. Standard Marquis preparations use 40% formaldehyde for alkaloid detection (6, 8, 10). A possible explanation for our results could be that the macerate preparations extracted had a lower concentration of alkaloid and that the amount of formaldehyde in the 10% formulation was sufficient to complex with the alkaloid present. Therefore, no more color changes would result with the addition of formaldehyde, as no more alkaloid-formaldehyde complexes would form at a higher concentration of formaldehyde. Furthermore, doubling the volume of formaldehyde used did not improve color development or intensity, and some precipitation was observed (**Figure 1B**). The addition of acetic acid seemed to help the formation of initial alkaloid-formaldehyde complexes, as preparations with acetic acid gave more intense colors than those without it (**Figure 1A**). Possibly, the increased amount of acid increased the solubility of formaldehyde or the rate of color development. Some Marquis reagents use acetic acid for dissolving the formaldehyde before adding sulfuric acid (10, 12, 13). Other preparations use a lower concentration of formaldehyde in the final Marquis reagent, such as the 10% formaldehyde Marquis reagent formulation that was the most sensitive in the positive control essays (12, 13).

The lavender macerate, which does not contain alkaloids, did not produce a color change; it remained dark greenish-brown following the addition of the Marquis reagent formulations and the sulfuric acid control. Therefore, we concluded that the Marquis reagent could be used as a specific test for the presence of alkaloids in medicinal plants.

Results from the tea extracts varied depending on the preparation method, but in general, the relaxing herbs mix, *T. diffusa*, *V. thapsus*, and *B. cavanillesii* all showed a color change indicating that all four contain alkaloids. Additionally, the concentration of alkaloids was higher in the relaxing herbs mix and *T. diffusa* samples as they had more robust color changes compared to *V. thapsus* and *B. cavanillesii*.

For the standard preparation method, the relaxing herb mix, *T. diffusa*, and *V. thapsus* samples changed colors. For the concentrated preparation method, the relaxing herbs mix, *T. diffusa*, *V. thapsus*, *B. cavanillesii*, *T. cordata*, and *H. brasiletto karst* samples changed colors. For the macerated preparation method, the relaxing herbs mix, *T. diffusa*, *T. cordata*, *H. brasiletto karst*, and *V. thapsus* samples changed colors (**Table 1**).

These color changes may support that all of these medicinal plants contained alkaloids, but for more reliable results, we compared the color changes with the samples exposed to only sulfuric acid in the control and no Marquis reagent (**Figure 7A & B**). We concluded that the relaxing herbs mix, *T. diffusa*, and *V. thapsus* contained alkaloids because the results were positive in the three preparations, as well as the sulfuric acid control, but the sulfuric acid control tests produced different colors than those with Marquis reagent, so the color change was not because of the sulfuric acid in the Marquis reagent but a specific Marquis reagent reaction with alkaloids.

Our results agree with previous studies that found alkaloids in the plants that tested positive in our study. One of the plants in the relaxing herbal mix, *V. officinalis*, contains two known alkaloids: catinine and valerian (14). One study reported the presence of the alkaloid caffeine in leaves and stems of *T. diffusa* (15). Although it is known to contain phenolic and saponins compounds and studies for alkaloids content are incomplete for this plant, *V. thapsus* tested positive for alkaloids (16). Nevertheless, *V. thapsus* belongs to the Scrophulariaceae family, which is a source of a variety of chemical constituents like saponins, monoterpene glycosides, iridoids, phenylethanoid glycosides, neolignan glycosides, flavonoids, steroids, phenolic acids, fatty acids, and spermine alkaloids that may explain its positive test (17). It is likely that *B. cavanillesii* also contains alkaloids because, although it produced no color change in the standard and macerated preparations, it did produce a color change in the concentrated preparation, which used half the volume of water as the other two methods. This difference in results along preparations methods indicates that concentration was an important variable for detecting color changes. *B. cavanillesii* has been shown to contain terpenes, terpene

derivatives, esters, ketones, aldehydes, and phenol-derived aromatic compounds (18). Also, *B. cavanillesii* belongs to the Asteraceae family, which is a source of pyrrolizidine alkaloids and may explain its positive result (19). Finally, *T. cordata* and *H. brasiletto karst* produced color changes in both the concentrated and macerated preparations tests; however, they likely do not contain alkaloids because the samples developed the same color when tested with the sulfuric acid control. Therefore, other compounds different than alkaloids were responsible for the color change observed with Marquis reagent. Most studies of color development of Marquis reagent have been done with known alkaloid drugs, but few have studied other related naturally-occurring compounds, such as terpenes and substituted allylbenzenes like safrole, which is used as a precursor for amphetamine-type drugs (6, 8, 9, 12, 20-22).

The method we used was a qualitative colorimetric method, performed with tea extracts and not pure alkaloids, so it is very difficult to compare colors obtained in the experiment with the standard Munsell Chart for colorimetry typically used for the determination of specific alkaloids in drugs and other known compounds (6). Therefore, it was difficult to elucidate the types of alkaloids present in medicinal plants. Additionally, the intensity of the color was much less than what is standard due to the lack of purity and the low concentrations of alkaloids present in the medicinal plants. Studies show that Marquis reagent produces pale colors when safrole concentration in essential oils is less than 15%, but it gives a dark blue-violet color in essential oils with safrole concentrations greater than 80% and with pure safrole (12). We believe that the concentration of alkaloids in the sample is important for both positive detection and color development.

Additionally, if two or more alkaloids are present in a certain plant, two possible scenarios arise. First, if one alkaloid is present in a higher concentration than others, then it would not substantially modify the final color; the mixture of the other colors with the one at the highest concentration would not be enough to change the result. Alternatively, if all the alkaloids are present at similar concentrations, then the resulting color would be a mixture of all the alkaloids present. This experiment only considered water-soluble alkaloids as they were the ones extracted by the hot water brewing method used in the tea preparations. Alkaloids that are not water-soluble were not detected, and they were not considered in this experiment. The medicinal plants that tested positive for alkaloids have the following health benefit claims, according to the seller from the local Mexican market: *T. diffusa*, nervous system alterations relief; *B. cavanillesii*, alleviating digestive and bile problems; *V. thapsus*, suppressing cough; and the relaxing herb mix, for relaxation.

To identify specific alkaloids in the preparations of medicinal plants that tested positive for alkaloids and to determine their concentration, more efficient extraction methods, and more specialized analytic instruments (i.e., high-performance liquid chromatography (HPLC) or gas chromatography-mass spectrometry (GC-MS) will be needed. However, the Marquis reagent could be used as an economical and rapid screening method for the detection of alkaloids in medicinal plants.

MATERIALS AND METHODS

Qualitative visual colorimetric analyses with the different Marquis reagent formulations were done to determine the presence of the alkaloids in the poppy seeds and the medicinal plants. If a color change was observed, the test was considered positive for the presence of alkaloids, independently of the color obtained.

Observation of color changes is subject since the interpretation of color may vary from person-to-person. To diminish differences in color interpretations, we took photos before and after the addition of the reagent with the best light possible to ensure color changes were only affected by the chemical reactions in the tests. We registered qualitatively positive tests when a color change occurred, independently of the color observed and its intensity.

Marquis Reagent Preparation

Two preparation methods of the Marquis reagent were tested, differing from the traditional Marquis formulation, by addition of acetic acid and by variation of formaldehyde concentration. These methods were included based on a study that stated with some alkaloids, specifically aspirin, the preparations showed reliable results (10). The procedure from this previous study was slightly modified to generate two preparations with or without acetic acid and using different concentrations of formaldehyde were tested for the Marquis reagent as described below.

Preparation A consisted of four formulations of Marquis reagent using 1 mL of 98% sulfuric acid and 0.1 mL of varying formaldehyde concentrations of 10%, 20%, 30%, or 38%. Then, the other four formulations of Marquis reagent were composed of 1 mL of 98% sulfuric acid and 0.2 mL of varying formaldehyde concentrations of 10%, 20%, 30%, or 38%. Preparation B consisted of four formulations of Marquis reagent using 0.1 mL of 10%, 20%, 30%, or 38% formaldehyde in 1 mL 99% acetic acid solution and 1 mL of 98% sulfuric acid. Then, the other four samples of Marquis reagent were composed of 0.2 mL of 10%, 20%, 30%, or 38% formaldehyde in 1 mL 99% acetic acid solution and 1 mL of 98% sulfuric acid.

Marquis Reagent Assay

After all formulations were prepared, a macerate of 30 mL of water and 15 g of poppy seeds was prepared for the positive control (morphine alkaloid present), and another macerate of 30 mL of water and 15 g of dry lavender was prepared for the negative control (no alkaloid present). Each macerate was prepared by blending the seeds or dry plant with water at medium speed for 30 s. The macerates were then filtered to mitigate any organic residues of the seeds or stems, which could be burned by the sulfuric acid in the Marquis reagent

and modify the color.

Preparations A and B were tested on both the poppy seed and lavender macerates to determine the best formulation of the Marquis reagent, using 1 mL of macerate and 2 drops of the Marquis reagent. The macerates and reagent were allowed to react for no more than 60 s to decrease sulfuric acid reacting with any remaining residue from the poppy seeds or the lavender and modifying the color. A reaction time of 45 s was considered to be sufficient because it was not so little time that the sample would not be able to change color and neither so much time that it would become dark. Photographs could also be taken within this 45 s. All tests were performed three times.

Medicinal Plants Extraction and Testing

Eleven medicinal plants from a local Mexican market were assayed for the presence of alkaloids. These plants, by scientific name and their use according to the seller, were the following: *T. cordata* (relaxing), *T. diffusa* (nervous system alterations), *E. arvense* (kidney diseases), *C. officinarum* (kidney function), P. calyculatus (kidney stones), *H. brasiletto karst* (blood circulation), *B. cavanillesii* (digestive and bile problems), *V. thapsus* (coughing), *M. grandiflora* (heart disease), *H. perforatum* (cicatrization), and a relaxing herb mix (improve relaxation) of *T. cordata*, *V. officinalis*, *P. incarnata* and *M. officinalis*.

Three different preparations were tested using the preparation B Marquis reagent composed of 10% formaldehyde in acetic acid, and 0.1 mL of this preparation was combined with 1 mL of concentrated sulfuric acid. All tests were performed three times.

The standard preparation consisted of steeping 2 ± 0.2 g of each of the dried or fresh plants in a beaker with 100 mL of water at 90°C for 5 min. The concentrated preparation consisted of steeping 2 ± 0.2 g of each of the dried or fresh plants in a beaker with 50 mL of water at 90°C for 5 min. The macerated preparation consisted of steeping 2 ± 0.2 g of each of the dried or fresh plants in a beaker with 100 mL of water at 90°C. For all preparations, 1 mL of each infusion was added to a porcelain tray. Then, 2 drops of the Marquis reagent were added, a reaction was allowed to occur for 45 s, and any color changes were recorded.

A final preparation consisted of reacting a sulfuric acid control solution with the 11 medicinal plant macerated extracts, using only sulfuric acid instead of the Marquis reagent. Using a similar procedure, 1 mL of macerate from each infusion was added to the porcelain tray, 2 drops of sulfuric acid were added to each sample, and any color development was observed within 45 s. This reaction was performed to compare color changes due to sulfuric acid only.

ACKNOWLEDGMENTS

The authors would like to thank fellow student Daniel Martin Uribe-Reza for supplying the materials needed to perform this study and for assisting Daniel Alejandro Ocampo-Bustos in the laboratory.

Received: May 14, 2020
Accepted: October 22, 2020
Published: December 21, 2020

REFERENCES

1. Thevis, Mario, *et al*. “Urinary concentrations of morphine and codeine after consumption of poppy seeds” *J. Anal., Toxicol*, vol, 27, no. 1, 2003, pp. 53–56, doi.org/10.1093/jat/27.1.53.
2. Moeller, Manfred R, *et al*. “Poppy Seed Consumption and Toxicological Analysis of Blood and Urine Samples.” *Forensic Science International*, vol. 143, no. 2-3, 2004, pp. 183–186, doi:10.1016/j.forsciint.2004.03.027.
3. Karila, Laurent. “Emergency of Synthetic Drugs in the General Landscape of Addiction.” *La Revue Du Praticien*, vol. 62, no. 5, 2012, pp. 661-663.
4. Kaur, Rajbir, and Saroj Arora. “Alkaloids-Important Therapeutic Secondary Metabolites of Plant Origin” *J. of Critical Reviews*, vol. 2, no. 3, 2015, pp. 1-8.
5. Stewart, CP Ed., and. Stolman, A Ed. “Toxicology. Mechanisms and Analytical Methods”. *New York, Academic Press*, vol. 2, no. 1, 1961, p. 247.
6. U.S. Dept. of Justice, “Color Test Reagents/Kits for Preliminary Identification of Drugs of Abuse”. *National Institute of Justice*, 2000, p. 4, www.ncjrs.gov/pdffiles1/nij/183258.pdf
7. Clarke, E.G.C., "Isolation and Identification of Drugs." *Pharmaceutical Press*, 1986, pp. 663-669, doi.org/10.1002/jps.2600760520
8. Toole, Kaitlyn E., *et al*. “Color test for the preliminary identification of methcathinone and analogues of methcathinone.” *Microgram J*., vol. 9, no. 1, 2012, pp. 27–32.
9. Glattstein B. “Method for the detection of compounds comprising methylenedioxyphenyl.” *US Patent* 3,374,946 B2, 2008, patents.google.com/patent/US7374946B2/en.
10. Gowda, Sandhya., *et al*. “Standardization of Marquis Reagent for the Detection of Aspirin”. *EC Pharmacology and Toxicology*, vol. 7, no. 2, 2019, pp. 92-102, www.academia.edu/38933320/Standardization_of_Marquis_Reagent_for_the_Detection_of_Aspirin
11. Prusinowska, Renata and Śmigielski, Krzysztof. “Composition, biological properties and therapeutic effects of lavender (Lavandula angustifolia l).” *Herba Polonica*, vol. 60, no. 2, 2014, pp. 56-66, doi: 10.2478/hepo-2014-0010.
12. Leitner, Andreas, *et al*. “Colour Tests for Precursor Chemicals of Amphetamine-Type Substances. Systematic study of colour tests for safrole and safrole-rich essential oils.” *United Nations Office on Drugs and Crime*, 2007, pp. 1-14. www.unodc.org/documents/scientific/SCITEC21_07fin.pdf.
13. United Nations International Drug Control Programme,

"Rapid testing methods of drugs of abuse. Manual for use by national law enforcement and narcotics laboratory personnel", *United Nations*, 1994, pp. 37-39, www.unodc.org/pdf/publications/st-nar-13-rev1.pdf.

14. Romero Jiménez, M. *Estudio antigenotoxicológico y de citotoxicidad de plantas medicinales de uso cotidiano y de sus fenoles más característicos*. 2013. Universidad de Córdoba, PhD dissertation. helvia.uco.es/xmlui/handle/10396/9785.
15. UNAM, "Biblioteca Digital de la Medicina Tradicional Mexicana", *Universidad Autónoma de México*, 2009, web.archive.org/web/20160409042048/http://www.medicinatradicionalmexicana.unam.mx/monografia.php?l=3&t=damiana&id=7387
16. Turker, Arzu Ucar and Ekrem Gurel. "Common Mullein (*Verbascum thapsus* L.): Recent Advances in Research." *Phytotherapy Research*, vol. 19, no. 9, 2005, pp. 733–739, doi:10.1002/ptr.1653.
17. Grigore, Alice, *et al*. "Correlation between Polyphenol Content and Anti-Inflammatory Activity of Verbascum Phlomoides (Mullein)." *Pharmaceutical Biology*, vol. 51, no. 7, 2013, pp. 925–929, doi:10.3109/13880209.2013.767361.
18. Eshiet, Etetor R., *et al*. "Chemical Characterization of Brickellia Cavanillesii (Asteraceae) Using Gas Chromatographic Methods." *Food Science & Nutrition*, vol. 2, no. 2, 2013, pp. 105–113, doi:10.1002/fsn3.52.
19. Viñas. René. *In vitro evaluation of the therapeutic and cytotoxic potential of Brickellia cavanillesi (Asteraceae) using HEPG2 cells*. 2007. Texas Tech University, M.S. dissertation. ttu-ir.tdl.org/bitstream/handle/2346/16297/Vinas_Rene_Thesis.pdf.
20. Winstock Adam R., *et al*. "Ecstasy pill testing: harm minimization gone too far?" *Addiction*, vol. 96, no. 8, 2001, pp.1139-1148, doi:10.1046/j.1360-0443.2001.96811397.
21. Ramsey, John D. *et al*. "A new method to monitor drugs at dance venues" *BMJ*, vol. 323, no. 7313, 2001, pp. 603-, doi.org/10.1136/bmj.323.7313.603.
22. Favretto, Donata *et al*. "When color fails: illicit blue tablets containing anabolic androgen steroids." *J Pharm Biomed Anal*. vol. 83, 2013, pp. 260-264, doi:10.1016/j.jpba.2013.05.024.

JOURNAL OF
EMERGING INVESTIGATORS

Article

Exploring a possible link between ADHD and inattentional blindness

[1]Zachary Younger, [2]Holly Bowen
[1]McKinney High School, McKinney, Texas
[2]Southern Methodist University, Dallas, Texas

SUMMARY

Attention Deficit Hyperactivity Disorder (ADHD) is characterized by impulsivity, hyperactivity, and inattention. These symptoms of inattention led us to wonder about a connection between ADHD and the phenomenon of inattentional blindness. We attempted to replicate a previous study done on this subject, and based on the results of that study, we hypothesized that people with ADHD would display more inattentional blindness in perceptually simple tasks and less inattentional blindness in perceptually complex tasks. Our results indicate that there is no significant correlation between ADHD and inattentional blindness in either type of task. This finding goes against our initial hypothesis and the conclusions from the only prior study on this topic. People with ADHD may not have the advantage of reduced inattentional blindness.

INTRODUCTION

For people without visual impairment, it would seem that object perception is an easy task. However, there is evidence that not all information we "see" is actually perceived. If an object is not the primary focus of attention, it could come into one's field of view without one being aware of and perceiving it. This phenomenon is known as inattentional blindness, and the phrase was first coined by Mack and Rock who described it as a failure to notice salient and foveated stimuli due to attention being engaged elsewhere (1).

Inattentional blindness is believed to be quite common and occur particularly when one is selectively focusing attention, but there have been few studies looking at inattentional blindness in individuals with Attention Deficit Hyperactivity Disorder (ADHD). Those with ADHD have difficulty focusing and selectively attending, and thus may be less prone to inattentional blindness compared to those without ADHD. Two studies have examined whether there is a difference in inattentional blindness in people diagnosed with autism, another disorder that is associated with attention dysfunction (2-3). In these studies, ability to detect change outside the focus of attention was assessed using tasks that involved static images: the Cross Detection Task and the Flicker Task. In the Cross Detection Task, participants are instructed to focus on a cross to determine which line is longer, while other shapes are flashed within the participants' fields of view. During the Flicker Task, presentation of an original image quickly alternates with a slightly manipulated image, with a blank screen inserted in between. The participant must actively seek to find the part of the image that is manipulated, or changed, during that brief blank screen. Researchers in both studies concluded that adults and children with autism have reduced rates of inattentional blindness, or that they perceive more information that is outside the focus of attention, compared to a control group (2-3).

To the best of our knowledge, only one study has examined the link between ADHD and inattentional blindness (4). These researchers found that participants with ADHD showed less inattentional blindness compared to neurotypical controls during the dynamic, and perceptually complex Monkey Business Illusion Task (5). Specifically, participants watched a short video of two teams passing several basketballs, which is the focus of the participants' attention, while a gorilla passes through the scene. The gorilla went largely unnoticed by those who were focused on the basketball passes, but those with ADHD were more likely to notice the gorilla than neurotypical control participants. These researchers also reported that those with ADHD showed greater inattentional blindness than control participants during a static, less perceptually complex task (the MOXO-Continuous Performance Task). Concentration on a dynamic, perceptually complex stimulus requires executive attention. Therefore, those with ADHD may find this difficult, as their attention wanders, which discourages inattentional blindness. In less perceptually complex tasks involving relatively static images, it may be easier for those with ADHD to focus attention, leading to levels of inattentional blindness comparable to controls. The major aim of our study was to replicate these previous results, emphasizing differences in inattentional blindness due to perceptual complexity.

The task-dependent distinctions in inattentional blindness for people with ADHD are theoretically supported by the hunter versus farmer hypothesis, which states that certain features of ADHD, such as impulsiveness, hyperactivity, and transient concentration, were once helpful in a hunter-gatherer society, but have become less useful in a farming society that heavily rewards intense focus on one task at a time (6-7). The perceptual load theory also hypothesizes that people with ADHD will have higher rates of distractibility in

tasks with a low perceptual load, but will have normal rates of distractibility in tasks with a high perceptual load (8-9). This was demonstrated in a recent study where participants with ADHD performed similarly to the non-ADHD participants in high load tasks (9). Thus, this model predicts that the participants with ADHD show more inattentional blindness in perceptually simple tasks, but will show similar rates of inattentional blindness in complex tasks compared to controls.

In the current study, we examined whether there is a link between ADHD and inattentional blindness by attempting to replicate the only other inattentional blindness experiments completed with participants diagnosed with ADHD (4). Specifically, we investigated whether inattentional blindness differs between those with and without ADHD symptomology during a perceptually simple task with static images and a more dynamic, perceptually complex task. We hypothesized that participants with ADHD would display more inattentional blindness than neurotypical control participants on the perceptually simple task, meaning they would be less likely to notice changes outside of the focus of attention, but less inattentional blindness than neurotypical control participants on the perceptually complex task, thus reporting greater perception of objects outside of attentional focus. Our hypotheses were based on the hunter versus farmer theory and the perceptual load theory detailed above. Overall, we failed to replicate prior work, and we did not find support for our hypotheses.

RESULTS

The Monkey Business Illusion Task

To test our hypothesis that participants with ADHD would display less inattentional blindness than neurotypical control participants in a complex task, participants watched the video titled “The Monkey Business Illusion” (5). This dynamic video involves a scene where two teams – one wearing black shirts and the other wearing white shirts – pass basketballs back and forth while the players move around a room. Participants are asked to count the number of passes made by one team. During the scene, three distracting things occur: (1) a person in a gorilla suit walks through, stops in the middle of the room, beats on their chest and exits; (2) the curtain hanging in the background changes color from red to gold; and (3) one of the players leaves the scene. Participants were asked to report how many passes the team wearing white made, as well as whether they saw these three distracting changes occur.

We found that 51 of 86 (59.3%) participants reported seeing the gorilla in the video. We also found that 12 of 97 (12.4%) participants reported seeing the background curtain change color and 27 of 97 (27.8%) noticed the player leaving the scene. Participants who had previously seen this exact video were excluded from analyses.

Participants were given an inattentional blindness score of 0 – 3 based on how many of the three unexpected events they reported seeing: the gorilla, the curtain changing color, and the player leaving the game. Higher scores indicate the participant reported seeing more of these changes and thus showed lower inattentional blindness. After excluding the participants who had already seen the gorilla video, we examined whether this inattentional blindness score differed for those who had ADHD symptoms (based on a score of 5 or higher on the ADHD Symptom Checklist). An independent t-test indicated that the difference in inattentional blindness scores between participants with ADHD symptoms (M = 1.97, SD = 0.73) and without ADHD symptoms (M = 2.07, SD = 0.69) was not statistically significant ($t(82) = 0.51$, $p = .05$) (**Figure 1A**). Furthermore, inattentional blindness scores and ADHD scores were entered into a correlation analysis as continuous variables (r = -0.01, p = 0.93), but again this relationship was not statistically significant. In contrast to our hypothesis that those with ADHD symptoms would show less inattentional blindness than neurotypical control participants in a complex task, the results suggest that participants with and without ADHD display equivalent levels of inattentional blindness in a dynamic, perceptually complex task.

The Cross Task

To test our hypothesis that participants with ADHD symptoms would display more inattentional blindness than neurotypical control participants in a simple, less cognitively demanding task, each participant completed the “Cross Task”. In this task, for six trials, a static cross shapeis briefly presented on the screen, and participants are instructed to report which line of the cross is longer, horizontal or vertical. On the sixth (critical) trial, a shape flashes in one quadrant of the cross, and participants are asked whether they saw the shape, what shape it was, and where it flashed on the screen.

We found that 44 of 98 (44.9%) participants noticed the surprise shape flashed in the cross on the sixth trial. Of those participants who noticed the shape, 11 (25%) reported a square, 10 (22.7%) a circle, 9 (20.5%) a triangle, 5 (11.4%) a rectangle, 1 (2.3%) a pentagon, 1 (2.3%) a diamond, 1 (2.3%) a cross, 1 (2.3%) reported it as “round”, 1 (2.3%) a shape of an angle, 1 (2.3%) a star, and 3 (6.8%) were not sure. Of those

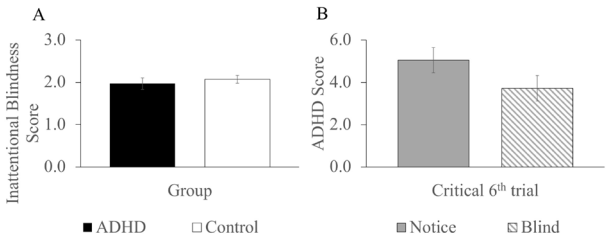

Figure 1. Outcomes of the Perceptually Complex and Perceptually Simple Task of Inattentional Blindness. (A) Average Inattentional Blindness scores (range 0 - 3) on the perceptually complex Monkey Business Illusion for participants with symptoms of ADHD (n = 36) and neurotypical control participants (n = 62). **(B)** Average ADHD Symptom Checklist scores for those who noticed the shape on the critical sixth trial of the Cross Task (Noticed; n = 44) and those who did not (Blind; n =54). Error bars = standard error of the mean.

participants who saw the shape, 14 (31.8%) reported it in the top left quadrant, 14 (31.8%) in the bottom left quadrant, 13 (29.5%) in the top right quadrant, and 3 (6.8%) in the bottom right quadrant.

An independent *t*-test indicated the ADHD symptom scores for participants who reported they noticed the shape (M = 5.05, SD = 3.97) and those who did not (M = 3.72, SD = 4.41) was not statistically different ($t(96) = 1.54$, $p = 0.13$) (**Figure 1B**). This suggests that those who reported the shape did not score higher on the ADHD symptom checklist than those who were "blind" and did not notice the shape. Furthermore, whether the critical shape on the sixth trial was noticed did not significantly differ between those in the ADHD group (M = 0.56, SD = 0.50) and those in the control group (M = 0.39, SD = 0.49) ($t(96) = 1.62$, $p = 0.11$). In contrast to our hypothesis, that participants with ADHD would display more inattentional blindness than neurotypical participants on a simple, less cognitively demanding task, the results indicate no significant differences between the two groups.

DISCUSSION

The main goal of our study was to compare inattentional blindness between adults with ADHD symptomology and a control group without ADHD. Specifically, we wanted to test the hypotheses that participants with ADHD symptomology would display more inattentional blindness on a perceptually simple task, but less inattentional blindness on a dynamic and perceptually complex task. These hypotheses were based on theories of ADHD and findings from the only other empirical investigation into differences in inattentional blindness between these two groups. We aimed to replicate this prior experiment using an online sample of MTurk workers (4).

Generally, we did not find support for these hypotheses, as the attention abilities did not differ between the two groups of participants in either the perceptually simple or complex task. Instead, we found that adults with and without ADHD symptomology performed similarly on both the Monkey Business Illusion and Cross Tasks. Participants across both groups noticed the unexpected events at the same rate, including the gorilla walking through the scene, the player leaving the scene, the curtain changing color, and the shape flashed in the critical sixth trial of the Cross Task.

Like the previous study on inattentional blindness and ADHD, we utilized the "Monkey Business Illusion" Task for our dynamic and perceptually complex task (4). However, we did not have access to the proprietary MOXO-continuous performance task used in the previous study, and instead opted to use the low perceptual load Cross Task that contains static images flashed briefly on the screen. The Cross Task has been utilized by other researchers examining inattentional blindness in participants with autism (2). We did not counterbalance the order of these tasks, and future research would benefit from randomizing the order to reduce the possibility that the Monkey Business Illusion Task influenced performance on the Cross Task. The other major difference between the current experiment and that of Grossman *et al*. is that those researchers tested a group of participants who had an ADHD diagnosis (4). In the current study, we utilized an online sample of MTurk workers that were not specifically recruited for an ADHD diagnosis. Instead, participants completed an ADHD questionnaire, and based on scores on that questionnaire were grouped as having ADHD symptoms or not. These differences in our methodology and paradigm may be partly responsible for the lack of differences between our two groups on inattentional blindness and the contrast of our results with those of previous experiments that examined inattentional blindness in participants with ADHD (4).

There are several other limitations that may account for why we did not replicate the prior findings in the literature. First, this was an online sample, and there may be characteristics about this online sample that differ from in-person samples. For example, individuals participating online may engage less with the task and be distracted by other things (e.g., television or outside noise), which would be less likely if they were physically present in a laboratory with a researcher explaining instructions and ensuring they complete the task diligently. Second, as noted, we did not specifically recruit participants who had an ADHD diagnosis but, for logistical reasons, chose to have all participants complete the ADHD symptom scale, and we classified participants into the two groups based on their scores. The number of participants who scored above the cutoff threshold and were included in our ADHD sample is much higher (~36%) than one would expect in a community sample (~4%) (10). It is possible that even though some participants scored high on this questionnaire, they would not meet the requirements for an ADHD diagnosis if assessed by a clinician. Furthermore, the ADHD group sample size was much smaller than the control group and may have lacked enough power to detect differences between the two groups.

In conclusion, the participants we classified as showing ADHD symptoms did not have different inattentional scores than neurotypical control participants on either the perceptually simple Cross Task or perceptually complex Monkey Business Illusion Task. We did not reach the same conclusions as prior studies that we were seeking to replicate (2–4). Inattentional blindness has significant implications for the real world, such as noticing changes in the environment while driving. It is possible that ADHD may provide an advantage and reduce inattentional blindness under some conditions, but specific details about our methodology could potentially account for our null findings. This is an important research area, and future studies should try to fill this large gap in the literature by examining differences between those with attentional dysfunction and those without.

METHODS

Participants

The study was approved by the Southern Methodist University Institutional Review Board, and all participants

gave informed consent. A total of 99 Amazon Mechanical Turk (MTurk; www.mturk.com) workers recruited through Cloud Research/Turk Prime (11) were compensated $4 for approximately 20 minutes of study participation. One participant was excluded from all analyses based on specific responses which suggested they were most likely a "bot" created to answer surveys, leaving a final sample of 98 participants. An additional nine participants failed an "attention check" where they were instructed to type "Silver" in a text box, but answered incorrectly because they did not carefully read the instructions. These nine participants were not excluded from any analyses since inattentiveness is ultimately what we were measuring in this study. There were 11 participants (5 with ADHD symptoms) who had seen a similar video so they were excluded from the Monkey Business Illusion analysis regarding whether they "saw the gorilla", but included in all other analyses. One additional participant had seen the exact video shown in the experiment, so they were excluded from all analyses regarding the Monkey Business Illusion.

The sample was on average 29 years old (SD = 4.0), had 15.14 years of education (SD = 1.89), and included 69 males and 29 female participants. All participants received an ADHD score based on the Adult ADHD Self-Report Scale (ASRS-v1.1) Symptom Checklist ranging from 0–18 (12)the World Health Organization (WHO. The average ADHD score was 4.32 (SD = 4.25). If the participants scored 5 or above on this measure they were considered to have symptoms of ADHD. Four participants (4.1%) self-reported they had been diagnosed with a learning disorder (e.g. ADHD, dyslexia), of which 3 were included in the 36 (36.7%) who were classified as showing ADHD symptoms by our measure. Additional demographic information including race, ethnicity, sex, education, and employment status was tabulated (**Table 1**).

Materials and questionnaires

The Monkey Business Illusion Task was completed first, and is considered dynamic and perceptually complex (5). Participants watched this video with the title edited out to eliminate any information about the stimuli. The scene consists of two teams of three people passing several basketballs back and forth, one team is wearing white and the other team is wearing black t-shirts. The participant is asked to count the number of passes made by the team wearing white. During the passing of basketballs, three unexpected events occur in the scene: (1) a person in a gorilla costume walks into the middle of the screen, beats on his chest for a few seconds, and then exits the scene; (2) the curtain in the background changes color from red to gold; (3) one player wearing a black t-shirt leaves the scene entirely. The video ends as soon as the players stop passing the basketballs and participants are then asked a series of questions about the unexpected events (see procedure section below).

For the second and perceptually simple task with static stimuli, we employed the Cross Task utilized in prior work (1). Participants are presented six trials where a cross appears briefly on the screen (110 ms), followed by a crosshatch mask (2000 ms). Participants indicate via button press which line of the cross is longer, the horizontal or the vertical line. Participants are given five regular trials and then on the sixth (critical) trial, a shape (circle, square, triangle, or star) briefly appears unexpectedly in one of the four quadrants of the cross. The participant is then asked to respond about whether they saw the shape, which shape they saw, and which quadrant it appeared in.

Lastly, participants completed three questionnaires: (1) the Shipley Institute of Living Vocabulary Test which asks participants to select the correct synonym among 4 choices for 40 target words (13); (2) the Behavioral Inhibition/Behavioral Approach Scales (BIS/BAS) which is a 24-item self-report questionnaire designed to measure the complementary

Table 1. Characteristics of the sample by ADHD group.

Characteristic	ADHD symptoms (n = 36)		non-ADHD (n = 62)	
ADHD score	9.1 (SD = 3.16)		1.5 (SD = 1.43)	
Race	Caucasian	66.7%	Caucasian	66.1%
	Black	16.7%	Black	14.5%
	Asian or Pacific Islander	11.1%	Asian or Pacific Islander	12.9%
	American Indian or Alaskan Native	5.6%	American Indian or Alaskan Native	1.6%
	"Other"	0%	"Other"	4.8%
Sex	Male	72.2%	Male	69.4%
	Female	27.8%	Female	30.6%
Ethnicity	Hispanic	16.7%	Hispanic	6.5%
	Not Hispanic	83.3%	Not Hispanic	93.5%
Education	High School	25.0%	High School	27.4%
	College	58.3%	College	66.1%
	Graduate Training	16.7%	Graduate Training	6.5%
Employment	Employed Full-Time	75.0%	Employed Full-Time	59.7%
	Employed Part-Time	11.1%	Employed Part-Time	14.5%
	Student	8.3%	Student	4.8%
	Not Employed	13.9%	Not Employed	24.2%
IB Score	1.96 (SD = 0.73)		2.07 (SD = 0.69)	
Cross Task		20.0%		24.0%

Note: ADHD = Attention Deficit Hyperactivity Disorder; IB Score = Inattentional Blindness.

motivational systems (14); (3) the Adult ADHD Self-Report Scale is a brief ADHD symptom checklist to determine the number of participants in our sample that met criteria for ADHD symptomatology. A score of 5 or above on this measure indicates symptoms of ADHD, but not a clinical diagnosis (12) the World Health Organization (WHO. All participants also provided demographic and general health information.

Procedure

Participants completed the experiment online via Qualtrics (www.qualtrics.com), and it was distributed to MTurk workers via CloudResearch/TurkPrime (11). After providing informed consent, participants watched the Monkey Business Illusion video and then were asked a series of questions: (1) how many times the people in white t-shirts passed the basketball, with the correct answer being 16, and (2) what was the color of the other team's shirt, which was black. These first two questions served as manipulation checks to ensure that participants were paying attention to the video. The next questions probed whether participants noticed the three unexpected events in a yes-or-no format. The last question asked whether they had seen this video before, with four options to choose from: (a) "No, I have never seen it", (b) "I haven't seen it, but I have heard about it", (c) "I've seen a similar video", or (d) "Yes, I've seen this exact video". The Monkey Business Illusion task was followed by the Cross Task detailed above.

After the two tasks, participants completed the Shipley Vocabulary Test that included an additional question to assess engagement and attention that required participants to select the word "GOWN" from the choices, rather than the synonym of the target word. Participants then completed the BIS/BAS, the Adult ADHD Self Report Scale, and responded to demographic and general health questions. The Shipley and BIS/BAS scores are not reported in this paper. The final question was a second attention check, which required that participants type the word "SILVER" into a text box after reading several lines of instructions.

Received: August 11, 2020
Accepted: December 16, 2020
Published: December 21, 2020

REFERENCES

1. Mack, A., and I. Rock. *Inattentional Blindness*. MIT Press, 1998.
2. Swettenham, J, *et al*. "Seeing the Unseen: Autism Involves Reduced Susceptibility to Inattentional Blindness." *Neuropsychology*, vol. 28, no. 4, 2014, pp. 563–70, doi:10.1037/neu0000042.
3. Ashwin, Chris, *et al*. "Differences in Change Blindness to Real-Life Scenes in Adults with Autism Spectrum Conditions." *PLOS ONE*, edited by Alastair Smith, vol. 12, no. 10, Oct. 2017, p. e0185120, doi:10.1371/journal.pone.0185120.
4. Grossman, Ephraim S., *et al*. "Beating Their Chests: University Students with ADHD Demonstrate Greater Attentional Abilities on an Inattentional Blindness Paradigm." *Neuropsychology*, vol. 29, no. 6, 2015, pp. 882–87, doi:10.1037/neu0000189.
5. Simons, D. "The Monkey Business Illusion." *YouTube*, uploaded by Daniel Simons, 29 April 2010, https://www.youtube.com/watch?v=IGQmdoK_ZfY&amp%3Blist=PLbiVpU59JkValOIEIo2Y65mBopHCjKvBo&amp%3Bindex=1.
6. Dein, S. "Hunters in a Farmer's World: ADHD and Hunter Gatherers." *Anthropology*, vol. *3*, no. 01, 2015, pp. 2332-0915, doi:10.4172/2332-0915.1000150.
7. Hartmann, T. *ADD Success Stories: A Guide to Fulfillment for Families with Attention Deficit Disorder: Maps, Guidebooks, and Travelogues for Hunters in This Farmer's World*. Underwood Books, 1995.
8. Lavie, N. "Attention, Distraction, and Cognitive Control Under Load." *Current Directions in Psychological Science*, vol. 19, no. 3, June 2010, pp. 143–48, doi:10.1177/0963721410370295.
9. Forster, S, *et al*. "Plugging the Attention Deficit: Perceptual Load Counters Increased Distraction in ADHD." *Neuropsychology*, vol. 28, no. 1, Jan. 2014, pp. 91–97, doi:10.1037/neu0000020.
10. NIMH. *Attention Deficit Hyperactivity Disorder*. 2017, https://www.nimh.nih.gov/health/statistics/attention-deficit-hyperactivity-disorder-adhd.shtml.
11. Litman, L., *et al*. "TurkPrime.Com: A Versatile Crowdsourcing Data Acquisition Platform for the Behavioral Sciences." *Behavior Research Methods*, vol. 49, no. 2, Apr. 2017, pp. 433–42, doi:10.3758/s13428-016-0727-z.
12. Kessler, R.C., *et al*. "The World Health Organization Adult ADHD Self-Report Scale (ASRS): A Short Screening Scale for Use in the General Population." *Psychological Medicine*, vol. 35, no. 2, Feb. 2005, pp. 245–56, doi:10.1017/s0033291704002892.
13. Shipley, W.C. "A Self-Administering Scale for Measuring Intellectual Impairment and Deterioration." *The Journal of Psychology*, vol. 9, no. 2, Apr. 1940, pp. 371–77, doi:10.1080/00223980.1940.9917704.
14. Carver, C.S., and T.L. White. "Behavioral Inhibition, Behavioral Activation, and Affective Responses to Impending Reward and Punishment: The BIS/BAS Scales." *Journal of Personality and Social Psychology*, vol. 67, no. 2, 1994, pp. 319–33, doi:10.1037/0022-3514.67.2.319.

Sponsorship

Editor's Circle $10,000+

ALLOY THERAPEUTICS

Patron $5,000+

NEW ENGLAND BioLabs® Inc.
enabling technologies in the life sciences

PORTFOLIOS WITH PURPOSE®

Institutional Supporters

HARVARD UNIVERSITY

HARVARD MEDICAL SCHOOL

Tufts UNIVERSITY

Charitable Contributions

We need your help to provide mentorship to young scientists everywhere.

JEI is supported by an entirely volunteer staff, and over 90% of our funds go towards providing educational experiences for students. Our costs include manuscript management fees, web hosting, creation of STEM education resources for teachers, and local outreach programs at our affiliate universities. We provide these services to students and teachers entirely free of any cost, and rely on generous benefactors to support our programs.

A donation of $30 will sponsor one student's scientific mentorship, peer review and publication, a six month scientific experience that in one student's words, 're-energized my curiosity towards science', and 'gave me confidence that I could take an idea I had and turn it into something that I could put out into the world'. **If you would like to donate to JEI, please visit https://emerginginvestigators.org/support, or contact us at questions@emerginginvestigators.org.** Thank you for supporting the next generation of scientists!

'Journal of Emerging Investigators, Inc. is a Section 501(c)(3) public charity organization (EIN: 45-2206379). Your donation to JEI is tax-deductible. '

emerginginvestigators.org